University of Strathclyde

Department of Biomedical Engineering

A computational and experimental investigation into the micropolar elastic behaviour of cortical bone

Jamie Campbell Frame

Engineering Doctorate in Medical Devices, 2013

Abstract

Cortical bone is a natural composite, heterogeneous material with a complex hierarchical microstructure. The description of this microstructure in terms of the mechanical properties of cortical bone may be important in the understanding of periprosthetic stress concentrations. Micropolar elasticity is a higher order continuum theory which may more effectively describe the influence of the microstructure in cortical bone on its mechanical behaviour. Micropolar elasticity predicts a size effect in three-point bending, which has been investigated computationally and experimentally on bovine mid-diaphyseal cortical bone. Computational models of an idealised heterogeneous material, with vascular canal-like structures running along the length of the beam, demonstrated a size effect in the longitudinal and transverse directions which was dependent on the surface condition of the beam. Idealised models with smooth surface layers increased in stiffness as specimens decreased in size, whilst idealised model beams intersected by the internal microstructure demonstrated an equally strong, yet opposite, effect. These FE size effects were further corroborated by analytical studies which demonstrated similar size effects. Experimental three-point bending studies of bovine cortical bone specimens orientated both longitudinally and transversely were consistent with the equivalent numerical models where the internal microstructure intersected the surface. These results suggest the micropolar characteristic length in bending is of the order of the size of the Haversian canal system in secondary osteons and the vascular channels in plexiform cortical bone. The ramifications of this are that the microstructure of cortical bone is of fundamental importance in understanding size effects and stress concentrations in the material. This finding is important in understanding and developing the design and longevity of prosthetic devices and in being able to improve the interaction between an implant and the surrounding cortical bone.

Acknowledgements

I would like to thank my supervisors Dr. Philip Riches and Dr. Marcus Wheel for their continuous support, patient and guidance throughout this research project. I would also like to acknowledge the EPSRC for their funding which made this EngD research project possible.

Thank you to my fellow Tissue Lab and Mechanical Engineering colleagues who have helped to make the work and research all the more enjoyable, through the good and bad.

And a special thank you is due to my parents, family and girlfriend for their unconditional support for the duration of this research project and my university education in general. I could not have done it without you.

Declaration

This thesis is the result of the author's original research. It has been composed by the author and has not been previously submitted for examination which has led to the award of a degree.

Signed:

Date:

Contents

List of figures

List of Tables

1 Introduction

1.1 Background and rationale

Cortical bone is a material with a complex hierarchical microstructure characterised by fibrous, porous and particulate features. It is thought that the microstructure has an important influence on the macroscale behaviour of cortical bone and should be considered mechanically and physiologically important (Sevostianov & Kachanov 2000; Ghanbari & Naghdabadi 2009; Hoc et al. 2006; Hogan 1992). Vascular channels such as associated with primary and secondary osteons are a microstructural feature which innervate and enable the flow of blood through cortical bone. The importance of these channels, if any, in the mechanical behaviour of cortical bone is not well understood. Moreover, there is significant evidence that the microstructure associated with porous features such as vascular channels may have contributing influences to the stress concentrations and stress shielding around implants (Bauer & Schils 1999; Abdel-Wahab et al. 2011; Sevostianov & Kachanov 2000). The design and integration of an implant with bone and understanding the bone prosthesis interface are important areas in prosthetic design. A better understanding of this interaction will enable more effective implants to be designed in the future

Currently classical elasticity is the most common material model used to describe and predict the behaviour of cortical bone. However, unless a geometrical model which includes all aspects of the microstructural morphology is created classical elasticity will not account for all of the microstructural detail of a heterogeneous material. Therefore, perhaps a more general continuum theory which more accurately accounts for the microstructural detail of cortical bone would be a more appropriate continuum model for describing the material. Micropolar elasticity is a higher order continuum theory which, in addition to the direct stresses of classical elasticity, includes a couple stress in the formulation. The effect of this is to add four additional material constants. This thesis investigates whether this additional description in the continuum formulation may better describe the microstructural complexity of heterogeneous materials such as cortical bone.

By modelling the behaviour of micropolar materials numerically and analytically through the creation of idealised analogues a better understanding of the relationship between the microstructure and macroscale material properties will hopefully be determined. Furthermore, by validating the numerical results with experiments on cortical bone it is hoped that a general impression of the potential micropolar behaviour of cortical bone can be created. This, in turn, will allow the future design of implants and prosthetic devices to be carried out with a more accurate and precise consideration for the influence of the microstructure on the general material behaviour.

1.2 Aims and objectives

The aims and objectives of this research project are:

- To model the behaviour of micropolar materials numerically using the finite element method (FEM) by creating an idealised heterogeneous material of a regular array of voids through a homogeneous matrix material. This will be achieved by creating a FE model and defining the material behaviour in axial and three-point bending simulations of various void sizes and arrangements.
- To complement the FEM computational study with an analytical study of similar geometrical models for materials with regular void patterns and laminated materials with heterogeneous material properties.
- To validate the numerical models with three-point bending experiments on cortical bone. This will be achieved by defining a robust experimental protocol and by carrying out experiments on bovine cortical bone specimens. The results of these experiments may then be compared to the numerical findings.
- Relate the size effects produced by the numerical models with those experimentally observed to provide the micropolar material properties of micropolar characteristic length and micropolar Young’s modulus for cortical bone.
- Advance the knowledge in both the numerical and experimental techniques in characterising micropolar material behaviour.

2 Literature Review

2.1 Bone Morphology

Bone is a complex composite material with varying degrees of hierarchical microstructure. The microstructure may be distinctly described at various length scales (Figure 1). In the most general sense a long bone may be categorised into two materials: cortical and cancellous bone. Within each of these types of bone there are unique forms of microstructure. In developed adult human cortical bone there is a network of vascular channels called Haversian canals which innervated and supply blood flow and nutrients to the osteocytes in the bone. Surrounding the Haversian canals are osteons: cylindrical structures consisting of lamellar layers of bone mineral and collagen fibres. At a lower length scale there are smaller channels within bone called canaliculi which link and intertwine between the lamellar layers of the osteons and allow adequate metabolite transfer to all locations in the bone. At the molecular level cortical bone is considered a composite material of two main phases: collagen and hydroxyapatite. This arrangement allows both strength and toughness in the material.

This study primarily focuses as an investigation into the material properties of cortical bone, however to give a background into the construction of long bones a brief section over-viewing the structural make-up of cancellous bone has been included. Cancellous or spongy bone is found at the ends of long bones. It is characterised by strut-like structures called trabeculae which are constructed from a collagen and hydroxyapatite composite and align themselves in an optimal arrangement for the loading conditions of the bone. Cancellous bone is a markedly heterogeneous material and is readily remodelled. The structural differences between cancellous and cortical bone mean that a material description of cancellous bone is significantly different than that of cortical bone.

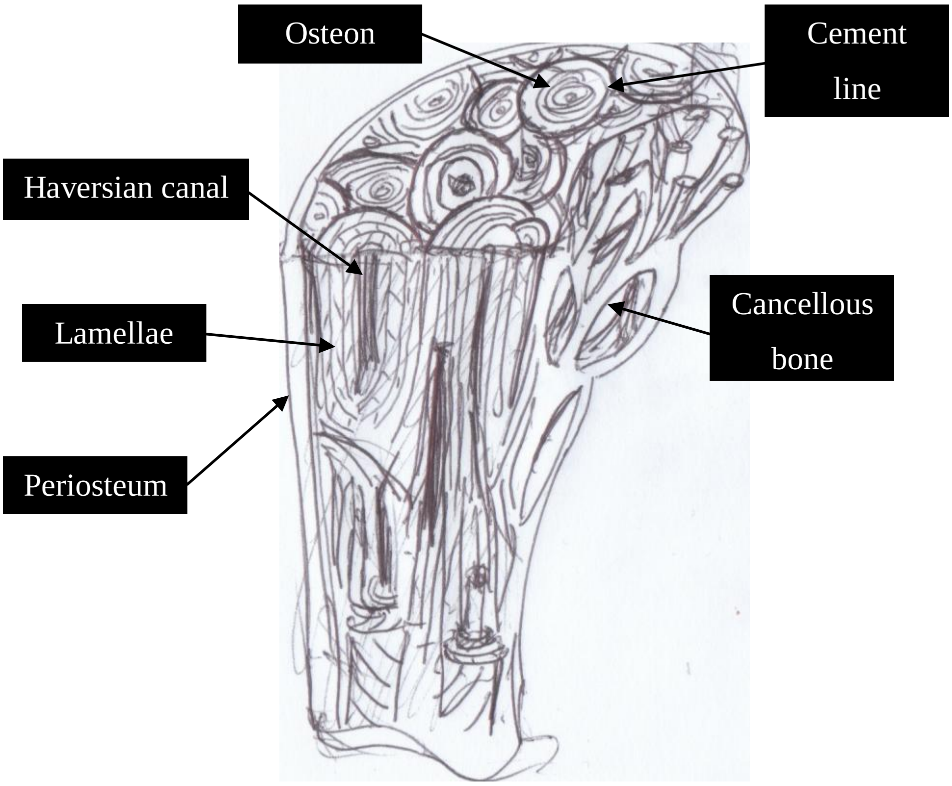

Figure 1 – Microstructure of the Haversian system in cortical bone.

2.1.1 Cortical bone microstructure

Cortical bone is the dense bone region found around the circumference of a long bone. The microstructure of cortical bone is organised in such a manner as to maximise the load bearing properties of the material, and moreover, is unique and adaptive to the loading environment of each bone. Secondary osteons are the primary microstructural feature of mature adult cortical bone (Figure 1). They are cylindrical structures made up of concentric lamellar layers. At the centre of the osteon is a vascular channel known as a Haversian canal. The Haversian canal is the main contributor to the porosity of cortical bone and typically contributes a porosity of between 7-14% in the material (Bayraktar et al. 2004). Haversian canals perform the function of vascularisation of the material which allows the transportation of nutrients to the osteocytes in cortical bone which need to be within 250µm of a vascular channel in order to access diffused nutrients. Osteons and Haversian canals vary in size depending on the region of the bone. Typically osteons are in the region of 300µm in diameter and a few millimetres in length (Pazzaglia et al. 2009; Black et al. 1974). Haversian canals are typically in the region of 50µm in diameter (Black et al. 1974; Pazzaglia et al. 2009). Osteons are aligned along the lines of greatest stress through a long bone. For example, in the mid-diaphysis region of a long bone osteons will be aligned longitudinally along the bone because this is the direction in which the majority of stresses act in this location. Moreover, there are limited transverse stresses acting across a long bone in the mid-diaphysis, therefore osteons tend not to be orientated transversely in this region. On the other hand, at the epiphysis of a long bone osteons are typically aligned to be perpendicular with the surface of the bone, this is particularly noticeable around the ball of a femur (Rho et al. 1997; Cowin 1989). A consequence of this is that the regions of greatest anisotropy in cortical bone are in the mid-diaphysis where the longitudinal Young's modulus is significantly higher than the transverse Young's modulus. Longitudinally aligned Haversian canals are connected through horizontal channels called Volkmann's canals. There are significantly fewer Volkmann canals than Haversian canals and their primary function is to aid the communication between neighbouring osteons.

Because of the dynamic nature of cortical bone and its continuous regeneration it is common for osteonal bone to be categorised according to its formation. Typically there are three types of osteonal bone divided into plexiform bone, secondary osteons and interstitial bone. Plexiform bone, which is constructed from primary osteons, is the material created by the rapid growth of new cortical bone and is found in younger bones and higher quantities in the long bones of quadrupeds (Mayya et al. 2013). Primary osteons follow a similar structure to that of a typical secondary osteon with a central vascular channel and lamellar rings concentrically aligned around the centre. However, the distinction between plexiform bone and secondary osteons is not purely semantic because primary osteons are generally not found in remodelled bone and are typically found to be a more compliant material with a higher degree of orthotropy (Cowin 1989). As bone ages and develops osteons are continually being created and destroyed in an ongoing remodelling process which adapts to the subtle changes in loading over time. When a new osteon is created by the boring out of a Haversian canal by an osteoclast, creating a secondary osteon, there will typically be a region of bone where an older osteon has been remodelled. This results in the region between cylindrical osteons being densely packed with the remainders of previous osteons. This region is known as interstitial bone. Nano-indentation studies have shown that interstitial bone is a harder, more mineralised material than primary osteons (Zhang et al. 2008; Rho et al. 2002) with a slightly higher Young's modulus. Around the outside of an osteon there is a thin layer known as a cement line. This region is commonly considered to be a demineralised region and is thought to be important in the control of microcracking and crack propagation through cortical bone. However, a study has suggested that cement lines are in fact a hyper-mineralized region and that this has an equally important role in controlling the propagation of microcracks through the material (Norman & Wang 1997; Najafi et al. 2007).

Secondary osteons are created by osteocytes as they remodel primary osteons into a microstructure which is better adapted to the unique loading conditions of that particular bone. They are constructed from concentric lamellae around the Haversian canal. The formation of the lamellar layers by osteoblasts reveals another layer of heterogeneity in cortical bone. The orientation of lamellae alternates between layers, in a similar structure to that of a plywood layered composite material. Within the lamellae layers there is a collagen-hydroxyapatite composite. The orientation of the collagen fibres in each lamellae is reversed between each layer (Bala et al. 2011; Rho et al. 1997; Akiva et al. 1998). This ultimately creates a strong and versatile composite structure within each osteon. Sandwiched between each lamellar layer are small pockets called lacunae. These small holes are the location of cortical bone where osteocytes are found. Lacunae contribute to the overall porosity of cortical bone and are an order of magnitude smaller than Haversian canals, so they can be thought of as another layer of heterogeneity below the microscale, within an osteon itself. Connecting each lacunae and between each lamellae there are small channels called canaliculi which are again an order of magnitude smaller than the Haversian system and their primary function is to aid intra-Osteon communication.

The fundamental building block of cortical bone is a composite of the organic phase: type I collagen; and the mineral phase: hydroxyapatite. The combination of these molecular structures enables bone to have longitudinal strength and toughness. These two phases are arranged with the apatite binding around a collagen fibril. The collagen-apatite fibres are arranged in parallel with one another which, once built up and compounded, create a lamellar layer in the osteon. The fundamental composite nature of cortical bone has led to structural analogies with composite materials (Najafi et al. 2009; Pidaparti & Chandran 1996; Belanche et al. 2011).

Cortical bone is a complex material. The combination of each of the levels of microstructure, from the molecular collagen-hydroxyapatite composite structure, to the intra-osteon detail of the canaliculi and lacunae microstructure and the lamellar layers surrounding each osteon, to the inter-osteon detail of the Haversian canal system and the distinctions between osteonal and interstitial bone suggests that to generalise such a material will exclude much of the detail which may be fundamental to its behaviour. Considering this, is it viable to describe such a material using classical elasticity when a main assumption of this theory is to assume the material behaves as a homogeneous continuum? The research hypothesis of this thesis is that a continuum theory which accounts for some of the microstructural detail would produce a more accurate description of cortical bone (Fatemi et al. 2002).

2.1.2 **Cortical bone mechanical properties**

The mineral and organic phases of cortical bone have a fundamental importance on the mechanical properties of the material. Unsurprisingly when the mineral content is reduced the stiffness of the material is noted to decrease (Burstein et al. 1975; Hasegawa et al. 1994). As the mineral content is increased in cortical bone the Young's modulus increases rapidly (Currey 1969). Yield stress and ultimate tensile stress have also been found to be markedly influenced by the mineralisation and the strain rate, where higher strain rates increase the stiffness of cortical bone (Currey 1975).

Cortical bone is often assumed to be either transversely isotropic, or orthotropic (mechanical properties are different in three orthogonal directions), but the assumption of transverse isotropy is not always sufficiently general (Cowin 1989). Using ultrasonic wave propagation measurements, the elastic stiffness coefficients were calculated for the human femur (Katz & Yoon 1984); Haversian bone was found to be transversely isotropic, whilst plexiform was more orthotropic in mechanical characteristics. The distinction between Haversian and plexiform bone is important in the interpretation of experiments on cortical bone as a specimen with a higher degree of plexiform bone may exhibit different material properties compared with a specimen with a fully developed secondary osteon system. In quadrupeds it has been observed that there is a higher degree of plexiform bone in load bearing regions where rapid bone growths occurs (Mayya et al. 2013). The porosity of cortical bone has a strong influence of the measured material Young’s modulus (Currey 1988). It has been observed that where the porosity of the Haversian system is factored out of the material properties by performing a regression analysis on axial loading results there was no influence on the material properties from the overall material porosity (Bayraktar et al. 2004). This suggests that the main contributing microstructural feature producing the anisotropy in cortical bone is the vascular channels in the material. Ultrasound techniques have been used to define the material stiffness and mineral content of cortical bone (Yamato et al. 2006) and suggest that a fully developed Haversian system exhibits orthotropic properties where the transverse radial and circumferential Young’s moduli are of similar magnitudes (10-14GPa) and the longitudinal modulus is significantly higher (18-20GPa) (Buskirk & Rice 1982). The orientation of collagen fibres has been related to the observed material properties of equine cortical bone (Martin et al. 1996) and three-point bending experiments have suggested that the organisation of the collagen fibres may be related to the localised stresses within the material and are linked to the porosity and mineral content which allow cortical bone to function more effectively depending upon the unique loading conditions (Martin & Boardman 1993). Nano-indentation further highlighted the importance of localised material properties where a dependence upon the individual lamellae which may exhibit different material properties within the same osteon (Zysset et al. 1999).

The viscoelastic nature of cortical bone has been investigated by experimentally analysing stress relaxation in the material and relating this to the water content (Sasaki & Enyo 1995). It was found that water content has a fundamental importance on the viscoelastic nature of the material. Because of the viscoelastic properties of cortical bone ultrasonic tests will tend to induce higher strain rates which will be below the relaxation times associated with viscoelastic effects (Lees et al. 1979). The result of this is that the material properties observed from ultrasound tests will reveal the upper bound of the elastic modulus. Where the strain rate is reduced a lower

Young’s modulus may be observed (Currey 1975). Furthermore, where the mineral content has been reduced due to specimen storage in saline solution it has been observed that the relaxation rate is significantly reduced compared to specimens stored in a Ca^{2+} solution (Sasaki et al. 2008). This again, highlights the importance in maintaining mineral content in cortical bone in order to produce reliable observed material properties. There is an important inter-relationship between the nature of microcracking in cortical bone and the viscoelastic properties of the material. Size effects in viscoelastic effects have been observed and have been attributed to the viscoelastic interfaces between lamellar layers in osteons (Buechner & Lakes 2003). This suggests that it is important to maintain consistency in the experimental protocol where elastic size effects are being investigated so as to avoid overlapping effects being observed. Viscoelastic models have been created which indicate that the viscoelastic effects may be broken down into nano-scale effects related to the collagen mineral interaction and microscale effects related to microstructural features (Iyo et al. 2004; Johnson et al. 2010).

The mechanical functions of bone may be related to the microstructural features where the mechanical behaviour is understood in terms of the observed mechanical properties. It has been shown that at lower strain rates the prominence and initiation of microcracks is increased as a mechanism for absorbing energy and as the strain rate is increased microcracks are less frequently initiated (Zioupos et al. 2008; Zioupos and Currey 1994). The microstructure of cortical bone creates a unique nature of microcracking within the material. Microcracks form in the lamellar rings of osteonal cortical bone and may perforate without communicating with other localised microcracks (Zioupos and Currey 1994). This feature of bone suggests it may not behave in the nature of a classically elastic material where the formation of the first microcrack leads to catastrophic failure of the material. The detailed nature of cortical bone’s microstructure allows microcracks to form and propagate in a controlled manner without threatening the integrity of the material on the macro scale. Voids and naturally occurring vascular networks within cortical bone are not the origin of microcracks in the material. Rather the microcracking is associated strongly with the areas of high mineralisation where the material is much more brittle compared to the less well mineralised regions (Zioupos and Currey 1994). How cortical bone behaves around artificially created voids and inclusions in the material, such as the creation of screw holes for implants, may be a more complicated proposition as the microstructural features which dissipate the microcracks in lamellar bone are disrupted and new stress concentrations are formed around voids. This would have an important influence on the understanding of the interface between prosthetic devices and cortical bone.

The nature of the lamellar rings surrounding the Haversian canals in osteonal bone have the influence of deflecting microcracks thereby creating a much more robust material where microcracking follows the pre-defined networks of microstructural channels within the material. Canaliculi (Ebacher et al. 2012) have been postulated as being the initiation region of many microcracks in compact bone where the microcracks originate at the mineralised collagen fibrils at the ultrastructural level (Vashishth et al. 2000). The many lamellar and sub-lamellar microcracks seen in cortical bone may be considered to be a feature of the microstructure as the microcracks follow the morphological nature of the microstructure itself. The variation through cortical bone from area of dense mineralisation to areas with lower mineralisation interspersed with varying morphological features has the impact of influencing the propagation speed and energy of microcracks, thereby controlling the impact on the overall macrostructure (Zioupos 1998). The degree of bone toughness is related to the ability of cortical bone to absorb microcracks, in turn this is related to the strain rate of the applied load, and in delaying the transition from a ductile to brittle material (Zioupos et al. 2008).

It can be seen that there is a great degree of complexity in describing both the physical microstructure and the material properties of cortical bone. Both are undoubtedly inter-related, and in order to gain a full understanding of the material properties of cortical bone a robust understanding of the impact of the microstructure on the macroscale material behaviour is required. Multiscale modelling is a traditional approach to model the microstructure of complex inhomogeneous materials. It attempts to represent the global material behaviour of a material by the formation of a representative volume element (RVE) (Ghoniem et al. 2003; Kouznetsova et al. 2002; Ghanbari & Naghdabadi 2009; Ladevèze 2004). The microstructure of cortical bone and the fundamental composite nature of the material lend themselves to a multiscale modelling approach (Hogan 1992; Braidotti et al. 1995; Ghanbari & Naghdabadi 2009; Bala et al. 2011). The observed behaviour from multiscale modelling generally attempts to generate a RVE which exhibits similar material behaviours to that of the global material and then describes the microstructure in terms of the observed behaviour. The RVE can them be altered in order to better match the observed material behaviour. In this study however, it will be attempted to show that from the first principles of the generalised continuum theory of micropolar elasticity the material behaviours created by the microstructure of cortical bone can be adequately described. The rationale for this is that the microstructure of cortical bone produces mechanical behaviours which can be generalised into material behaviours which are described by micropolar elasticity.

2.2 Micropolar elasticity and higher order continuum theories

2.2.1 Background

All materials contain length scale specific microstructure. This may vary from the macro scale in metal foams and many biomaterials to the micro scale and below in apparently homogeneous continua such as metals and plastics. Ultimately the molecular structure can be considered as the basic structure of all apparently homogeneous materials. In such homogeneous materials the microstructure is sufficiently small that it has a minimal influence on the macro scale deformations. However, for materials where the microstructure is comparable to the overall scale homogeneity can no longer be assumed. In such cases an approach that incorporates the microstructure may better describe the material behaviour and be a more effective method for describing the interaction between the microstructure and the macroscale material behaviour. This is because the microstructural detail will have already been accounted for in the continuum model and a more simplified numerical model could be created without modelling the intricacies of the microstructure.

Generalised continuum theories attempt to quantify the character of a heterogeneous material rather than model the intricacies of the material microstructure. Although the fundamental structural complexities of the material may not be fully modelled the character of the material can be sufficiently described so as to provide a functional representation of the material behaviour. When considering the complexity of many composite materials a generalised continuum theory that averages the discrete idiosyncrasies of the material into a global continuum may prove to be a more practical method of modelling material behaviour than modelling with classical elasticity.

In classical elasticity theory the forces acting upon a point depend only upon the location. When the influence of neighbouring points is considered on the forces acting upon a point a non-local theory may be developed. The forces acting on a point in the material are dependent upon the location and the neighbourhood in a non-local theory. An intrinsic length scale is associated with the material joining the location and neighbourhood. The non-local effect will become more pronounced as the length scale becomes more significant in the geometry being analysed. For larger geometries with relatively small length scales the non-local effects will lose their significance, and a local theory may describe the material effectively.

Micropolar elasticity is a higher order generalised continuum theory. It includes a micro rotation into the formulation in addition to the direct stresses of classical elasticity. This has the effect of enabling the requirement of complimentary shear stress pair to be relaxed. To maintain equilibrium couple stresses are included which have an associated intrinsic length scale. The addition of the extra degree of freedom causes micropolar elasticity to predict different material behaviours compared with classical continuum elasticity. This is especially apparent in the dispersion of stress waves, stress concentration factors and the prediction of a size effect in bending and torsion.

2.2.2 **Constitutive equations**

The incorporation of a couple stress into the formulation of micropolar elasticity in addition to the familiar direct stresses of classical elasticity, results in four additional elastic constants (six in total) compared with those produced by classical elasticity (Figure 2).

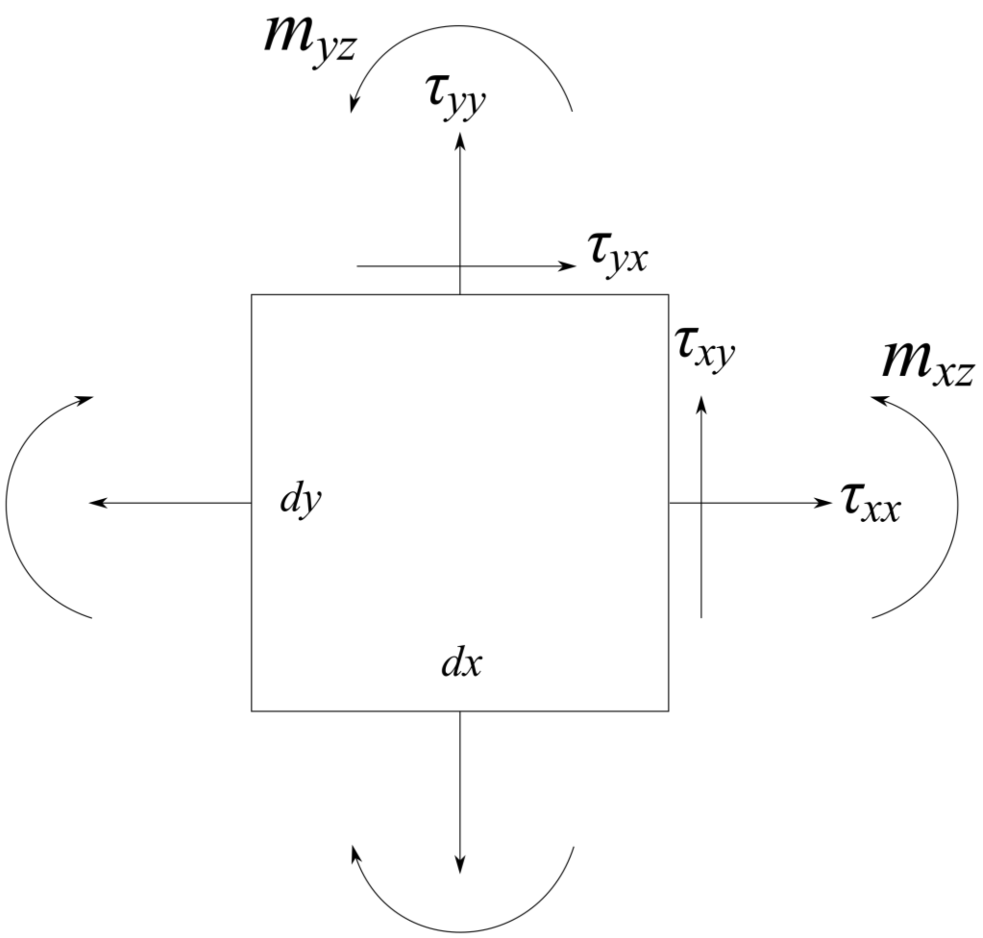

Figure 2 – Micropolar differential stress element

For an isotropic linear elastic micropolar material the constitutive equations are (Eringen 1966):

Equation 1

$$\tau_{ij} = \lambda \varepsilon_{kk} \delta_{ij} + \left(2\mu^* + \kappa\right)\varepsilon_{ij} + \kappa e_{ijk}\left(\theta_k - \phi_k\right)$$

Equation 2

$$m_{ij} = \alpha \phi_{k,k} \delta_{ij} + \beta \phi_{i,j} + \gamma \phi_{j,i}$$

where δ_{ij} is the Kronecker delta, e_{ijk} is the permutation tensor and λ and μ are the material dependent Lamé constants of classical elasticity. Conventional stress and strain tensors are represented by τ_{ij} and $\varepsilon_{\mathrm{ij}}$ respectively while θ_{k} represents the usual macrorotation. The couple stress and microrotation are given by m_{ij} and $\varphi_{\mathrm{i,j}}$

respectively. The remaining moduli κ, α, β and γ represent the additional micropolar constitutive properties which will tend to zero on approaching classical behaviour. In the planar case these elastic constants can be reinterpreted in terms of just four independent technical or engineering properties, E_M, υ_M, l_b and N (Gauthier & Jahsman 1975; R. Lakes 1995). The first two of these correspond to the Young's modulus and Poisson's ratio that govern uniform dilatational and distortional straining with the subscript M being used here to distinguish them from their classical counterparts. The characteristic length in bending, l_b, reflects the size scale of the intrinsic heterogeneity by specifying the range of the couple stresses while the coupling number, N, characterizes any asymmetry in the shear stresses that must be balanced by the couple stresses.

2.2.3 **A micropolar beam in 3-point bending**

The derivation of the stiffness of a micropolar beam in 3-point bending is given in (Beveridge 2011) and is included here. The radius of curvature of a slender beam bent through a small angle is:

Equation 3

$$\frac{1}{R} = \frac{d\theta}{dx} = \frac{d\phi_z}{dx} = -\frac{d^2 v}{dx^2}$$

Considering only the in plane couple stress, m_{xz} and direct stress, τ_{xx}

Equation 4

$$m_{xz} = \gamma \frac{d\phi_{xz}}{dx}$$

Equation 5

$$\tau_{xx} = E_m \frac{y}{R}$$

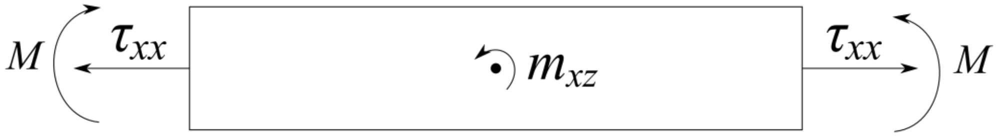

Figure 3 – Stress acting upon a planar micropolar beam

By taking the internal resisting moment equal to the external applied moment, M (Figure 3):

Equation 6

$$M = \int_A (y\tau_{xx} + m_{xz})dA$$

Or by substituting for m_{xz} and τ_{xz},

Equation 7

$$M = \frac{1}{R}\int_A (y^2 E_m + \gamma)dA$$

Completing the integration and substituting terms for the area, *A*, and second moment of area, *I*, the moment curvature relationship is:

Equation 8

$$\frac{d^2v}{dx^2} = -\frac{M}{E_m I + \gamma A}$$

From the moment curvature relationship the maximum deflection of a micropolar beam under 3-point bending is:

Equation 9

$$v_{\max} = \frac{Wl^3}{48(E_m I + \gamma A)}$$

where *l* is the length of the beam. By dividing the applied load *W* by the maximum deflection v_{max} the stiffness of the beam can be calculated. For a square cross sectioned beam of breadth *b* and depth *d* the equation for the stiffness of a micropolar beam in 3-point bending can be represented as:

Equation 10

$$K = 4E_m b \frac{d^3}{l^3}\left(1 + \frac{l_c^2}{d^2}\right)$$

where E_m is the micropolar Young's modulus, and l_c is the micropolar characteristic length. It can be seen that the stiffness is dependent on the characteristic length as well as the length to depth aspect ratio. In short a size effect is observable where smaller beams will be relatively stiffer compared to larger beams of the same length to depth aspect ratio.

Equation 11

$$K = 4Eb\frac{d^3}{l^3}$$

Equation 11 shows the equivalent stiffness relationship for a classically elastic beam in 3-point bending. Therefore, the term included within the brackets in Equation 10 is the additional term which is responsible for the micropolar size effect.

Equation 10 describes the plane stress closed form three-point bending stiffness of a micropolar material. This equation assumes there is no transverse stresses in the beam. From the size effect described by Equation 10 it is possible to extract the micropolar material properties of micropolar Young's modulus, E_m, and micropolar characteristic length, l_c. The micropolar characteristic length in bending, l_b, is related to the characteristic length in Equation 10 by $\frac{l_c}{\sqrt{12}}$. The distinction between the characteristic length and the characteristic length in bending is that in Equation 10 the characteristic length allows the micropolar size effect to be represented more succinctly, the characteristic length in bending of square cross sectioned beam is related to the micropolar material constant γ by $l_c = \sqrt{\frac{12\gamma}{E_m}}$ (Beveridge 2011). The micropolar Young's modulus may be thought of as the flexural equivalent of the modulus obtained from a micropolar beam loaded axially. The micropolar characteristic length may be considered to be a description of the linear size effect observed between stiffness and reciprocal of depth squared and may be considered to characterise the predominant microstructural features in the material and is related to the moment arm of the couple stress that the microstructural features produce in the material (R. Lakes 1983; Eringen 1967; Beveridge et al. 2013; Park & R. Lakes 1986; R. Lakes 1995).

There are similarities in structure between an idealised heterogeneous material of regularly arranged voids and that of the observable microstructure in bone. For example in remodelled bone the Haversian canal network approximately creates a regular array of voids through the osteonal matrix or the lacunae and canaliculi microstructural features are arranged within the osteon to create a regular heterogeneous material. Using micropolar elasticity, it may be possible to describe the heterogeneity of cortical bone, at a chosen length scale, thereby enabling a more accurate representation of the material behaviour.

2.2.4 **Experiments on micropolar materials**

Attempting to identify microscopic level size effects at the macroscopic scale is understandably a challenging task. For this reason many early attempts to extract micropolar material properties were unsuccessful. Gauthier and Jahsman pioneered an experimental technique which was able to separate and quantify all six micropolar material constants (Gauthier & Jahsman 1975). To do this, analytical expressions were required for the mechanical response in bending and torsion for an idealised material with rigid inclusions. These predict a relative stiffening of smaller specimen sizes. When analysing a material in both torsion and bending loading conditions it is possible to extract all six of the micropolar material properties from the size effects. The results were inconclusive and Gauthier and Jahsman were unable to derive all six micropolar properties due to the negative size effects of some results (Gauthier & Jahsman 1975). It has since been suggested that the main cause of the negative size effect was because the inclusions in the idealised material were stiffer than the matrix material and a positive micropolar size effect is only observed where the inclusions are less stiff than the matrix material (Bigoni & Drugan 2007).

Lakes has been the most prolific author with regards to experimental work in micropolar materials. His review of experimental methods in micropolar materials provides a general overview of the experimental techniques used to determine micropolar material properties (Lakes 1995). However, although his work has focused on many materials including polyurethane foams, porous solids and cortical and cancellous bone (Anderson & Lakes 1994; Lakes 1983; Lakes 1995; Lakes 1985; Yang & Lakes 1982) the experimental methods have not been corroborated with numerical analyses to confirm the causes of the observed size effects.

In some cases the size effects appear to show a size softening anti-micropolar size effect which is not predicted by analytical solutions and it has been suggested that the cause of the observed size effect is a masking of the true micropolar behaviour by surface effects (Anderson & Lakes 1994; Brezny & Green 1990). Lakes and Anderson have suggested that the surface region of a micropolar material may be considered as a region of damage caused by the preparation process of the specimens and thus masks the true material behaviour (Anderson & Lakes 1994). Brezny and Green have suggested that there is a critical cell size to weight ratio which will reduce the influence of any surface region to the observed micropolar material properties (Brezny & Green 1990). Both of these studies highlight that one of the major problems with experimentally deriving the properties of a micropolar material is the issues regarding surface effects. If the condition of the surface is affecting the results then the true micropolar material properties will not be observed. A computational investigation and validation of the influence of the surface on the observed micropolar size effect trend would enable future experimental analyses to be more accurate. Furthermore, it would enable a greater insight into the relationship between sample preparation and observed mechanical behaviour.

Beveridge has shown a micropolar size effect may be observed computationally by creating an array of voids through a homogeneous matrix material thus creating a planar idealised heterogeneous material (Waseem et al. 2013; Beveridge et al. 2013; Beveridge & Wheel 2010; Beveridge 2011). The micropolar size effects produced through three-point bending analyses computationally were concurrent with those observed in experiments on an equivalent idealised heterogeneous material. This also revealed that the characteristic length in bending of a micropolar material is of the order of the void size and is related to the density of the voids in the material. Attempts have been made to characterise the micropolar material properties in terms of the microstructural detail. This has been done by modelling a deliberately simplified heterogeneous material with discrete sections of different material properties (Forest et al. 2000). This would suggest that where a micropolar material behaviour is observed experimentally it may be possible to relate the observed size effect directly to the microstructure.

It has also been suggested that cortical bone exhibits micropolar size effect trends (Yang & Lakes 1982; Buechner & Lakes 2003; Park & Lakes 1986; Lakes 1995). The most prominent of these studies into the micropolar behaviour of cortical bone was the work of Yang and Lakes (Yang & Lakes 1982) and Park and Lakes (Park & Lakes 1986). In these papers it is postulated that one of the causes of a micropolar size effect in cortical bone may be the effects of the cement lines between osteons. It is hypothesised that the hypo-mineralised cement lines are a region of relatively lower material stiffness where shear stresses are not transmitted in the material and result in sliding between osteons, rather than the material acting in unison. This theory ties in well with the shear stress imbalance used in the formulation of micropolar elasticity and would suggest that the characteristic length of cortical bone should be of the order of the diameter of an osteon (around 350μm). The observed size effects from these studies indicated that the micropolar characteristic length of cortical bone was 200μm broadly consistent with the hypothetical predictions. One of the issues with this work is the length scales over which the specimens were tested. The smallest specimen is greater than 1mm in diameter and therefore is not approaching the scale of the microstructure being tested as it is significantly larger than the diameter of an osteon. This suggests the size effect may be more attributable to natural variation in the material properties of each specimen rather than a fundamental material property. Furthermore, because there is no validation of the experimental results with computational models it is unclear whether the material properties are being derived free from the influence of a surface effect.

Choi observed size effects in cortical bone during three-point bending tests of specimens ranging from 1000μm to 200μm (Choi et al. 1990). This is of the length scale of the microstructure of cortical bone. Although Choi did not directly relate his finding with micropolar theory the results are of significance as they clearly show a negative size effect is present in cortical bone under three-point bending. This work is in direct contrast with the findings of Yang and Lakes (Yang & Lakes 1982), which found a positive size effect in bending tests on cortical bone. The main differences between both studies were the length scale of the tests - where Choi has tested significantly smaller specimens - and the cross sectional shape of the specimens: Lakes tested circular cross sections; Choi tested square cross sections. This may suggest that Choi's results show a more significant relationship between specimen stiffness and size. The length scale of the specimens tested is approaching the microstructural level of cortical bone, and therefore may be revealing the influence of the Haversian system more prominently in the recorded stiffness values. Moreover both the results of Lakes and Choi broadly agree in the stiffness of the larger specimens. This may suggest that at a larger length scale the influence of the microstructure of the Haversian system is less prominent and natural variation between bone specimens is the more important factor influencing the material stiffness. However, it may also indicate that there are various microstructural influences which could produce a size effect in cortical bone; one study may have detected the influence of osteons and the cement line interface, and another may have detected the influence of the Haversian canal system.

The Choi data show a clear negative size effect which is opposite to that predicted by micropolar elasticity. Because the surface condition of each specimen was not recorded it is unclear whether the negative size effect could be attributable to some kind of surface damage. However, if this was the case it would add further weight to the theory that surface effects have a strong influence on the behaviour of micropolar materials and may be a contributing factor in experimental detection of the micropolar material properties (Choi et al. 1990). Nevertheless, it is noteworthy that Lakes found a positive size effect in cortical bone and it remains unclear why there is an inconsistency between similar studies on the same material (Park & Lakes 1986).

Recently there have been some studies which have attempted to describe cancellous bone as a micropolar material (Goda et al. 2012; Ramézani et al. 2012). Cancellous bone has a less dense microstructure and is more relatable to polyurethane foam type materials, which have been analysed for micropolar behaviour in the past (Anderson

& Lakes 1994; Forest et al. 2000). These types of material show that where the microstructure is on the scale of the global geometry the magnitude of the size effect observed will be much more pronounced. On the other hand in cortical bone it is thought that the micropolar size effects may be observed from the microstructure itself, rather than at the macroscale. For this reason experimental observation of micropolar size effects in cortical bone requires specimens of the order of size of the Haversian system, whereas in cancellous bone it is the interaction between trabeculae at the macroscale which are thought to cause micropolar behaviour and therefore cancellous specimens of a larger scale can be used.. This research project will focus on characterising cortical bone however the advances currently occurring in the mechanical description of both cortical and cancellous bone seem to indicate that micropolar elasticity is an appropriate continuum model for describing microstructure.

2.3 Cortical Bone as a Micropolar Material

The complex hierarchical microstructure of cortical bone raises the question of whether classical elasticity is adequate in describing this detail. Classical elasticity assumes a homogeneous material. In the case of cortical bone it is a broad generalisation to ignore the microstructure and describe the material as a purely homogeneous continuum. However, in the most general cases the approximation of cortical bone as a homogeneous material may not an unreasonable assumption. This is because at larger sample sizes the scale of the microstructure is well below that of the macroscale where larger deformations would be observed. This was mentioned previously in the diverging results between Lakes and Choi; where the scale of specimens is larger than the microstructural detail Lakes observed a positive size effect (Park & Lakes 1986); on the other hand Choi observed a negative size effect where the scale of specimens were in the region of the Haversian system (Choi et al. 1990).

The reasons for the difference in size effect trends is ambiguous and may be related to surface preparations, however, micropolar theory relies upon the microstructure becoming significant in relation to specimen size when using the method of size effects. For this reason it may be important to note that in circumstances where the microstructure is of the scale of the surrounding geometry micropolar elasticity could be a more appropriate continuum theory for describing cortical bone. Whereas, in situations where the microstructure is of a relatively smaller scale than the surrounding geometry, classical elasticity may suffice in its description of cortical bone (Fatemi et al. 2002).

A fundamental problem in the design of artificial joint replacements is in full interfacing of a non-biological component with living tissue. In particular the design of many implants is based upon a correct load transfer from the foreign prosthesis onto living bone. This can only be achieved if the stress behaviour of the biological bone is properly understood and modelled. This is of particular significance at the length scale of the microstructure where stress concentrations may become distorted by the morphological features. Implants, prosthetic and periprosthetic devices interact with cortical bone during their normal functions. The interaction between prosthetic devices and cortical bone fundamentally involves the contact between the microstructure and the surface of the prosthetic device either directly or through a cement interface (Hogan 1992). How this interaction occurs and develops over time is of importance to understanding the lifecycle of prosthetic devices (Huiskes 1990). Micropolar elasticity predicts a reduction in stress around a stress concentration such as a circular hole or rigid inclusion in a micropolar material when compared to a classically elastic material (Eringen 1966; Gitman et al. 2010). If cortical bone can be described as a micropolar material, then the description of material behaviour using classical elasticity may no longer be a completely accurate representation. Subsequently, where an implant may be considered to be a rigid inclusion through that continuum, micropolar behaviour would produce a significantly different material behaviour than that predicted by classical elasticity. This would represent a scenario where micropolar elasticity was a more appropriate continuum model for describing the stress and stress concentrations in cortical bone.

Where stress concentrations are relatively higher or lower than expected in cortical bone then the resulting bone will remodel itself over time to the new loading conditions. This may result in stress shielding around implants, where there is a relatively lower stress than there otherwise would be, and osteolysis may begin to occur. Recent studies have shown that the level of stress shielding that occurs post implant is dependent on the type of implant device and the interaction between the implant and the bone (Cristofolini et al. 2009; Sathappan et al. 2009; Ellison et al. 2009). It has been suggested that the size of an implant can be related to the potential failure mechanisms (Baggi et al. 2008). For aseptic implant failures loosening of implants is among the most common failure mechanisms. This may be related to particle wearing from the implant and casing changes in loading patterns or due to the micromotion of the implant itself (Bauer & Schils 1999). If micromotion of implants can be better described by a more representative continuum model then a more accurate description of the behaviour of the implant may be modelled. Where there is an increase or decrease in stress in a particular location then this will undoubtedly influence the fatigue behaviour of that region in the bone and may lead to osteolysis and an unpredictable alteration in the mechanical loading on the bone (Bauer & Schils 1999; Baggi et al. 2008; J.-H. Lee et al. 2005). Understanding the fatigue behaviour and the probability of microcracking to occur and propagate through cortical bone is important in determining how the bone will remodel itself under new loading conditions (Taylor & Lee 1998). Microcracking is an important aspect of the interaction between implants and cortical bone. The microstructure at various scale levels is thought to have an important influence on the propagation of cracks through cortical bone. In fact it is thought that the location and organisation of the heterogeneity in cortical bone is a key factor in controlling the occurrence of microcracks (Rho et al. 2002; Tai et al. 2007). Moreover where there is a change in the stress concentration the likelihood of microcracking to occur will also be changed. There is evidence that microcracking is of vital importance to the development of bone and bone remodelling (Reilly & Currey 2000; Ebacher et al. 2012; Reilly & Currey 1999; Vashishth et al. 1997); this would ultimately alter the interaction between prosthetic implant and the surrounding material where the stress concentration is different from what has been predicted. If cortical bone can be shown to behave in accordance with micropolar elasticity it will enable more accurate numerical modelling of prosthetic devices. Furthermore, a better understanding of the interaction between an implant and cortical bone will be achievable. This would further the design potential of prosthetic devices to interact with cortical bone in the most effective way possible. Thereby, increasing the lifecycle of implants and improving their functionality.

3 Numerical analysis of idealised heterogeneous materials

3.1 Background

Previous studies have found that idealised planar heterogeneous model materials can be created which exhibit micropolar behaviour (Waseem & Beveridge 2013). These studies modelled beams in three point bending and demonstrated the relationship between micropolar characteristic length and the microstructural features. It was also shown that for beams with lower length to depth aspect ratios a non-linear size effect trend occurred from which the micropolar coupling number could be calculated.

An idealised 2-dimensional planar heterogeneous material can be created by introducing an array of voids or inclusions of a different material property into a homogeneous matrix material (Beveridge 2011) as shown in Figure 4. This material is designed to mimic the variation in material properties, inherent heterogeneous character and possible anisotropy of many composite materials. The geometrical characteristics of this material are defined by the void radius, V_R, the void separation in the x-axis, S_X, and the void separation in the y-axis, S_Y. By varying these parameters the geometry of the material can be altered resulting in varying degrees of both heterogeneity and anisotropy. The material properties of the isotropic, intra-void matrix are defined by the Young's modulus and Poisson's ratio. When S_Y is $1/\sqrt{2}S_X$ this material is macroscopically transversely isotropic, the material exhibits isotropy within the 2D x-y plane, and otherwise the material is anisotropic with the degree of anisotropy depending on the ratio of S_X to S_Y.

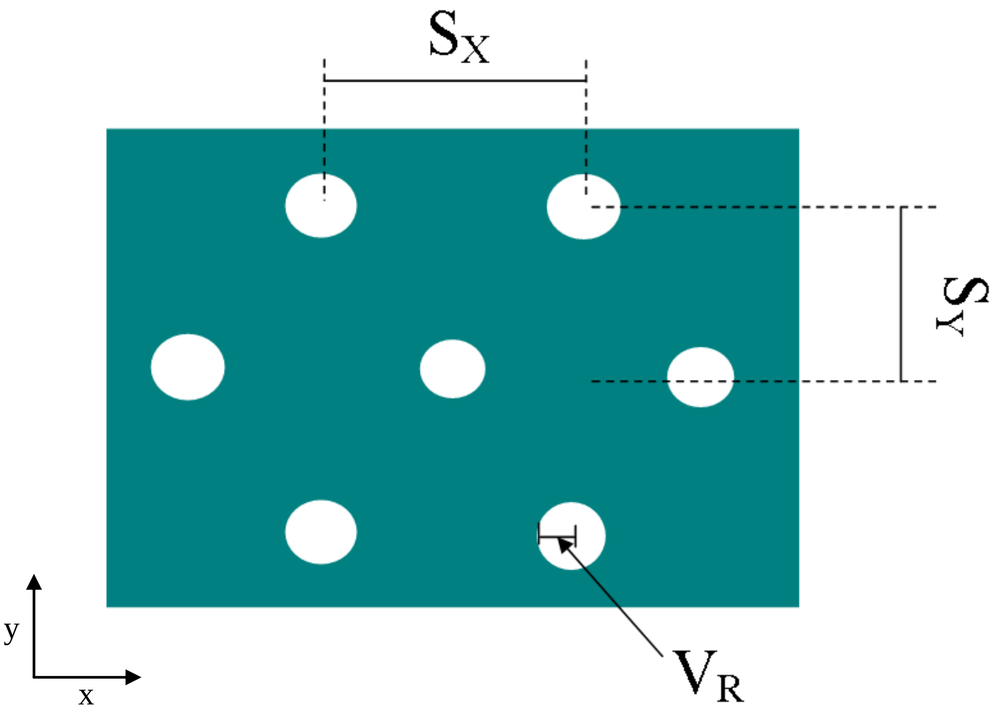

Figure 4 - Idealised planar heterogeneous material

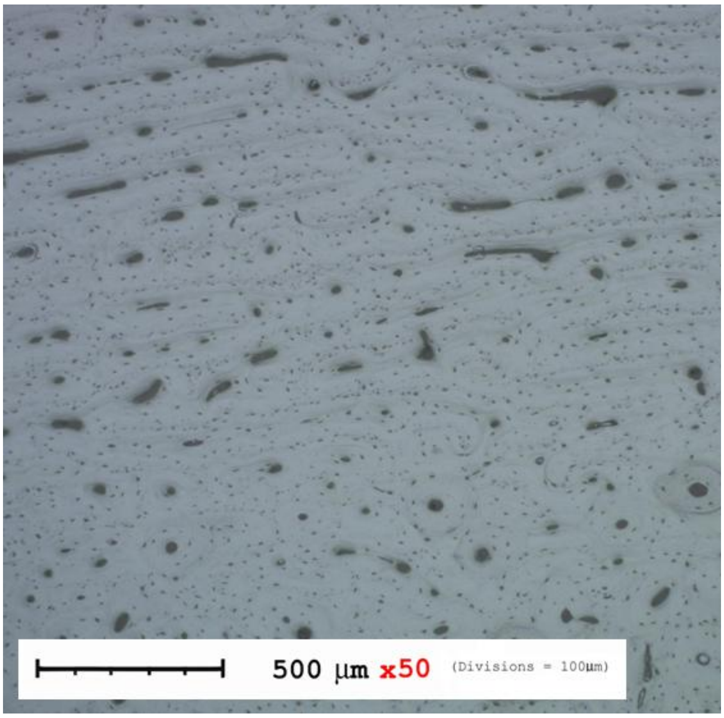

Figure 5 – A cross section of bovine cortical bone showing the detail of the Haversian canal system (bottom) and primary osteons (top).

Cortical bone shows various levels of hierarchical microstructural detail. At the scale of the vascular system in cortical bone there is a direct comparison that may be drawn between the idealised heterogeneous material in Figure 4 and the imaged cross section shown in Figure 5. It can be seen that cortical bone has a comparable array of voids through the material and, although they are randomly dispersed, the voids may be represented by an idealised version of the material where the voids are arranged in a hexagonal array. In turn this idealisation may be used to understand the underlying material properties attributable to the microstructure (Hogan 1992; Braidotti et al. 1995). It is important to note that cortical bone displays numerous levels of microstructural detail and by reducing the length scale the most significant microstructural feature will change. At the macroscopic scale primary and secondary osteons are the most significant porous microstructural feature and although plexiform bone has a higher degree of orthotropy associated with voids running transversely, the longitudinal modulus is significantly higher than the radial and circumferential moduli (Yamato et al. 2006; Macione et al. 2010) suggesting that the majority of vascular channels run longitudinally along the long axis in plexiform bone at the mid-diaphysis region of a long bone. Therefore it may be assumed that the void arrangement in the idealised heterogeneous material shown in Figure 4 is a general representation of the anisotropy created by osteons in cortical bone.

3.2 Axial loading of the idealised planar heterogeneous material

In order to determine the degree of anisotropy in the idealised planar heterogeneous material in Figure 4 a series of Finite Element (FE) simulations were undertaken loading the material axially in both the x and y directions. This was done over a range of void arrangements to analyse the relationship between the void arrangement and the degree of anisotropy evident.

3.2.1 **Method**

The finite element program ANSYS 12.1 was used to analyse the material in Figure 4. The mesh as shown in Figure 6 was created using the linear-elastic 8-noded element 183 with the material properties of 20GPa for Young’s modulus and 0.3 for Poisson’s ratio for the matrix material – commonly quoted material properties of cortical bone (Jae Young Rho et al. 1993; Evans et al. 1990; J Y Rho et al. 1997a). A refine function was added to the mesh generation to enable versatile mesh convergence analysis. A mesh convergence study was done for each void arrangement and void radius. This basic unit cell as shown in Figure 6 was then layered vertically and horizontally to create a global heterogeneous material (Figure 7)(X. Wang & Ni 2003).

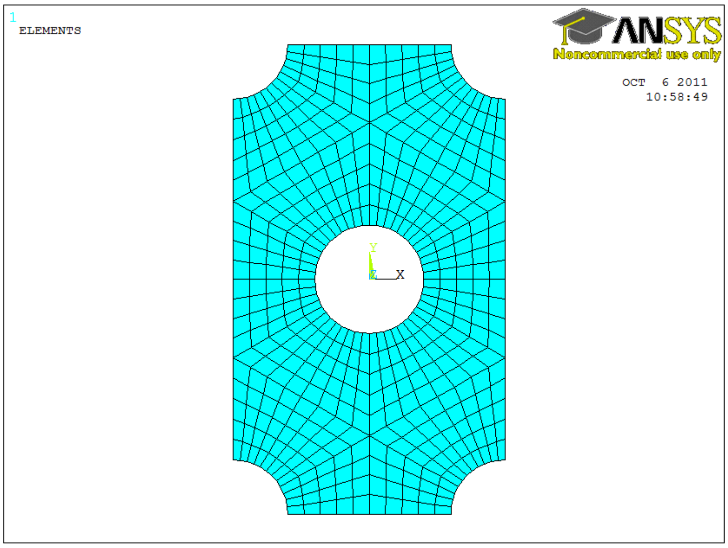

Figure 6 - Mesh used for generating heterogeneous material for axial analyses and corrugated surface beam bending analyses

The material was loaded in both the x and y directions respectively in two separate analyses. The beam was fixed horizontally at one end, with a single node constrained vertically in the centre of the fixed end to provide a y constraint and at the free end a unit pressure was applied on the surface as shown in Figure 7. The effective pressure applied to the beam could then be calculated by determining the surface area over which the applied pressure was distributed. This was scaled to the entire cross sectional area of the beam. In axial loading this is equivalent to the stress through the cross section of the beam along the length. The FE strain results were then used to calculate the Young's Modulus of the global material from the uniaxial relationship $E = \frac{\sigma}{\varepsilon}$ using the effective pressure as the stress through the material cross section.

Figure 7 - Axial loading in the x-direction: horizontally fixed at the left end with the central node pinned in the y-direction on the left end and a uniform pressure applied at the free end.

The variables S_X, S_Y and V_R were altered to determine the influence of each on the overall anisotropy of the material. The variable S_X was maintained at unity through the analyses, and the variable S_Y was altered between 1, 0.866 and 0.707, to create differing arrays of voids. At each geometrical arrangement the void radius was set at 0.1, 0.2 and 0.3, which can be translated into respective void fractions, V_F, of 0.036, 0.145 and 0.326 for $S_X = 1$ and $S_Y = 0.866$.

3.2.2 Results and discussion

The results in Table 1 show the axial Young's modulus decreases as the void fraction is increased. This is an expected result as the material density is significantly reduced with an increase in void radius. It is also apparent that the transverse anisotropy in Young's Modulus of this material is relatively low in the x-y plane for smaller void sizes and increases as the void radius is increased. For example a void fraction of 0.036 produced an axial Young's modulus of 18.22 GPa in the x direction, whereas when the void fraction was increased to 0.326 the Young's modulus decreased to 9.74 GPa in the x direction.

The void pattern was also shown to have an important influence on the axial anisotropy. Where the angle between voids is at 45° (S_X=1, S_Y=0.707) it is apparent that the material behaves in a manner congruent with plane isotropy. However, as this orientation is altered towards an equilateral 60° (S_X=1, S_Y=0.866) orientation between voids there is an increasing degree of plane anisotropy (Table 1).

This effect may be a result of the changing material distribution in the x and y dimensions respectively depending on the arrangement of the voids. At 45° there is an approximately equal distribution of mass along the x and y axes, however as the angle between voids is altered so too is the distribution of mass in either the x or y axes, therefore contributing proportionately to the observable stiffness in each axis, and the increase in anisotropy in the material.

Table 1 – Young's Modulus for varied void arrangements and void radii

		Void Fraction, V_F					
		0.036		0.145		0.326	
S_X (m)	S_Y (m)	E_X (GPa)	E_Y (GPa)	E_X (GPa)	E_Y (GPa)	E_X (GPa)	E_Y (GPa)
1	1	18.22	18.22	14.20	14.00	9.74	9.05
1	0.866	17.94	17.94	13.20	13.11	7.94	7.63
1	0.707	17.46	17.49	11.46	11.51	5.06	5.03

Interestingly for the matrix Young's modulus of 20GPa used in this study and a void fraction of approximately 0.25 the apparent Young's modulus of the material is similar to published values for the radial and circumferential directions in cortical bone (Pope 1974; Akiva et al. 1998; C H Turner et al. 1995). This may suggest that the void arrangement in cortical bone is important in producing the underlying anisotropy in observed material properties.

This study reveals the idealised planar heterogeneous material created in Figure 4 behaves as an approximately isotropic material in the x-y plane. It should be noted that the defining parameter of the Young's modulus of the matrix material is representative of an isotropic matrix material and may be scaled to better compare with a real material such as cortical bone. Cortical bone typically has a void fraction of between 0.1 and 0.15 (X. Wang & Ni 2003) indicating that the void fraction for the closest matching results, of approximately 0.25, is higher than of those observed naturally.

3.3 Three-point-bending of the idealised planar heterogeneous material

A size effect can be produced through three-point bending simulations of an idealised planar heterogeneous material (Waseem & Beveridge 2013; Beveridge 2011). These studies demonstrated how the micropolar material properties of Young's modulus and characteristic length can be determined from a size effect produced in an idealised heterogeneous material by applying Equation 10 to a plot of the bending stiffness against the reciprocal of depth squared. This assumes a slender beam and the same length to depth aspect ratio are maintained throughout all beam sample sizes.

Although the ability to determine micropolar properties from bending experiments has been established, a complete description of an idealised planar heterogeneous material and the understanding of how to experimentally describe the nuances of a real heterogeneous material have not thus far been assessed. In short, any similarity between the idealised material models and the real material behaviour has yet to be established. In particular the surface condition between theoretical idealised materials may differ significantly from that actually encountered in the preparation of a real material sample. Specifically, in the latter case the main question is: Is it likely to produce a perfectly smooth surface from a pseudo-random heterogeneous material? It can be identified that even in the idealised case there are extremes of surface condition that can exist. Two extremes may be considered: a perfectly smooth surface and; half a cell out of phase in the y-axis, a surface pitted by surface voids, where the internal microstructure intersects the surface creating a corrugated effect (Figure 8).

Understanding the difference between these two extremes of material behaviour may improve the evaluation of the validity of the three-point bending size effect technique in identifying micropolar material properties in real materials.

3.3.1 **Methodology**

To evaluate the heterogeneous material shown in Figure 4 in bending two separate cases were considered, that of a continuous smooth surface, not intersected by the internal microstructure, and that of a corrugated surface intersected by the internal microstructure. The two cases of continuous beams and corrugated beams represent the two extremes of geometrical preparation from the idealised planar heterogeneous material. This is demonstrated in Figure 8 where two sets of beams with and without surface perforations are shown. An equilateral array of voids was used for the bending analyses by defining S_X equal to unity and S_Y equal to 0.866, to maintain a 60 degree angle between voids. For each set of equivalent beams the void volume fraction or porosity was maintained constant so that the underlying material microstructure remained comparable between beams.

Figure 8 - Beams with and without surface perforations with constant length to depth aspect ratio and varying depths

The finite element program ANSYS 12.1 was used to create and analyse both sets of beams in 2-dimensional bending. Figure 6 and Figure 9 show the different meshes used around each void for beams with and without surface perforations respectively. The mesh used for the beams with a corrugated surface, Figure 6, is the same as that used for the axial loading analyses. It is of note that the mesh used to analyse the beam with the corrugated surface can produce a material where the void diameter is greater than the vertical separation between voids, whereas the mesh for the smooth surface cannot be created with voids of a greater diameter than the vertical separation. For this reason the axial loading analyses were more effectively analysed using the mesh in Figure 6 as a greater void fraction range could confidently be meshed.

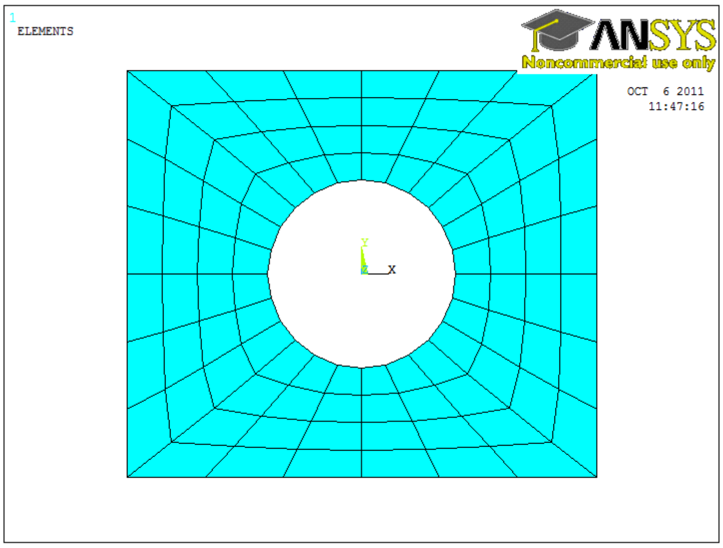

Figure 9 - Mesh used for smooth smooth 2-D beams in bending

For both meshes representative material properties of cortical bone (E = 20GPA, υ = 0.3) and the linear-elastic 8-noded element 183 were used. The breadth of the beam perpendicular to the meshed plane was set to unity and plane stress behaviour assumed. A refine function was added to the mesh generation to enable versatile mesh convergence analysis.

To model a size effect in 3-point bending, beam models were created by repeatedly generating the meshes in Figure 6 and Figure 9 as appropriate to produce an array of voids representing the beam geometry; four with a smooth surface and four with a corrugated surface in accordance with the geometries shown in Figure 8. This enabled the same material to be represented at varying length to depth aspect ratios for both cases with and without surface voids. Each beam was constrained with two single vertical constraints defining the length of the beam and a point load of 100N, constrained horizontally, applied in the centre of the upper surface of the beam. The boundary and loading conditions for the three-point bending simulations can be seen in Figure 10. Care was taken to ensure the point load was placed midway between adjacent voids and not directly over a single void.

In order to maintain the same aspect ratio between each discrete beam depth alternative boundary conditions were used in particular cases. Figure 11 shows the boundary conditions used for beams with an odd number of voids through the depth (1 or 3). For these cases using the boundary conditions shown in Figure 10 would result in the applied load or the supports being located next to a void rather than between adjacent voids producing inconsistent simulations across all four depths. For this reason the alternative boundary conditions incorporating symmetry were adopted for beams where a full model was not applicable. Symmetry was applied through the depth of the beam in the axial plane (Figure 11) and a point load was applied at the far end of the beam, equivalent to half a beam length away. A vertical constraint was added to the centre point along the symmetry plane.

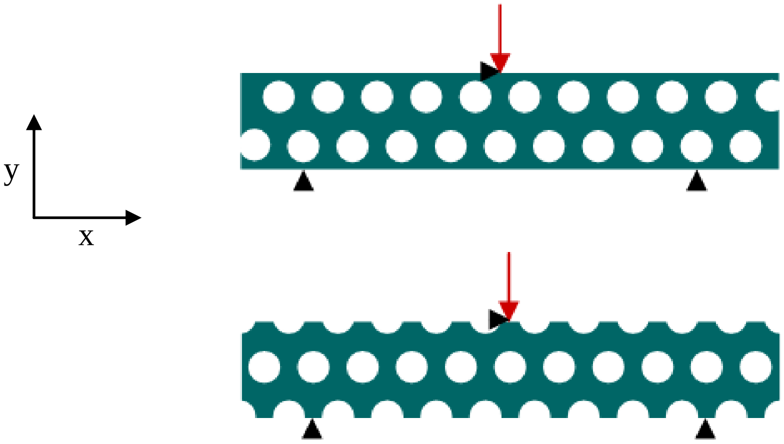

Figure 10 - Three-point-bending loading conditions for equivalent beams with and without surface perforations.

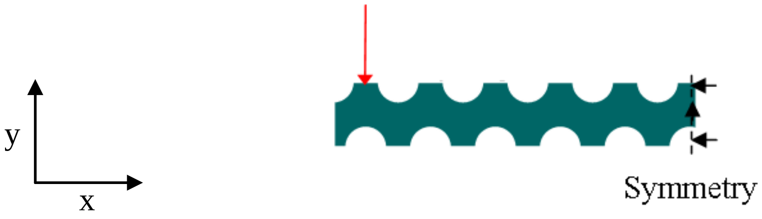

Figure 11 – Three-point bending loading conditions using symmetry to simplify the model.

Analyses were conducted over three different length to depth aspect ratios (5.8:1, 10.4:1 and 20.8:1) which were determined by the separation of the voids in the x and y axes. For example, where the depth was one void deep (0.866) then the length was set to be 9 voids long, therefore producing a 9:1 cell length to cell depth aspect ratio and a 10.4:1 absolute length to absolute depth aspect ratio. For each aspect ratio the void radius was varied in 0.05 intervals from 0.1 to 0.3. This enabled the influence of void size on the stiffness of the constitutive material in bending to be analysed. Void radius was normalised by dividing by the void separation in the y-axis, S_Y. The flexural stiffness was calculated by dividing the applied load by the calculated deflection on the lower surface of the beam below the centrally applied load. A size effect could then be determined for both the corrugated and smooth surface beams by plotting the flexural stiffness against the reciprocal of the depth squared in accordance with Equation 10. Where there is a linear relationship between the flexural stiffness and reciprocal of depth squared the y-intercept and gradient of the linear relationship can be used to determine the micropolar Young's modulus and micropolar characteristic length using Equation 12 and Equation 13 respectively.

Equation 12

$$y = 4E_m b\left(\frac{d^3}{l^3}\right)$$

Equation 13

$$gradient = \frac{4E_m bd^3}{l^3}\frac{l_c^2}{d^2}$$

3.3.2 **Results and discussion**

The computational analyses revealed that the idealised planar heterogeneous material behaves as a typical micropolar material for beams with smooth surfaces. Figure 12, Figure 13 and Figure 14 show the stiffness plotted against 1/depth^2 for varying void dimensions at 20.8:1, 10.4:1 and 5.8:1 aspect ratios respectively revealing the inherent size effects in the idealised 2-dimensional heterogeneous material. The nature of the size effect present is different between each aspect ratio. It can be seen that for the 20.8:1 aspect ratio (Figure 12) the size effect trend is in accordance with the closed form analytical solution (Equation 10) as the aspect ratio is reduced to 10.4:1 (Figure 13) the size effect remains almost linear. However, as the aspect ratio is reduced further to 5.8:1 (Figure 14) the size effect does not follow a true linear relationship between flexural stiffness and reciprocal of depth squared. This can be attributed to the shorter aspect ratio causing the beam to behave as a shear beam and therefore the analytical micropolar equation for a slender beam in three-point bending no longer holds. As the aspect ratio is increased above 10:1 the relationship between stiffness and reciprocal of depth squared tends to a linear relationship. This is because the beam now behaves as a slender beam in three-point bending and shear effects can be neglected. Classical elasticity does not predict a size effect with alterations in specimen size for homogeneous materials. Therefore, the existence of a size effect in slender beams of the same material of different size in three-point bending suggests that classical elasticity is an inappropriate continuum model for describing that material in the absence of microstructural detail. However, micropolar elasticity is able to describe a linear relationship between the beam stiffness and size for three-point bending of slender beams. Consequently micropolar elasticity may be a more appropriate continuum model for describing a material which displays size effects in three-point bending.

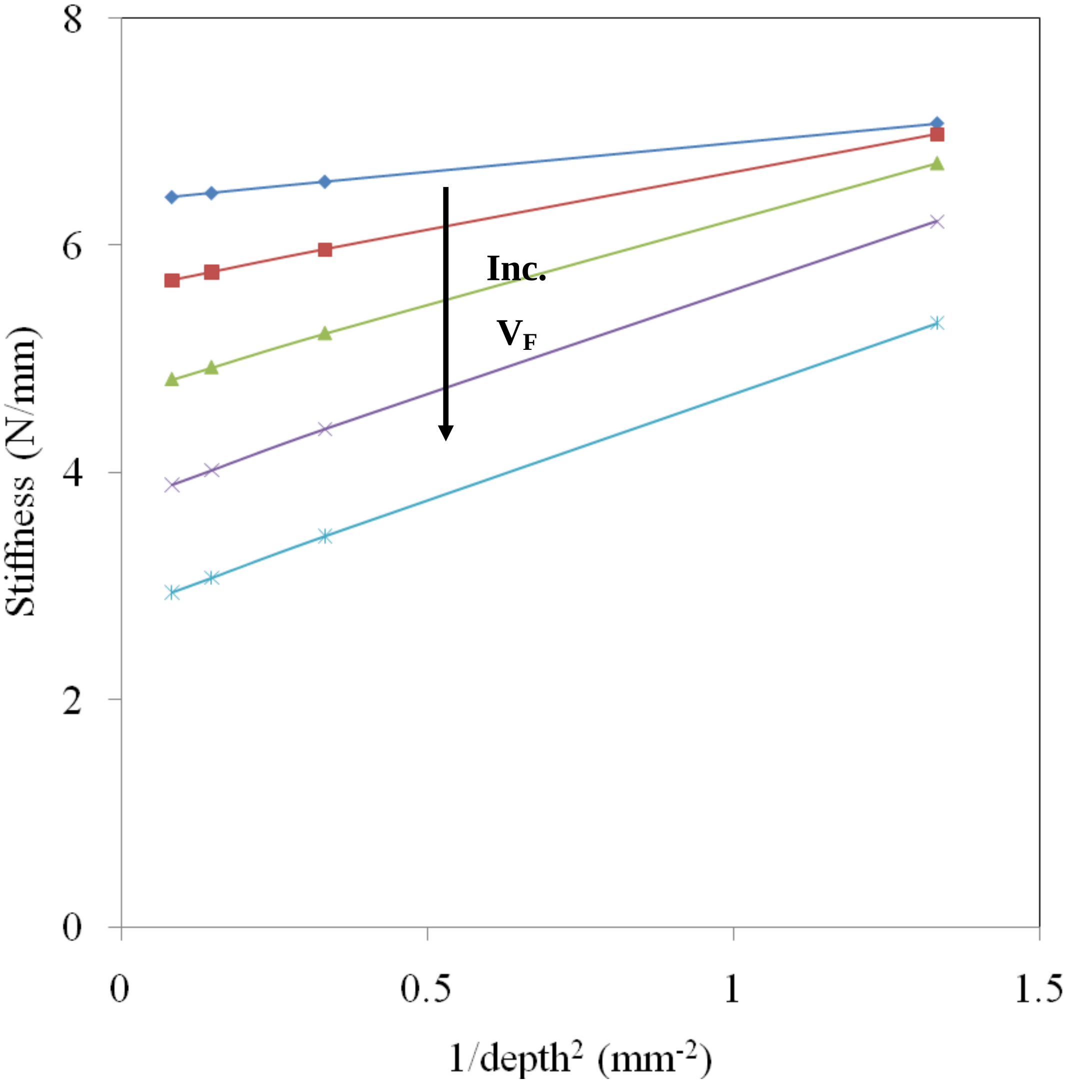

Figure 12 - Stiffness against the reciprocal of depth squared for smooth beams at a 20.8:1 length to depth aspect ratio for varying normalised void radii, V_R/S_Y. Each line represents a different void radius: blue

diamonds, V_R/S_Y=0.12; red squares, V_R/S_Y=0.17; green triangles, V_R/S_Y=0.23; purple circles, V_R/S_Y=0.29; blue stars, V_R/S_Y=0.35.

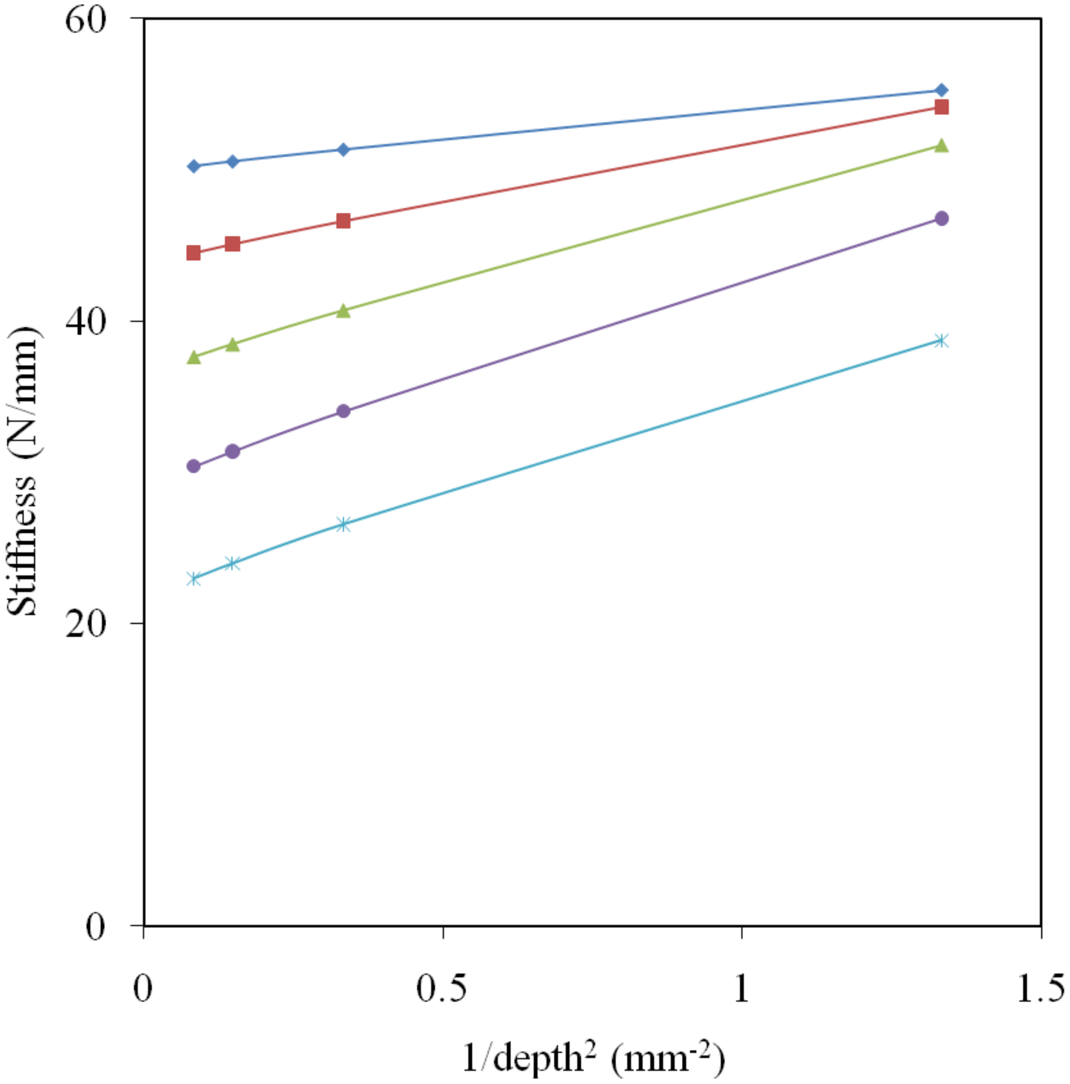

Figure 13 - Stiffness against the reciprocal of depth squared for smooth beams at a 10.4:1 length to depth aspect ratio for varying normalised void radii, V_R/S_Y. Each line represents a different void radius: blue diamonds, V_R/S_Y=0.12; red squares, V_R/S_Y=0.17; green triangles, V_R/S_Y=0.23; purple circles, V_R/S_Y=0.29; blue stars, V_R/S_Y=0.35.

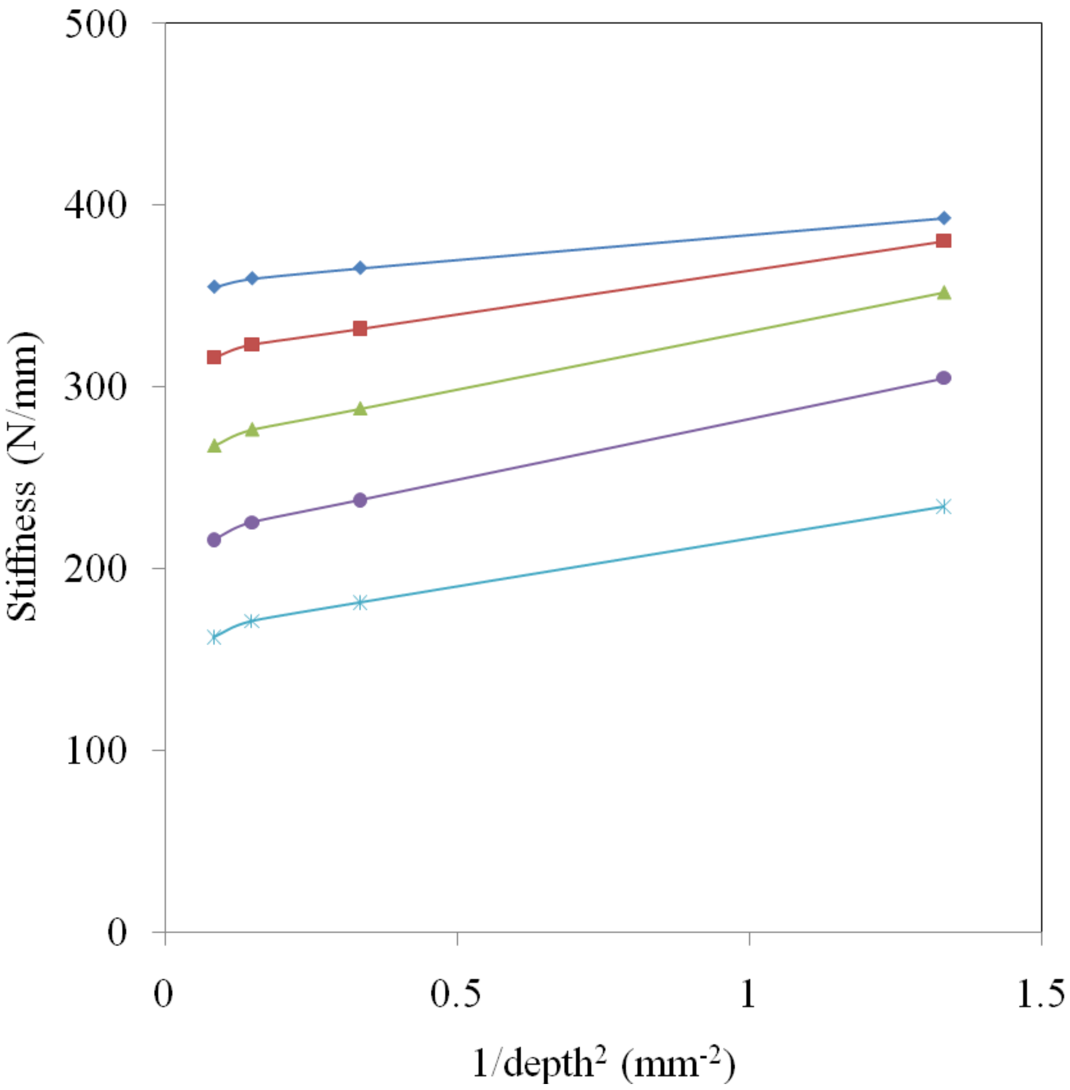

Figure 14 - Stiffness against the reciprocal of depth squared for smooth beams at a 5.8:1 length to depth aspect ratio for varying normalised void radii, V_R/S_Y. Each line represents a different void radius: blue diamonds, V_R/S_Y=0.12; red squares, V_R/S_Y=0.17; green triangles, V_R/S_Y=0.23; purple circles, V_R/S_Y=0.29; blue stars, V_R/S_Y=0.35.

From the plot of the trend lines the characteristic length and micropolar Young's modulus were determined from the gradient and intercept in Figure 12 and Figure 13 for the 20.8:1 and 10.4:1 aspect ratios (Equation 10) (Beveridge 2011). The characteristic length was found to be slightly greater than the diameter of the internal voids and is thought to represent the microstructure of the heterogeneous material by describing the void dimensions or the distance between fibres (Tekoglu & P Onck 2008; R. Lakes 1995; R. Lakes 1985). Additionally, there is a suggestion of a relationship between the geometrical organisation of voids and their distribution through the material in defining the characteristic length (Tekoglu & P Onck 2008; R. Lakes 1995).

Beams with surface microstructure display the opposite size effect. A noticeable size softening was observed: a size softening “anti-micropolar” effect. Figure 15, Figure 16 and Figure 17 display the results for the varying void dimension for 20.8:1, 10.4:1 and 5.8:1 aspect ratios respectively for such beams plotting the stiffness against 1/depth^2.

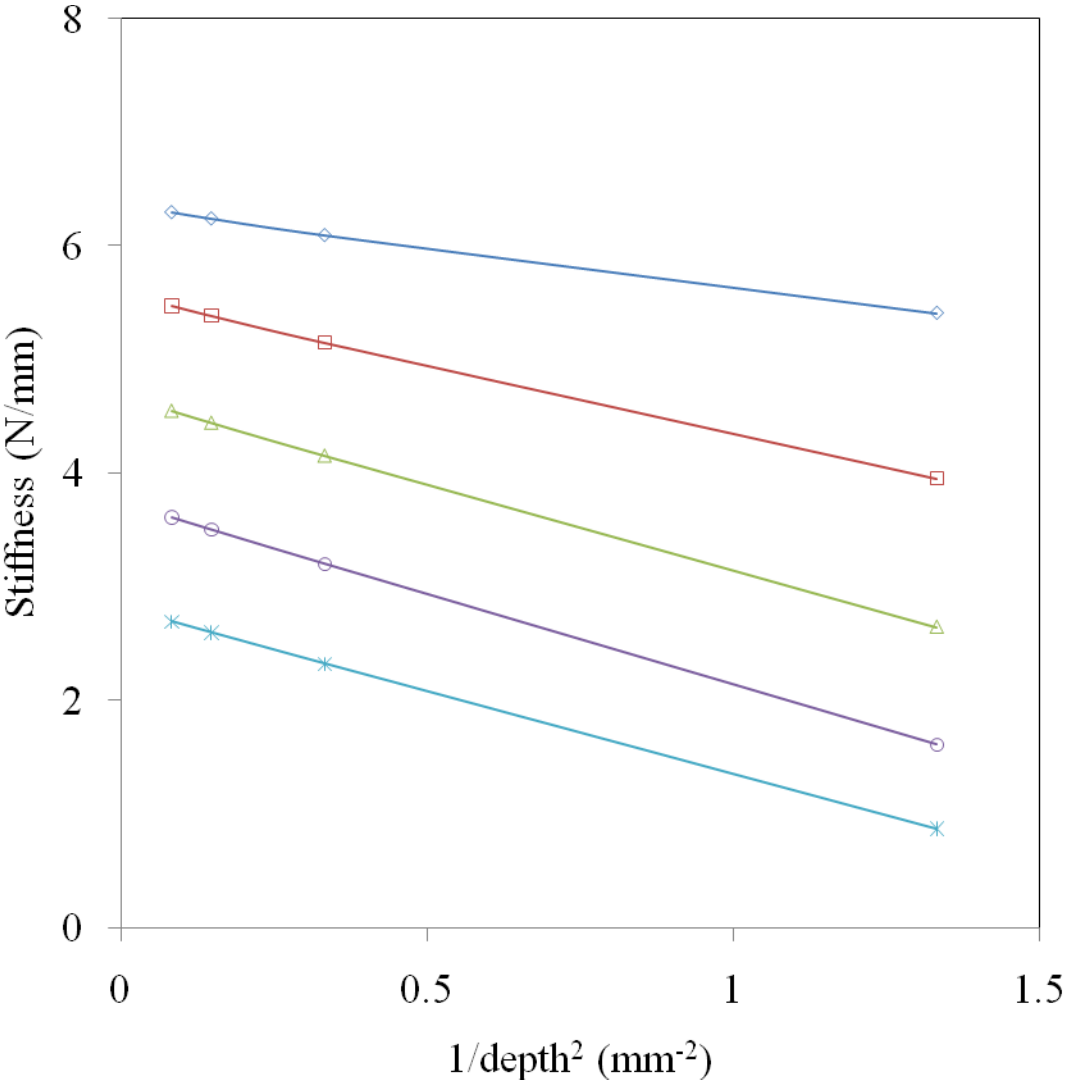

Figure 15 - Stiffness against the reciprocal of depth squared for corrugated beams at a 20.8:1 length to depth aspect ratio for varying normalised void radii, V_R/S_Y. Each line represents a different void radius: blue diamonds, $V_R/S_Y=0.12$; red squares, $V_R/S_Y=0.17$; green triangles, $V_R/S_Y=0.23$; purple crosses, $V_R/S_Y=0.29$; blue stars, $V_R/S_Y=0.35$.

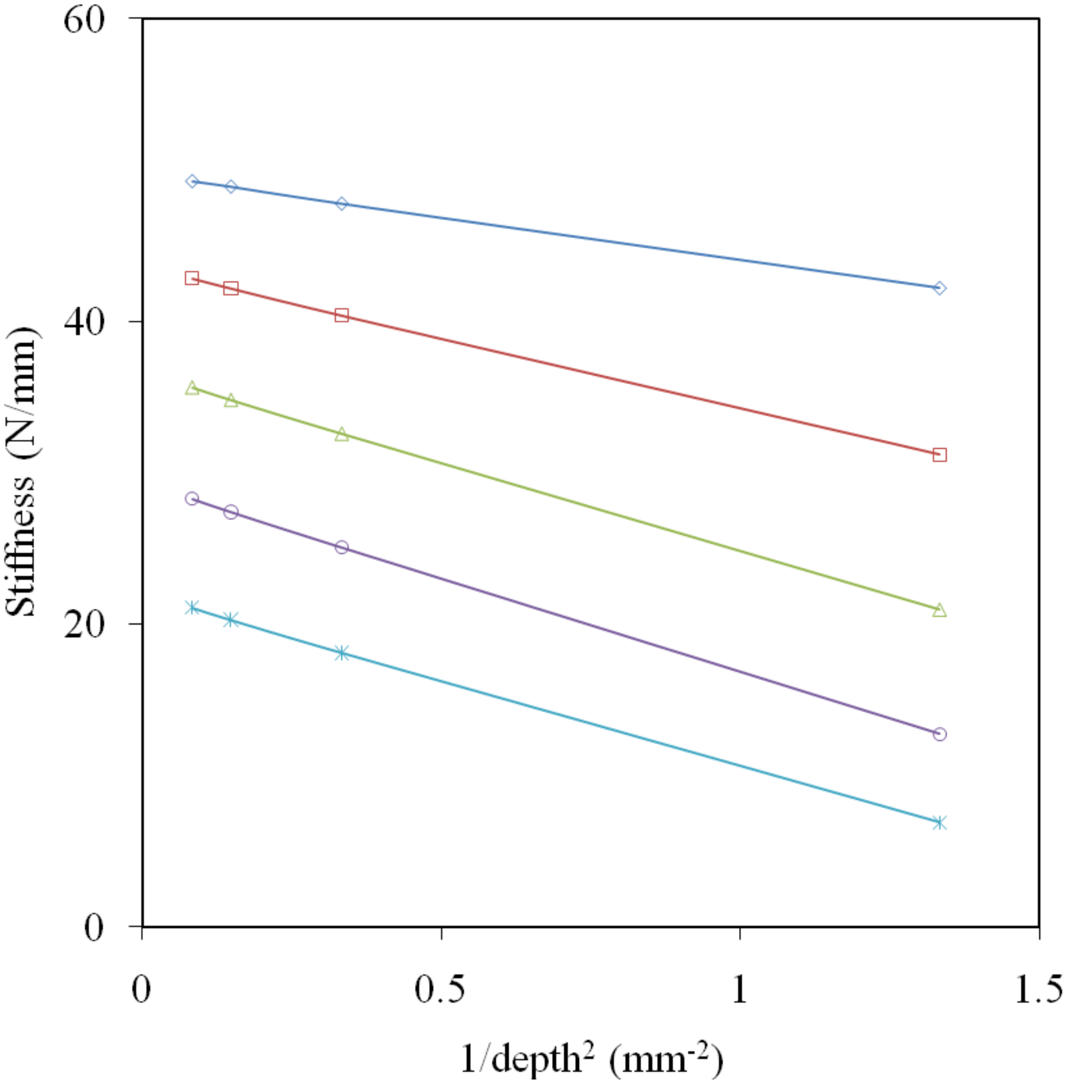

Figure 16 - Stiffness against the reciprocal of depth squared for corrugated beams at a 10.4:1 length to depth aspect ratio for varying normalised void radii, V_R/S_Y. Each line represents a different void radius: blue diamonds, $V_R/S_Y=0.12$; red squares, $V_R/S_Y=0.17$; green triangles, $V_R/S_Y=0.23$; purple crosses, $V_R/S_Y=0.29$; blue stars, $V_R/S_Y=0.35$.

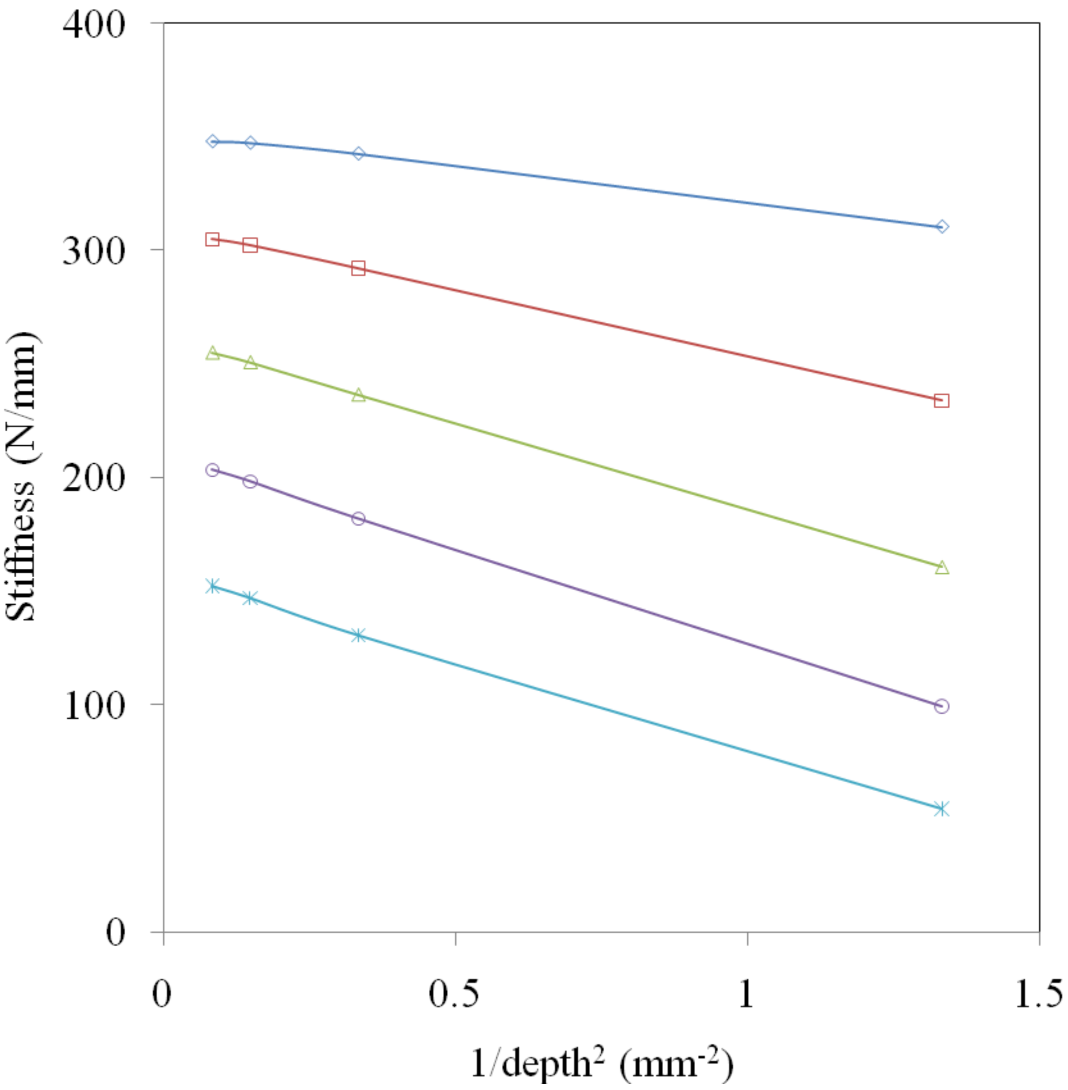

Figure 17 - Stiffness against the reciprocal of depth squared for corrugated beams at a 5.8:1 length to depth aspect ratio for varying normalised void radii, V_R/S_Y. Each line represents a different void radius: blue diamonds, $V_R/S_Y = 0.12$; red squares, $V_R/S_Y = 0.17$; green triangles, $V_R/S_Y = 0.23$; purple crosses, $V_R/S_Y = 0.29$; blue stars, $V_R/S_Y = 0.35$.

It is notable that the y-intercept for both continuous and corrugated beams (the y-intercept describes the stiffness of an infinitely deep beam) occur at the same point when comparing continuous and corrugated beams of the same void fraction and aspect ratio. Moreover, both continuous and corrugated beams produce a micropolar Young's modulus (calculated from the y-intercept) equivalent to the Young's Modulus determined through axial loading of the equivalent arrangement of voids. This suggests confidence and continuity in the results and that the micropolar

Young’s modulus can be successfully calculated through both bending and axial loading analyses.

It is not possible to calculate a real characteristic length from the negative gradient by applying Equation 10 however it is possible to compare the magnitude of the gradient between micropolar and “anti-micropolar” size effects. Figure 18 shows a plot of the magnitude of the size effect against void size, for both the corrugated and smooth beams at a 20.8:1 aspect ratio. The gradient produced by the corrugated beams follow a similar trend to that of the continuous beams but is of an opposite value. The results show that there is not an exact correlation between the gradient of smooth and corrugated beams, this is demonstrated in Figure 19 which shows the percentage difference between the smooth and corrugated size effects at each void radius. It is apparent that as the void radius is altered the relationship between the opposing size effects from each model changes. A normalised void radius of 0.23 shows the optimum correlation between continuous and corrugated beams. The magnitudes of the size effects showing near perfect agreement at this void size. The largest differences between positive and negative size effects occur where the normalised void radius is at the extremities of the void sizes tested. A contributing factor towards the inconsistencies between the positive and negative gradients may be attributable to the differences between the meshes used for each finite element model because the mesh used for the smooth surfaced beams was different to that used for the corrugated beams. However, this may also be a real effect and there may be a more fundamental reason for the difference in size effects between continuous and corrugated beams not being exactly equal in magnitude. What can be observed are the similar trends which indicate opposing material behaviours for beams with and without surface voids. The maximum percentage difference between complimentary size effects are approximately 30% and occur at the lowest and highest void fractions. These void fractions are significantly different than that of cortical bone. The closest agreement between positive and negative size effects occurs where the void fraction is approximately 0.23, this is a realistic void fraction for cortical bone and suggests that it may be possible to directly compare observed negative size effects in cortical bone with those of a the equivalent positive size effect in a micropolar material.

Considering the similarities between opposite size effects of continuous and corrugated beams it may be considered possible to describe the micropolar material behaviour of the beams with corrugated surfaces in terms of the smooth continuous beams. This would hold true if both cases were describing the extremes of the possible surface conditions in the idealised material: where a smooth beam has no voids intersecting the surface and a corrugated beam has the maximum void depth and distribution on the surface. However, it is important to remember that such a description is only an approximate observation of empirical evidence based on numerical experiments which suggests that beams with a smooth surface follow a micropolar trend and beams with surface voids follow a close to symmetrically opposite anti-micropolar trend. At present there is no theoretical basis to corroborate this observation. Nevertheless, in situations where a negative size effect is experimentally observed this chapter would provide strong numerical evidence that the micropolar material properties may still be calculated from the equivalent positive size effect which would occur in a continuous beam.

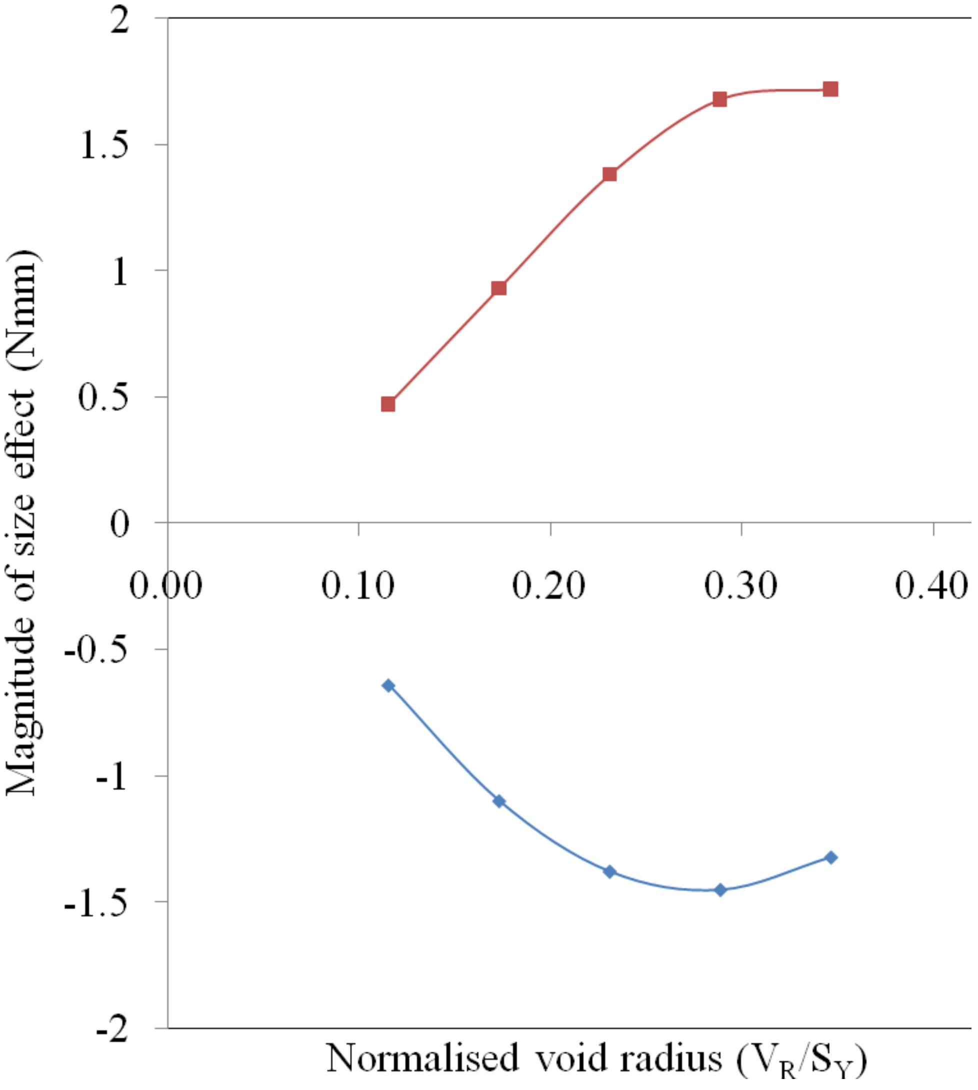

Figure 18 – The magnitude of the size effects plotted against normalised void radius, V_R/S_Y, for 20.8:1 length to depth aspect ratio. The smooth surfaced beams are shown by the red squares and the corrugated surfaced beams are shown by the blue diamonds.

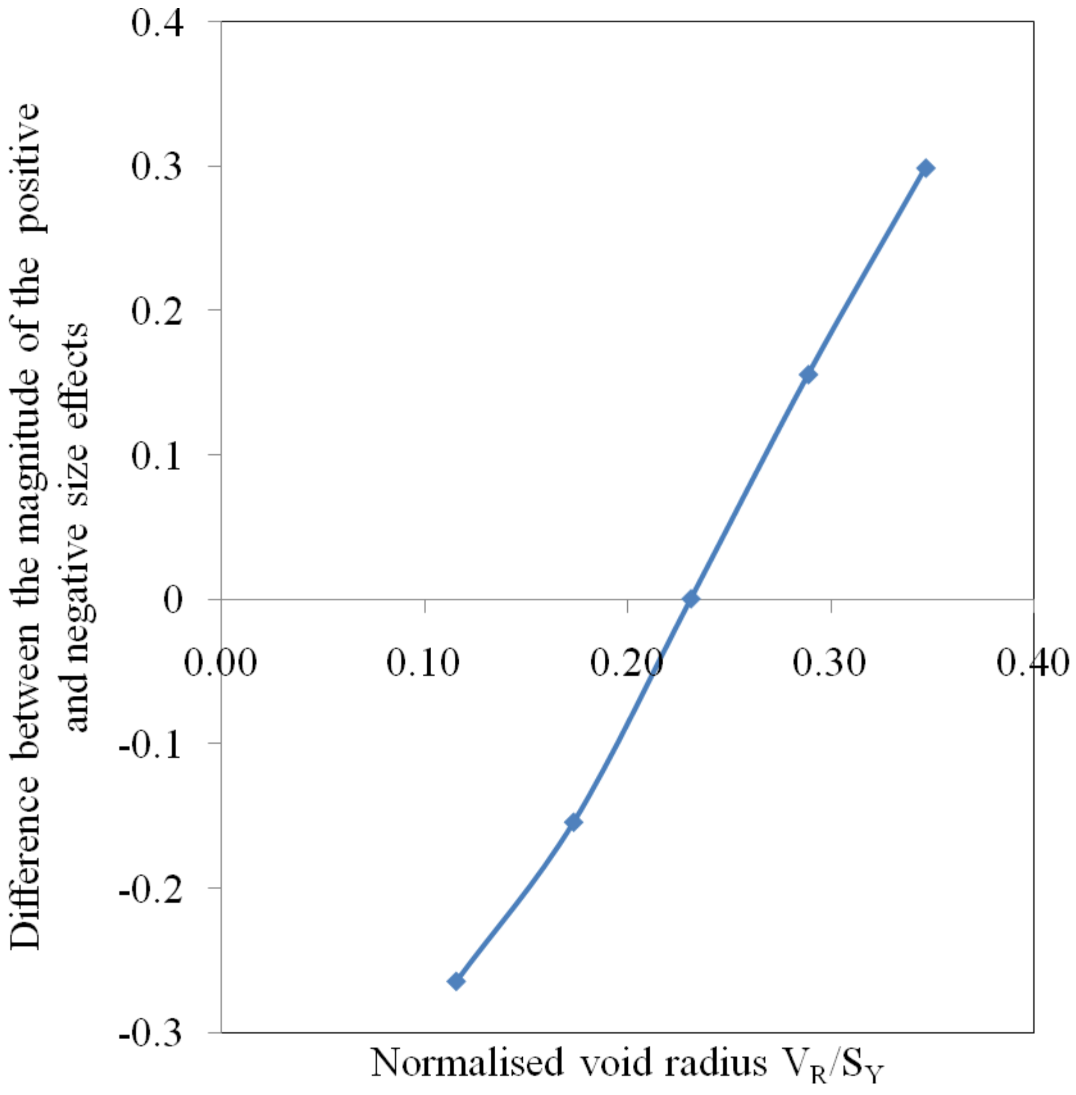

Figure 19 – The fractional difference in magnitude of negative and positive size effects for corrugated and smooth surfaced beams at 20.8:1 aspect ratio plotted against normalised void radius V_R/S_Y

The results revealed the characteristic length has a dependence on the length to depth aspect ratio. Table 2 shows a comparison of characteristic length against length to depth aspect ratio for each varying normalised void size (V_R/S_Y). This indicates that the difference between the 10.4:1 and 20.8:1 aspect ratios are relatively insignificant, but suggests that the 20.8:1 ratio will provide more accurate material properties. For the lower aspect ratio beams the assumptions taken in the formulation of the bending stiffness in Equation 10 are no longer valid. Therefore the 5.8:1 aspect ratio beams have been excluded from the results analysis. This is because the beam is not in idealised bending, there is a significant contribution of shear deformation in the beam (Beveridge, A., Wheel 2010; Beveridge 2011), unaccounted for in Equation 10. This is evidenced in Figure 14 where the size effect for lower 5.8:1 aspect ratio beams can be seen. There is a similar size effect in these beams, but it is not a true linear relationship between stiffness and reciprocal of depth squared. This effect is more pronounced in the beams with proportionately larger voids, and to determine the true characteristic length for such materials relies upon significantly larger aspect ratios in bending.

Table 2 – Comparison of the characteristic lengths for different void radii at 10.4:1 and 20.8:1 length to depth aspect ratios.

Void Diameter, V_d (mm)	**Void Fraction V_F**	**Normalised void radius V_R/S_Y**	**Characteristic length (mm)**	
			10.4:1 aspect ratio	**20.8:1 aspect ratio**
0.2	0.036	0.12	0.28	0.28
0.3	0.082	0.17	0.42	0.43
0.4	0.145	0.23	0.55	0.57
0.5	0.227	0.29	0.66	0.70
0.6	0.326	0.35	0.75	0.82

A significant finding may be noted in the relationship between the micropolar characteristic length calculated from the observed positive size effect and that of the void diameter (Figure 20). When the micropolar characteristic length is linearly regressed with void diameter it was found that $l_c = 1.39V_D$ with and R^2 of 0.99, this relationship may be observed in Table 2. This suggests that there is a strong association between the observed micropolar characteristic length and the physical size of the voids in the idealised heterogeneous material. Therefore this result suggests that it is possible to predict the micropolar material properties from the physical geometry of the microstructure.

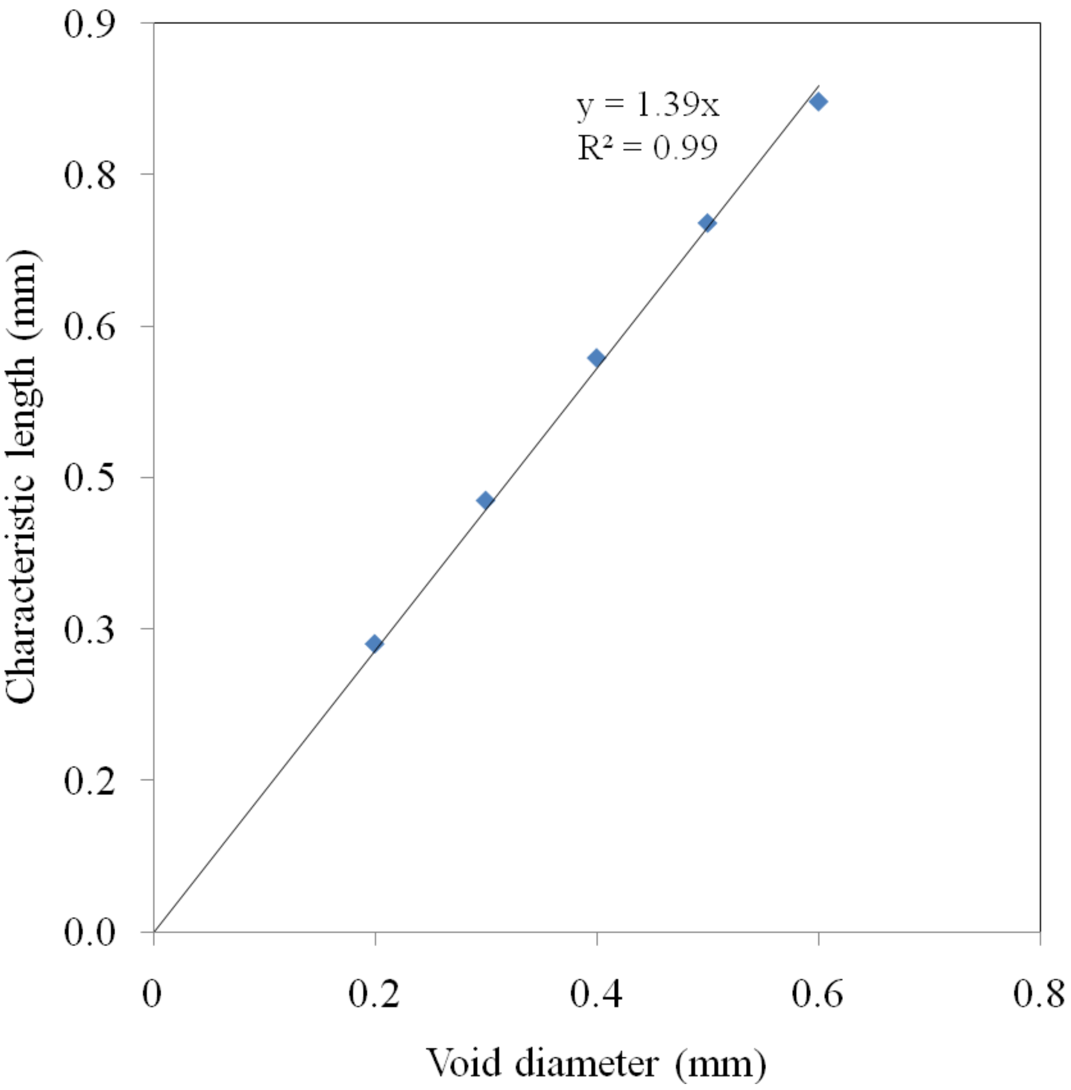

Figure 20 - Linear regression of the micropolar characteristic length against the void diameter for 2-D 20.8:1 aspect ratio beams

Brezny and Green (Brezny & Green 1990) described the influence of surface damage on materials in bending and proposed a composite model accounting for the surface layer. This was taken further by Anderson and Lakes (Anderson & R. Lakes 1994; R. Lakes 1995) who applied these considerations to micropolar elasticity. As the extremities of a beam in bending take the highest stresses it is intuitive to imagine the beams with surface perforations or surface damage having a reduced bending stiffness. Such a composite model of different phases of material at the surface and core in bending raises the question of whether micropolar size stiffening is attributable to the opposite effect: a relatively stiff surface layer with internal material damage. Furthermore, in both cases as the region close to the surface is proportionately greater in the smaller beams the influence of the surface layer will become more significant. Conversely larger beams will have a proportionally smaller surface region.

Therefore this modelling suggests the fundamental cause of micropolar behaviour observed in this idealised planar heterogeneous material may be attributed to a surface effect. As this leads to opposing observed size effects, for beams with and without surface voids, it may be appropriate to describe the two types of beams as extremes of a global material behaviour. This would imply that the negative size effect is not caused by surface damage but by the existence of surface microstructure. The surface microstructure in effect reduces the stiffness of the surface layer in beams with internal voids corrugating the surface layer and in continuous beams the surface region is maintained. Because bending stresses are not constant through a cross section, but rather larger at the surface this will lead to more significance on the surface regions. Moreover, smaller beams will show a greater dependence upon the nature of this surface region in terms of their overall observed material stiffness.

3.4 3D heterogeneous material

To extend the process of numerically evaluating the micropolar material properties of idealised heterogeneous materials a 3 dimensional computational analogue of the microstructure of cortical bone was created. This model was designed to mimic the character and geometric nature of primary and secondary osteons cortical bone orientated along the long axis of the mid-diaphysis region of a long bone. Extruding the idealised planar heterogeneous material discussed previously (Figure 4) in the z-axis it is possible to create a 3-dimensional material with cylindrical voids running along the length (Figure 21). This is similar to the microstructural nature of cortical bone in the mid-diaphysis region of long bones and although plexiform bone shows some transverse vascular channels, the majority are aligned longitudinally along the long axis. Figure 22 shows an image of a section taken from a long bone orientated with the vascular channels running diagonally along the image, in the direction of the arrow.

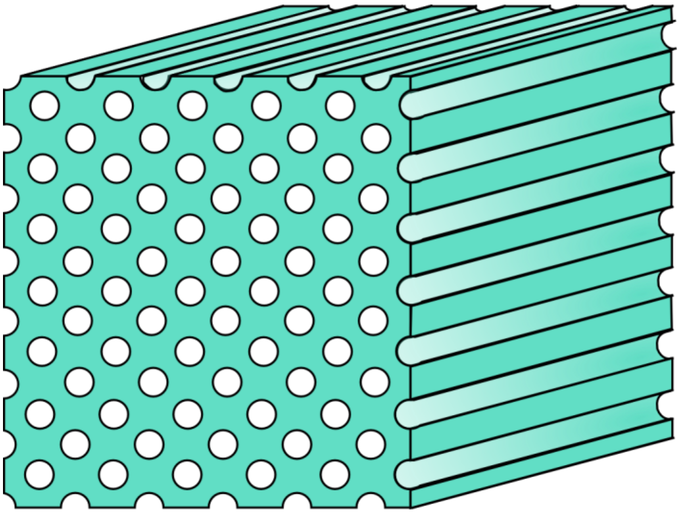

Figure 21 – Extrusion of the 2D idealised planar heterogeneous material into a 3D channel material mimicking the structure of primary and secondary osteons in cortical bone.

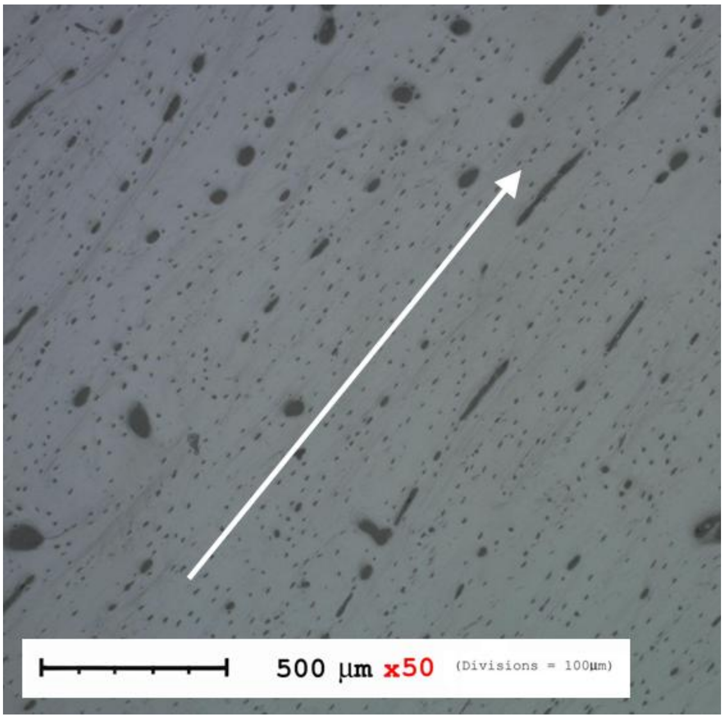

Figure 22 – Longitudinal view along the length of the long axis of bovine cortical bone. Haversian canals and vascular channels associated with primary and secondary osteons can be seen to be aligned along the long axis of the bone (white arrow).

3.5 Axial loading of a 3D heterogeneous material

The two dimensional planar heterogeneous material displayed limited anisotropy when loaded axially (along the x and y directions), however, as the void radius was increased the anisotropy increased. This indicated a degree of anisotropy in this material that is dependent on the void radius and void spacing; for a fixed void spacing the anisotropy increases as the void radius is increased. To further develop the understanding of the material behaviour of such an idealised heterogeneous material the longitudinal axial Young’s modulus, with the voids running along the length of the beam, was analysed. This allows an insight into the relationship between the material properties in the transverse plane and the longitudinal axis and may help in identifying the degree of transverse anisotropy in the idealised 3-dimensional material.

3.5.1 **Methodology**

To analyse the longitudinal elastic modulus a three dimensional finite element model was created using ANSYS 12.1. The two dimensional heterogeneous material in Figure 4 was extruded into the z-axis so as to maintain the underlying microstructural character of the original material.

The same fundamental mesh as those used for the two dimensional planar analyses shown in Figure 6 and Figure 9 were used. However, they were applied to a three dimensional model with the 20-noded three dimensional linear elastic element 186. The material properties of cortical bone were again used ($E = 20GPa$, $\upsilon = 0.3$), this enabled direct comparisons to be made with the two dimensional results.

Axial loading along the z axis was applied to the three dimensional material by fixing one end of the beam and applying a unit pressure to the free end (as in Figure 7 but with the pressure applied normal to the x-y plane, and displacements measured along the z-axis). The applied pressure was scaled to the beam cross sectional area by calculating the surface area over which the load was applied and adjusting for the entire cross sectional area. The displacements of the beam in axial loading were calculated and subsequently the stress and strain values were used to calculate the axial Young’s modulus.

3.5.2 **Results and discussion**

Longitudinal axial loading revealed the Young’s modulus varied depending on the void size in the material. This is an expected result as the density of material is reduced significantly with increasing void size. Table 3 displays the result obtained for the longitudinal axial Young’s modulus for the three dimensional FE model, where the void fraction has been varied. The table also includes the 2-dimensional results for a comparison between all three axes in the idealised material where $S_X = 1$ and $S_Y = 0.866$. This reveals that there is a degree of transverse isotropy in the material with a significantly stiffer longitudinal axis. This indicates that the idealised 3-dimensional heterogeneous material effectively replicates the transversely isotropic behaviour of cortical bone.

Table 3 - Longitudinal Young's modulus, E_Z, calculated using ANSYS 12.1 for axial loading on a 3D mesh. Results from the 2D analysis, E_X & E_Y are included for comparison.

	Void fraction, V_F		
	0.036	0.145	0.326
Longitudinal Young's Modulus, E_Z (GPa)	**19.3**	**17.1**	**13.5**
Transverse Young's Modulus, E_X (GPa)	17.94	13.20	7.94
Transverse Young's Modulus, E_Y (GPa)	17.94	13.11	7.63

3.6 Three point-bending of a 3D heterogeneous material

3.6.1 Methodology

Figure 23 – Examples of beam cross sections for beams with and without surface perforations for 3D simulations

Bending analyses were also carried out on the three dimensional material. This analysis was designed to identify if size effects were present when the voids run axially along the beam in bending. Figure 23 shows the cross sections both of the smooth surfaced and corrugated beams where the beam breadth is one unit cell, or the separation of voids in the x axis, S_X. Figure 24 shows how the modelling of these geometries could be reduced to a quarter the size by applying symmetry boundary conditions along the y-z and x-y planes. A line of nodes were pinned in the y-axis along the centre of the beam to give a vertical constraint to the model. Similarly a line load was applied along the edge of the beam in the x-axis. A load of 100N was distributed between the nodes along this line. Applying these boundary conditions allowed a cantilever model to represent a three-point bending model. The reduction in the size of the model greatly increased the speed of the computational process.

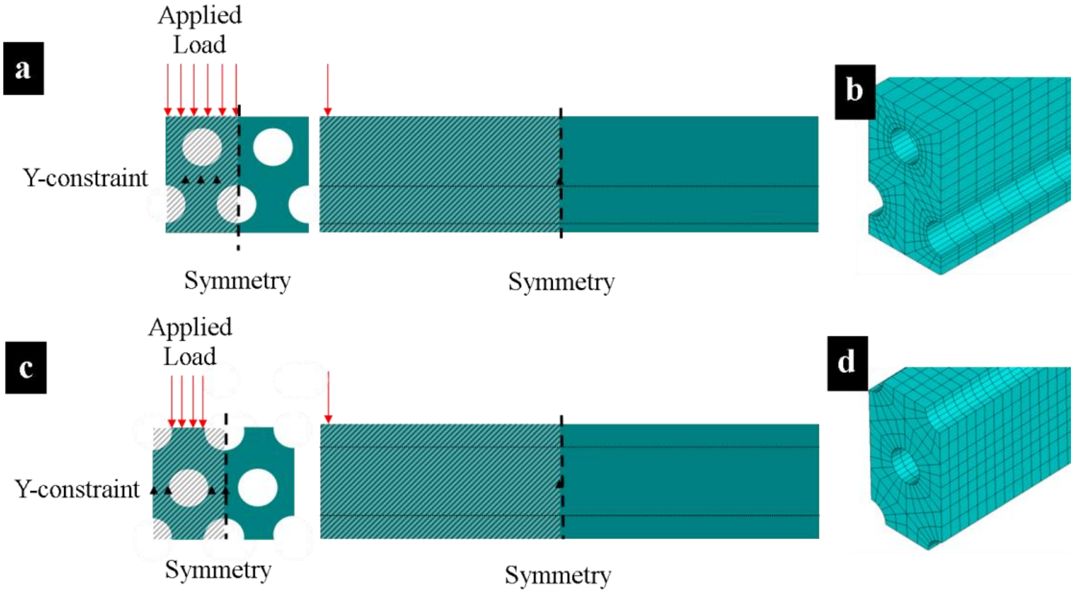

Figure 24 – The boundary conditions applied to the three-dimensional FEM model. Symmetry was used to reduce the model to a quarter the size and a line load was applied to the nodes to simulate three-point-bending as a cantilever beam. a. The boundary conditions for a continuous beam b. the mesh used to model the continuous beam in ANSYS c. The boundary conditions applied to the corrugated beams d. The mesh used to model the corrugated beam in ANSYS.

Beams at every depth were created with the same length to depth aspect ratio to observe the changes in stiffness with alterations in size (Equation 10). These aspect ratios were chosen to match as best as possible the aspect ratios used in the 2-dimensional analyses.

Similar to the two-dimensional models, beams were created with and without surface corrugations running along the length of the beam (Figure 24b and d), to determine if the same effects were observable as in the planar case. Two 3-dimensional mesh variants were created equivalent to the meshes used in the 2-dimensional simulations. These used the 20-noded 128 brick element; exemplar meshes are shown in Figure 24. Three length to depth aspect ratio were chosen (6:1, 10:1 and 20:1) with the same depth dimensions as those for the two dimensional model material ($S_X = 1$, $S_Y = 0.866$). Six void radius values were chosen to determine the influence of the void fraction on the material properties: these ranged from 0.05 to 0.3mm in increments of 0.05mm. The material properties of the matrix material were set to be the same as the previous studies and consistent with the material properties of cortical bone (E = 20GPa and ν = 0.3). The deflection of the beam was taken as the maximum displacement on the lower face of the beam below where the line load was applied. The micropolar Young's modulus and characteristic length were calculated using Equation 12 and Equation 13 $\left(y = 4E_m b\left(\frac{d^3}{l^3}\right), gradient = \frac{4E_m bd^3}{l^3}\frac{l_c^2}{d^2} \right)$ obtained from the size effect relationship in Equation 10.

3.6.2 **Results and discussion**

Table 4 - Characteristic length and micropolar Young's modulus for varying void radii calculated from 3-point-bending analyses on continuous beams with breadth equal to 1 at an 20:1 aspect ratio

Normalised void radius, V_R/S_Y	**Micropolar Characteristic Length, l_c, (mm)**	**Micropolar Young's Modulus, E_{mz}, (GPa)**	**Void diameter (mm)**	**Void fraction**
0.06	0.079	19.7	0.1	0.009
0.12	0.161	19.1	0.2	0.036
0.17	0.242	18.2	0.3	0.082
0.23	0.323	17.0	0.4	0.145
0.29	0.401	15.3	0.5	0.227
0.35	0.477	13.3	0.6	0.326

Three-point bending analyses revealed that for beams with smooth continuous surfaces the same effects were observed as seen in the two dimensional case: a size stiffening size effect trend. Figure 25, Figure 26 and Figure 27 show the plot of the stiffness against 1/depth^2 for varying normalised void radius (V_R/S_Y) in beams with a smooth continuous surface and breadth equal to one unit cell at a 20:1, 10:1 and 6:1 length to depth aspect ratios respectively. The micropolar material properties of micropolar Young's modulus and characteristic length were calculated using Equation 10. Although this equation assumes isotropy, and the idealised 3-dimensional heterogeneous material is anisotropic, Equation 10 is nevertheless a valid approximation because the deformation in the bending analyses is predominately flexural. This enables the axial properties to be reasonably accurately characterised despite the anisotropy in the material. The micropolar characteristic length, l_c, was found to be less than the void diameter (Table 4). A linear regression of the micropolar characteristic length with the void diameter revealed $l_c = 0.8V_D$ with $R^2 = 0.99$ (Figure 28). This suggests that the micropolar material property of characteristic length is predictable from the geometrical features of the microstructure as it scales almost linearly with the void diameter. This is a significant finding which indicates that micropolar material properties have a direct relationship with the microstructure. For an equivalent void fraction in the two dimensional material the characteristic length is noticeably larger, therefore demonstrating the dependence of the characteristic length on the orientation of the voids through the material in bending.

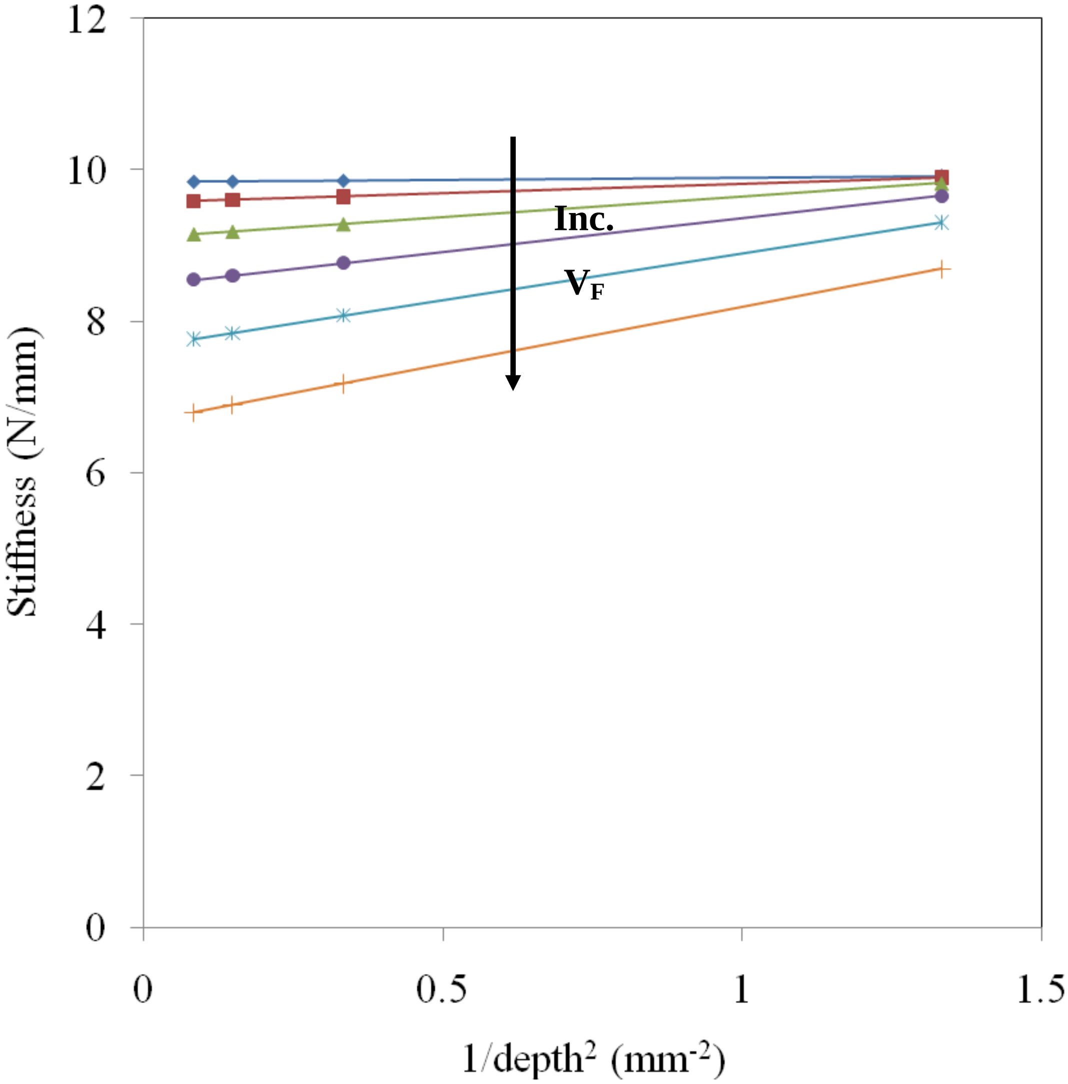

Figure 25 - Stiffness against the reciprocal of depth squared for smooth continuous beams at a 20:1 length to depth aspect ratio for varying normalised void radii, V_R/S_Y. Each line represents a different void radius: blue diamonds, V_R/S_Y=0.06; red squares, V_R/S_Y=0.12; green triangles, V_R/S_Y=0.27; purple circles, V_R/S_Y=0.23; blue stars, V_R/S_Y=0.29; orange crosses, V_R/S_Y=0.35.

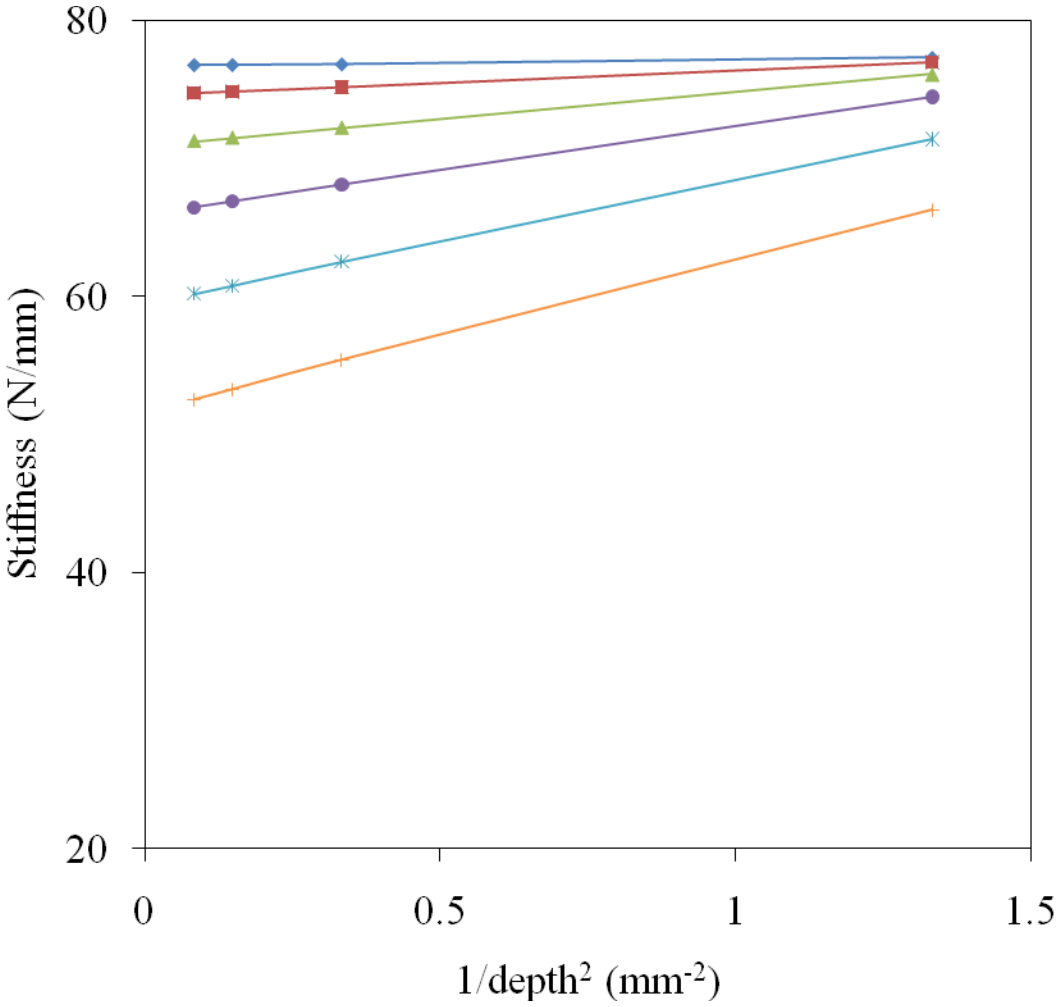

Figure 26 – Stiffness against the reciprocal of depth squared for smooth continuous beams at a 10:1 length to depth aspect ratio for varying normalised void radii, V_R/S_Y. Each line represents a different void radius: blue diamonds, $V_R/S_Y=0.06$; red squares, $V_R/S_Y=0.12$; green triangles, $V_R/S_Y=0.27$; purple circles, $V_R/S_Y=0.23$; blue stars, $V_R/S_Y=0.29$; orange crosses, $V_R/S_Y=0.35$.

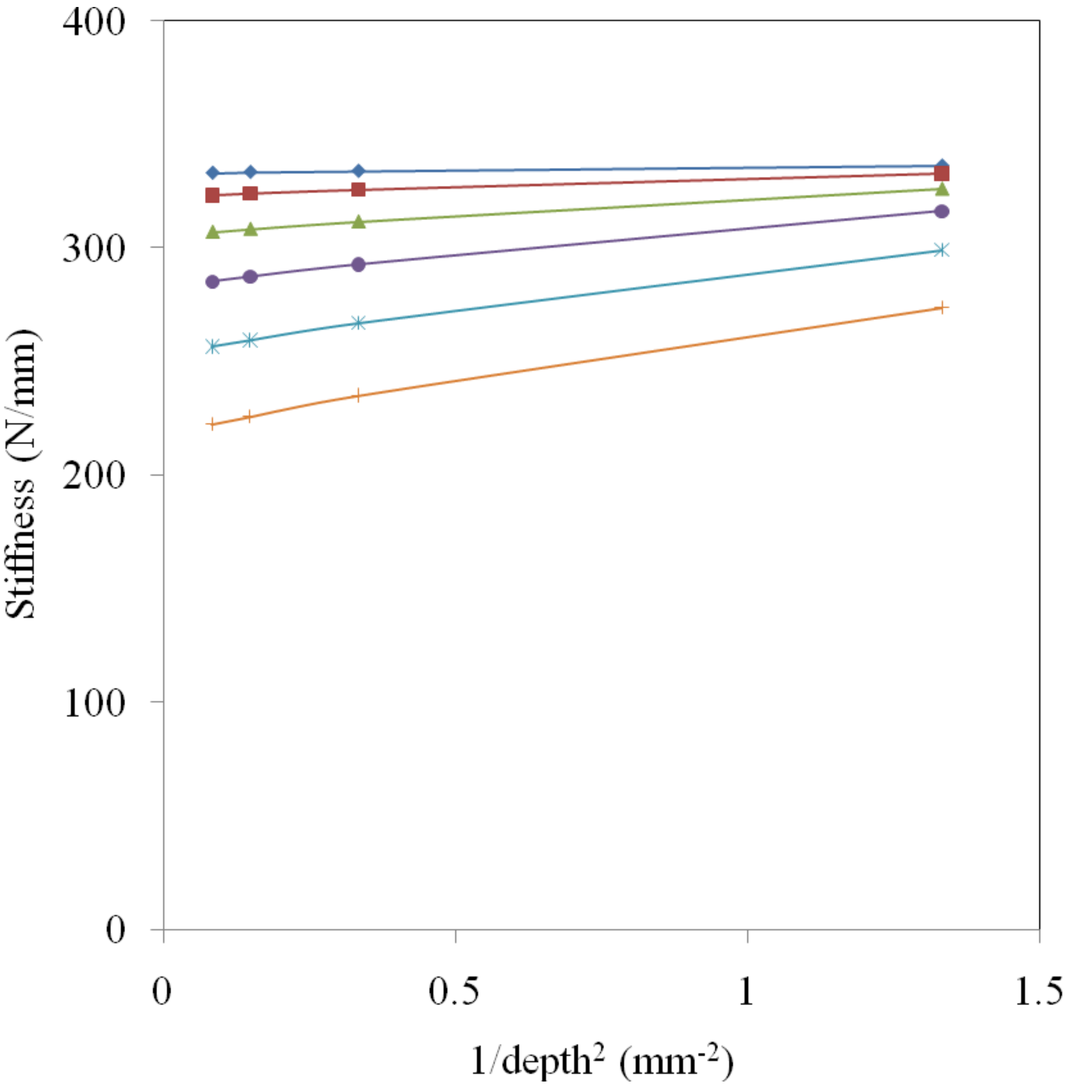

Figure 27 - Stiffness against the reciprocal of depth squared for smooth continuous beams at a 6:1 length to depth aspect ratio for varying normalised void radii, V_R/S_Y. Each line represents a different void radius: blue diamonds, $V_R/S_Y = 0.06$; red squares, $V_R/S_Y = 0.12$; green triangles, $V_R/S_Y = 0.27$; purple circles, $V_R/S_Y = 0.23$; blue stars, $V_R/S_Y = 0.29$; orange crosses, $V_R/S_Y = 0.35$.

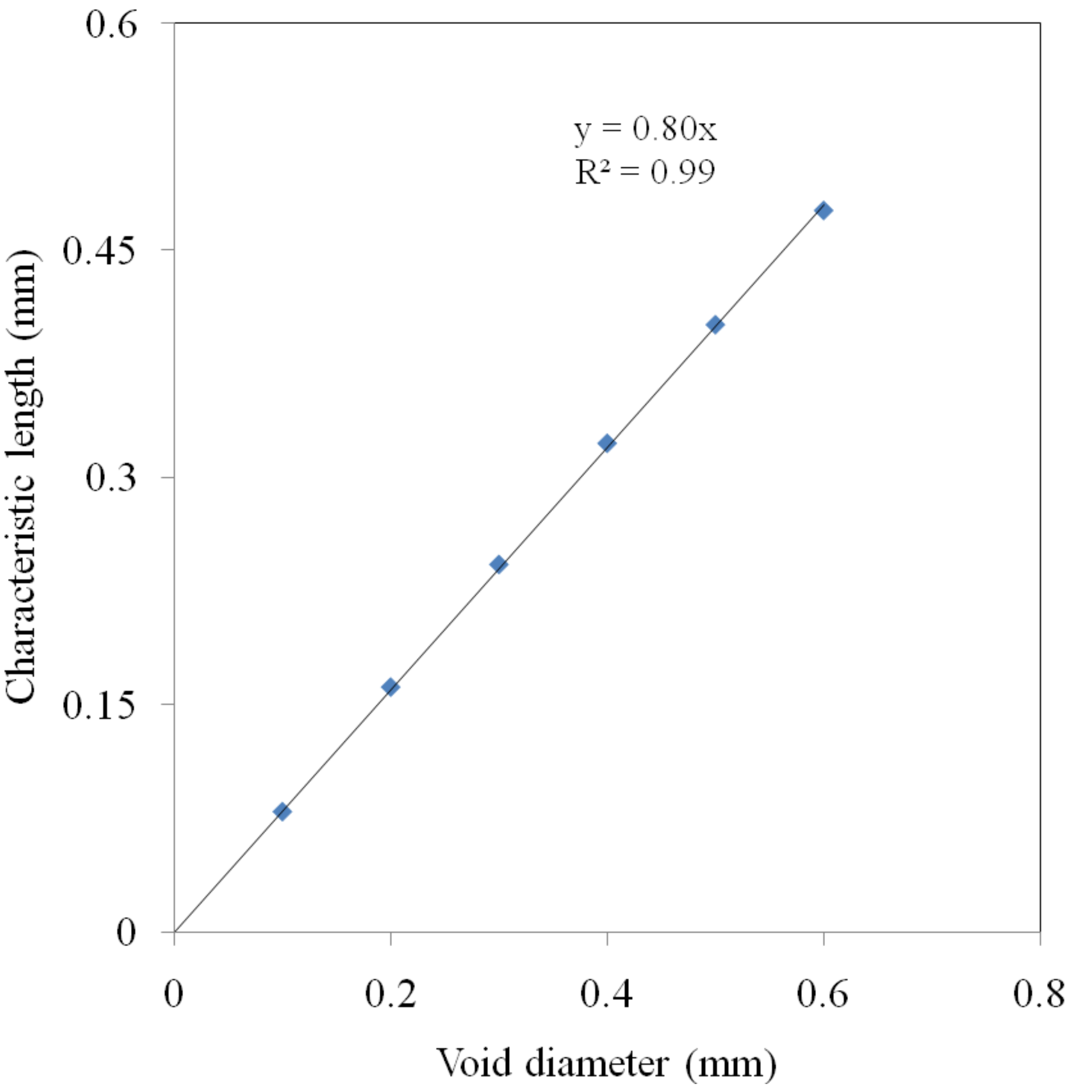

Figure 28 - Linear regression of the micropolar characteristic length against the void diameter for 3-D 20.8:1 aspect ratio beams

Figure 29, Figure 30 and Figure Figure 31 show the stiffness plotted against the reciprocal of depth squared for beams with surface perforations running longitudinally along the surface for length to depth aspect ratios of 20:1, 10:1 and 6:1 respectively. It can be seen that the same trends are present as in the two-dimensional scenarios: a size softening “anti-micropolar” effect. As before, a real characteristic length could not be calculated from the negative gradients, however the micropolar Young’s modulus was calculated from the y-intercept, and was revealed to be equivalent for both the smooth and corrugated beams. This again repeated the trend observed in the two dimensional planar case.

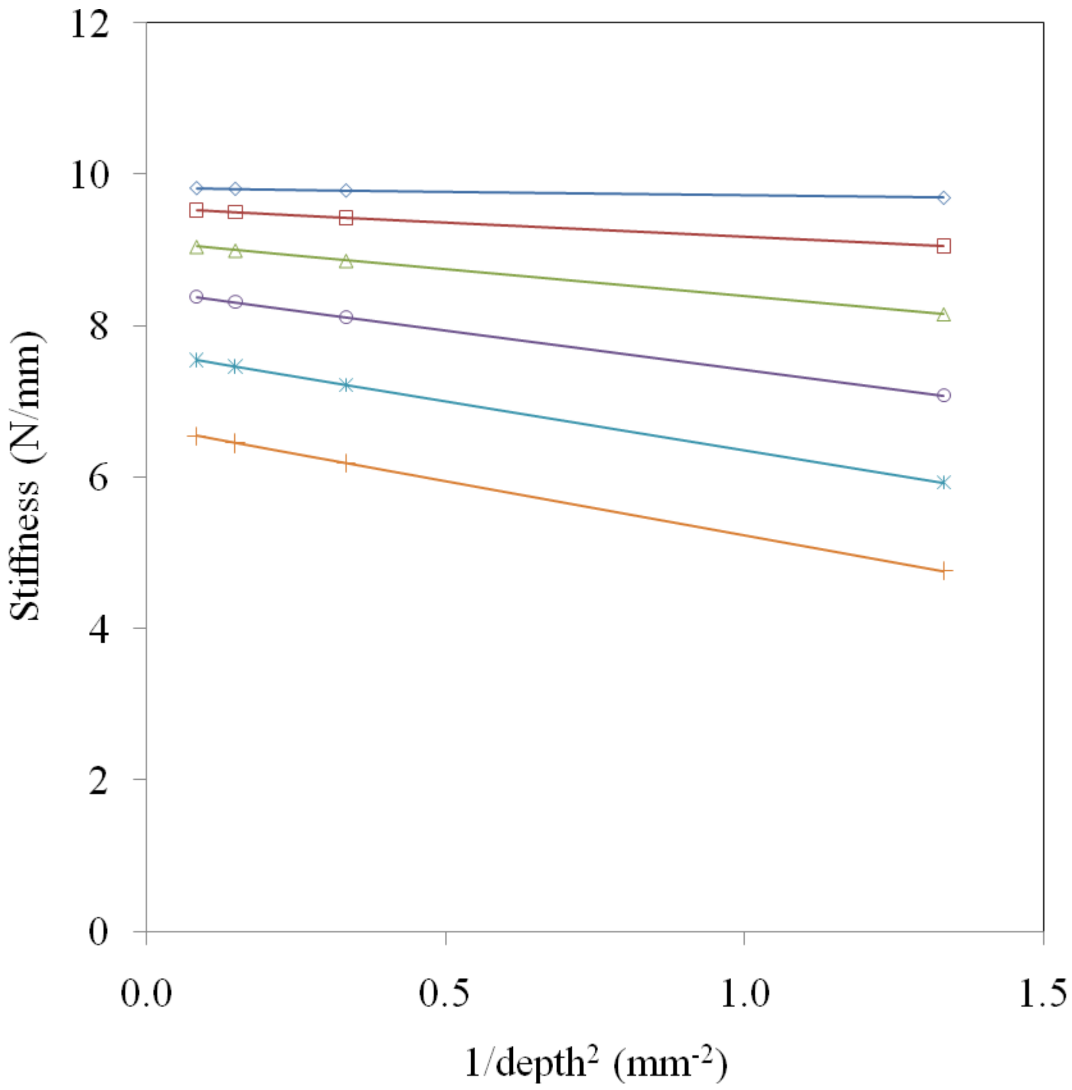

Figure 29 - Stiffness against the reciprocal of depth squared for corrugated at a 20:1 length to depth aspect ratio for varying normalised void radii, V_R/S_Y. Each line represents a different void radius: blue diamonds, V_R/S_Y=0.06; red squares, V_R/S_Y=0.12; green triangles, V_R/S_Y=0.27; purple circles, V_R/S_Y=0.23; blue stars, V_R/S_Y=0.29; orange crosses, V_R/S_Y=0.35.

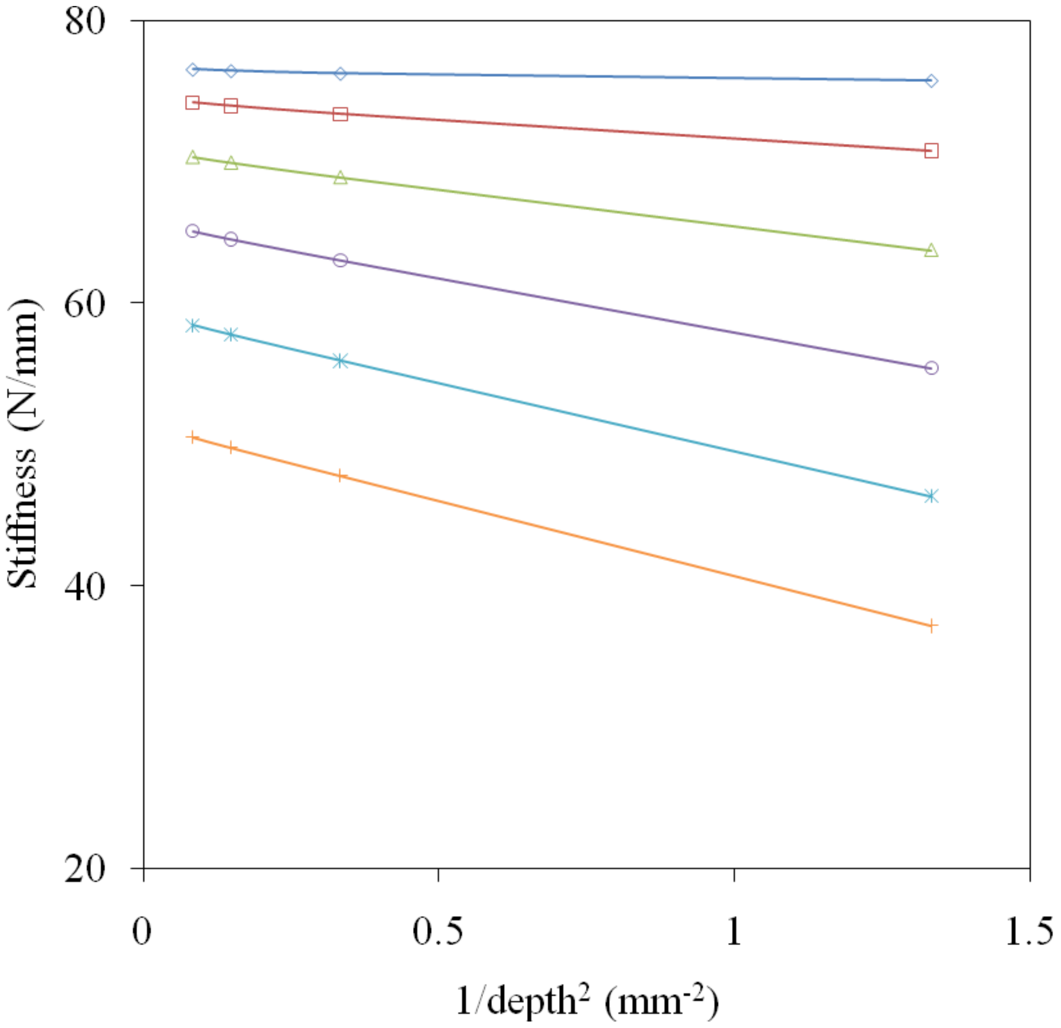

Figure 30 - Stiffness against the reciprocal of depth squared for corrugated at a 10:1 length to depth aspect ratio for varying normalised void radii, V_R/S_Y. Each line represents a different void radius: blue diamonds, V_R/S_Y=0.06; red squares, V_R/S_Y=0.12; green triangles, V_R/S_Y=0.27; purple circles, V_R/S_Y=0.23; blue stars, V_R/S_Y=0.29; orange crosses, V_R/S_Y=0.35.

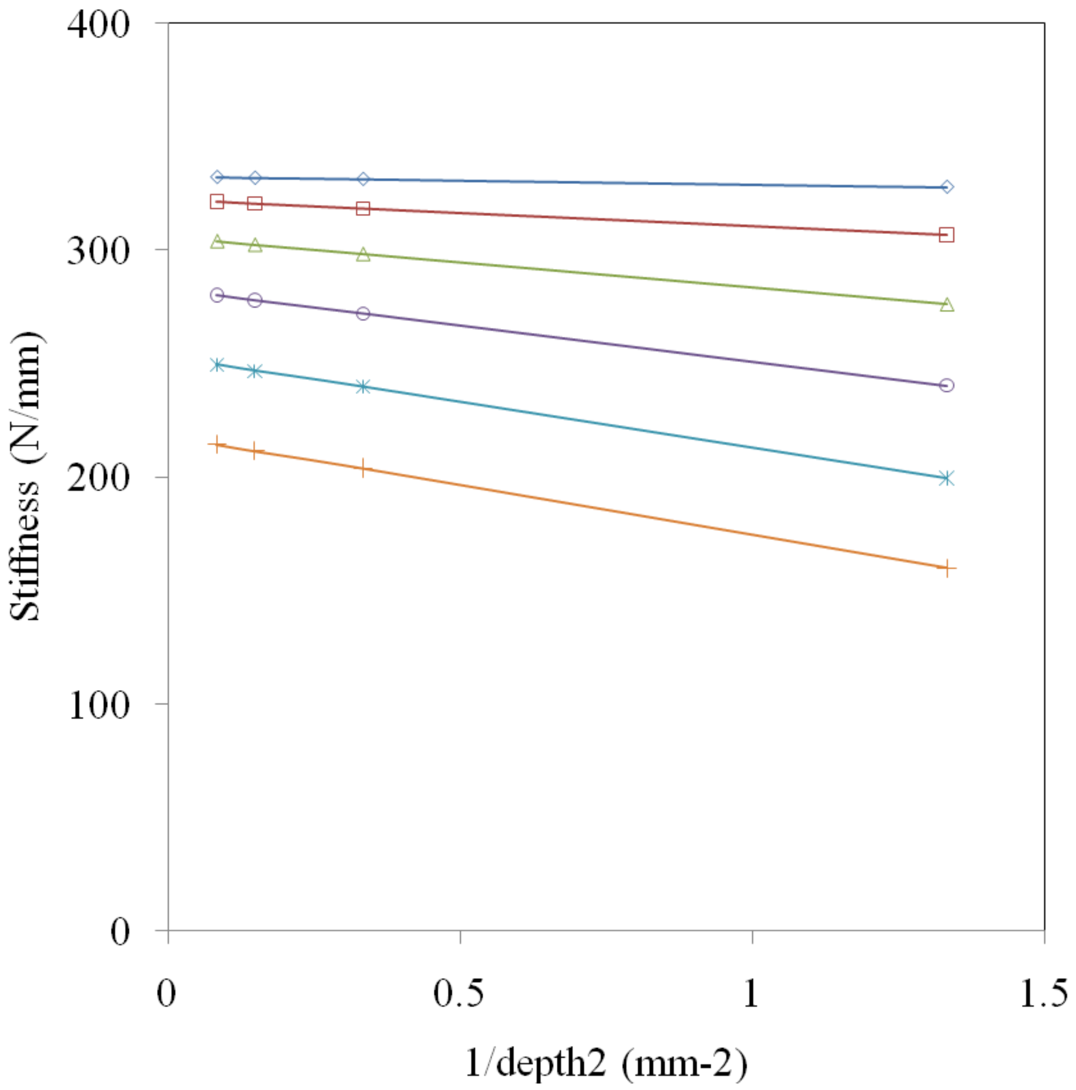

Figure 31 - Stiffness against the reciprocal of depth squared for corrugated beams at a 6:1 length to depth aspect ratio for varying normalised void radii, V_R/S_Y. Each line represents a different void radius: blue diamonds, $V_R/S_Y=0.06$; red squares, $V_R/S_Y=0.12$; green triangles, $VR/S_Y=0.27$; purple circles, $V_R/S_Y=0.23$; blue stars, $V_R/S_Y=0.29$; orange crosses, $V_R/S_Y=0.35$.

Table 5 shows the values for characteristic length in the 3D simulations. It is not possible to take a reliable characteristic length value for below 10:1 aspect ratio as the beams do not follow the closed form analytical linear trend necessary to apply Equation 10.

Table 5 - A comparison of the characteristic lengths for different void radii at 10:1 and 20:1 length to depth aspect ratios for 3D models.

Normalised void radius V_R/S_Y	Characteristic length (mm) 10:1 aspect ratio	Characteristic length (mm) 20:1 aspect ratio	Void diameter (mm)
0.06	0.07	0.08	0.1
0.12	0.16	0.16	0.2
0.17	0.23	0.24	0.3
0.23	0.31	0.32	0.4
0.29	0.39	0.40	0.5
0.35	0.46	0.48	0.6

As in the planar idealised heterogeneous material case a better impression of the relationship between the positive and negative size effects observed between smooth and corrugated beams can be created by plotting the respective magnitude of the gradients against normalised void radius (Figure 32). It can be seen in Figure 32 that both size effects follow similar trends as the void size is increased, and could be considered to mirror one another. Again, as in the 2-D case the difference between both size effects was plotted against void size (Figure 33). For perfectly complementary size effect trends to be present in both the corrugated and smooth surfaced beams there would have to be no difference in the magnitude of the observed size effects. However, it is apparent in Figure 33 that for smaller void sizes there is a significant divergence between positive and negative size effects. As the void size is increased the difference between size effects reduces. This implies that a normalised void radius in the region of 0.25 produces the most comparable results between positive and negative size effects. However, it is important to note that at lower size effects a small change in the gradient will not majorly affect the calculated values for micropolar characteristic length and Young's modulus. Therefore, even at smaller void radii it nevertheless remains a fairly accurate generalisation to describe the positive and negative size effects as mirroring one another. Moreover, where the experimental testing of a real material is considered, the difference between positive and negative size effects are within the regions of experimental errors. The opposing size effects, although not exactly opposite in magnitude follow strikingly similar opposing trends. This may allow the micropolar material properties to be inferred from the opposing complimentary size effect allowing predictions from data which would otherwise not enable the material properties to be calculated

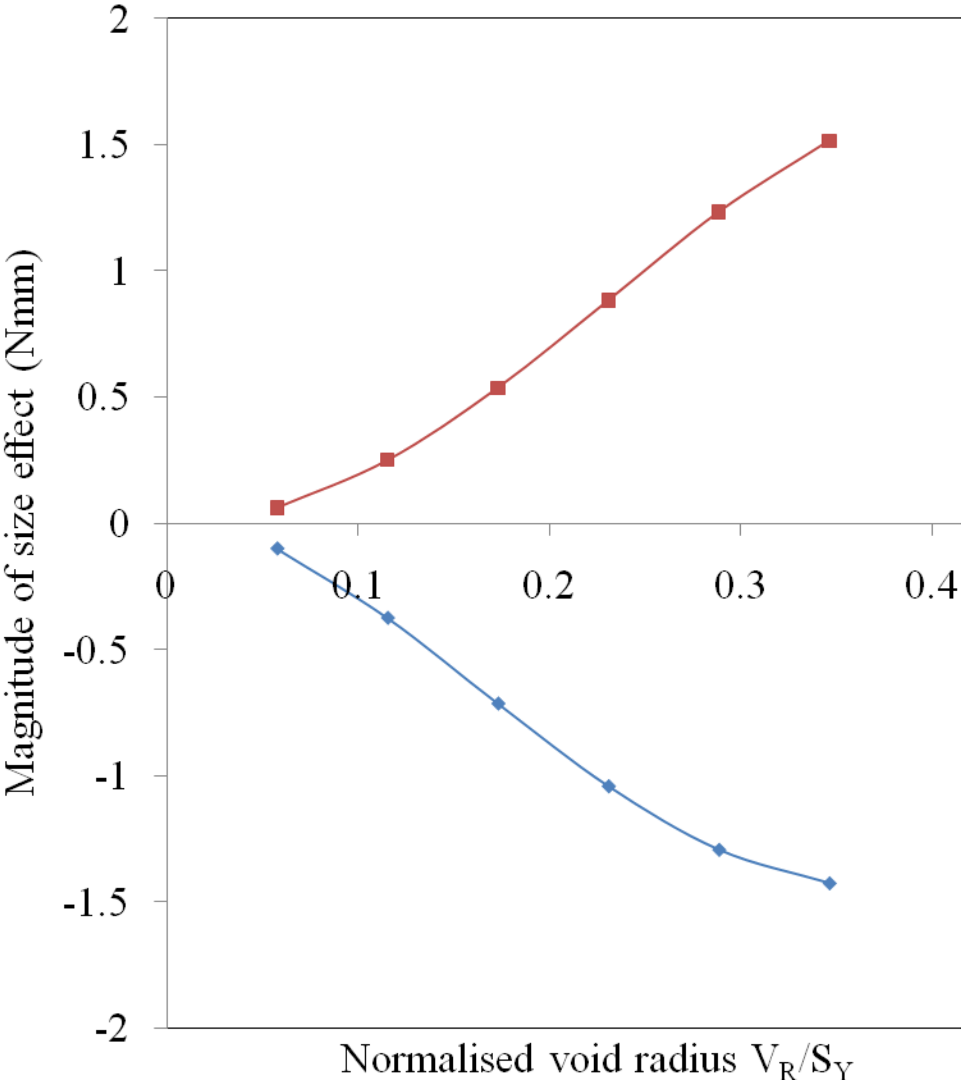

Figure 32 – Magnitude of size effect plotted against normalised void radius, V_R/S_Y, for 20:1 length to depth aspect ratio for beams with voids running longitudinally along the axis of bending. The blue diamonds are for beams with continuous surfaces and the red squares represent beams with surfaces corrugated by the internal microstructure.

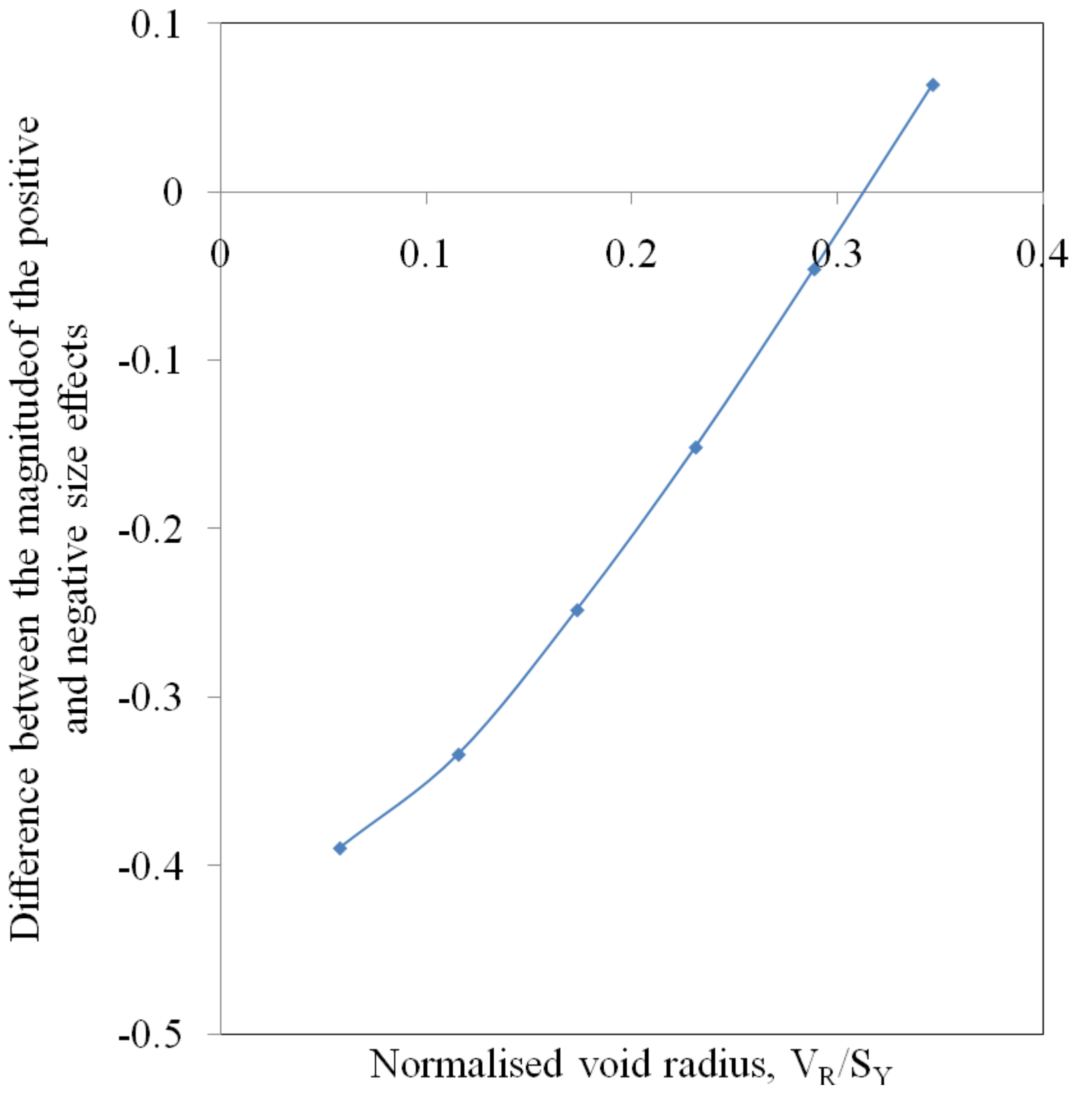

Figure 33 – The difference in the magnitude of size effects between the positive (smooth surfaced) and negative (corrugated) plotted against the normalised void radius, V_R/S_Y

Three dimensional FE models demonstrate the transverse isotropy in the 3D idealised heterogeneous material. The 2-dimensional models revealed that there was limited anisotropy in the x-y plane, but the 3-dimensional model clearly demonstrates that along the long axis (where the voids run along the length of cortical bone) the material is significantly stiffer. This suggests close to plane isotropy in the idealised 3-dimensional model; a finding which is consistent with current models of transverse isotropy in mid-diaphyseal cortical bone (Dong & Guo 2004; Remond & Naili 2005; Turner et al. 1995).

The bending analyses further reveal the size effect trends apparent in the idealised material. Not only is there a significant size effect recorded in the 2-dimensional cases – where continuous and corrugated surfaces follow opposing size effect trends – but the same size effect trends are apparent in the longitudinal axis also. This indicates that a full three dimensional micropolar model of the idealised heterogeneous material is required to effectively describe the micropolar behaviour. If the idealised FE models are representative of the Haversian canals system in cortical bone then there will be two unique size effects observed for the longitudinal and transversely orientated specimens, each describing the characteristic length of the microstructure at each orientation.

Another significant finding from both the 2-dimensional and 3-dimensional FE models has been that the length to depth aspect ratio has an important influence on the observed size effect. The analytical solution for a micropolar beam in three point bending highlights a linear size effect relationship between the flexural stiffness and the reciprocal of depth squared. For beams with a 20:1 length to depth aspect ratio a near linear relationship is observed. As this aspect ratio is reduced the assumptions of the analytical solution become less valid. At a 10:1 aspect ratio the linear relationship is still maintained, but as the aspect ratio is reduced below 10:1 there is no longer a linear relationship between stiffness and reciprocal of depth squared. This means that for experimental analyses of cortical bone at least a 10:1 aspect ratio will have to be used. For the practicalities of the experiments a larger length to depth aspect ratio could prove problematic and for this reason a 10:1 length to depth aspect ratio was determined to be the most practical for experiments and effective for establishing micropolar material properties.

A significant finding from both the two and three-dimensional models was that the micropolar characteristic length can be predicted from the diameter of the internal microstructural voids. It was found empirically that micropolar characteristic length varies directly with void diameter. This implies that a general geometric observation may be made of the microstructure in a heterogeneous material and allow the characteristic length to be inferred from that geometry. It has also be observed that the orientation and character of the microstructure has an important influence of the observed characteristic lengths with the 2-D and 3-D geometries showing different relationships with void diameter. Nonetheless this finding has demonstrated the predictability of knowledge of the microstructure in identifying micropolar material properties. Moreover it has shown a direct link between the underlying microstructure (which causes the material heterogeneity) and the material properties which are associated with the global material behaviour.

3.7 Three dimensional hexagonal models

3.7.1 Background

The previous results have shown that surface effects have an overwhelming influence on the observed size effect. In rectangular cross sections the influence of the surface region is influential to the overall beam behaviour in bending because this is where the highest stresses occur in three-point bending. However, in beams with circular cross sections the surface regions are noticeably less significant in determining the overall material behaviour in three-point bending. In a circular cross sectioned beam the influence of the upper and lower surface regions are not as prominent. It may be possible to observe similar micropolar size effect in beams with continuous surfaces and beams corrugated by the internal microstructure because the surface regions have a less significant influence on the overall material behaviour. Considering the contrasting findings between similar the experimental analyses of Lakes and Choi in bending tests on cortical bone specimens (Park & R. Lakes 1986; Choi et al. 1990) it is plausible that the cause of these differences is due to the cross sectional area of the test specimens rather than systematic difference between the tests. This section tests this hypothesis.

3.7.2 Methodology

To determine if a more circular geometry would produce more consistent results between corrugated and smooth beams a series of hexagonal three-point bending models were created in ANSYS 12.1 to approximate the geometry of a circular cross section. The behaviour of a micropolar beam of hexagonal cross section in three-point bending is derived from the three-point bending equation:

Equation 14

$$K = \frac{48EI}{l^3}$$

where E is the Young's modulus, I is the second moment of area and l is the length of the beam. The second moment of area of a hexagonal cross section is given by:

Equation 15

$$I_{hexagon} = \frac{5\sqrt{3}r^4}{16}$$

where r is the radius of the hexagon. By substituting Equation 15 into Equation 14 an expression for a hexagonal beam in three –point bending may be formed:

Equation 16

$$K = \frac{5\sqrt{3}}{3} E_m \frac{d^4}{l^3}$$

The equivalent micropolar expression for a hexagonal cross sectioned beam is therefore given by:

Equation 17

$$K = \frac{5\sqrt{3}}{3} E_m \frac{d^4}{l^3} (1 + \frac{l_{c,HEX}^2}{d^2})$$

where $l_{c,HEX}$ is the micropolar characteristic length of a hexagonal beam in bending and is given by $l_{c,HEX} = \sqrt{\frac{72\gamma}{5E_m}}$. For a rectangular beam $l_{c,RECT} = \sqrt{\frac{12\gamma}{E_m}}$ and for a circular beam $l_{c,CIR} = \sqrt{\frac{16\gamma}{E_m}}$. The difference between characteristic lengths arises from the change in second moment of area between beam cross sections and therefore to compare the hexagonal models accurately with the rectangular geometries a comparison between the characteristic lengths in bending is required.

By dividing Equation 17 through by the depth the length to depth aspect ratio can be maintained as the parameter by which the size effect is determined.

Equation 18

$$\frac{K}{d} = \frac{5\sqrt{3}}{3} E_m \frac{d^3}{l^3} (1 + \frac{l_{c,HEX}^2}{d^2})$$

where the symbols have their usual meaning. This allows the micropolar Young's modulus and characteristic length to be calculated from the linear relationship between stiffness per unit depth and the reciprocal of depth squared $\left(y - \text{int}\, ercept = \frac{5\sqrt{3}}{3} E_m \left(\frac{d^3}{l^3} \right), gradient = \frac{5\sqrt{3}}{3} E_m \left(\frac{d^3}{l^3} \right) \left(\frac{l_{c,HEX}^2}{d^2} \right) \right)$.

The same three-dimensional FE mesh was used for the hexagonal beams as was used in the previous section for the three-dimensional models with surface perforations and rectangular cross sections (Figure 6 and Figure 34). Four models were created with one void radius of 0.3 used to analyse the hexagonal beam models. The main purpose was to determine if a negative size effect occurred in hexagonal (circular) cross sectioned beams and therefore only one void radius was initially analysed.

Symmetry and anti-symmetry boundary conditions were applied to simplify the model and reduce the computational time. A 10:1 length to depth aspect ratio was maintained for the four depths of model created. A line load of 100N was applied along the top surface to simulate three point bending in each model. The deflection was taken as the displacement on the bottom surface of the beam directly below the line where the load was applied. The flexural stiffness of the beam was determined by dividing the applied load by the calculated deflection.

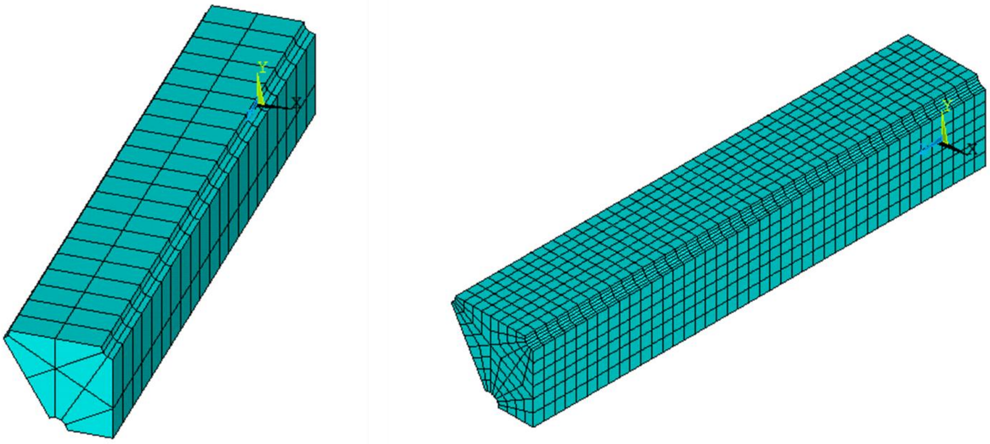

Figure 34 – The mesh used for the smallest hexagonal cross sectioned beams. Anti-symmetry boundary condition was applied to the upper x-z plane and symmetry was applied to the x-y plane in order to reduce the size of the model.

3.7.3 Results and discussion

The flexural stiffness value obtained from the FEA was divided by the depth for each model to enable the stiffness per unit depth to be plotted against the reciprocal of depth squared and determine the magnitude and direction of any observable size effects (Equation 18). This also allowed the size effect to be compared with the equivalent rectangular beam of the same void fraction. A negative size effect in agreement with anti-micropolar size softening was observed in the FE results (Figure 35). This suggests that hexagonal cross sectioned beams follow the same trend as rectangular cross sectioned beams in that where the surface is corrugated by the internal microstructure a size softening size effect is observed. The primary purpose of this analysis was to determine if a negative size effect trend occurred in hexagonal models and therefore beams without surface voids were not created. Despite this the micropolar material properties may be inferred by assuming similar behaviour to the rectangular beams where a complementary positive size effect would occur in smooth surfaced hexagonal beams. The micropolar characteristic length and Young's modulus were calculated using Equation 18 and were found to be 0.59mm and 12.8 GPa respectively. The characteristic length in bending for the hexagonal model is therefore 0.15mm. These are comparable to the values obtained from the rectangular cross sections of equivalent void size and void fraction at a 20:1 length to depth aspect ratio (l_b = 0.14mm and E_m = 13.3GPa).

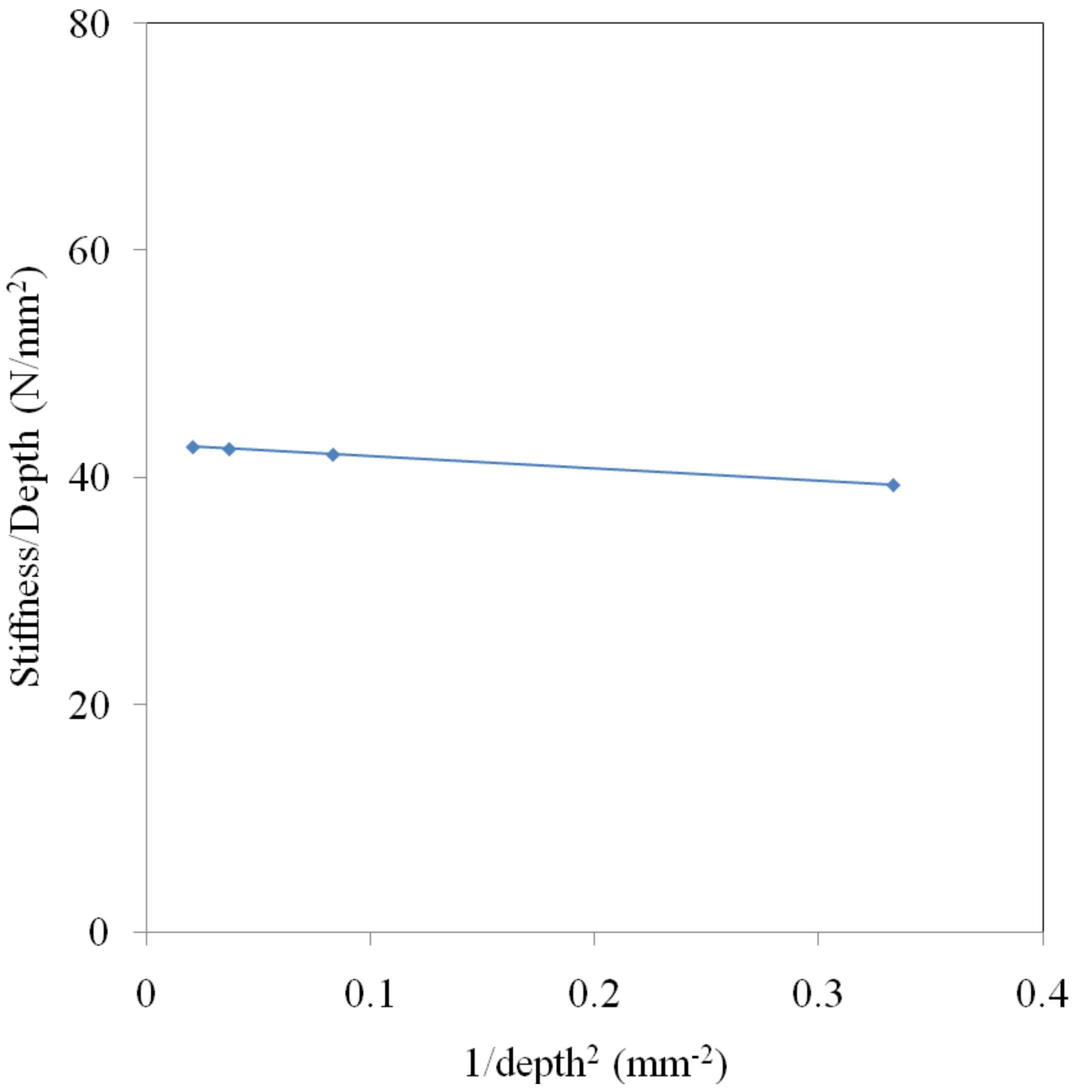

Figure 35 – Stiffness per unit depth plotted against the reciprocal of depth squared for the four hexagonal beams modelled at a void radius of 0.3.

Lakes investigated the micropolar behaviour of cortical bone in the 1980s (R. Yang & Lakes 1982; R. Lakes 1985; J. Yang & R. Lakes 1982). In these studies specimens of circular cross section were analysed. Because Lakes' conclusions suggest that cortical bone exhibits a positive size effect consistent with micropolar elasticity the hypothesis was that the circular cross section had an influence upon whether such a size effect is predicted by numerical modelling.

A negative anti-micropolar size effect was found numerically in hexagonal cross sectioned beams contrary to that experimentally observed by Lakes (Yang & Lakes 1982) for circular cross sectioned beams. This suggests that the experiments by

Lakes are observing a different size effect to that predicted by the computational models. One possible explanation of the discrepancy is the lack of an analysis of specimens of a length scale approaching the scale of the microstructure in Lakes' investigation. The smallest specimen size tested by Lakes was of the scale of 1mm in diameter; this is considerably larger than the microstructure of the Haversian canal system which is being modelled in the numerical models in this study. Therefore it may be argued that the positive size effect observed by Lakes is not directly comparable to the hexagonal models investigated here. Moreover, it would be expected that a circular cross sectioned beam experimentally tested at below the 1mm diameter size would begin to reveal a significant decrease in stiffness concurrent with the numerical predictions. This may also suggest that results from Lakes' work should perhaps not be taken as a definitive quantification of the micropolar behaviour of cortical bone but rather may be an indication of the natural variation of the material at that length scale and not representative of the constitutive behaviour of the material.

3.8 Two dimensional models with a varied surface thickness

3.8.1 **Background**

In the models created thus far there has been continuity in the distribution of voids through the material in both the continuous and corrugated beams. If these cases represent extremes of the geometrical preparation of the idealised heterogeneous material then it follows that a beam may be created which is representative of a preparation between those two extremes. To create such a beam a series of models were created with discretely smaller surface voids thereby reducing the thickness of the compliant surface layer on the beam. The surface voids were maintained at the same porosity as the internal microstructure but the radius of each void was reduced. These models were designed to represent a scenario where the surface of the beam has had an artefact introduced onto it; the artefact may have arisen from the preparation process (i.e. cutting, polishing and lapping) and is smaller than the internal microstructure but cannot be ignored as a negligible influence on the beam stiffness. In fact the real situation may be a combination of surface microstructure and preparation artefact.

By understanding the situations between the extremes of size effect behaviour in beams in three-point bending a more complete picture of the predicted experimental behaviours may be developed.

3.8.2 **Methodology**

A series of beams were created with surface voids of half the radius of the internal microstructure. The same size effect methodology as was used in previous numerical experiments was applied where the aspect ratio of length to depth was maintained throughout for larger and smaller beams. The same aspect ratio of 10.4:1 was used for all models.

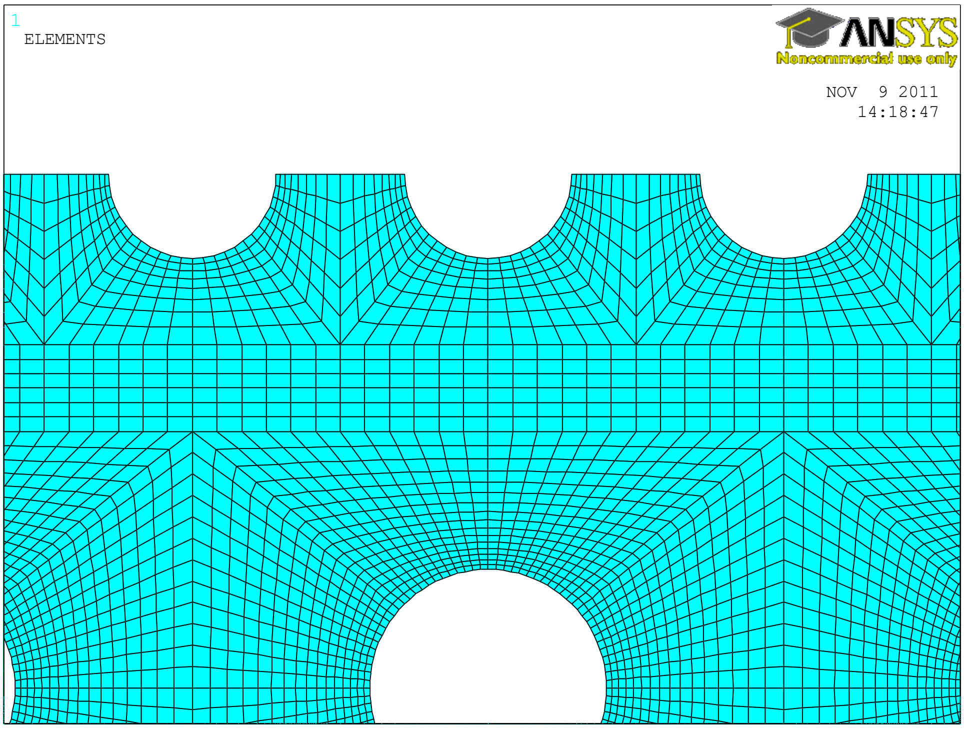

Figure 36 – Example mesh for a 2D beam with double the surface voids to internal voids. The porosity is consistent throughout the model.

A new mesh was created to model the surface region for the halved radius voids; the mesh was created using the same equilateral array of voids as in the previous 2-dimensional analyses (Figure 36). Because the void radius was halved and the porosity of the beam was to remain constant this meant that the number of voids on the surface doubled.

The same boundary conditions were used as those applied in the previous section for 2-dimensional models in three-point bending (Figure 10). Two supports were simulated by pinning two vertical points on the lower edge of the beam thus defining the length of the beam. A vertical point load of 100N was applied to the midpoint of the beam on the upper surface and was pinned in the x direction. Care was taken to apply the constraints between voids to reduce localised effects. The material properties of 20GPa for the matrix material Young's modulus and 0.3 for Poisson's ratio were used as representative of cortical bone.

Five void fractions were analysed: 0.036, 0.082, 0.145, 0.227 and 0.326 these are the same void fractions used in the previous 2-dimensional analyses and therefore were deemed to be directly comparable.

3.8.3 **Results and discussion**

Figure 37 shows the results for beams with voids of half the size on the surface. It can be seen that there is a non-linear relationship between the stiffness of the beams and the reciprocal of depth squared. This non-linear effect, which becomes more pronounced as the void fraction of the material is increased, is not consistent with micropolar elasticity and for this reason Equation 10 may not be used to describe a linear trend between size and stiffness. Therefore it is not possible to extrapolate micropolar material properties from these results.

It is apparent that there is both a size softening trend and a size stiffening trend exhibited by the non-linear relationship.

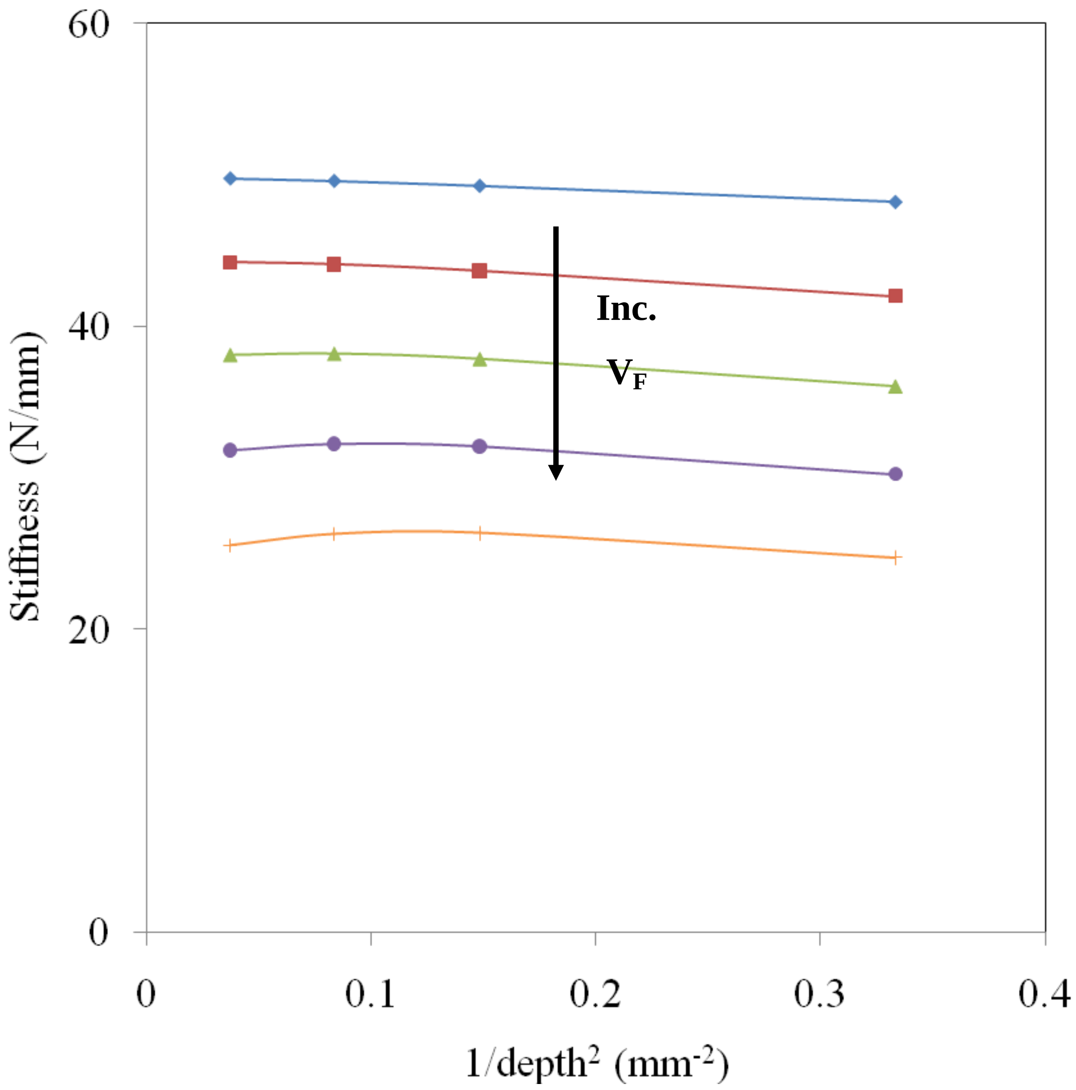

Figure 37 - Stiffness against the reciprocal of depth squared for beams with double the number of surface voids at a constant porosity for a 10.4:1 length to depth aspect ratio for varying normalised void radii, V_R/S_Y. Each line represents a different void radius: blue diamonds, $V_R/S_Y = 0.06$; red squares, $V_R/S_Y = 0.12$; green triangles, $V_R/S_Y = 0.27$; purple circles, $V_R/S_Y = 0.23$; blue stars, $V_R/S_Y = 0.29$; orange crosses, $V_R/S_Y = 0.35$.

Although there is not a linear size effect trend exhibited by the results of beams with variable surface voids it is possible to draw some interesting conclusions. Firstly, there is a noticeable size softening trend indicative of an anti-micropolar size effect. This compares to the FE models of beams with surface voids of the same radius as the internal microstructure. Despite the lack of linearity in the results it is possible to identify the micropolar trend as being generally of a negative size effect and therefore related to the presence of surface voids.

Where the surface voids have the most influence on the stiffness of the beam – i.e. where the surface layer is most significant: in the smaller beams – it is apparent that the beams are more compliant. For larger beams, where the surface layer is less significant in the overall beam stiffness, the beam appears stiffer. The differing influence of the surface regions of larger and smaller beams may account for the non-linear size effect trends observed for these type of surfaces. This expresses itself in the stiffness against depth plot as a positive micropolar size effect in larger specimens and a negative micropolar size effect in the smaller specimens.

It may be possible to infer the micropolar material properties from the positive size effect trend of the larger specimens, where the influence of the surface region becomes less important. To do this the intercept and gradient of the line at the intercept would be used in the closed form micropolar formulation of a beam in three-point bending.

The variable surface void models are an important tool for understanding the preparation of specimens for the experimental testing of real materials. If a standardised surface artefact is produced on the surface of each specimen thereby creating a consistent surface for each specimen then a size effect trend concurrent with micropolar elasticity may be established. It would be important to establish a finer grain size of the artefact on the surface than the internal microstructural features of the constitutive material. This would enable the influence of the induced surface voids to be reduced therefore allowing any discernable size effect trend to be related to the internal microstructure rather than the imparted artefact.

3.9 Numerical modelling conclusions

The 3-dimensional idealised heterogeneous material created to mimic the microstructure of cortical bone has been shown to behave closely in accordance with plane isotropy while the longitudinal z-axis shows significantly stiffer material properties than the x-y plane. Micropolar size effects were observed in both the 2-dimensional and 3-dimensional models. However, there is an overwhelming importance in the nature of the surface regions in both models. Where the surface is corrugated by voids a negative, anti-micropolar, size effect is observed and where the surface is continuous a positive micropolar size effect is observed. This suggests that the surface needs to be characterised in order to fully interpret any size effect behaviour in experiments on a real material.

It has been shown that the micropolar material properties of characteristic length in bending and micropolar Young's modulus can be found from a positive size effect. It has also been demonstrated that the micropolar characteristic length varies linearly with the void diameter. It was calculated that for the 2-D case $l_c = 1.35V_D$ and for the 3-D case $l_c = 0.79V_D$. This highlights the predictive nature of the microstructure on the macroscale material properties and may allow micropolar constitutive properties to be inferred from geometrical measures of the microstructure itself. This is a significant finding as it directly links the heterogeneity of the microstructure to size effects in the material.

The opposing size effects for continuous and corrugated models are approximate mirrors of one another. This suggests that the micropolar material properties may be inferred from the negative size effect, as it is a mirror of the relevant positive size effect in the models without surface voids. It was also noticed that the length to depth aspect ratio plays an important role in the observed size effect. Where the length to depth aspect ratio is maintained above 10:1 the results are fairly consistent with the closed form analytical solution, however, where the aspect ratio falls below 10:1 the analytical solution is no longer valid as the influence of shear deformation become significant in the bending of the beam.

Further analyses were done on hexagonal beam geometries to investigate whether opposing size effects occurred where the surface region had less of a significant impact on the beam geometry. However, this further corroborated the earlier findings on rectangular cross sectioned beams and further revealed the opposing size effects in beams with and without surface corrugations.

In order to further understand the importance of the surface region on the bending size effects, models were created with a varied size of surface voids. This revealed an intriguing finding where a linear relationship between beam stiffness and reciprocal of depth squared was not evident, but rather a non-linear relationship which shows both size stiffening and softening trends. It may be that the non-linear relationship is descriptive of the differing influence that the surface region imparts upon larger and smaller beams. This finding is important in the future experimental work as it further highlights the importance of consistent surface preparation.

Finally, it is important to note that many of the effects modelled are small (i.e. a small % difference in stiffness). Inherent biological variation and non-idealised heterogeneity in bone may mask these numerically predicted size effects. Furthermore, positive, neutral and anti-micropolar behaviour is all possible from an idealised heterogeneous material depending on the surface finish. If a lack of size effect is present this does not necessarily mean that the material follows classical elasticity. Clearly, surface finish on small samples plays an important role.

4 Analytical models of idealised materials

4.1 Analytical models for 3D beams in bending

The numerical analysis revealed opposing size effects in the 3-dimensional idealised heterogeneous material created in ANSYS. It is possible to create complementary analytical models of the FE simulations by calculating the second moment of area of the cross section of each simulated beam. From this it is possible to calculate the stiffness of each beam in three-point bending. Such an examination of the micropolar size effects observed in the FE analysis may enlighten the underlying causes of the micropolar size effects and reveal a method for extracting the micropolar behaviour from a beam showing a negative size effect.

4.1.1 **Methodology**

Equation 11 may be represented by an equivalent expression which includes an unspecified second moment of area.

Equation 19

$$K = \frac{48EI}{l^3}$$

where E is the matrix material Young's modulus, I is the second moment of area of the cross section and l is the length of the beam. The second moment of area, I, of a rectangular cross sectioned beam is given by: $bd^3/12$, where b and d are the breadth and depth of the section respectively.

Because the beam cross-section is uniform in each of the three dimensional beams along the axis of bending (Figure 23) it is possible to calculate the second moment of area for each beam by subtracting the voids using the parallel axis theorem. Therefore, it is possible to validate the finite element results for the three dimensional beams using Equation 19. A Young's modulus representative of cortical bone (20GPa) was used for the matrix material to maintain consistency in the methodology. Because the analytical solution assumes that the beam is loaded in three-point bending there would be no discrepancy in varying the aspect ratio. For this reason only one length to depth aspect ratio (20:1) was calculated. The 20:1 aspect ratio was chosen for the analytical models because this ratio was the largest used in the FE analyses and simulated the closest approximation to pure bending. Analytical solutions were calculated for beams both with and without surface voids in order to compare the size effects produced.

4.1.2 Results and discussion

The same size effect trends were observed as in the computational models. Beams with continuous surfaces showed a micropolar size stiffening size effect (Figure 38) and beams with surface perforations showed an anti-micropolar size softening size effect (Figure 39). Both set of results quantitatively match those produced for a 20:1 length to depth aspect ratio in the FE analyses (Table 6 and Table 7).

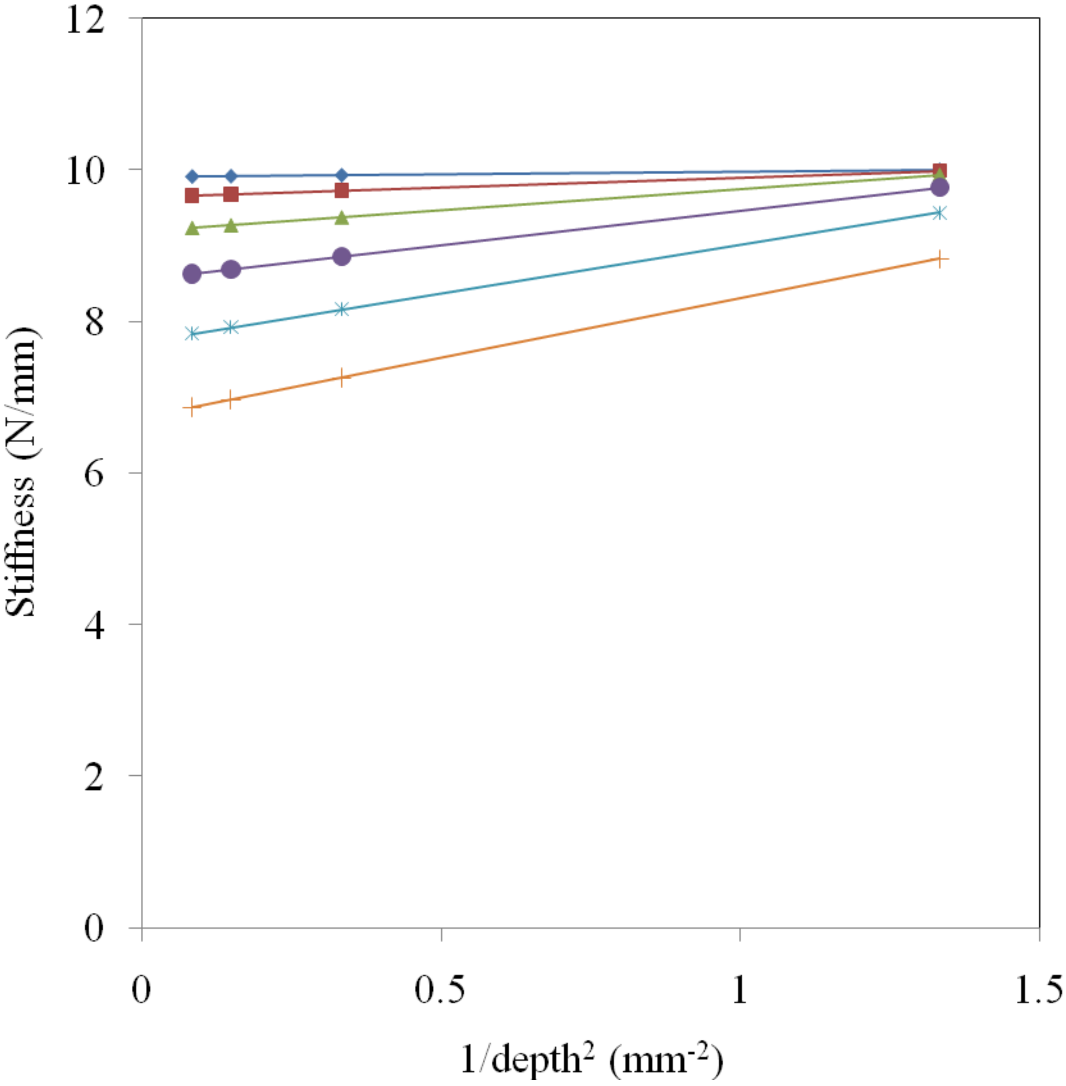

Figure 38 – Analytical stiffness against the reciprocal of depth squared for smooth continuous beams at a 20:1 length to depth aspect ratio for varying normalised void radii, V_R/S_Y. Each line represents a different void radius: blue diamonds, $V_R/S_Y = 0.06$; red squares, $V_R/S_Y = 0.12$; green triangles, $V_R/S_Y = 0.17$; purple circles, $V_R/S_Y = 0.23$; blue stars, $V_R/S_Y = 0.29$; orange crosses, $V_R/S_Y = 0.35$.

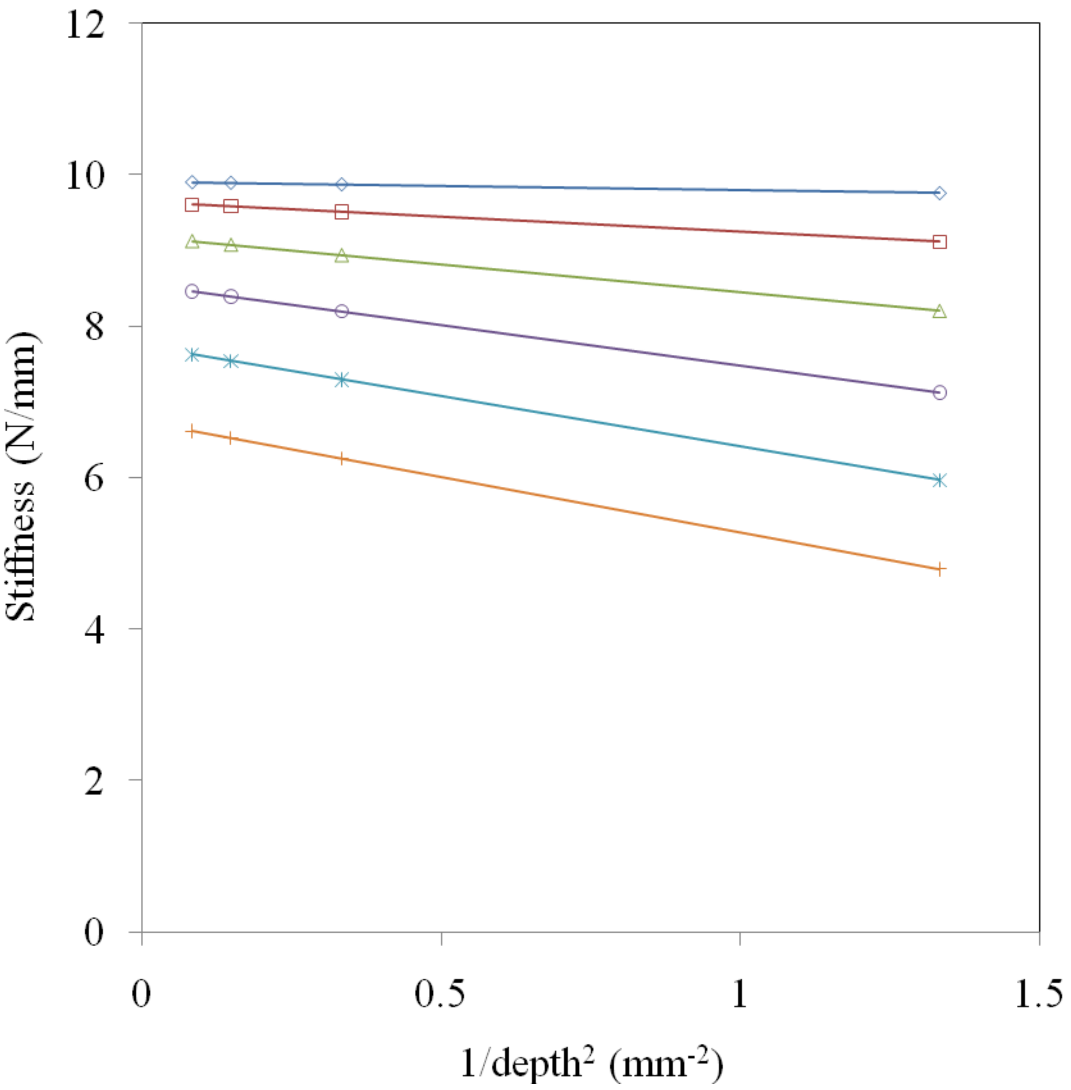

Figure 39 - Analytical stiffness against the reciprocal of depth squared for corrugated beams at a 20:1 length to depth aspect ratio for varying normalised void radii, V_R/S_Y. Each line represents a different void radius: blue diamonds, $V_R/S_Y = 0.06$; red squares, $V_R/S_Y = 0.12$; green triangles, $V_R/S_Y = 0.17$; purple circles, $V_R/S_Y = 0.23$; blue stars, $V_R/S_Y = 0.29$; orange crosses, $V_R/S_Y = 0.35$.

The same value for Young's modulus was produced from the analytical results as that obtained from the axial FE model for three dimensional beams (Table 6). However, the values obtained from three-point bending show a slightly lower micropolar Young's modulus. This may be because even a 20:1 aspect ratio does not exactly simulate the conditions used in the analytical model to describe pure bending. As the FE simulations will generate a numeric result which includes element approximations for the particular geometry being analysed it is unlikely to produce a result exactly the same as an equivalent analytical solution. Moreover, the analytical solution does not account for the anisotropy in the 3-dimensional material which the finite element calculations will include. Despite this the values for micropolar Young's Moduli are strikingly similar and suggest the analysis technique is showing a true material behaviour, and, that size effects are apparent in 3-dimensional extruded heterogeneous materials.

Table 6 - Longitudinal Young's modulus for varying void fractions comparing computational and analytical results over a 20:1 length to depth aspect ratio.

Longitudinal Young's Modulus, E_z (GPa)	**Void fraction, V_F** *0.036*	*0.145*	*0.325*
FE three-point-bending (20:1)	19.1	17.0	13.3
FE axial loading	19.3	17.1	13.5
Analytical three-point-bending	19.3	17.1	13.5

The micropolar characteristic length predicted by the analytical methods closely matches the values calculated using FE analysis. Table 7 shows a comparison between the analytical and FE values for both Micropolar Young's Modulus and characteristic length for models simulated at a 20:1 length to depth aspect ratio. This shows the FE predictions to be closely matched by the analytical validation. Again this suggests that the geometrical difference between models can be quantified through the difference in the second moment of area.

Table 7 – A comparison between the analytical and FE Micropolar characteristic length and Young's Modulus for beams with a 20:1 length to depth aspect ratio.

Normalised void radius, V_R/S_Y	**Analytical Micropolar Characteristic Length, l_c, (mm)**	**Analytical Micropolar Young's Modulus, E_{mz}, (GPa)**	**FE Micropolar Characteristic Length, l_c, (mm)**	**FE Micropolar Young's Modulus, E_{mz}, (GPa)**	**l_c % difference**	**E_{mz} % difference**
0.06	0.082	19.8	0.079	19.7	3.66	0.51
0.12	0.165	19.3	0.161	19.1	2.42	1.04
0.17	0.246	18.4	0.242	18.2	1.63	1.09
0.23	0.327	17.1	0.322	17.0	1.53	0.58
0.29	0.406	15.5	0.401	15.3	1.23	1.29
0.35	0.482	13.5	0.477	13.3	1.04	1.48

4.2 Analytical models for 2D beams: Size effects in layered heterogeneous materials

4.2.1 Background

Idealised heterogeneous materials can be represented by creating an array of voids in a homogeneous material. Such idealised materials are intended to represent a form of physical microstructure; alternatively such an arrangement may induce a characteristic material feature such as anisotropy in material properties through the material.

Previously the method of representing inhomogeneity by an arrangement of voids in a homogeneous material has shown a size effect consistent with micropolar elasticity when simulating three-point-bending using FE analysis (Section 3.3). However, a micropolar size effect - where stiffening is observed for smaller beams in three-point bending with consistent aspect ratio – is only observed where the surface of the material is not intersected by the internal material voids. An opposite "anti-micropolar" size effect is observed when the surface is corrugated by the material voids. In this case the beams become more compliant as size is reduced at the same three-point-bending aspect ratio. This raises the question: What is the mechanism by which the same material is able to portray inherently opposite material behaviours depending on how the sample boundaries are positioned relative to the prescribed microstructure?

It has also been demonstrated that the alterations in stiffness of the 3-dimensional FE simulations may be attributed to a change in the second moment of area between beams of varying size. This quantity describes the change in geometrical distribution of material through the beam cross section and is relatively straight forward to determine for a continuous cross section. However, for the case where the cross section alters along the length of a beam it is more challenging to calculate a value for the second moment of area applicable over the beam length. For example in the 2-dimensional FE simulations a value for the cross sectional second moment of area will change depending on the location of the cross section along the major axis of the beam, because of the alternating location of voids through the depth.

An alternative possibility is to redefine the microstructure of the heterogeneous material in terms of material property variations rather than geometrical features (Figure 40). By representing the heterogeneity in the idealised planar material as a series of stiff and compliant layers, as opposed to modelling detailed microstructure, it is hoped that a more detailed relationship between the influence of the microstructure and the observed micropolar material properties may be formed. The rationale for this approach is that first principles define a material as being micropolar when the material is unable to transfer shear forces equally through the material. Such behaviour appears to be effectively simulated by creating regular voids in a material; the areas with voids represent compliant layers and areas without voids represent stiff layers.

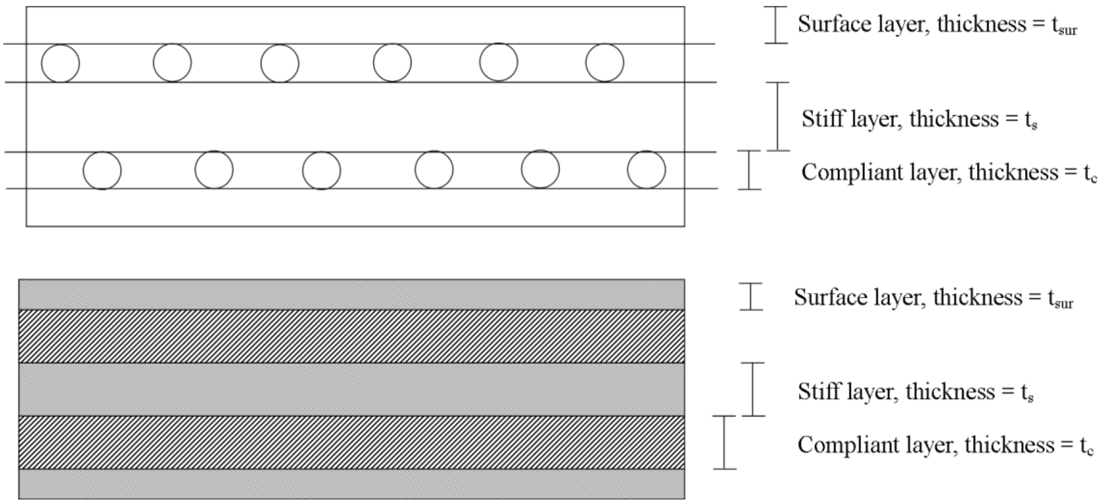

Figure 40 - Laminated model of stiff and compliant layers representing the internal microstructural voids.

The hypothesis that a similar micropolar trend to that which has already been shown in the idealised heterogeneous material of regularly arranged voids distributed through a homogeneous material will be observed in a laminated style material of stiff and compliant layers as in Figure 40.

For beams where the surface is intersected by the internal microstructural voids a compliant layer may be defined on the surface. Where the surface is continuous a stiff layer may be defined on the surface.

4.2.2 Methodology

Equation 20 is used to calculate the stiffness of a homogeneous beam in three-point-bending.

Equation 20

$$K = \frac{48EI}{l^3}$$

where K is the geometric stiffness of the beam, E is the Young's Modulus, I is the second moment of area and l is the length of the beam.

For beams constructed from alternating stiff and compliant layers as shown in Figure 40 the Young's Modulus and cross sectional second moment of area varies between each layer. Therefore the second moment of area of the entire beam about the centre of the beam cross section can be calculated in order to evaluate the overall beam stiffness. In effect the stiffness of each layer about the central plane of bending can be summated to give the total stiffness of the beam as shown in Equation 21.

Equation 21

$$K = \frac{48}{l^3}\left(\sum_{i=1}^{n} E_i I_i\right)$$

where K is the stiffness of the beam, E_i is the Young's Modulus, I_i is the second moment of area of the *ith* layer, l is the length of the beam and n is the number of layers in the material.

This method was repeated for 5 beams. For the smallest beam there were three layers, one in the centre and two surface layers. For the largest beam there were eleven layers altogether. The analysis was set up with five discrete input parameters which could be adjusted for each beam globally. The defined inputs used to calculate the beam stiffness were: compliant layer thickness, t_c; stiff layer thickness, t_s; coefficient of surface layer thickness, t_{SUR}; Young's Modulus of the stiff layer, E_s; Young's Modulus of the compliant layer, E_c (Figure 40). A length to depth aspect ratio of 10:1 and a breadth of unity were chosen for these analyses.

The coefficient of surface layer thickness represents the ratio of the thickness of the surface layer to the thickness of the internal stiff layers, thereby allowing the importance of the thickness of the surface layer to be analysed. The stiff and compliant layers could be reversed in the beam and therefore allow the surface layer to be compliant. In this case the coefficient of surface layer thickness was set to be half the thickness of the compliant layer.

In order to standardise the analysis procedure and enable a comparison with the 2-D FE analyses the input parameters were defined in terms of the equivalent void radius in the FE models. By using the same equilateral array of voids used in the FE analyses (Figure 4) where S_X and S_Y define the arrangement of voids in the x-y plane the void radius, V_R was used to define the input parameters (Figure 40). The input parameters are detailed in Table 8 where it can be seen that the void radius defines the void fraction, stiff layer thickness and compliant layer thickness. The void fraction and Young's modulus of the stiff layers in turn were used to define the

Young’s modulus of the compliant layers. This was done by proportionately scaling the Young’s modulus of the compliant layers by the reduction in material caused by the size of the voids in the layer.

Table 8 – Input parameters for the 2-D analytical models of beams of stiff and compliant layers

Void radius, V_R (mm)	**Void fraction, V_F**	**Compliant layer thickness, t_C (mm)**	**Stiff layer thickness, t_S (mm)**	**Coefficient of surface layer thickness, t_{SUR}**	**Young’s modulus of stiff layer, E_S (GPa)**	**Young’s modulus of compliant layer, E_C (GPa)**
0.1	0.036	0.2	0.667	0.5	20	18.5
0.15	0.082	0.3	0.567	0.5	20	16.7
0.2	0.145	0.4	0.467	0.5	20	14.2
0.25	0.227	0.5	0.367	0.5	20	10.9
0.3	0.326	0.6	0.267	0.5	20	6.9

In total five discrete compliant layer thicknesses were analysed ranging from a void radius of 0.1 to 0.3 in 0.05 increments. The Young’s modulus of the stiff layers was set to 20GPa. To reverse the order of layers in the material between stiff and complaint the values of E_s and E_c were reversed. This allowed analyses to be carried out for beams with stiff surfaces and the equivalent beams with complaint surfaces.

Additionally, to investigate the influence of the surface layer thickness on the nature of the size effect, the depth of the surface layers were altered. This was done by varying the coefficient of surface thickness, t_{SUR}, between three values 0.25, 0.5 and 1 for beams with stiff surfaces and for beams with compliant surfaces. All other parameters were maintained at constant values of $t_S = 0.5$, $t_C = 0.5$, $E_S = 20$GPa and $E_C = 1$Pa for these analyses. It was hoped that the influence of the surface region on the observed size effects could be better understood through this analysis.

4.2.3 Results and discussion

Figure 41 shows the micropolar size effect for beams with stiff surface layers. By reversing the values of E_S and E_C the case where the surface layers are compliant was also simulated. Figure 42 shows the resulting anti-micropolar size softening effect produced in the latter case.

Both trends agree qualitatively with those observed in the FE analysis of 2-dimensional beams with and without surface corrugations. This suggests the size effects predicted by FE analysis are attributable to the distribution of the stiff and complaint layers in the material, and on the nature of the surface material itself. Furthermore, both opposing complementary size effect trends are opposite in direction and show gradients of perfectly equal and opposite magnitudes (Figure 43). As this shows the gradients to be equal in magnitude and opposite in direction it follows that the micropolar material properties may be inferred from the negative gradient.

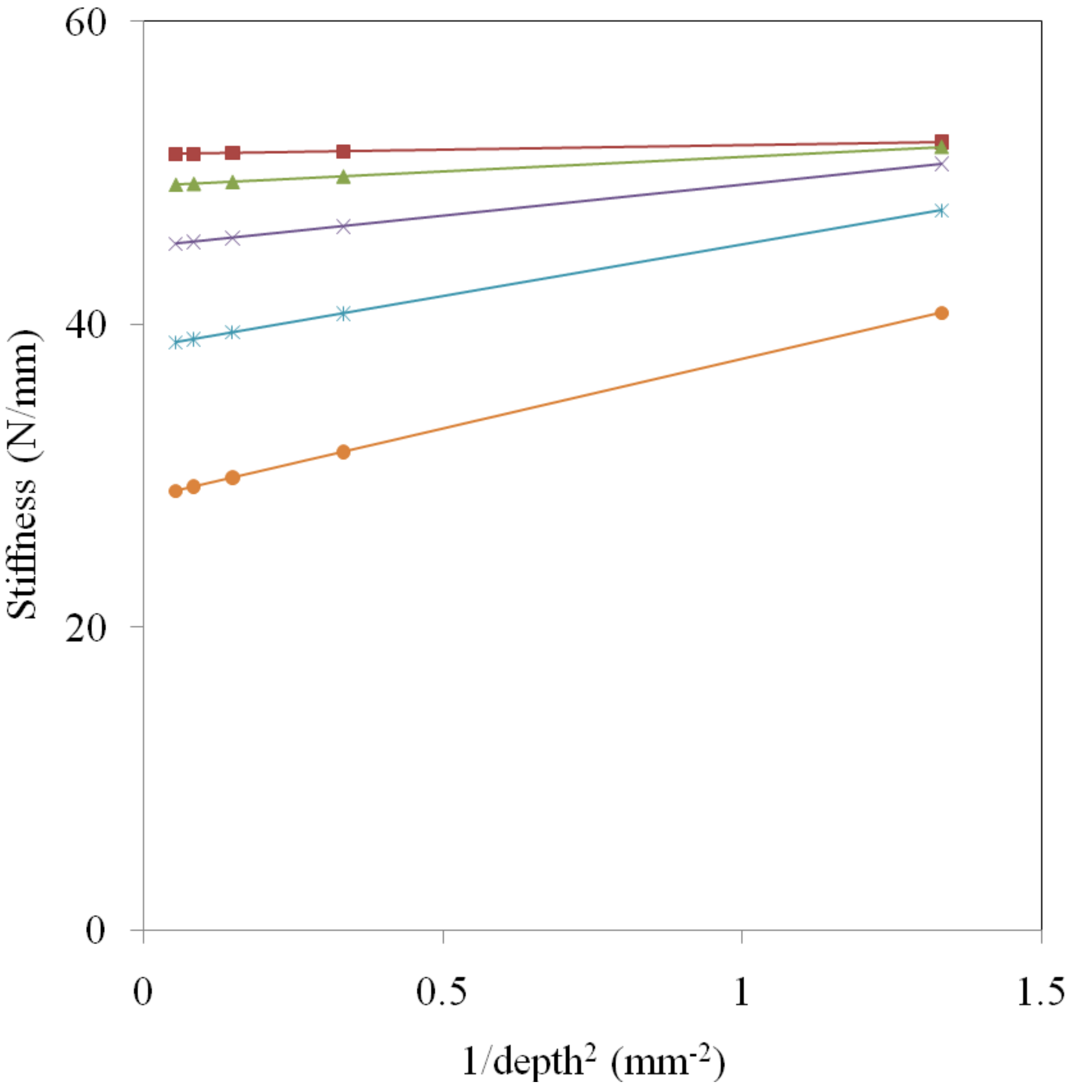

Figure 41 - Analytical stiffness for 2-D laminated model beams plotted against the reciprocal of depth squared for beams with stiff surfaces at a 10:1 length to depth aspect ratio for varying normalised void radii, V_R/S_Y. Each line represents a different void radius: Red squares, $V_R/S_Y = 0.12$; green triangles, $V_R/S_Y = 0.17$; purple crosses, $V_R/S_Y = 0.23$; blue stars, $V_R/S_Y = 0.29$; orange circles, $V_R/S_Y = 0.35$.

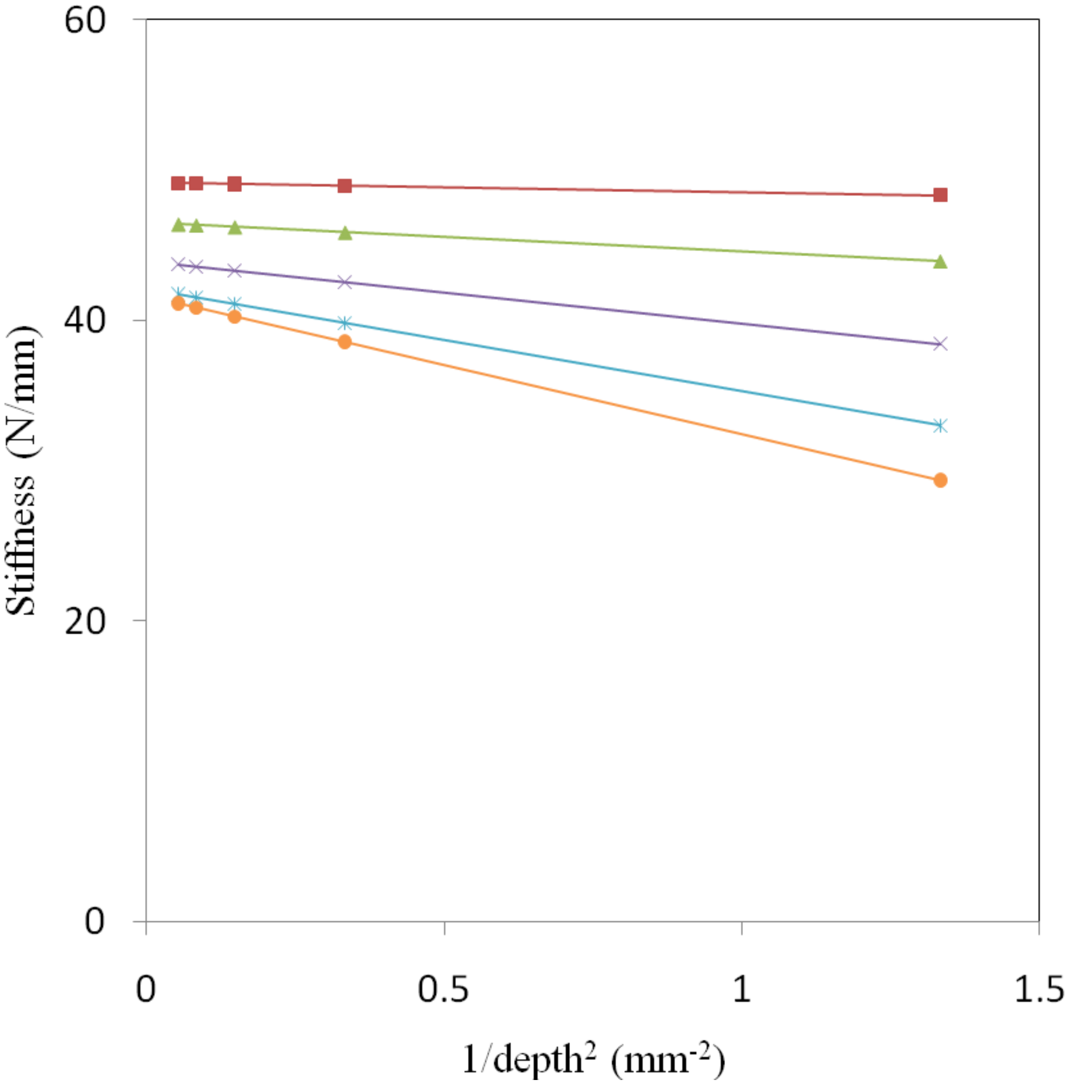

Figure 42 - Analytical stiffness for 2-D laminated model beams plotted against the reciprocal of depth squared for beams with compliant surfaces at a 10:1 length to depth aspect ratio for varying normalised void radii, V_R/S_Y. Each line represents a different void radius: Red squares, $V_R/S_Y = 0.12$; green triangles, $V_R/S_Y = 0.17$; purple crosses, $V_R/S_Y = 0.23$; blue stars, $V_R/S_Y = 0.29$; orange circles, $V_R/S_Y = 0.35$.

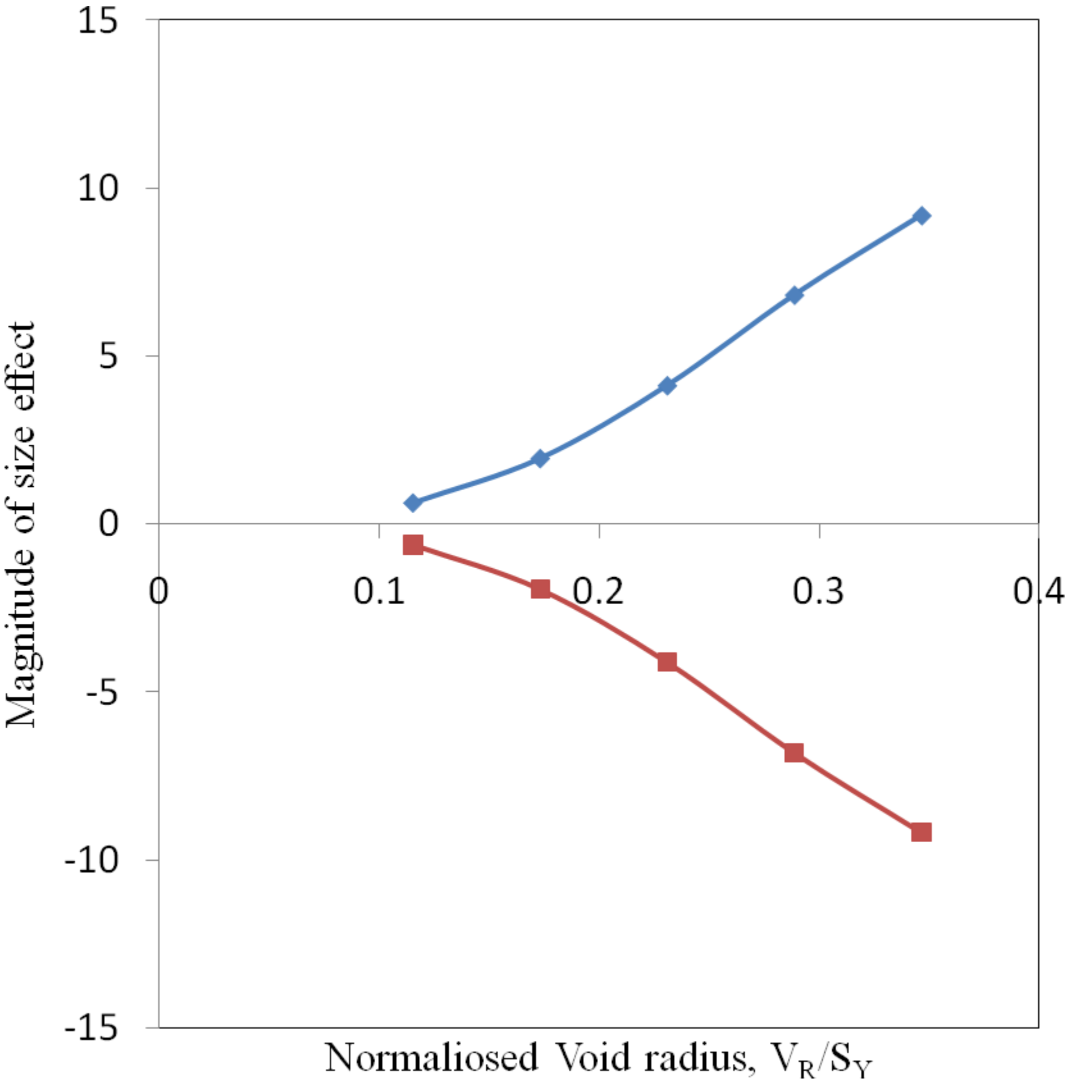

Figure 43 - Magnitude of size effect plotted against normalised void radius, V_R/S_Y for analytical 2D models where the microstructure is represented by stiff and compliant layers. The blue diamonds are for beams with continuous surfaces and the red squares represent beams with surfaces corrugated by the internal microstructure.

The surface layer thickness was varied by altering the coefficient of surface layer thickness. The results for these analyses revealed that a non-linear relationship was observed in which both micropolar and "anti-micropolar" size effect co-exist.

Figure 44 show the trends where the coefficient of surface layer thickness has been varied to either $t_{SUR} = 0.25$ or $t_{SUR} = 1$. It is apparent that the identification of any size effect present under such conditions is partially masked by the surface condition. It can be seen that for the models where the surface layer is compliant and the thickness is less than the internal layer thicknesses (Figure 44d) the same non-linear trend is observed as was exhibited in the FE models for beams with smaller surface voids (Figure 37). This adds further evidence to the influence of the surface regions as being of fundamental importance in understanding the micropolar size effect trends observed in real materials

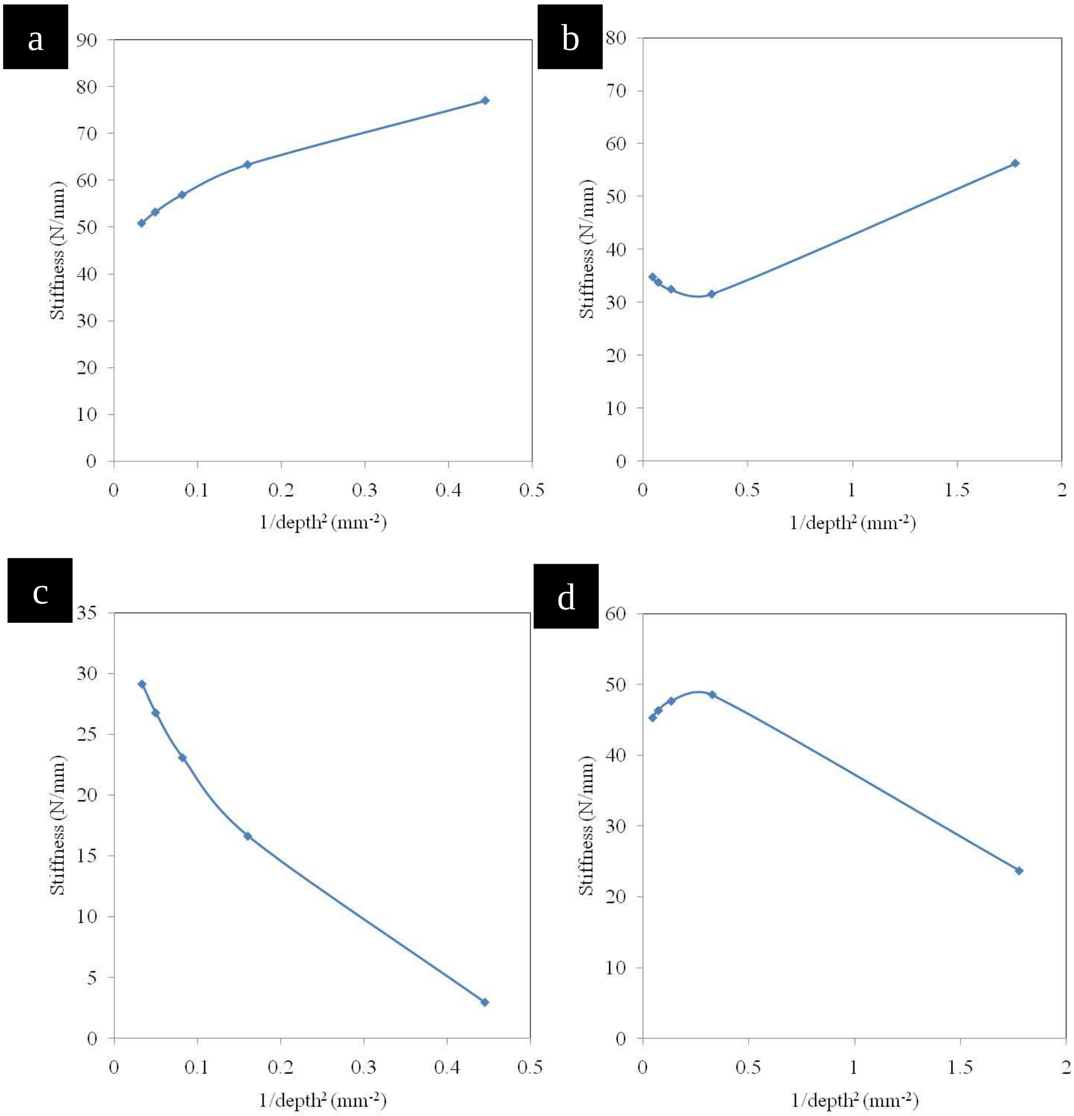

Figure 44 – a. Size effect trend produced where t_{SUR} = 1 for beams with a stiff surface b. Size effect trend produced where t_{SUR} = 0.25 for beams with a stiff surface c. Size effect trend produced where t_{SUR} = 1 for beams with a compliant surface d. Size effect trend produced where t_{SUR} = 0.25for beams with a stiff surface

4.3 Analytical models for 2D beams: Relationships between micropolar material properties and microstructural features

It has already been demonstrated in the FE analysis section that there is a strong relationship between the microstructure of heterogeneous materials in the form of the void diameter and the micropolar characteristic length. It follows that where the microstructure is represented as a series of compliant and stiff layers that a relationship between stiff and compliant layer thicknesses, stiff and complaint Young's moduli and micropolar material properties may exist. In order to investigate this, a parameter study was undertaken where the input parameters of the layer thicknesses and Young's moduli were varied and compared with the output parameters of micropolar characteristic length and micropolar Young's modulus.

4.3.1 **Methodology**

The same input parameters were defined as in the previous section investigating the size effect trends in idealised layered 2-D models. For this study the coefficient of surface layer thickness was maintained at 0.5 in order to ensure a linear size effect trend was created for each analysis. The four other input parameters were defined as the thickness of the stiff layer, t_S, the thickness of the compliant layer, t_C, the thicknesses of the stiff and compliant layers.

4.3.2 **Results and discussion**

The micropolar Young's modulus is related to the axial modulus of the summated heterogeneous beam as the equivalent modulus representative of the entire material. The combined Young's Modulus for the composite beams corresponds with the proportional summation of each constituent material in the beam and is given by Equation 22.

Equation 22

$$E_M = \frac{T_S}{T_S + T_C} E_S + \frac{T_C}{T_S + T_C} E_C$$

where T_S is the total thickness of the stiff layers, T_C is the total thickness of the compliant layers. It was found empirically that for scenarios where the Young's modulus of the stiff and compliant layers were of significantly different orders of magnitude, where the compliant layer had a stiffness of effectively zero in comparison to the stiff layer, that the characteristic length was defined by Equation 23.

Equation 23

$$l_c^2 = 2t_c^2 + t_c t_s$$

Equation 23 demonstrates that where the ratio of E_S to E_C approaches infinity (as defined in the assumptions where $E_S >> E_C$) the characteristic length is described by the thicknesses of the stiff and complaint layers alone. However, for situations where the Young's Moduli of the stiff and compliant layers were of similar orders of magnitude Equation 23 was found to not hold true. For materials where the stiffness of each individual layer is of a similar order of magnitude a more general form of Equation 23 is needed. This case is more relevant to cortical bone where the heterogeneity in the material may be more attributable to voids reducing the local stiffness and some regions of demineralisation.

A second empirical analysis was conducted where the Young's modulus of each layer was set to similar orders of magnitude to one another and the layer thicknesses were maintained at the same values of 0.5 each. In this scenario it was observed that the micropolar characteristic length followed an asymptotic relationship when plotted against the ratio of stiff to compliant Young's Moduli as is shown in Figure 45.

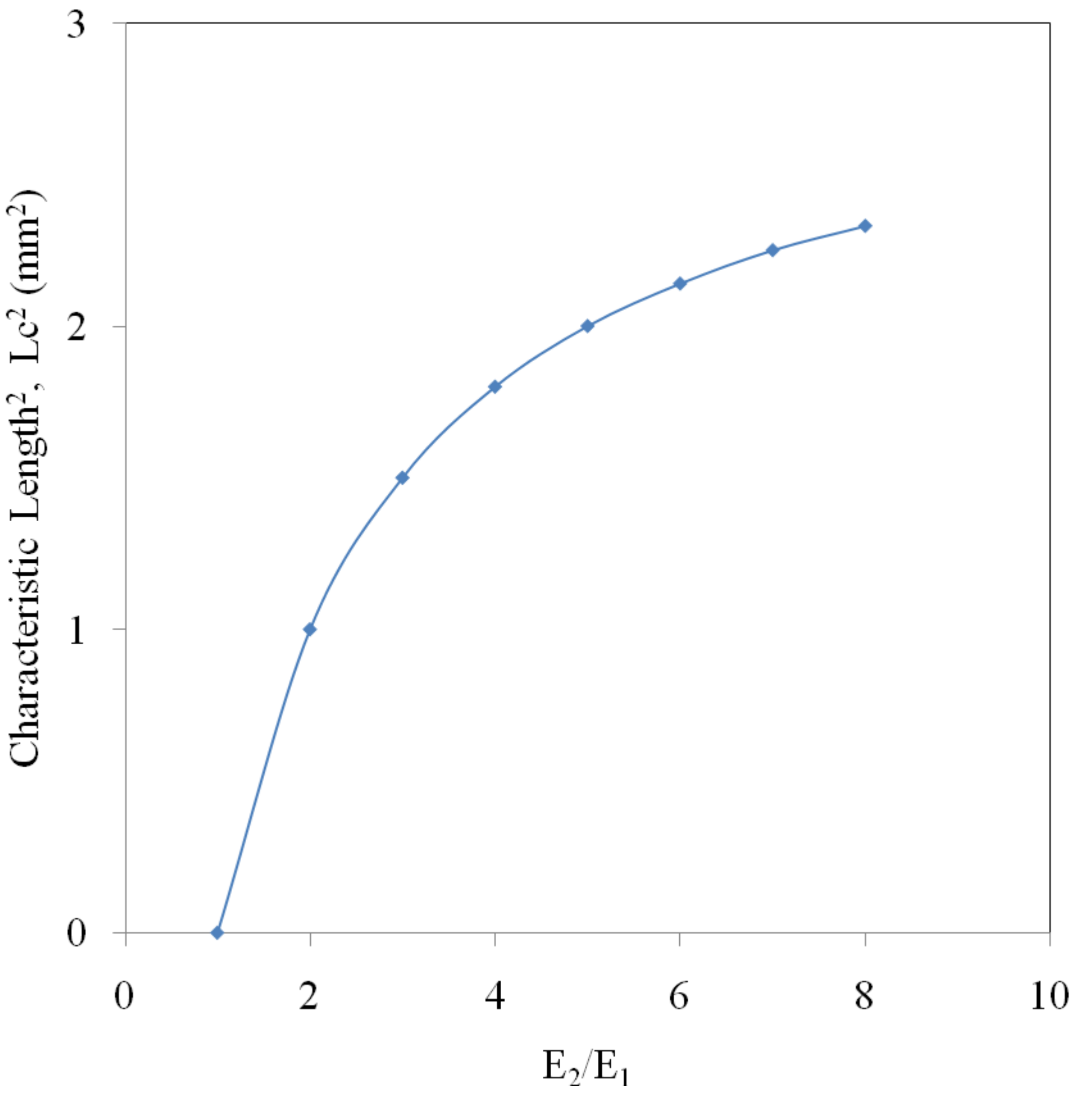

Figure 45 - Relationship between characteristic length and ratio of stiff to complaint Young's Moduli for the 2D layered beam models

The relationship between the four input parameters of stiff and compliant layer thickness and stiff and complaint Young's Moduli was obtained empirically and is given in Equation 24.

Equation 24

$$l_c^2 = \frac{(2t_c^2 + t_c t_s)(E_s - E_c)}{(E_s + E_c)}$$

It is worth noting that the characteristic length is defined by the same expression as in Equation 23 with an additional term relating the Young's modulus values of the stiff and compliant layers. The additional term relating Young's modulus values will tend to unity as the ratio of stiff to compliant modulus approaches infinity therefore producing Equation 23. From Equation 24 it is apparent that the degree of size effect present in a heterogeneous material can be predicted by the geometrical nature and character of the microstructure and its constituent phases.

Table 9 – A comparison between the empirical equations and the closed form analytical equation for the micropolar characteristic length.

Compliant layer thickness, t_C (mm)	**Stiff layer thickness, t_S (mm)**	**Complaint layer Young's modulus, E_C (GPa)**	**Stiff layer Young's modulus, E_S (GPa)**	**l_c^2 from Equation 24 (mm^2)**	**l_c^2 from Equation 23 (mm^2)**	**l_c^2 from Equation 10 (mm^2)**
0.5	0.5	1E-9	20	0.750	0.750	0.750
0.4	0.8	1E-9	20	0.640	0.640	0.640
0.5	0.5	18	20	0.039	0.750	0.039
0.4	0.8	18	20	0.034	0.640	0.044

However, a general expression for all four input variables has not been empirically observed. Table 9 highlights the accuracy of the empirically found expressions for characteristic length with that of the closed form analytical solution of Equation 10. It can be seen that for conditions where the Young's moduli of the stiff and compliant layers are of significantly different orders of magnitude Equation 23 provides an accurate value for the micropolar characteristic length. As the Young's moduli for stiff and compliant layers approach one another it can be seen that Equation 23 no longer accurately predicts the micropolar characteristic length and that Equation 24 gives a more accurate value. However, for input values where the thicknesses and the Young's moduli of the stiff and compliant layers significantly differ Equation 24 no longer accurately predicts the micropolar characteristic length. A general equation which accurately predicts the micropolar characteristic length for all input conditions has not been found.

4.3.3 **Validation of empirical expressions**

To validate the appropriateness of Equation 23 and Equation 24 an analytical study was undertaken to determine if the same expressions were derivable from analysis of the layered material in bending.

The stiffness of a two layered beam (a beam with one compliant layer in the centre and stiff layers on each surface) may be represented in terms of the input parameters t_S, t_C, E_S and E_C.

Equation 25

$$K = \frac{48}{l^3}\left[\frac{E_c b t_c^3}{12} + 2E_s\left(\frac{b\left(\frac{t_s}{2}\right)^2}{12} + b\left(\frac{t_2}{2}\right)\left(\frac{t_c}{2}+\frac{t_s}{4}\right)^2\right)\right]$$

If the assumptions are made that the thickness of the stiff and compliant layers are equal ($t_C = t_S = t_L$) and the Young's modulus of the stiff layer is several orders of magnitude stiffer than the compliant layer ($E_S >> E_C$) so that the stiffness of the compliant layers may be considered to be effectively zero Equation 23 and Equation 24 are simplified to:

Equation 26

$$l_c^2 = 3t_L^2$$

and Equation 22 becomes:

Equation 27

$$E_m = \frac{E_S}{2}$$

Then Equation 25 may be simplified to

Equation 28

$$K = \frac{48b}{l^3}\left[\frac{E_s t_L^3}{4} + \frac{9E_s t_L^3}{16}\right] = \frac{28b}{l^3}\left[E_s t_L^3\right]$$

Equation 28 may also be arrived at by directly inputting the expressions for micropolar characteristic length and micropolar Young's modulus into Equation 10. If the depth of a layered beam is defined as

Equation 29

$$d = nt_L$$

where n is the number of layers in the beam (in this case for a double layered beam n = 2).

Equation 30

$$K = 4\frac{E_S}{2}b\frac{d^3}{l^3}\left(1+\frac{3t_L^2}{(nt_L)^2}\right) = \frac{28b}{l^3}\left[E_S t_L^3\right]$$

This demonstrates that for this simplified scenario, where the stiff and compliant layers are of the same thickness and the Young's moduli of the stiff and compliant layers are of several orders of magnitude difference, it is possible to extract micropolar material properties analytically from an analytical three-point bending analysis. For more complex conditions where the stiffness of the different layers approach one another in terms of magnitude and the dimensions of the layers are divergent an analytical derivation of the micropolar material properties in terms of the geometrical features is no longer resolvable by straight forward analytical means.

4.4 Analytical modelling discussion

The analytical models show that the size effect trends predicted by the FE models are attributable to the geometrical microstructural features of the models. The second moment of area is the primary descriptive measure of the distribution of mass in each beam, and as such allows a quantitative description of the void arrangement and how this influences the beam stiffness. In terms of the micropolar material properties it may be possible to understand the relationship between stiffness and second moment of area in terms of the fundamental micropolar stress formulation. Where the micropolar second moment of area is reduced from the classically elastic value it is in effect describing the inability of shear forces to be transferred through the material because of material discontinuities (Figure 46). This is manifested in a reduced second moment of area. Moreover it may also be expressed through a reduced Young's modulus for discrete regions of the material.

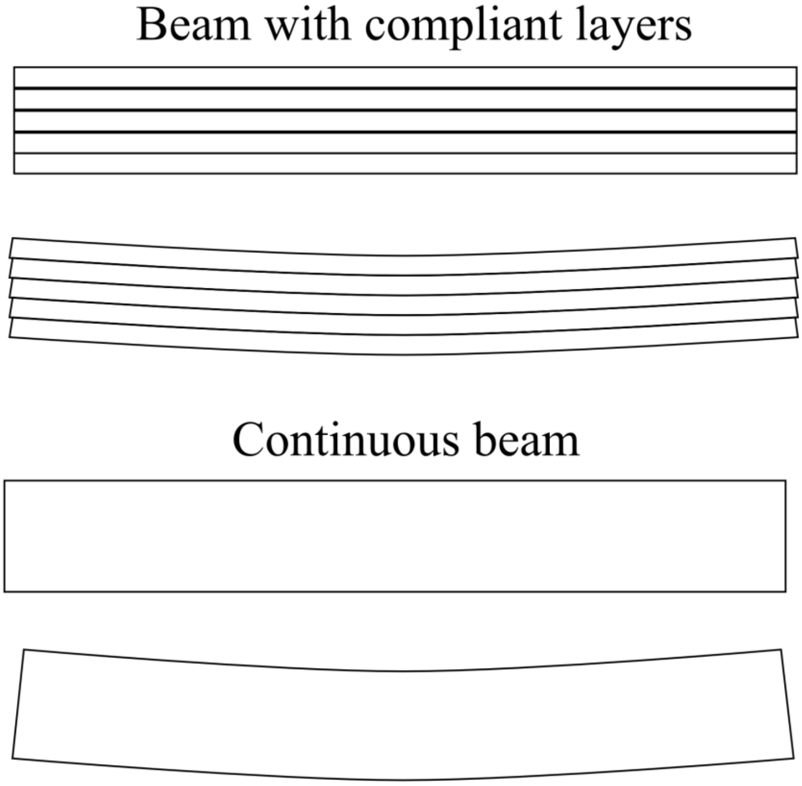

Figure 46 – The difference between a continuous beam and a beam with compliant layers in bending.

In relation to cortical bone a reduction in localised material stiffness may be a consequence of the presence of vascular channels or could also be caused by the variation in material properties throughout the constitutive components of the material. For example cement lines are regarded as hypo-mineralised regions of cortical bone and may indicate a location where loading is not transferred through the material. A similar method has been used previously to investigate the behaviour of a single osteon by modelling the structure of the lamellar layers as elastic compound models (Braidotti et al. 1995). The model created here tLakes the single osteon model further by averaging the entire microstructure of cortical bone into discrete layers of differing elastic properties (Forest et al. 2000). Lakes hypothesised this to be one of the fundamental reasons for the micropolar behaviour which was observed in torsion and bending tests on cortical bone (Park & R. Lakes 1986; R. Yang & Lakes 1982). Because of the complexity of cortical bone and the multiple heterogeneous features of its microstructure it may be true that Lakes' observed micropolar material properties are describing various microstructural features in the material. For example, the micropolar characteristic length in bending could be describing a material characteristic associated with the distance between cement lines and the separation of vascular channels. Therefore the simplified descriptions used here would not fully predict the full extent of Lakes' experimentally observed material behaviour.

For the experimental testing of a real material such as cortical bone the results from the analytical analyses reveal that the determination of the character of the surface region is of the utmost importance in being able to quantify the micropolar material properties. Where the surface region is not only broken by the internal microstructure, but is also influenced by varying degrees of surface thickness and quality then a non-linear size effect trend is predicted. This effect validates the numerical analysis of beams with smaller surface voids which indicates that where the surface exhibits smaller surface voids than the internal microstructure a non-linear anti-micropolar size effect trend is predicted. However, in practice, the preparation of the surface layer will induce an artefact onto the surface but will not remove the underlying internal microstructure. This implies that although there is an artefact on the surface the microstructure of the material itself will also be present. It is therefore important in the experimental analysis of cortical bone to be aware that where the surface is prepared to be smooth there will be microstructure revealed and therefore a negative anti-micropolar size effect would be more expected than a positive trend. Moreover, the nature of the size effect might be more likely to follow a linear trend with perhaps a slight non-linearity induced through the introduction of an artefact attributable to the preparation methods.

4.5 Conclusion

The analytical models confirm the size effect observed in the FE models associated with microstructural detail. The analytics agree with the FE models which include this microstructural detail. This has helped in identifying the underlying causes of the material behaviour and the planning for experimentation on cortical bone. Size effects in three-point bending tests on heterogeneous materials are highly dependent of the nature of the surface. Understanding the size effect experimentally observed is dependent on the nature of the surface of the test specimen and the character of the surface layer in relation to the underlying material microstructure.

It has also been shown that the micropolar material properties can be related to the geometrical and localised material features in the global material. This is a relevant finding for understanding the causes of size effects and in relating the observed size effect to the geometry of the microstructure. It also indicates the predictive ability of detailed knowledge of the microstructure in being able to understand the micropolar material properties of heterogeneous materials. This is consistent with the findings of the FE study which indicated that the void diameter was a predictive feature for the micropolar Young’s modulus. The closed form analyses which have been looked at in this chapter indicate that for materials with microstructures it is possible to simplify the model in broad regions of microstructure which will then be relatable to the global micropolar constitutive material properties. In short, it has been demonstrated that micropolar material properties have a physical significance which is related to the microstructure of the heterogeneous material which micropolar elasticity is describing.

5 Anticlastic effects

5.1 Background

Experimentally testing small specimens is a potentially challenging task. It becomes increasingly difficult when it is important for the surface condition of each specimen to be controlled. For this reason a study into the possibility of creating suitably wide specimens for experimentation was undertaken. Wide beams would enable a consistent surface condition to be maintained even as the specimen sizes were reduced.

The flexural stiffness of a beam in three-point-bending may be expressed as

Equation 31

$$K = 48E^{*}I/L^{3}$$

Where K is the flexural stiffness, E* is the apparent material Young's modulus, I is the second moment of area, and L is the Length of the beam. For a beam with a narrow cross section where the depth is larger than the breadth the beam may be considered as behaving in plane stress. For the plane stress condition the apparent Young's modulus, E*, of the material in bending is equal to the true material Young's modulus, E, as would be observed in an extension or compression test. This is demonstrated in Equation 32 and holds true where the Young's modulus of the beam is independent of the strain.

Equation 32

$$K = 48EI/L^{3}$$

One of the assumptions in Equation 32, in relation to a beam of rectangular cross section, is that the beam behaves in plane stress through the breadth of the beam. This approximation is true for narrow beams, however for beams with a significantly large breadth to depth ratios this assumption no longer holds (Figure 47). Where the breadth becomes significantly large in relation to the depth of the beam plate bending theory more accurately describes the behaviour. In plate bending theory for a "wide beam" the beam may be thought of as acting according to plane strain rather than plane stress in the “narrow beam” case. Therefore, for a “wide beam” the stiffness expression may be written as (Swanson 2001).

Equation 33

$$K = 48\left(\frac{E}{1-\upsilon^2}\right)I \Big/ L^3$$

where the symbols have their usual meanings and ν represents Poisson’s ratio. It can be seen from the equation above that a wider beam will appear relatively stiffer than the narrow beam. This is due to the influence of Poisson’s ratio on the material and the constraint on the transverse contractions during bending.

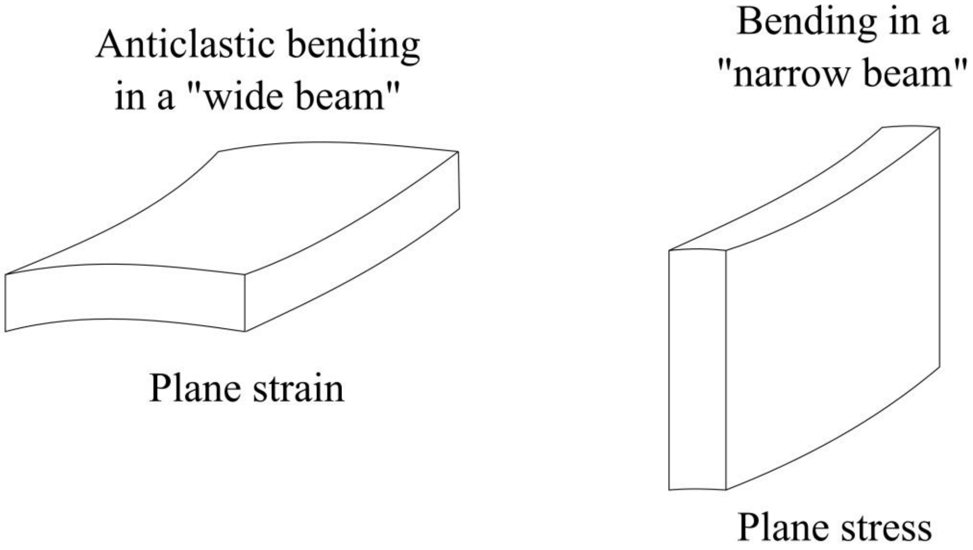

Figure 47 – Plane strain bending in a “wide beam” showing the anticlastic effect and plane stress bending in a “narrow beam”

Ambiguity emerges where the beam is neither obviously narrow nor obviously wide, or is neither behaving in accordance with plane stress nor plane strain, but somewhere between. This is specifically important for ratios of breadth to depth between 2:1 and 5:1. In such cases the transverse stresses in the beam become significant enough to produce an anticlastic bending (Figure 47), however the effect is not pronounced enough to produce the plane strain condition required for the pure plane strain conditions of plate bending.

Saint-Venant (1856) derived a series solution for three-point flexure under the assumption that no transverse stresses occur in the specimen (Equation 34). It can be adapted to estimate the variation of apparent elastic modulus with breadth to thickness ratio and Poisson's ratio (Equation 35).

Equation 34

$$E*(b/d\,,\nu) = E\bigg/\left\{1 + 12\left(\frac{\nu}{\pi}\right)^2 \sum_{n=1}^{\infty} \frac{(-1)^n}{n^2 \cosh(n\pi\, d/b)}\right\}$$

Equation 35

$$E* = E/((1-(f(b/d))\upsilon^2))$$

Where the symbols have their usual meaning; *d* represents the beam depth and *b* is the beam breadth, *f(b/d)* is a function of the breadth to depth ratio which describes the transition between plane stress and plane strain. The apparent modulus E^* is related to the Young's modulus by *f(b/d)* which represents the transition between plane stress and plane strain. When *f(b/d)* is equal to unity the apparent modulus, *E**, is equivalent to the plane strain modulus, $E/(1-v^2)$. On the other hand when *f(b/d)* approaches zero the beam behaves in accordance with plane stress where the apparent modulus, *E**, is equivalent to the material Young's modulus, *E*.

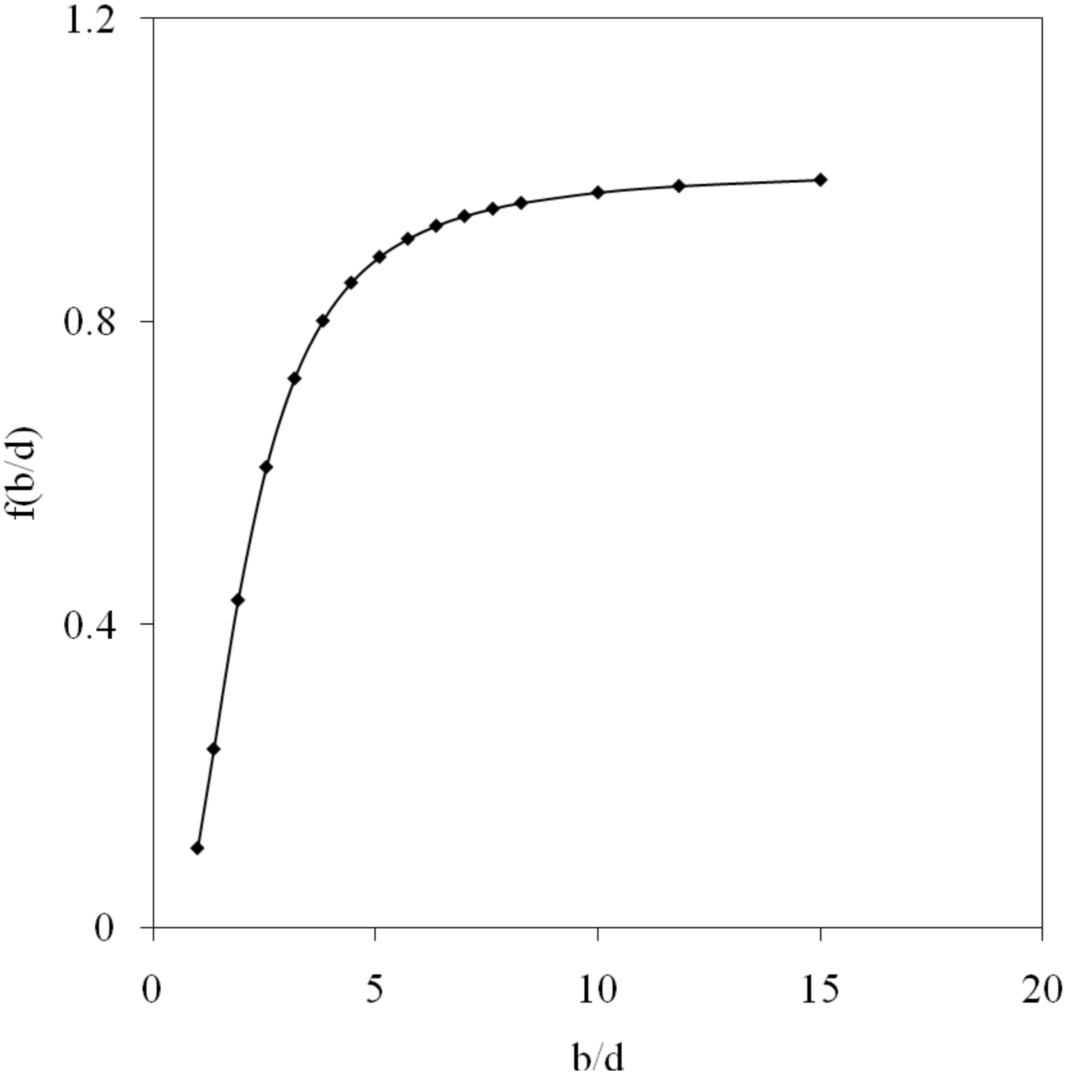

Figure 48 – The function of b/d relating the apparent and true Young's Modulus of the material when 40 term were taken in the Saint-Venant series solution to represent infinity Equation 34.

The transition between plane stress and plane strain was calculated for the Saint-Venant series solution where 40 was chosen to represent infinity as a good approximation thus allowing the function *f(b/d)* in Equation 35 to be defined, this function is plotted against the ratio of breadth to depth in Figure 48.

An investigation into the significance of the anticlastic effects and their importance towards future experiments on cortical bone was undertaken. In particular to obtain a fuller understanding of the transition region between plane stress and plane strain in both the computational models and the experimental results FE models were created where the breadth to depth aspect ratio was altered and the apparent Young’s modulus was calculated.

5.2 Finite Element Analysis of the anticlastic effect in three-point bending

A series of finite element models were created in order to analyse the influence of the anticlastic effect on flexural three-point bending experiments.

5.2.1 **Methodology**

A quarter size FE model was created using ANSYS 12.1 using the same boundary and loading conditions as in the 3-dimensional FE bending analyses (Figure 24 section 3.6.1 p66). The models created for this study were isotropic and did not contain any microstructural voids, this was to reduce the complexity of the models and allow a clear interpretation of the anticlastic effect in the results. Symmetries and anti-symmetries were utilised to reduce the complexity of the model. A line load was applied to represent the supports in three point-bending and the beam was pinned in the y-axis along the x-centre line at half the length of the beam.

The beam length and depth were maintained at 50 and 5mm respectively while the beam breadth was varied at intervals between 5 and 50mm in order to simulate a full range of breadth to depth ratios. Isotropic material properties were used with a Young’s modulus of 20GPa and Poisson’s ratio of 0.3. The linear elastic 20-noded brick element 183 was used for the analysis.

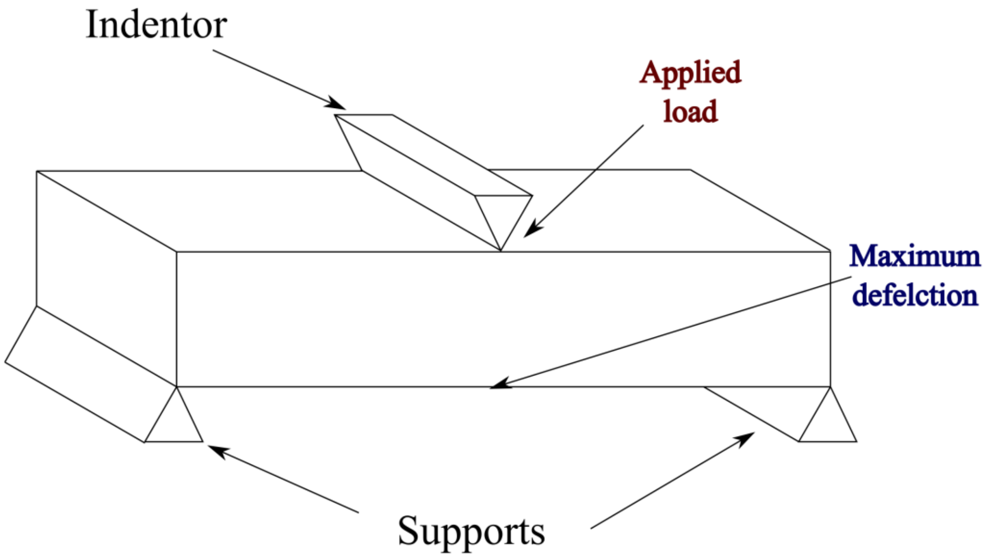

Figure 49 - Three-point bending loading conditions and load deflection measurement locations. These loading conditions were used for the global simulations and measurements.

In addition to a three point-bending model (Figure 49) a pure bending moment model was created (Figure 50). For this model the same quarter size geometry was used as in the three-point bending model but a linearly varying pressure load was applied to the end of the beam to replicate a pure moment action. This model used the same material properties and mesh as the 3-point-bending model. The same range of lengths, breadths and depths were analysed for both models.

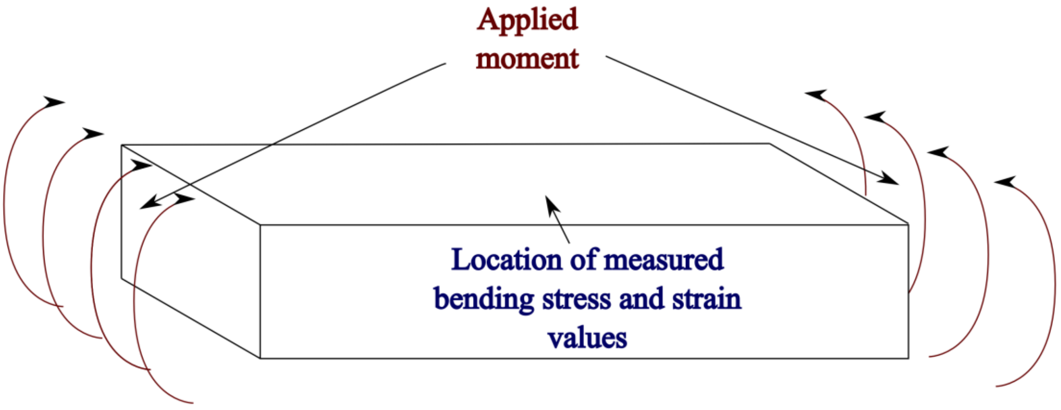

Figure 50 - Pure moment loading conditions showing the location of the measured bending stress and strain values. These loading conditions were used for the local simulations and measurements.

For both methods the apparent Young's modulus, E^*, of the beam was calculated. In addition, by using the change in apparent modulus and the change in the ratio of *b/d*, the value of *f(b/d)* was calculated. The apparent Young's modulus was calculated from both stress-strain (local) values and load-deflection (global) values for both models.

For the three-point bending model the flexural deflection was read as the value on the centre of the bottom surface of the beam directly below where the load was applied. The flexural stiffness was then calculated from the applied load divided by the deflection. From this value the apparent Young's modulus of the beam in bending was calculated. After varying the breadth the change in Young's modulus was compared to determine the influence of breadth to the stiffness of the beam.

In conjunction with this nodal stress and strain values along the main axis of bending were taken at the top surface centre point in the beam, where the highest localised stress was likely to occur. From this the apparent Young's modulus was calculated directly from the ratio of localised nodal stress to strain.

For the pure moment bending analysis the same process was undertaken; both load-deflection and stress-strain (global and local) results were calculated. The applied load was calculated from the applied moment value and the Young's modulus calculated from the applied moment-deflection values as shown in Equation 36.

Equation 36

$$E^* = \frac{ML^2}{8\delta I}$$

where E^* is the apparent Young's modulus, M is the applied moment, L is the length of the beam, δ is the beam deflection, and I is the second moment of area.

5.2.2 **Results and discussion**

Figure 51 and Figure 52 show the results for the applied moment and three-point bending simulations. Local calculations for the apparent Young's modulus in both the moment and three-point bending simulations follow the trends predicted by the analytical solutions in Equation 33 and shown in Figure 48. However, the global load-deflection results follow a less dramatic trend and the anticlastic effect appears to have a much lower impact upon the change in flexural stiffness compared to local Young's modulus values in the material. Although this trend follows for both the pure moment and three-point bending models, there is more of a noticeable influence of the anticlastic effect in beams under three-point bending loading than under pure bending. In pure bending the maximum influence of the anticlastic effect on the flexural stiffness occurs at a 10:1 breadth to depth aspect ratio where *f(b/d)* is 0.2. The equivalent value for the three-point bending results show *f(b/d)* to be higher at around 0.5. Both of these values are significantly lower than those predicted by Saint-Venant analytical solution and those calculated from the localised stress-strain results from the same models.

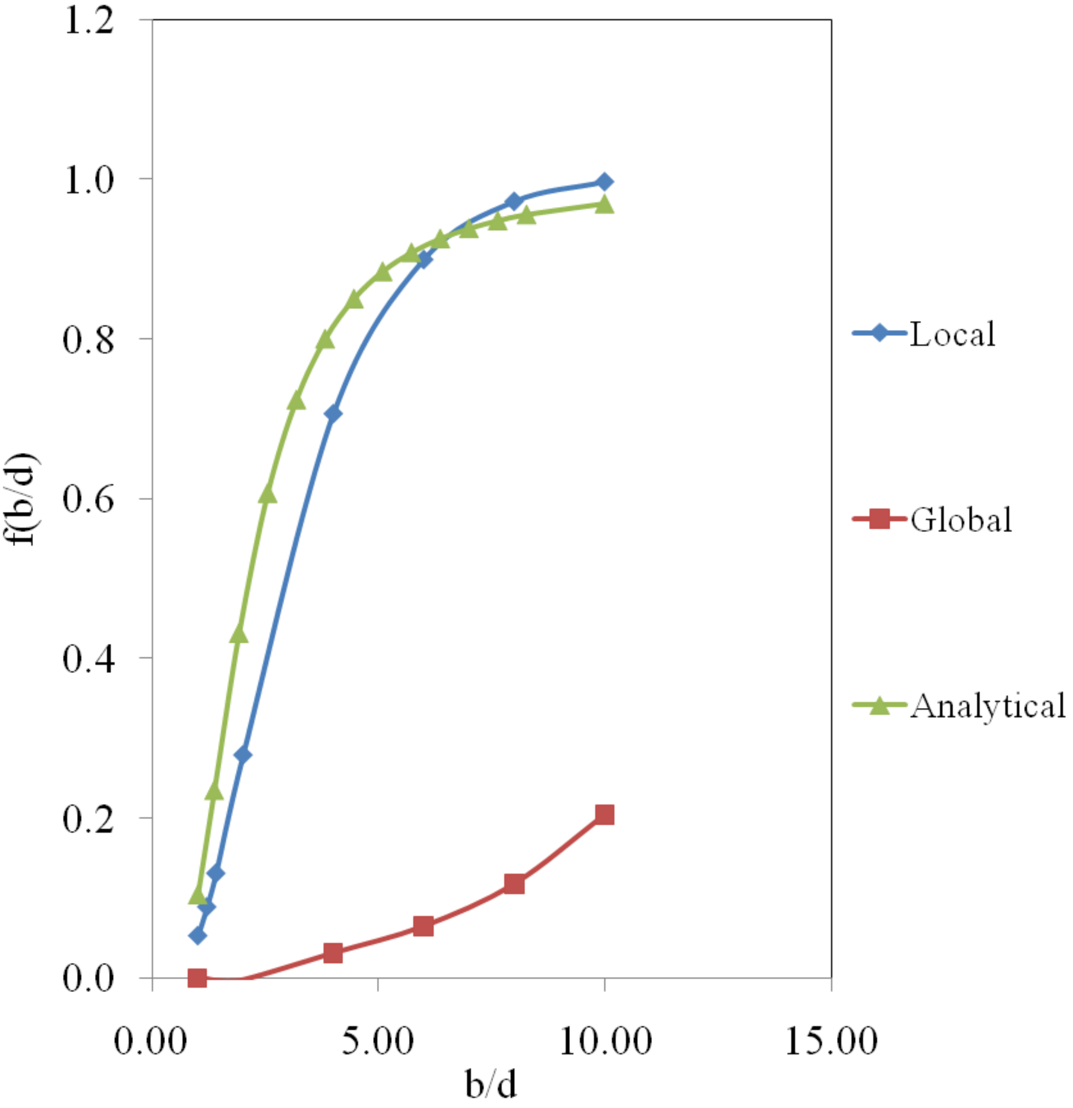

Figure 51 – Comparison of the pure bending moment results of f(b/d) against b/d for load-deflection and stress-strain with the analytical solution. The local results are shown by the blue diamonds. The global results are shown by the red squares. And the analytical solution is shown by the green triangles.

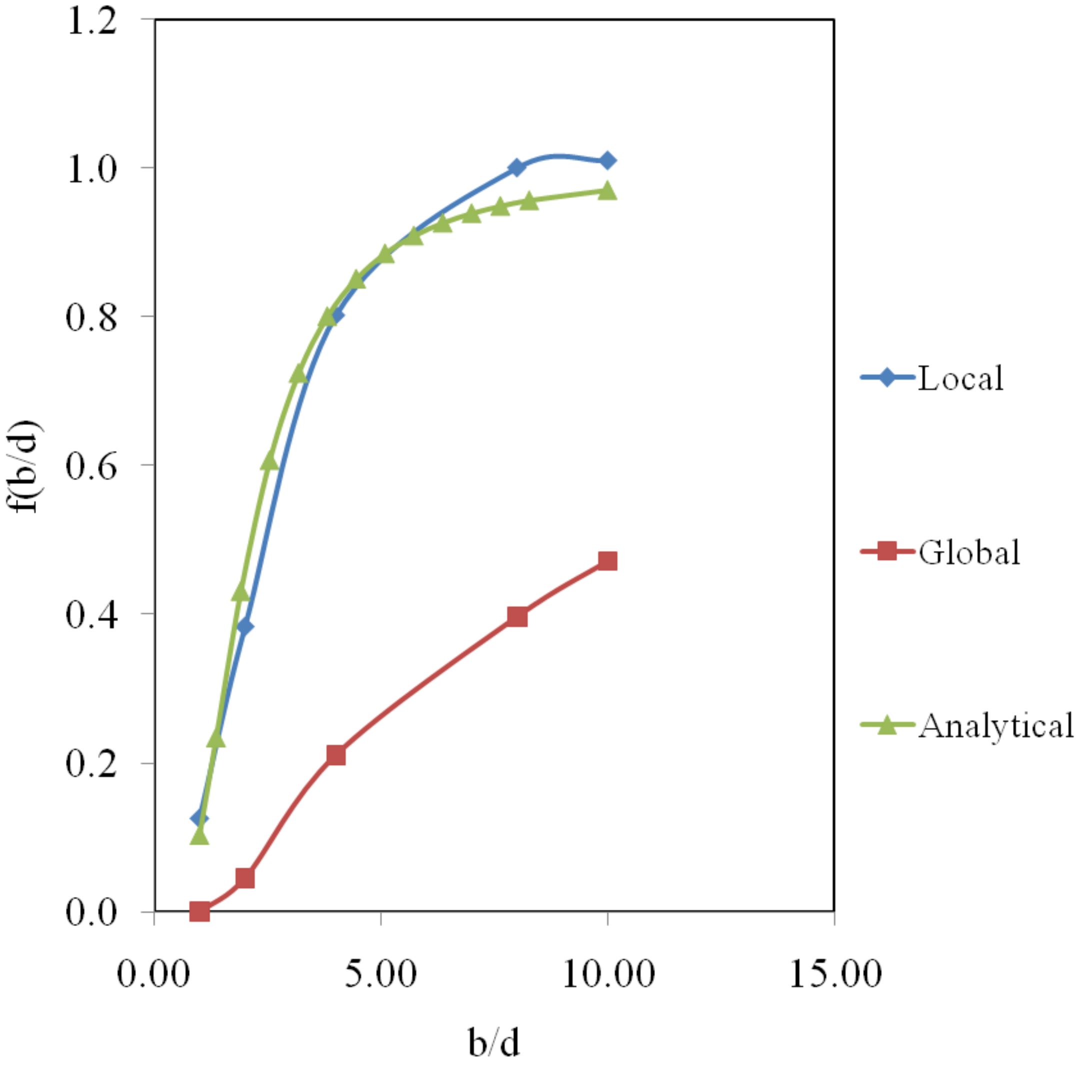

Figure 52 - Comparison of the three-point bending results of f(b/d) against b/d for load-deflection and stress-strain with the analytical solution. The local results are shown by the blue diamonds. The global results are shown by the red squares. And the analytical solution is shown by the green triangles.

The finite element analysis results suggest that anticlastic effects in beams in three-point-bending follow analytical trends. However, there is a discrepancy between global and local trends for beam stiffness. Stress-strain (local) values for Young's modulus follow the analytical trend of anticlastic behaviour, however the load-deflection (global) values show a much less significant variation in stiffness as the beam breadth is increased.

The results suggest that anticlastic effects are important in local stresses in the material in bending, especially along geometrically significant regions, such as the centre line of the beam. However when the global geometry is considered the influence of anticlastic transverse stresses become much less significant (the results suggest the effect is at least halved for the largest *b/d* aspect ratio), and are averaged for the entire geometry. As a result the general plane stress analytical expression for a beam in three-point bending where the apparent Young's modulus is represented by the material Young's modulus appears to hold for "wide beams" in three-point bending, and may be considered a close approximation to the true bending behaviour independent of beam breadth.

By taking the global results from the three-point bending analyses an upper extreme may be calculated for the influence of the anticlastic effect in three-point bending experiments. From Figure 52 a b/d aspect ratio of 10:1 produces a value for *f(b/d)* of approximately 0.5. Applying this value to Equation 35 shows that for a Poisson's ratio of 0.3 the apparent Young's modulus is less than 5% different than that predicted by the plane stress solution in Equation 32. This change is well below that predicted by the analytic solution for anticlastic behaviour and suggests it falls within the region of potential experimental error. For this reason the plane stress solution for the flexural stiffness of a beam in three-point bending has been deemed to be a close approximation of the global beam stiffness in wider beams despite the influence of the varying breadth to depth aspect ratio.

5.3 Summary of findings and relevance to subsequent experimental procedure

In order to detect a size effect experimentally a series of specimens need to be tested at varying sizes in three-point bending. The geometric dimensions of the specimens produced should be of the order of the microstructure which is thought to influence the material behaviour. In the case of cortical bone the microstructure is of the scale of the Haversian canal system. Therefore, to detect an observable size effect, specimens below 1mm in depth are required. The practicalities of generating specimens of a 1mm square cross section are quite restrictive. Furthermore it has been demonstrated that surface preparation is of fundamental importance to understanding the experimental results. To control the surface condition sufficiently wide beams are much more pragmatic in terms of consistent experimental protocol.

A more practical approach to specimen preparation is to create specimens of a standard breadth and a variable length and depth. The implied complication with this approach is that as the beams are reduced in depth the ratio of breadth to depth increases therefore increasing the stiffness of the beam through the anticlastic effect.

What the FE results suggest is that, when the flexural stiffness is measured, the anticlastic effect has a much reduced influence on the beam’s stiffness than has been suggested in the analytical solution of Saint-Venant. The results suggest the plane stress conditions are an accurate representation of the global stiffness of a wide beam in three-point bending and show that even at a 10:1 breadth to depth aspect ratio the anticlastic effect is roughly half what is predicted by the analytical solutions..

For this reason it was deemed viable in experiments to maintain the beam breadth and vary the depth and length of the beams between tests as although anticlastic effects are not insignificant they are within the experimental error which would be expected in such experiments. Moreover the practicalities of consistently preparing specimens with a fixed breadth are far more practical than preparing specimens with square cross sections.

6 Experimental Methodology Development

6.1 Background

Before three-point bending experiments could be carried out on bovine cortical bone specimens several factors had to be considered in order to enable the most effective experimental protocol to be devised. The following discusses the most important pre-experimentation factors which were considered.

The mineral content of cortical bone is reported as being between 70 to 75 g/cm^3 which accounts for approximately 75% of bone content (Burstein et al. 1975; Martin & Boardman 1993; J Y Rho et al. 1998). Both the mineral and organic phases contribute towards the material stiffness of cortical bone however the mineral content is the main contributor towards the Young's Modulus before yield. After yield the organic phase contributes to the toughness of the material (Burstein et al. 1975). Together they make a strong and tough material, but when either phase is reduced or the balance between mineral and organic phases is altered the material properties are dramatically changed. Where the mineral content is slightly reduced there is a dramatic reduction in the pre-yield Young's Modulus value. The demineralization of cortical bone is observed to significantly reduce the strength of bones in osteoporotic patients and is a main cause of bone fractures in elderly patients (Hasegawa et al. 1995). For this reason it was decided that the mineral content of the test specimens should be monitored.

The FE analysis revealed that in idealised heterogeneous materials the nature of the surface is of primary importance in understanding the mechanical response of the material in bending. If the surface is intersected by the internal microstructure a size softening size effect is observed whereas if the surface is continuous and smooth a size stiffening size effect is observed. For this reason the quantification of surface roughness was taken as an important measure of the degree to which the surface was either intersected by the underlying microstructure or damaged by the preparation methodology. Moreover, it was decided that the surface of each specimen should be prepared to be as smooth as possible with the available equipment in order to remove the influence of surface artefacts introduced by the preparation equipment, such as the bone saw. Polishing itself would introduce surface relief where bone tissue would be removed preferentially in areas of specific HAP orientation. Although this would interfere with the surface character and introduce an artefact itself which would not normally be exhibited it would enable the surface to be prepared to a standard condition which could be replicated in every specimen. If this induced surface condition could then be quantified then it would be possible to determine a better impression of the true material properties. Furthermore, if the surface was prepared to be as smooth as possible then the artefact produce on the surface would be considerably smaller than the scale of the microstructural features thought to be responsible for cortical bone's micropolar behaviour such as the Haversian canals.

It was decided that silicon carbide paper should be used to prepare the surface of specimens before testing. Increasingly smooth grades of silicon carbide paper were used from 200 to 2500 grade. The particle size of the smoothest grade of paper (2500) is 6 μm significantly less than the diameter of the microstructural features associated with primary or secondary osteons. Therefore this suggested that surface preparation would produce a surface where the artefact is significantly smaller than the underlying microstructure. It was hoped that this would allow the material properties of the internal microstructure on the surface of the cortical bone samples to be of the foremost influence in the mechanical testing.

Surface roughness is a measure of the texture of a surface. The standard method for quantifying the nature of a surface is by running a needle tip along the length of the surface. The resulting perturbations of the needle give a two-dimensional profile of the character of the surface. From the movement of the needle various measures of the surface can be obtained. The most commonly used surface roughness measure is the R_a value: this is a value which represents the arithmetical average of all the normal displacements in the profile. Other useful measures include R_t (the maximum peak to valley in the profile) and R_z (the average peak to valley in the profile). These values can be related to the microstructural features of cortical bone, and may give an indication towards identifying whether the surface contains artefacts which would reduce the stiffness of the specimen.

Cortical bone is a viscoelastic material (Wirtz et al. 2000; J Y Rho et al. 1998; R. Lakes 1979; N Sasaki & Enyo 1995; Yamato et al. 2006). The importance of this for mechanical testing is that there will be a degree of stress relaxation apparent in a static three point bending experiment. Viscoelastic materials also exhibit strain rate dependence rather than the strain dependence seen in elastic materials (P Zioupos 1994; Gupta & P Zioupos 2008). To calculate the strain on the outermost fibres in the centre of a beam in three-point bending the following equation may be used:

Equation 37

$$\varepsilon = 6\delta d / L^2$$

where ε is the strain δ is the defection of the beam at the mid-span d is the depth where the strain is being calculated and L is the length of the beam. Viscoelastic effects also contribute to the time dependence of the measured elastic modulus of cortical bone, where the strain rate is higher a higher elastic modulus will be observed. Ideally a consistent strain rate should be used between specimens in order to maintain the comparability of the observed stiffness values (Zioupos & Currey 1994; Peter Zioupos et al. 2008).

The results from the finite element analyses into idealised heterogeneous materials showed that the micropolar material properties observed were dependent on the length to depth aspect ratio of the specimens. The true micropolar Young’s modulus and characteristic length were observed where the length to depth aspect ratio approached infinity. On the other hand where the aspect ratio was shortened to significantly below 10:1 anticipated mechanical behaviour deviated significantly from those of longer aspect ratios. This occurs because, at shorter aspect ratios, in beams in three-point bending the influence of shear deformation becomes important and the beam no longer follows the analytical predictions.

Therefore, it is important to produce samples with aspect ratios which are as large as possible in order to obtain the most accurate material properties. However, the experimental practicalities of producing a 20:1 or greater length to depth aspect ratio specimen are prohibitive. Therefore, a shorter aspect ratio of 10:1 was chosen as a practical compromise. At this aspect ratio the beam still behaves according to the analytical predictions of a beam in three-point-bending but without the impracticalities of testing over impractically long lengths.

6.2 Pilot experiments on bovine cortical bone

The main objective of the preliminary experiments was to gain a deeper understanding of experimental tests on cortical bone and the challenges that occur especially when dealing with particularly small specimens. In order to simplify the experiments various assumptions were made regarding the preparation and testing.

Specimens were taken from the mid-diaphysis region of a long bone, but there was no significance placed on the location circumferentially or radially around the shaft.

Viscoelastic effects were initially not analysed to reduce the complexity in the software of the testing experiment. Displacement and displacement rate were therefore maintained for each specimen irrespective of the specimen depth.

Specimens were prepared at random depths ranging from 5 to 0.9 mm.

6.2.1 **Pilot experimental methodology**

Five bovine femurs were obtained from a local abattoir and frozen at -20 °C until required. The mid-diaphysis section was used for extracting samples as this is the region of long bones with the highest degree of heterogeneity (Katz & Yoon 1984; Macione et al. 2010; Pope 1974)**.** To prepare the samples a diamond bladed sectioning saw (Smart Cut 6001, UKAM, USA) was used to cut the diaphysis into approximately 5 mm thick longitudinal slices. Each slice was then hand polished under fluid to within 0.05 mm of 5 mm thickness using increasingly smooth grades of silicon carbide paper and measured using a micrometer. From these slices, 51 samples were obtained ranging in depth from 5.5 mm to 1mm. The breadth of each specimen was maintained at 5 mm. The samples were then polished with increasing grades (up to 2500 grade) of silicon carbide paper and stored in PBS in a tissue fridge at 3°C for up to 48hours. It was deemed important to prepare the surface to be as smooth as possible in order to remove surface artefact resulting from the preparation procedure which could interfere with the measurements of underlying mechanical properties.

A BOSE Electroforce 3200 mechanical testing machine with a 3-point bending jig and temperature controlled saline bath was used to perform the bend tests (Figure 53 and Figure 54), using a 450N load cell. Each specimen was tested in a 0.9M saline water bath at a controlled temperature of 37°C in order to replicate the conditions of normal bone function. The span of the 3-point-bending supports was altered to give a 10:1 aspect ratio (length:depth) for each specimen. Specimens with a depth above 3 mm were displaced at the mid-section by 1 mm whilst specimens with a depth below 3 mm were displaced at the mid-section by 0.5 mm. Displacement rate was constant for all specimens at 0.1 mms^{-1}. Force displacement graphs were created for each specimen and the linear portion of the curve was used to determine the stiffness of each beam.

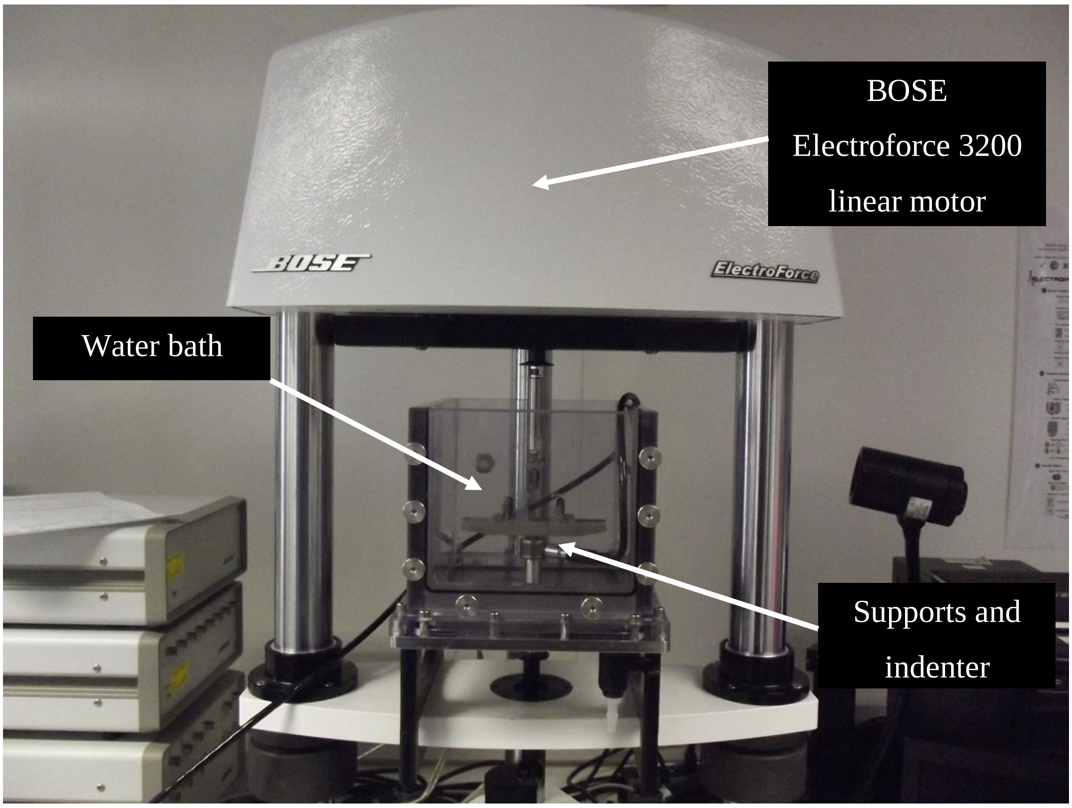

Figure 53 – Bose Electroforce 3200 with water bath and three point bending test jig.

Specimens were taken for surface roughness measurements where R_a values were obtained using a Talysurf surface roughness measuring machine. All specimens had their wet weight and density determined by measuring their volume and weight with a micrometers and a balance. All specimens were then dried at 100 °C for 24 hours and then reweighed to give the dry weight and density. Each specimen was finally ashed at 800°C for 24 hours and reweighed to determine the ash weight, the mineral and collagen contents.

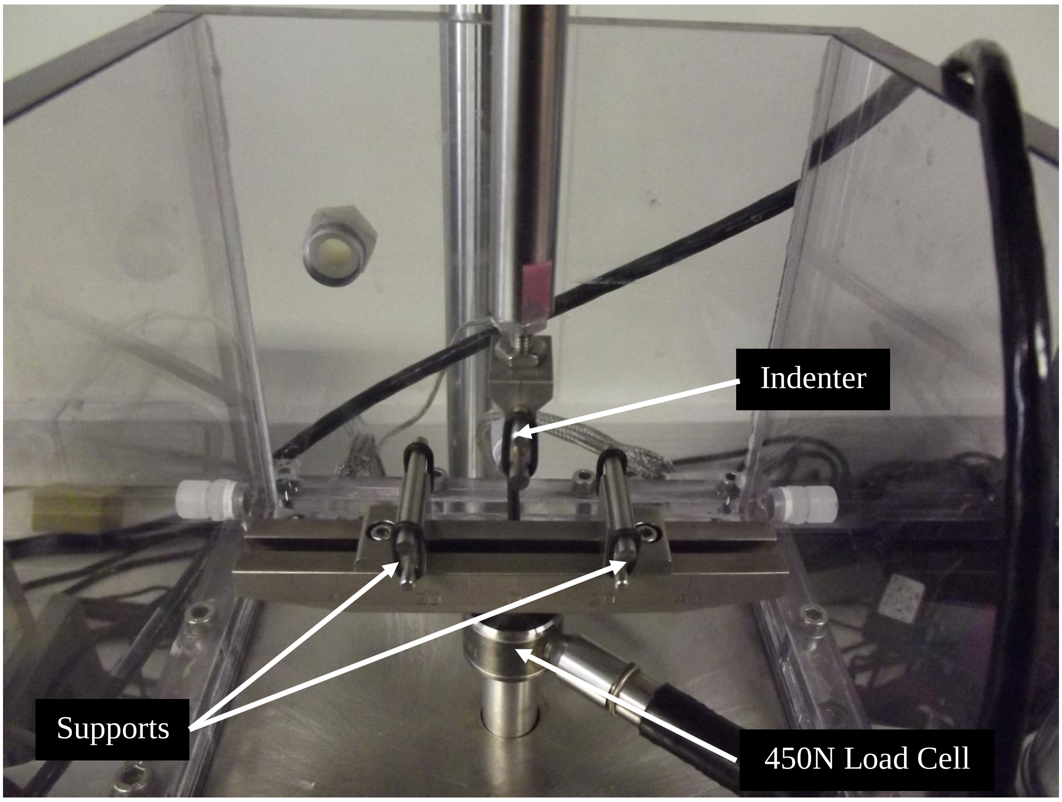

Figure 54 – The temperature controlled water bath and three-point bending experimental jig.

6.2.2 **Pilot experimental results**

The initial experimental results showed a wide variance in stiffness when plotted against the sample size as represented by reciprocal of depth squared (Figure 55). Although there is a suggestion of a negative size effect the lack of a definite linear trend from these results meant it was difficult to extract micropolar material properties. The results do indicate there may be a size softening trend however they also suggest that there is a weak negative relationship between the mineral content and specimen size (Figure 56) (correlation coefficient = -0.477) . This is indicated by the smaller specimens tending to have a lower mineral content. Figure 57 shows a plot of the specimen stiffness against the mineral content which demonstrates how the mineral content is of fundamental importance to the observed stiffness of each specimen. It also shows that where there is a link between the specimen size and mineral content then the smaller specimens are more likely to show a lower stiffness, due to their lower mineral content. Moreover, there are a significant number of specimens with a recorded mineral content lower than 0.7g/mm^3, which would suggest that there has been a leaching of mineral in these specimens and a subsequent reduction in measured stiffness (J. D. Currey 1969; Burstein et al. 1975). Because of this the stiffness was recalculated to account for the variation in stiffness with mineral content. This was done by performing a linear regression of stiffness against mineral content and scaling the stiffness values depending upon the recorded mineral content of each specimen. This produced the plot of stiffness against reciprocal of depth squared shown in Figure 58.

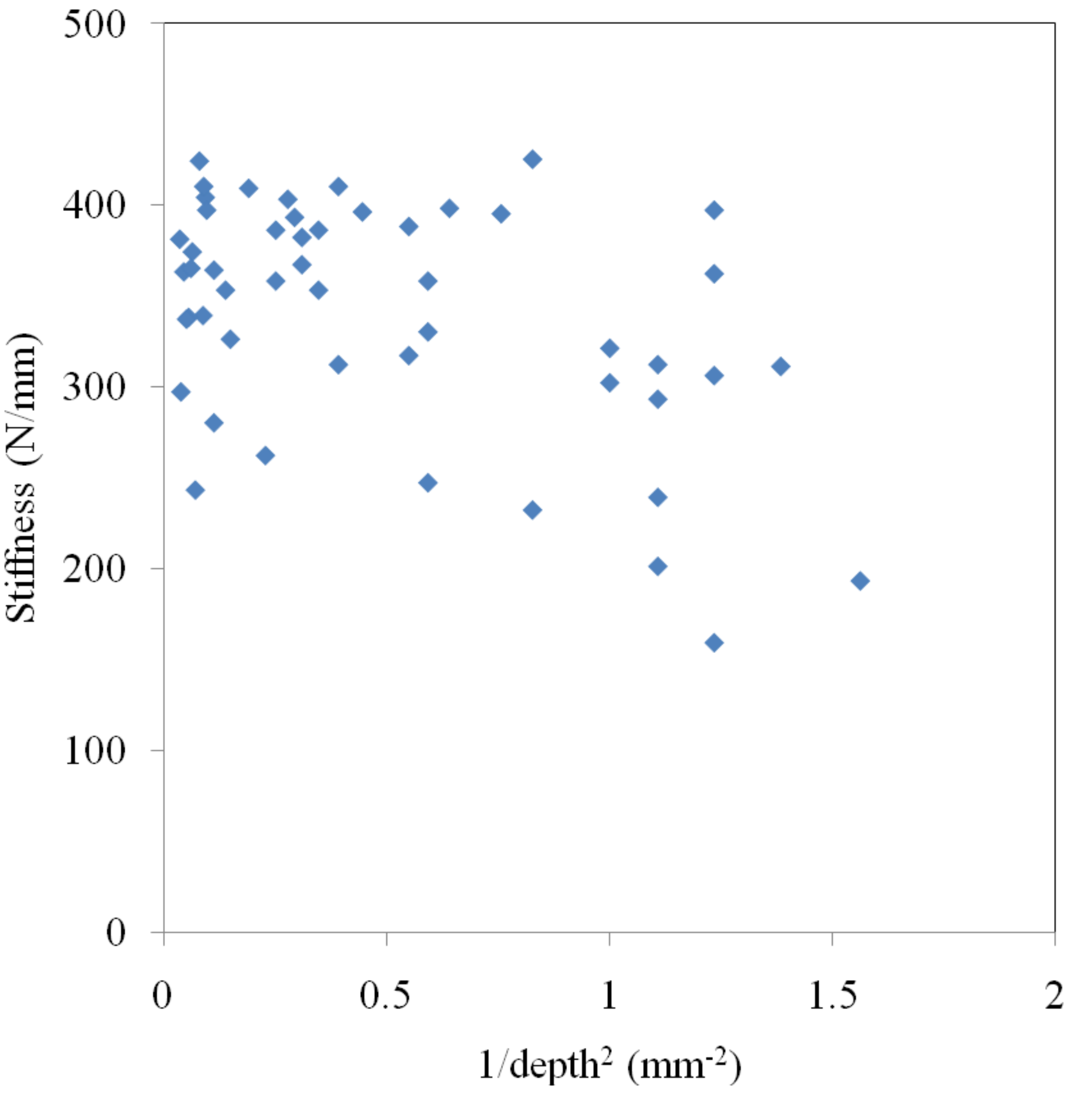

Figure 55 - Experimental results of stiffness plotted against reciprocal of depth squared.

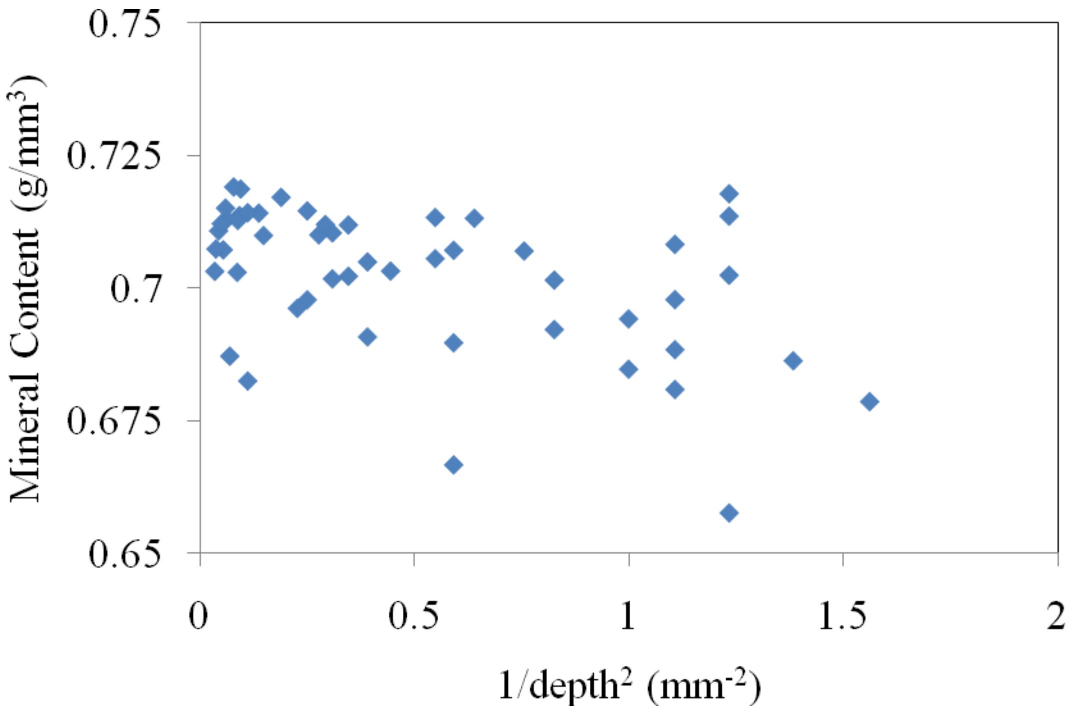

Figure 56 - Experimental results showing mineral content plotted against specimen size for all specimens.

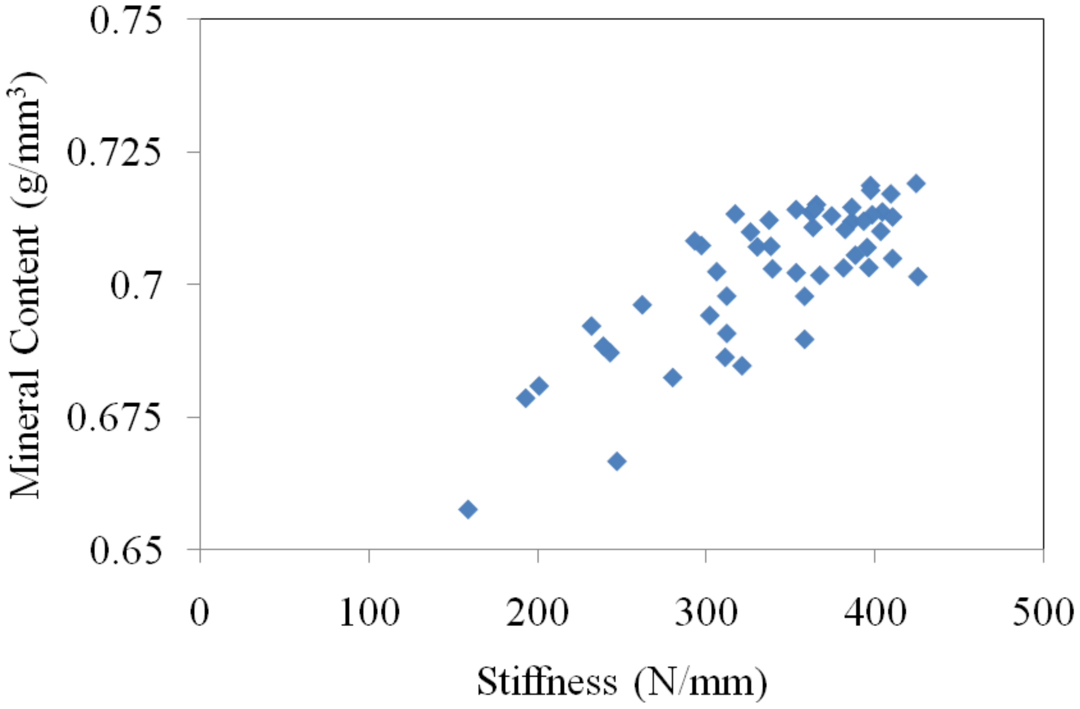

Figure 57 - Plot showing the relationship between mineral content and stiffness for all specimens.

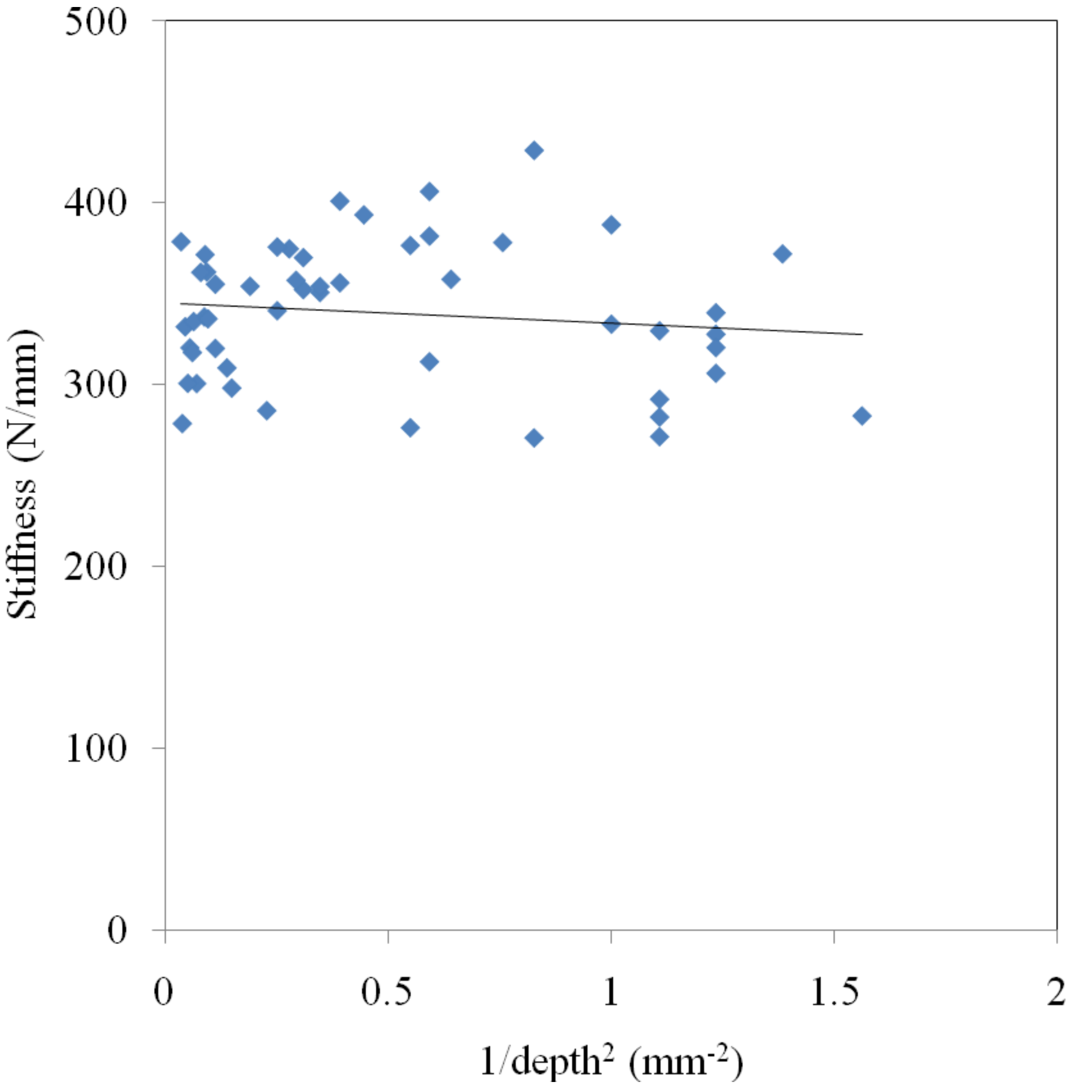

Figure 58 - Experimental results of stiffness plotted against reciprocal of depth squared with the stiffness corrected for the variation in mineral content with trend line showing the negative size effect.

The size effect trend shown in Figure 58 represents the stiffness values after they have been corrected for the variation in mineral content. From the trend line produced in this plot it was possible to extract the micropolar material properties of micropolar Young's modulus and micropolar characteristic length in bending.

Table 10 – Micropolar material properties from the stiffness against size plot for corrected values for mineral content.

Specimen	Size effect	Micropolar Young's modulus (GPa)	Micropolar characteristic length (µm)	Micropolar characteristic length in bending (µm)
All specimens	negative	17.2	181	52

Surface roughness results show the majority of the values obtained were between 0.1 and 0.2 mm Ra values. There were a significant number of outlying values which suggest that the surface roughness readings produced inconsistent results as the surfaces of all specimens were produced using the same method. Figure 59 shows the surface roughness Ra values plotted against the specimen size. It can be seen that there is an indication of a size dependent trend between surface roughness and specimen size suggesting that a reduction in stiffness may be attributable to a rougher surfaces in the smaller specimens.

The reliability of the surface roughness measurements taken in this experiment were questionable primarily because the Talysurf machine used to measure the surface roughness had no internal check to determine if the readings met ISO standards for surface roughness measurements. For many of the readings taken the length of sample measured was below the ISO standard required length meaning that the surface roughness results do not have a statistical significance. It was decided that future experiments would require the surface roughness measurements to meet the ISO standard.

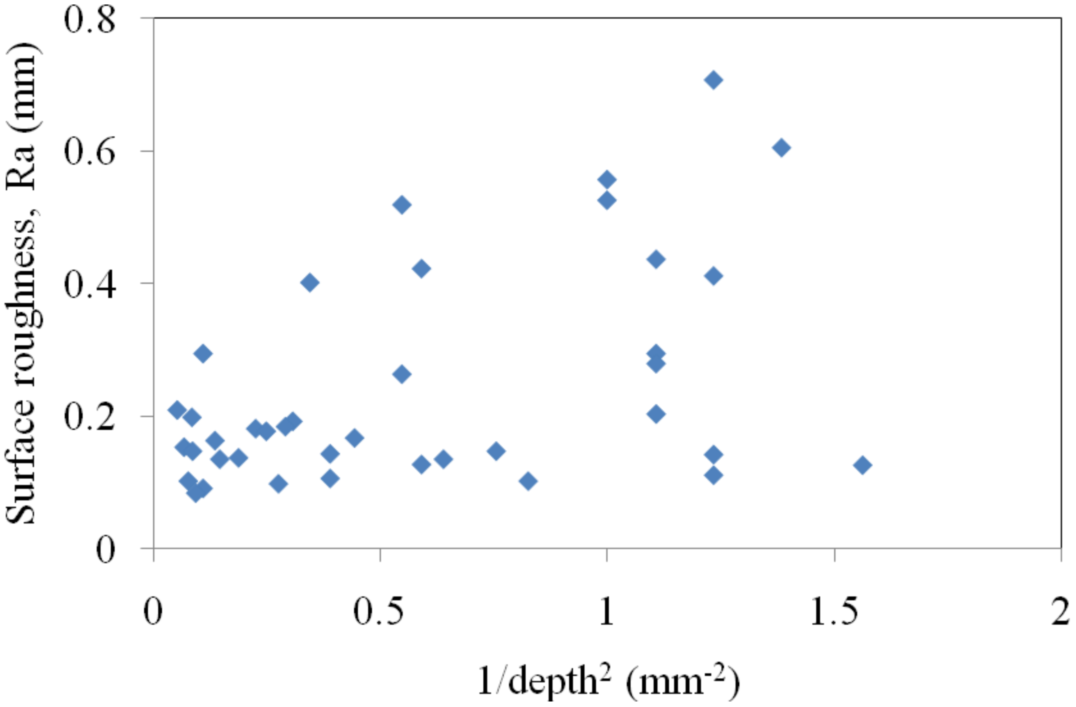

Figure 59 - Surface roughness plotted against the reciprocal of depth squared for all specimens.

6.2.3 Discussion

The initial experiments of bovine cortical bone proved to be a useful developmental experience for the further improvement of the experimental protocol. Although a size effect trend was identified the reliability of the result was dependent upon correcting the stiffness results for the lower mineral content observed in some specimens. Moreover, a solid understanding of the procedure required to determine the existence of a size effect was gained. This was a good starting point for further experiments.

There was a large degree of demineralisation which was observed, especially with the smaller specimens. Although the stiffness values were corrected for the variation in mineral, the contributing influence of lower mineral content on the recorded stiffness may have a more profound impact on the actual size effect in cortical bone. The potential causes of the demineralisation were considered to be related to the preparation method. Specimens were kept in 0.9M saline overnight before testing which would have allowed the leaching of mineral (Ca^{2+}) out of the specimens (Naoki Sasaki et al. 2008b; N Sasaki & Enyo 1995). Moreover, the smaller specimens have a larger surface area to volume ratio and therefore it would be conceivable to observe a greater mineral loss in the smaller specimens. This is consistent with what was observed in the relationship between mineral content and specimen size (Figure 56). To prevent mineral loss in future experiments it was decided that Phosphate Buffered Saline (PBS) solution was more appropriate instead of saline to hinder the movement of mineral from the bone to the solution. A further step to reduce mineral loss was to reduce the time between the preparation of specimens and testing as this would significantly reduce the opportunity for mineral to leach from the bone.

Each specimen was tested at one unique depth. Although this allows for comparisons between specimens and to generate an overall impression of the mechanical properties of cortical bone, it includes potentially significant inter-specimen stiffness variation. To improve the experimental procedure further it was decided to prepare all specimens from each bone to the same initial dimensions. Once the specimens were tested they would be re-prepared and re-tested in order to produce several unique depths for each specimen. This approach would enable a comparison to be made between intra-specimen variability and size effects and an overall inter-specimen variability and size effect. A comparison between the intra-specimen stiffness values may also prove a more reliable measure of the influence of the microstructure on the overall material stiffness, especially when analysing size effects, as the internal microstructure between discrete depths may be more consistent in the same specimen.

The inadequacy of the surface roughness values removed any meaningful analysis regarding surface roughness trends with size and/or stiffness. It was decided that future readings would be made on a non-invasive Alicona surface roughness machine to standardise the process and allow conformation with ISO standards. This would also allow cross validation with images of the surface and the surface roughness values measured in that region.

Comparable specimens should be taken from the same location around the diaphysis to prevent inconsistencies and variance arising from different mineral contents and microstructure architectures at different locations in the bone.

Future experiments should apply a consistent strain and strain rate depending on the depth at which each specimen was being tested. This was because of the viscoelasticity of cortical bone and the dependence on strain rate rather than displacement rate.

6.2.4 **Conclusions**

The preliminary experiments suggested a size softening negative size effect relationship between specimen size and stiffness. However there was a high degree of variance in the values obtained. Moreover, there were a significant number of specimens with a reduced mineral content and as a result the stiffness values were adjusted to account for this. The surface roughness values obtained were deemed to be inadequate for analysis.

Proposed revisions to the experimental protocol included: the use of PBS instead of saline to reduce mineral loss, reduce the time between specimen preparation and testing, use the Alicona surface roughness machine to standardise surface roughness measurements, test each specimen at a range of depths to determine intra-specimen variability as well as inter-specimen variability and load specimens to a consistent strain at a consistent strain rate.

6.3 Revised experimental methodology

6.3.1 Methodology

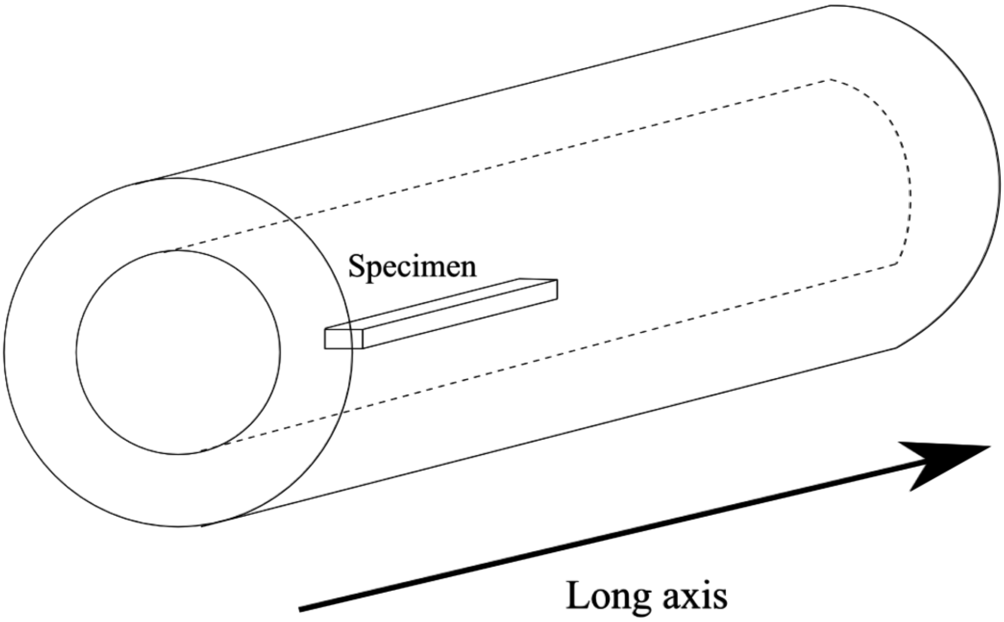

Figure 60 – Orientation of specimens along the long axis of the bovine femurs

Five new bovine femurs were obtained from a local abattoir and frozen at -20 °C until required. One specimen was extracted from the anterior region of the mid-diaphysis for each femur using a hacksaw and a diamond bladed sectioning saw (Smart Cut 6001, UKAM, USA) to produce five specimens in total. All five specimens were prepared to have the dimensions of 50 mm length, 5 mm breadth and 5 mm depth. The specimens were prepared to have the long axis of the femur running along the length of the specimen (Figure 60).

Each of the five specimens was polished under irrigated conditions with phosphate buffered saline (PBS) solution using incrementally smooth silicon carbide paper (grades 200, 500, 1200 and 2500) to within 0.05 mm of the desired dimensions as measured by a micrometer. The specimens were then stored in PBS solution at 3 °C for less than a day prior to testing. Such storage would have a negligible effect on the mechanical properties of the specimens (N Sasaki & Enyo 1995).

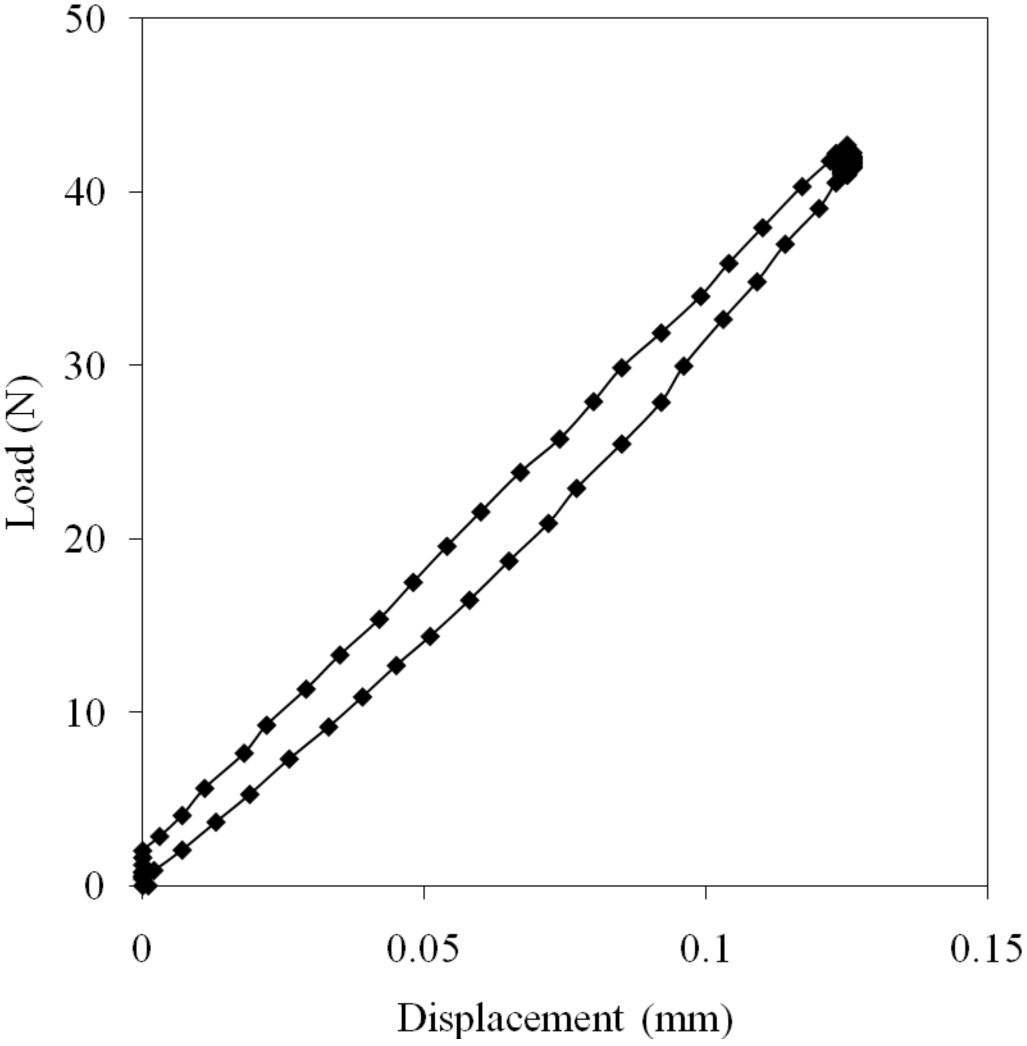

Figure 61 – A typical load-displacement graph for specimen 1 at a depth of 1.5 mm. The linear region of the load-displacement curve was used to determine the geometric stiffness of the specimen. Slight hysteresis can be seen and a stress relaxation of approximately 5%.

The same test equipment and load cell were used as in the previous experiments. Each specimen was tested in a PBS bath at 37°C. Each specimen was ramp loaded to a surface strain of 0.005 at a strain rate of 0.0025s^{-1} and held for 10 seconds before being unloaded to zero displacement. Each specimen was then re-orientated to swap the compression and tension surfaces in bending and the loading repeated. In total each specimen was loaded three times. A cutting was subsequently taken from the end of each specimen for surface roughness and tissue property data to be acquired.

This testing procedure was applied each time after the specimen depth was reduced by removing material from the upper and lower surfaces with increasingly refined grades of silicon carbide paper to maintain as smooth a surface as possible. Each specimen was tested at seven unique depths: 5 mm, 4 mm, 3 mm, 2.1 mm, 1.5 mm, 1.2 mm and 0.9 mm. As the depth of each specimen was systematically reduced the supports of the bending jig were moved progressively closer to maintain a constant 10:1 length to depth aspect ratio.

The flexural stiffness at each depth for each specimen was taken as the gradient of the linear relationship between load and displacement (Figure 61). Surface images were taken from the cuttings removed during the experimental procedure and surface roughness characteristics were analysed using an Alicona InfiniteFocus surface imager. After surface imaging the cuttings taken during experimentation were used to calculate the mineral content using the same method as in the pilot experiments.

Two-way repeated measures ANOVA was used to determine whether the stiffness varied with specimen depth and repeated measure. Linear regression and correlation was subsequently used to assess the nature of the relationship between stiffness, mineral content and surface roughness with $1/d^2$. All statistical analysis was performed using IBM SPSS Statistics v21 (IBM, New York, USA) and statistical significance was assumed if $p <= 0 .05$.

6.3.2 **Results**

The pilot experiments indicated that there were a significant number of specimens with reduced mineral content. This was thought to be attributable to the leaching of mineral during the specimen preparation process. Figure 62 shows the relationship between specimen mineral content and specimen size. There was no significant size effect trend attributable to mineral content observed ($p = 0.358$). This suggests that the revised methodology was successful in maintaining the mineral content of each specimen between the preparations and testing stages. This was further supported by Figure 63 showing a plot of the mineral content against the specimen stiffness which indicates that there is a much less dramatic influence of mineral content on stiffness than in the previous experiments (Figure 55 and Figure 56) and that the mineral content of all specimens are consistently higher than in the preliminary experiments suggesting that the revised protocol is better at maintaining a consistent level of mineral for all specimen depths.

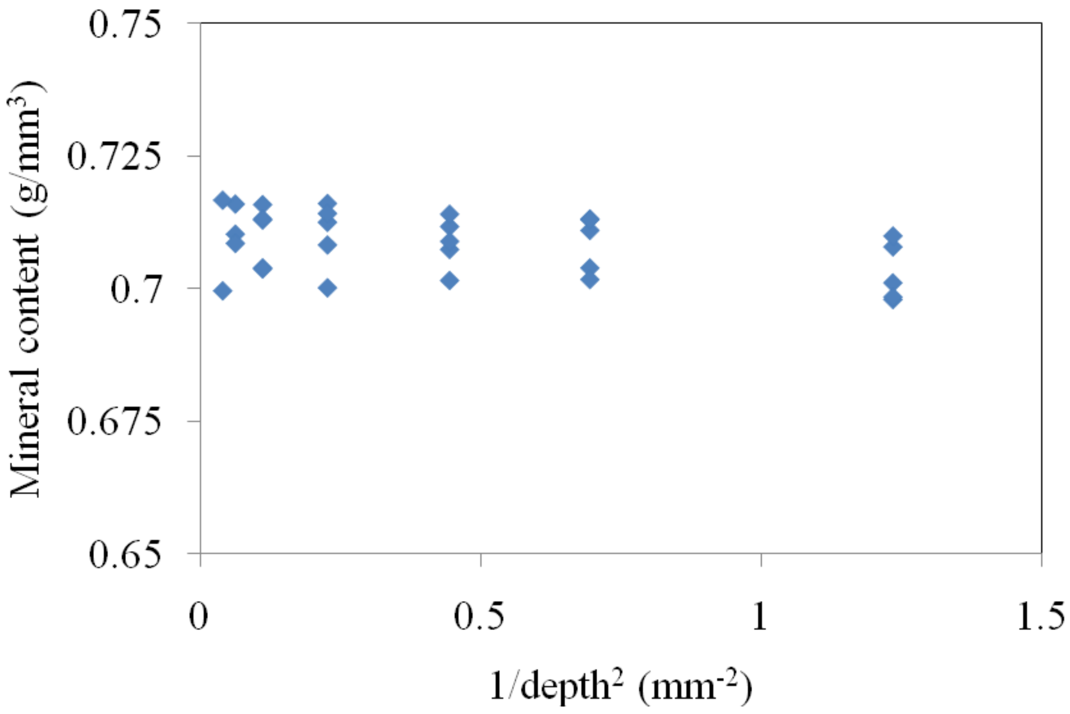

Figure 62 – Reciprocal of depth squared plotted against mineral content for all specimens.

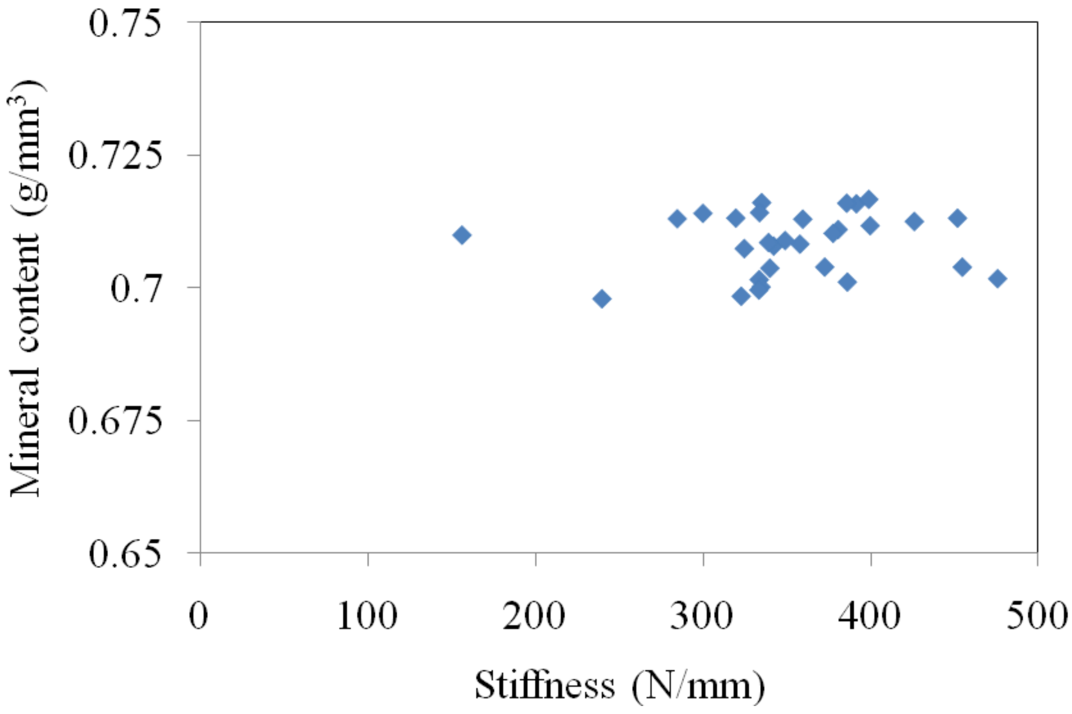

Figure 63 - Mineral content plotted against stiffness for all specimens.

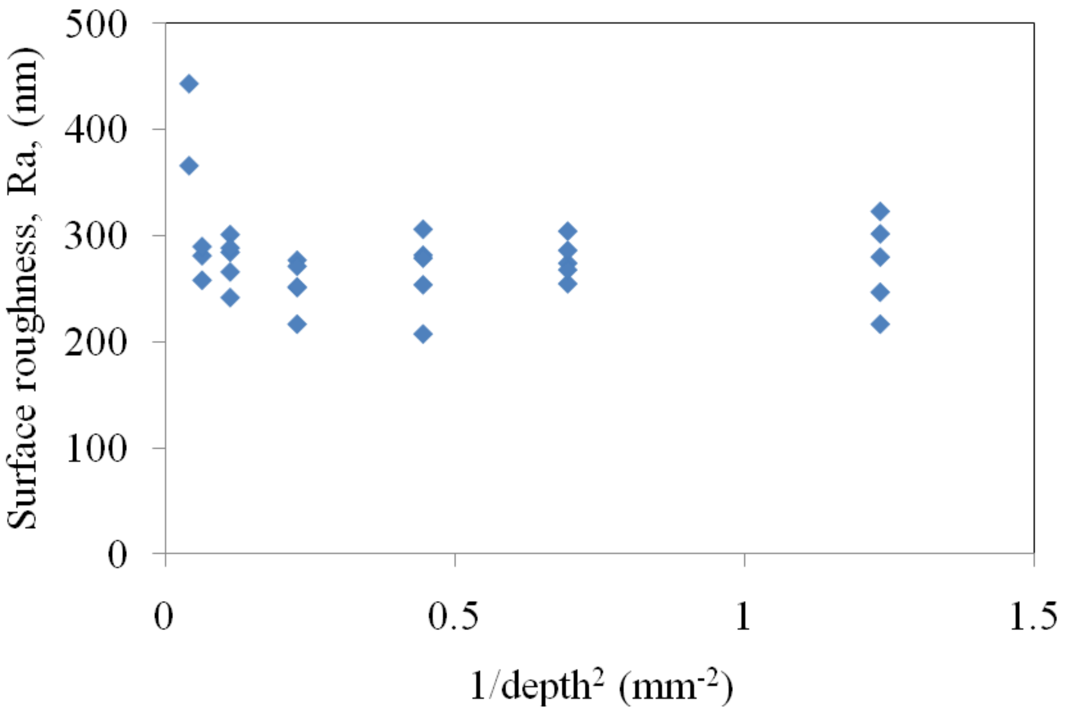

Figure 64 - Surface roughness, Ra, plotted against the reciprocal of depth squared.

Figure 64 plots the surface roughness (Ra) against the specimen size. It shows that while there are a few outlying surface roughness values the general trend shows there to be no significant effect of size on surface roughness ($p = 0.156$). This suggests that the surface roughness was maintained between specimens. Other measures of surface roughness were also taken from the Alicona results. In addition to the Ra value which represents an arithmetical average of surface perturbations (and is a good measure of the general degree of surface roughness) the Rmax and Rz values were also taken. These values represent the maximum and mean surface peak to trough distances and in the case of these cortical bone experiments are an interesting representative measure of the size of voids on the surface of each specimen. The values of Rmax, Rz and Ra are shown in Table 11. This shows that the typical maximum peak to trough dimension is in the region of 5µm and the mean peak to trough values are slightly lower in the region of 3µm. The values for Ra are an order of magnitude lower, typically in the region of 280nm, this is because the Ra values take an average of all surface perturbations across the selected profile and do not only consider the peak to trough values.

Table 11 – Mean Rmax, Rz and Ra values with standard deviations for all specimens.

Depth (mm)	1/depth^2 (mm^{-2})	Mean Rmax ± st. Dev (µm)	Mean Rz ± st. Dev (µm)	Mean Ra ± st. Dev (nm)
0.9	1.23	5.12 ± 3.13	2.85 ± 1.07	273 ± 42
1.2	0.69	4.64 ± 2.18	2.50 ± 0.56	277 ± 18
1.5	0.44	4.38 ± 1.54	2.62 ± 0.46	265 ± 37
2.1	0.23	3.25 ± 1.18	2.10 ± 0.29	253 ± 23
3	0.11	4.69 ± 2.35	3.29 ± 1.48	280 ± 29
4	0.06	3.13 ± 0.81	2.18 ± 0.34	276 ± 16
5	0.04	7.02 ± 1.83	4.69 ± 1.59	331 ± 40

The stiffness against reciprocal of depth squared plots are shown in Figure 65 which shows each result for all five specimens and Figure 66 which shows the combined results with a mean and standard deviation for each depth. A p value of 0.127 was calculated from the two-way repeated measures ANOVA suggesting that any size effect, although observable in Figure 66, is not statistically significant.

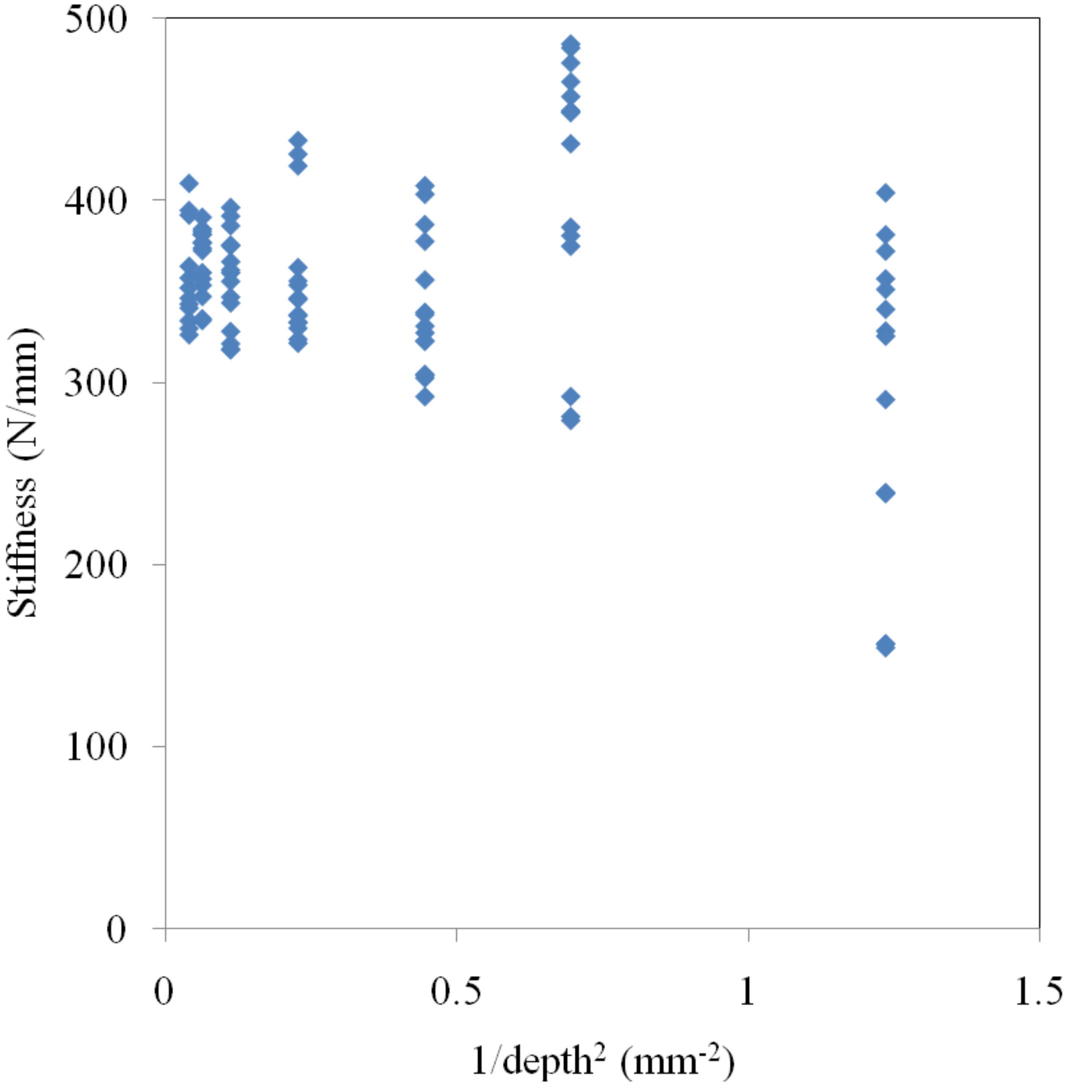

Figure 65 – Stiffness plotted against reciprocal of depth squared all discrete values from all specimens.

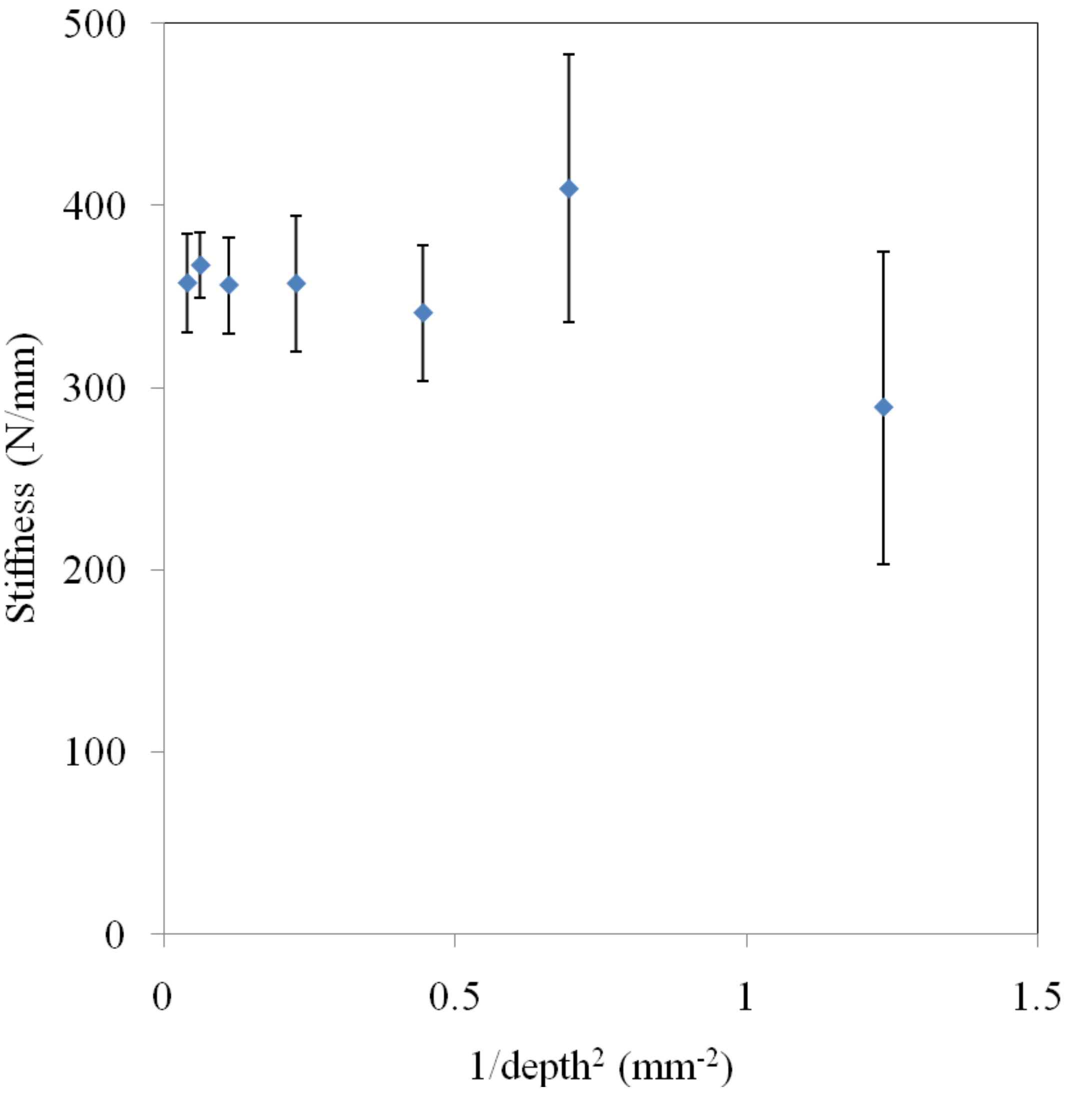

Figure 66 - Combined results for all specimens (1 to 5) plotting stiffness against reciprocal of depth squared with the standard deviation.

Table 12 shows the micropolar Young's modulus and characteristic length in bending where the negative size effect trend shown in Figure 66 is used to calculate micropolar material properties. The micropolar Young's modulus was calculated as being 18.5 GPa. This value is calculated from the intercept of the best fit line on the stiffness against reciprocal of depth squared plots above and Equation 10. It is a comparable value to those recorded for the Young's modulus of cortical bone in the literature (Evans et al. 1990; Hernandez et al. 2001; J Y Rho et al. 2000). The micropolar characteristic length in bending was also identified from these plots by taking the magnitude of the gradient of the best fit line. The characteristic length may only be obtained from a positive gradient, however, if the gradient is negative the magnitude of the gradient may be used to infer the equivalent characterise length that would produce the size effect if the surface had not been intersected by the internal microstructure. The combined results give a micropolar characteristic length in bending of 0.095 mm.

Table 12 – Micropolar Young's modulus and characteristic length values all specimens individually and combined with standard deviations.

Specimen	Size effect	Micropolar Young's modulus (GPa)	Micropolar characteristic length (mm)	Micropolar characteristic length in bending (mm)
All specimens	negative	18.5 ± 1.1	0.33 ± 0.23	0.095 ± 0.066

6.3.3 Discussion

There was no discernable size effect for either the mineral content nor surface roughness which suggests that the methodology for preparing and analysing specimens has improved sufficiently to remove these as confounding factors in influencing any observed size effect in stiffness. The surface roughness values suggest that the surface has been prepared to a level where the surface artefact is significantly lower than that of the internal microstructure. This suggests that the surface is being intersected by the internal microstructure; in other words the surface scratches created by the preparation technique are much smaller than the size of the voids on the surface created by the microstructure.

By confirming that the mineral content and surface roughness are consistent throughout all specimens at each depth, and are not influencing the specimen stiffness, it is possible to confidently identify a relationship between stiffness and size.

The combined size effect of stiffness plotted against size for all five specimens showed a negative size effect trend consistent with the surface being intersected by the internal microstructure of cortical bone however this size effect trend was not statistically significant. Despite this it was possible to infer from the negative size effect trend the micropolar material properties of characteristic length in bending and Young's modulus by comparing this to the equivalent beam without surface corrugations. This analysis assumes that a continuous surface and a corrugated surface represent the extremes of the material behaviour, from which the likelihood of a negative size effect caused by the surface being corrugated by the internal microstructure is higher.

Figure 65 demonstrates the high variance in the results and highlights the difficulty in ascertaining any definite size effect trend in cortical bone because of the natural biological variation in the material. However, considering the finite element analysis has shown that there is potentially a wide discrepancy in material behaviour between specimens with continuous surfaces and specimens with corrugated surfaces it is understandable that there would be an equally high degree of variation in the experimental results. Moreover, because five unique specimens were tested from five different bones there is a greater likelihood to observe a higher variation in material properties across all specimens.

Although there are no obvious systematic errors in the experiments which can only be attributed to the 1.2 mm depth it cannot be ruled out as a plausible explanation for the discrepancy in stiffness observed at this depth.

Microdamage begins to permanently influence the structural stiffness in cortical bone at strains of around 0.005 (Zioupos & Currey 1994). As this is the maximum strain on the outer surface of the cortical bone specimens loaded in these bending experiments microdamage will only have begun to influence the outermost surface. Microdamage is related to strain rate in that lower strain rates will be more likely to induce microcracking in cortical bone. This is thought to be a mechanism through which bone absorbs energy at lower strain rates (Zioupos et al. 2008). In this study the strain rate was maintained at a low level of $0.0025s^{-1}$ thereby suggesting that the possibility for microdamage to occur. This strain rate is in the regions of normal everyday cycles for cortical bone and may more effectively replicate the loadings cycles which typically occur on bones. After testing, the surface region of each specimen was removed and re-prepared to a new depth. In doing this the region where the most strain had been imparted in the previous test was removed, subsequently removing the region most likely to contain microdamage.

Previous work by Choi et al has indicated that there is a size dependency in human cortical bone (Choi et al. 1990). Although Choi et al's work focused on human cortical bone it is nevertheless a worthwhile comparison with the size effect observed in this work. Figure 67 shows the comparison between this study and the work of Choi et al. It can be seen that there are similarities between the results indicating a similar size effect. The largest specimen tested in Choi et al's work is 1mm deep which is only slightly larger than the smallest specimen tested in this study. To fully compare the size effects smaller specimens are required where the depth is as small as 0.5 mm. This depth is approaching the microstructural size of the Osteon system in cortical bone, suggesting that the influence of the microstructure will be more prevalent.

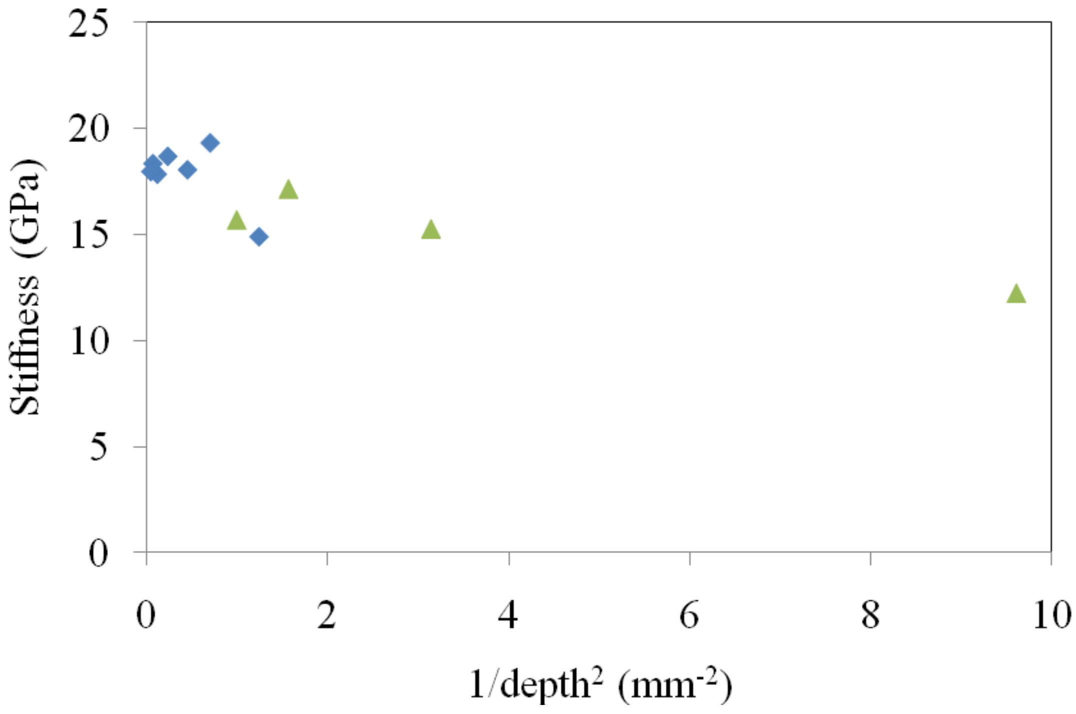

Figure 67 – Comparison between the results in this study(blue diamonds) with those of Choi et al (Choi et al. 1990) **(green triangles).**

To further understand the degree of the size effect evident in bovine cortical bone a further set of specimens are required at a series of smaller depths where the influence of the microstructure is higher. For this reason a new series of experiments testing specimens at four unique depths from 1.3 mm to 0.5 mm deep would allow a more detailed impression of the size effect to be formed. This would fully integrate this study's results with the findings of Choi et al.

A demonstrable size effect was observed in bovine cortical bone this showed that the micropolar Young's modulus was 18.5 GPa and the micropolar characteristic length in bending was 0.095 mm. These values are comparable to the microstructural features found in cortical bone where Haversian canals are typically 0.03 - 0.07 mm in diameter.

Further experiments at smaller depths are required to fully confirm the size effect and compare it with previous studies in observed size effects in cortical bone.

6.4 Experimental Development Conclusions

The development of the experimental protocol was an iterative process. The initial attempts at detecting a size effect were ultimately unsuccessful because of the inconsistent mineral content results and limiting assumptions. However, the process enabled detailed development in both understanding and procedural competence. The finite element analysis has shown that the surface condition is of primary importance in determining and understanding the observed material properties of a heterogeneous material. For this reason surface roughness properties were measured as a way to introduce a standardised preparation technique.

In the initial set of experiments the mineral content showed a high degree of variation and indicated demineralisation may have caused some of the specimens to reduce in stiffness. This reduced the reliability of the results from the first round of experiments and for future experiments mineral content was controlled by reducing the time between preparations and testing in conjunction with using PBS solution instead of saline solution for storage. This proved successful as the latter experiments showed no significant variation in mineral content with specimen size.

Once a consistent experimental protocol was defined a size effect was observed which showed the micropolar material properties of Young's modulus and characteristic length in bending to be 18.5GPa and 0.095 mm respectively which compared to the values in literature for Young’s modulus and the diameter of a typical Haversian canal. However to gain a more detailed impression of the size effect observed in bovine cortical bone more specimens at smaller depths are required. This should enable a more detailed analysis of the size effect where the length scale approaches that of the microstructure. This will further allow a better comparison with previous studies into size effects in human cortical bone.

7 Longitudinal and transverse size effects

The previous chapter detailed the process of the development of a robust repeatable experimental protocol. Once this protocol had been established a new series of experiments was carried out. This time two series of experiments were carried out using the previously establish protocol: one where the specimens were orientated longitudinally along the long axis of the femur; and another set orientated in the transverse plane with the vascular channels predominantly running through the breadth of each specimen. Both set of experiments used smaller specimens than in the previous chapter in order to gain a more detail impression of potential size effects at smaller specimen sizes.

7.1 Methodology

The same experimental methodology was used as had been devised in the previous chapter. Five bovine femurs were used to produce 10 specimens in total. From each femur two specimens were produced: one orientated longitudinally along the long axis of the femur as before (Figure 60); and the other orientated transversely across the radial-circumferential plane so that the vascular channels would predominantly run through the breadth of the specimens, this produced five specimens for each orientation. Each specimen was prepared to an initial length of 20mm, breadth of 5mm and depth of 1.3mm. Four unique depths were tested for each specimen: 1.3mm, 1mm, 0.7mm and 0.5mm. Specimen stiffness, surface roughness and mineral content were measured and quantified as with the established protocol.

Two-way repeated measures ANOVA was used to determine whether the stiffness varied with specimen depth and repeated measure. Linear regression and correlation was subsequently used to assess the nature of the relationship between stiffness, mineral content and surface roughness with $1/d^2$. All statistical analysis was performed using IBM SPSS Statistics v21 (IBM, New York, USA) and statistical significance was assumed if $p <= 0 .05$.

7.2 Experimental Results

7.2.1 **Specimens orientated longitudinally along the long axis.**

The longitudinal experimental results show a statistically significant size softening size effect (p = <0.001) but not with repeated measure which is in accordance with an anti-micropolar size effect trend. Figure 68 shows the combined results for all five femurs for specimens orientated longitudinally along the long axis of the femurs. These results confirm a size softening size effect in three point bending. Table 13 summarises the micropolar material properties calculated from inferring positive size effect trends from the negative size effect. This shows the micropolar Young's modulus of bovine cortical bone to be 17.97 GPa and the micropolar characteristic length in bending to be 0.080mm. Both of these values are comparable to the quoted values for axial Young's modulus in cortical bone and the size of Haversian canals and vascular channels in secondary and primary osteons (Black et al. 1974; Smit et al. 2002; Jae Young Rho et al. 1993; Zhang et al. 2008).

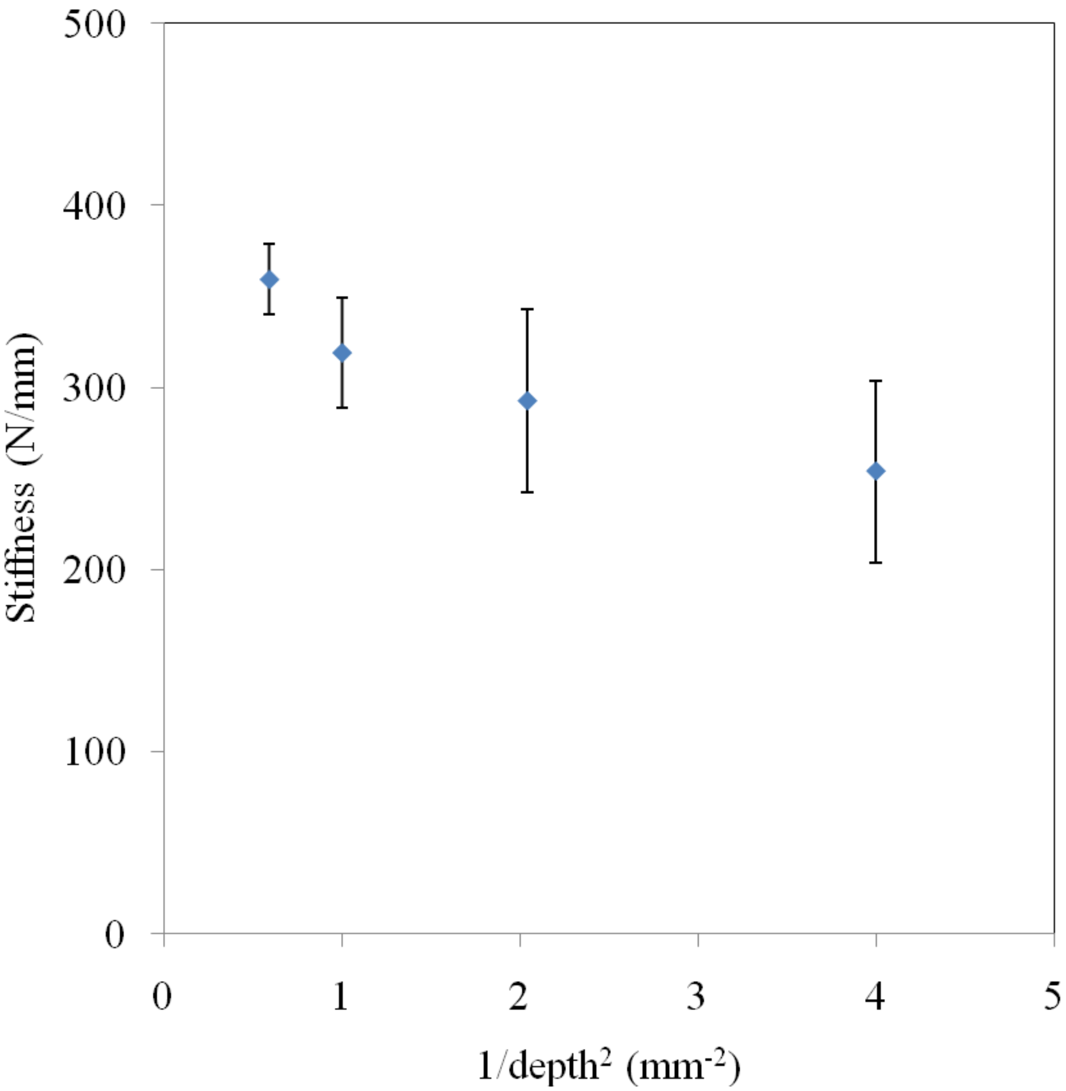

Figure 68 – Combined experimental results across all five specimens orientated longitudinally along the long axis of five bovine femurs.

Figure 69 shows the mineral content plotted against the reciprocal of depth squared for all specimens. For these results the mineral content does not fall below 0.7 g/mm^3 suggesting consistency in the procedure. The higher consistency with mineral content suggests the results are more reliable than previous experiments for determining material properties. Moreover the consistency in mineral content indicates that this has no significant influence on the observed size effect ($p = 0.108$) and points towards the size effect in stiffness being attributable to the influence of the material's microstructure rather than changes in mineral content. This is further corroborated by Figure 70 which shows the surface roughness plotted against the reciprocal of depth squared for all specimens. There is no discernable size effect in surface roughness with depth (p = 0.725).

Table 13 - Micropolar Young's modulus and characteristic length values for all specimens combined with standard deviations

Size effect	**Micropolar Young's modulus (GPa)**	**Micropolar characteristic length (mm)**	**Micropolar characteristic length in bending (mm)**
negative	17.9 ± 1.0	0.28 ± 0.05	0.080 ± 0.016

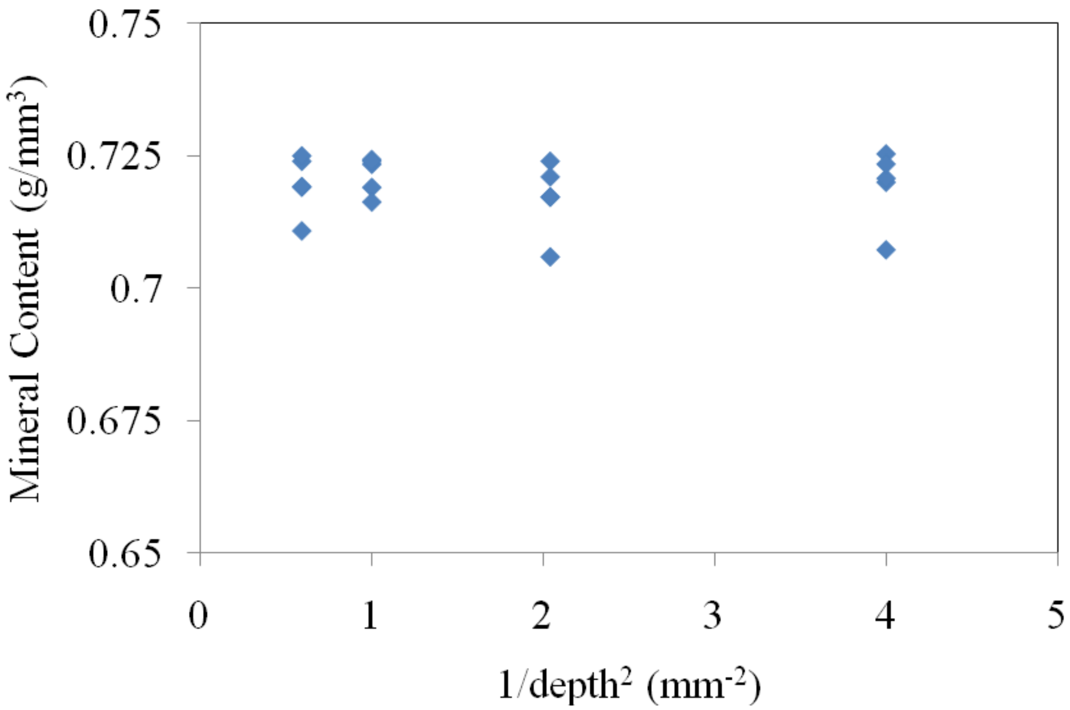

Figure 69 - Mean mineral content plotted against reciprocal of depth squared for all specimens.

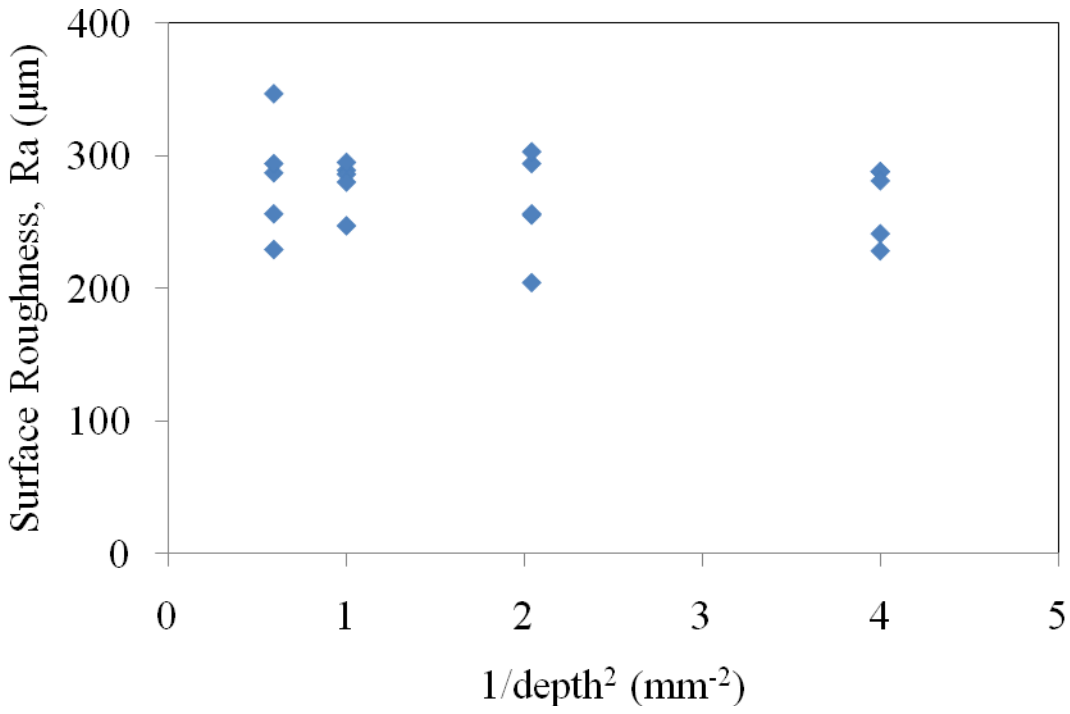

Figure 70 – Reciprocal of depth squared plotted against the mean surface roughness, Ra, for all specimens.

The longitudinal results show that there is a significant of the negative size softening size effect observed in bovine cortical bone. This is further emphasised by the repeatability of the results which suggests that cortical bone as a unitary material exhibits behaviours which are concurrent with micropolar elasticity theory. The values obtained for micropolar Young's modulus and characteristic length in bending are comparable to those quoted in literature for the material properties of bovine cortical bone.

7.2.2 Transverse specimens orientated with voids running through the breadth.

The size effect trend for the five transverse specimens is shown in Figure 71. This shows a negative size softening size effect trend which may be described by micropolar elasticity. However, the size effect trend shows a p-value of 0.166 which suggests the results are not statistically definitive. Moreover the large standard deviations suggest a high variation of the measured stiffness at each depth.

Nevertheless there is a noticeable drop in stiffness with specimen size which is indicative of a size effect in the material.

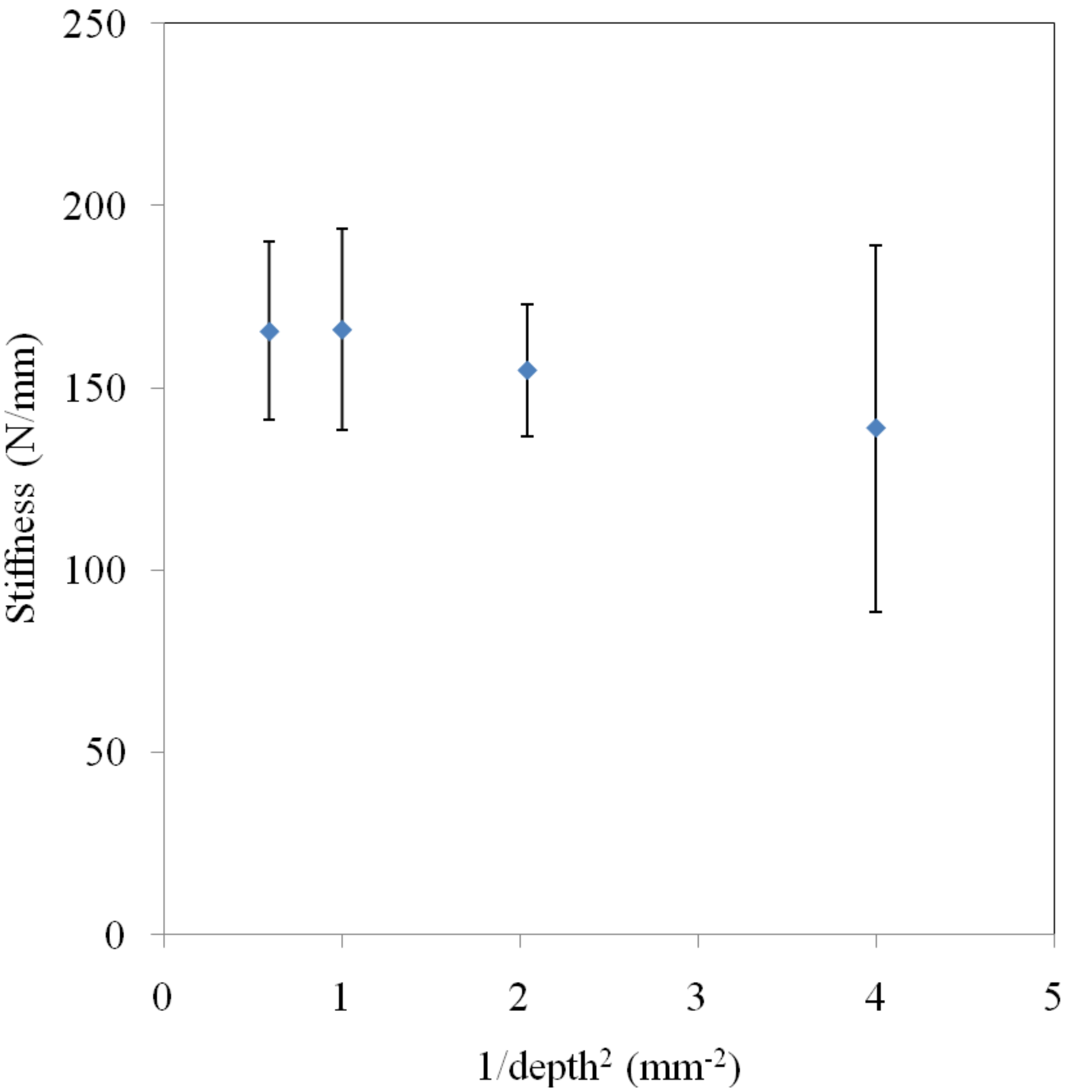

Figure 71 - Radial circumferential combined results plotting mean specimen stiffness against the reciprocal of depth squared with standard deviation.

Table 14 summarises the micropolar size effects and micropolar material properties calculated form the size effect. The micropolar Young's modulus of 8.6GPa shows the reduced transverse stiffness of cortical bone. The micropolar characteristic length in bending is 63μm which is in agreement with published values for the Haversian canal diameters in bovine cortical bone (Black et al. 1974; Rho et al. 1998).

Table 14 - Micropolar Young's modulus and characteristic length values for all specimens combined with standard deviations

Size effect	Micropolar Young's modulus (GPa)	Micropolar characteristic length (mm)	Micropolar characteristic length in bending (mm)
negative	8.6 ± 0.7	0.22 ± 0.11	0.063 ± 0.033

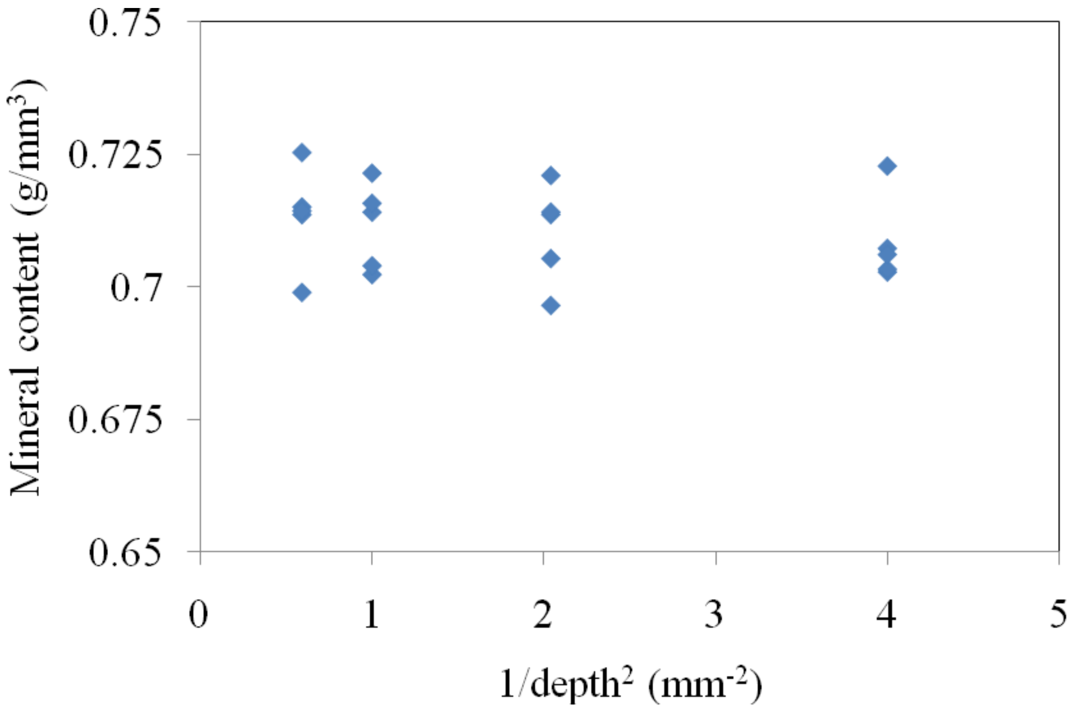

Figure 72 - Mean mineral content plotted against reciprocal of depth squared for all specimens.

Figure 72 shows the mineral content plotted against the reciprocal of depth squared for all specimens. The consistency in mineral content indicates that this has no significant influence on the observed size effect ($p = 0.828$) and indicate that the size effect in stiffness may be attributable to the influence of the material's microstructure. This is further corroborated by Figure 73 which shows the surface roughness plotted against the reciprocal of depth squared for all specimens. There is no discernable size effect in surface roughness with depth ($p = 0.361$).

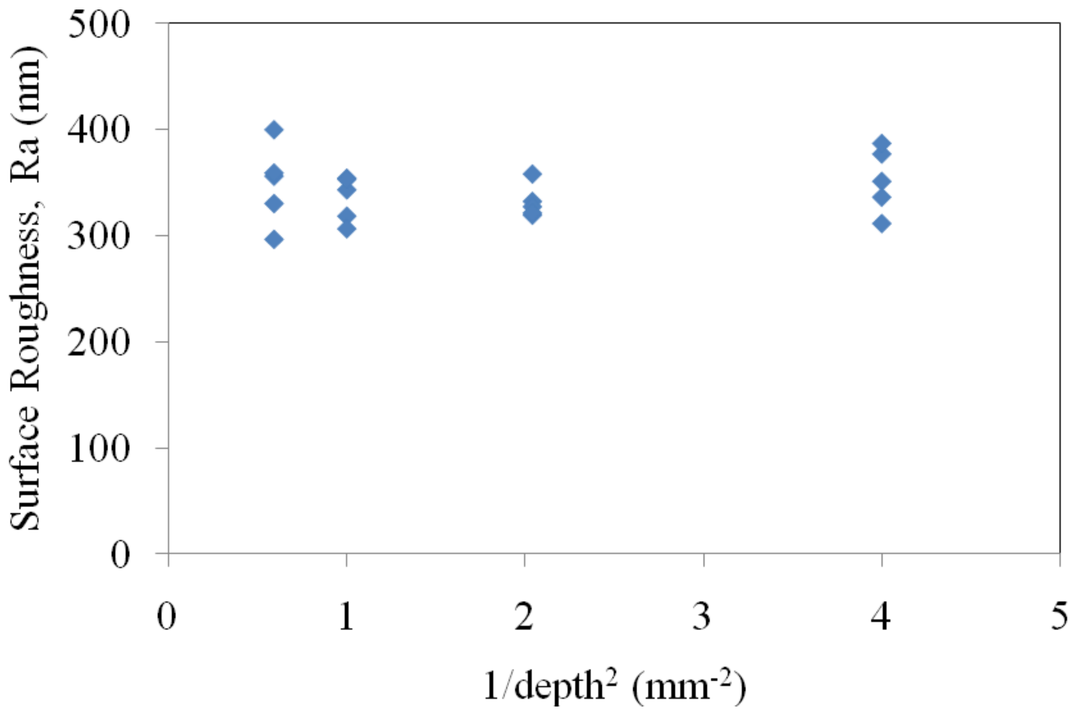

Figure 73 - Reciprocal of depth squared plotted against the mean surface roughness, Ra, for all specimens.

7.2.3 Discussion

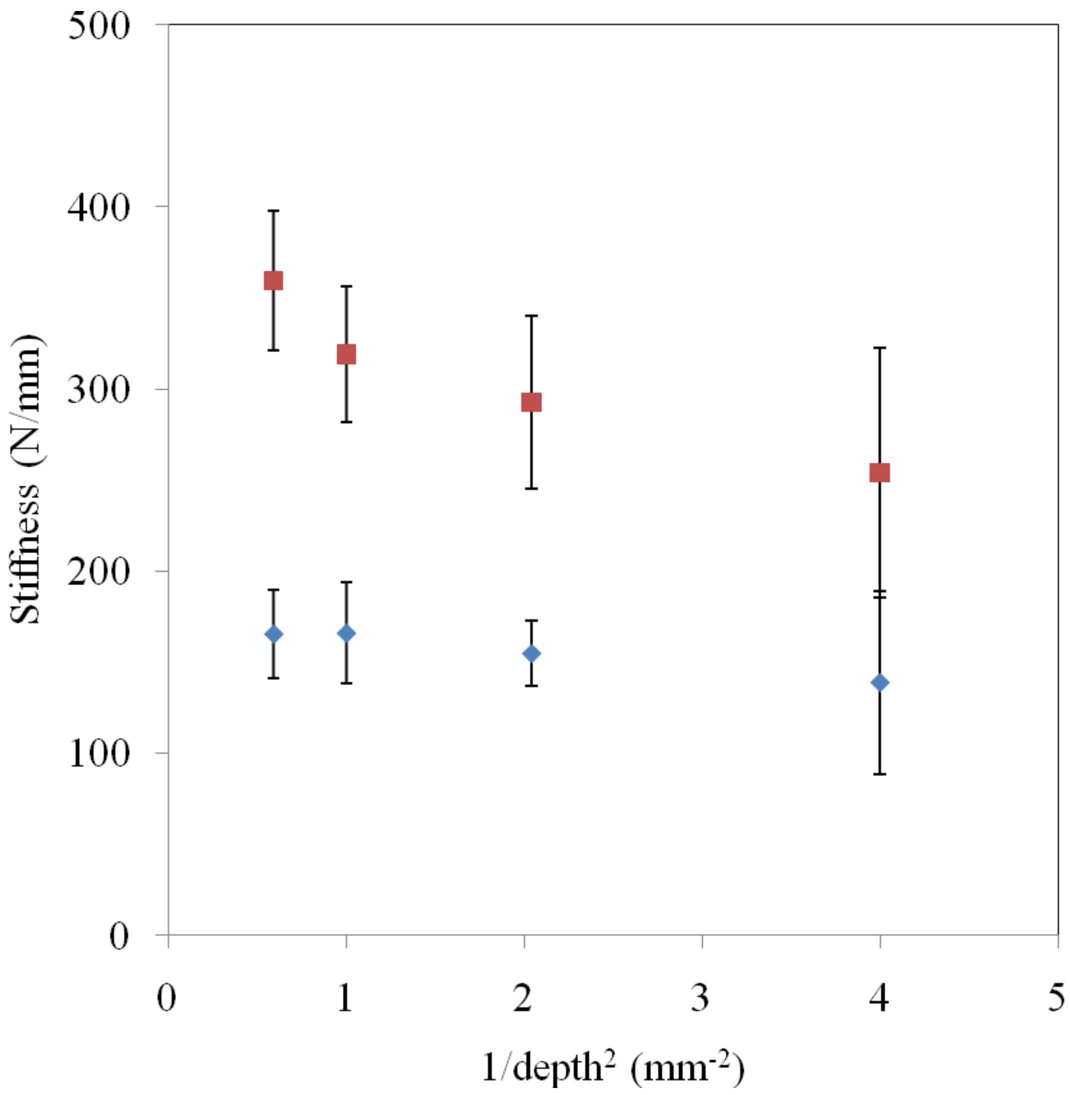

Figure 74 – Mean stiffness values plotted against the reciprocal of depth squared for specimens orientated longitudinally (red squares) and radial-circumferentially (blue diamonds) with standard deviations.

Experimental data exhibits a size softening trend for both the specimens orientated in transversely and longitudinally (Figure 74) with the longitudinal results showing statistical significance.

The micropolar Young's modulus and characteristic length were calculated using Equation 12 and Equation 13 obtained from the size effect relationship in Equation 10 $\left(y = 4E_m b\left(\frac{d^3}{l^3}\right), gradient = \frac{4E_m bd^3}{l^3}\frac{l_c^2}{d^2}\right)$ where the magnitude of the negative gradient was used to calculate the micropolar characteristic length. This revealed that where the specimens were orientated with vascular channels predominantly running along the length of the specimen the characteristic length in bending was 80μm and the micropolar Young's modulus was 17.9 GPa. Where the specimens were orientated in the radial circumferential plane with vascular channels predominantly running through the breadth of the specimen the micropolar characteristic length in bending was 63μm and micropolar Young's modulus was 8.61GPa.

Figure 75 shows a comparison between three sets of stiffness value plotted against the reciprocal of depth squared. The stiffness values have been modified to represent a Young's modulus value in order to compare the results in this study with those of Choi et al. This was done by calculating the equivalent Young's modulus for the flexural stiffness of each specimen. The length, breadth, depth and flexural stiffness were used to recalculate and represent the stiffness in terms of Young's modulus. The three groups are the initial group of five specimens prepared from the five bovine femurs, prepared at larger depths and tested over seven unique depths from 5mm to 0.9mm. These are shown by the blue triangles. The second group is the five specimens from the same five bovine femurs tests conducted over four unique depths from 1.3mm to 0.5mm. These are shown in the red squares on the graph. The final group is the results from three-point bending experiments performed by Choi et al (Choi et al. 1990). These experiments were done on smaller specimen sizes than were used in the current experiments and the specimens were orientated along the long axis of human femurs. They clearly show an extension of the size effect trend and strongly corroborate the findings of this study. Micropolar behaviour however was not inferred from the negative size effects observed by Choi et al. As the trend in Choi's study follows a similar trend to that observed in this study it is possible to relate both to micropolar size effects.

It can also be observed that all ten specimens tested longitudinally follow similar size effect trends. Although the ten specimens were tested individually there is conformity in the size effect trend produced between each specimen. This demonstrates a correlation between inter and intra specimen variability suggesting that, on average, bovine cortical bone will show a size softening anti micropolar size effect when tested in three point bending. This confirms the size effect for each femur. As both specimens for each femur were tested independently, mineral content remained consistent and surface roughness showed no discernable variation with size it may be concluded that the consistent size effects are attributable to the influence of the microstructure becoming more significant as specimen size approaches the depth of the specimen.

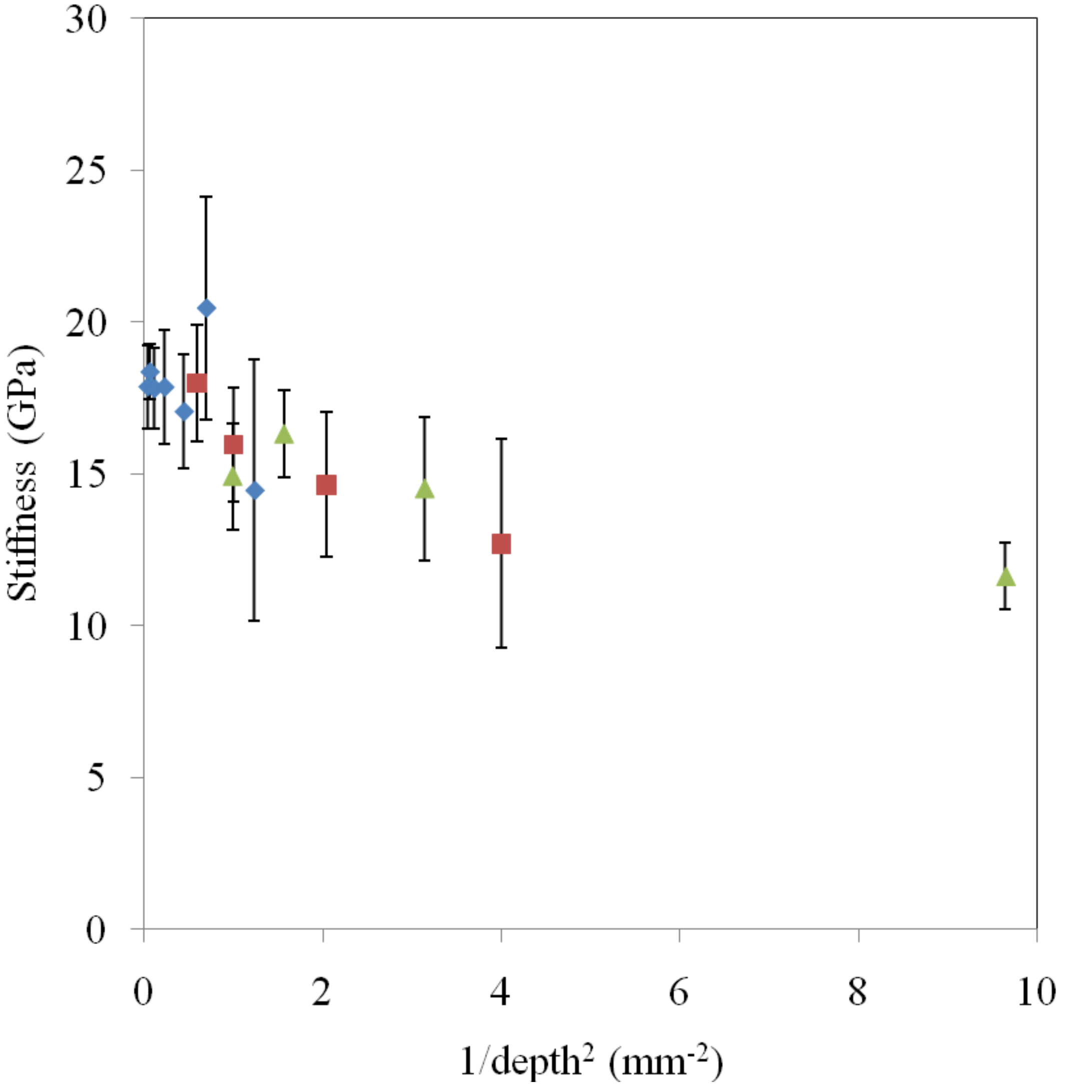

Figure 75 Mean stiffness (Young's modulus values) plotted against the reciprocal of depth squared with standard deviations comparing the initial five specimens with the second group of specimens and the results of Choi. Blue diamonds are the intial five specimens, red squares are the second group of smaller specimens and the green triangles are results of Choi (Choi et al. 1990)**.**

It is possible that successive testing on the same specimen would lead to surface damage and a loss of stiffness with size. However, to negate the effects of microdamage specimens were loaded at a low strain rate of 0.0025s^{-1} and to a maximum outer surface strain of 0.005. This is below the strain where microdamage begins to propagate in cortical bone (Zioupos et al. 2008). Furthermore, as the outermost surface of each specimen was removed between tests then the area most likely to have been affected by microdamage would have been removed.

The continuity in results between the initial five specimens tested over larger depths and the second group tested over smaller depths adds further weight to the argument that microdamage has a limited effect on the observed size effect. As the first specimen tested in the second group shows a stiffness value in accordance with the values observed in the smallest depths of the first group it can be deduced that microdamage has a limited influence during the experimental process itself. However, this does not remove the possibility of microdamage occurring during the preparation process which may have induced damage into the specimens before testing therefore reducing the overall recorded stiffness. Microdamage may also account for the higher standard deviation values seen in the smaller depths from each group of specimens and could be a possible explanation for the heteroscedasticity of the experimental results shown in Figure 65 and Figure 68. This would attribute the higher standard deviation as a consequence of the gradual introduction of microdamage during each loading cycle. However, as the size effect trend is noticeably similar between specimens from the same femurs it may be reasonable to assume that microdamage has had a limited influence on the global inter specimen size effect trends.

7.3 Summary

It has been shown that bovine cortical bone exhibits size effect trends in three-point bending which act in accordance with those predicted by micropolar elasticity. The anti-micropolar size softening size effect follows the trend predicted in the finite element analysis for beams where the surface has been intersected by the internal microstructure. The specimens in this study were prepared to remove the surface artefact and allow the internal microstructure to perforate the surface. By comparing this negative size effect to the corresponding positive size effect observed in beams without microstructure perforating the surface the micropolar material properties of micropolar Young's modulus and characteristic length in bending may be inferred.

Two groups of specimens were tested: the first group of specimens were orientated along the long axis of the femur with vascular channel predominately running alon g their length and the second group was orientated transversely with vascular channels predominantly running through the breadth of each specimen. The results showed the micropolar Young's modulus was 17.9 GPa longitudinally and 8.6 GPa transversely. The micropolar characteristic length in bending was 80μm longitudinally and 63μm transversely. Both of these value are in accordance with those quoted in literature for the physical properties of cortical bone (Rho et al. 1993; Choi et al. 1990; Hogan 1992; Hoc et al. 2006; Black et al. 1974).

Possible alternative causes of a size effect in cortical bone not attributable to the microstructure include demineralisation, inconsistent surface properties and the influence of microdamage were considered. Demineralisation was discounted as there was no significant correlation found between mineral content and specimen size. Surface roughness equally showed no discernable correlation with specimen size. Care was taken to test specimens to a strain no higher than 0.005 where microdamage begins to propagate. Moreover, because of the consistency between specimens and the repeatability of the size effect between specimens from the same bone the size effect observed in these experiments is consistent with those predicted by micropolar elasticity and may be attributed to the microstructure of cortical bone.

8 Comparison between numeric and experimental results

8.1 Background

Computational models of an idealised heterogeneous material, created to mimic the geometry of cortical bone, revealed micropolar size effects in three-point bending. The nature of the observed size effect depends upon the nature of the surface of the beam in bending. If the beam has a surface which is intersected by the internal microstructure, creating a corrugated surface, the beam then shows an anti-micropolar size softening size effect. On the other hand if the surface is continuous and not broken by the internal microstructure a micropolar size stiffening size effect is observed. Similar size effect trends were shown to exist in both the longitudinal and the transverse orientations of the idealised material, albeit of different magnitudes, indicating a three dimensional anisotropic micropolar material.

The experiments on bovine cortical bone revealed an anti-micropolar size effect in three-point bending. Similar size effects were observed in beams orientated both longitudinally and transversely, however the magnitude of the size effect differed between both cases.

The qualitative and quantitative similarities between the computational and experimental results suggested a structural equivalence between both the idealised and the real materials. By direct comparison between both sets of results an enhanced picture of the micropolar material properties of cortical bone may be determined. Similarly, a more detailed gauge of the accuracy of the computational models may also be obtained. This may enable a fuller understanding of the role which the microstructure of cortical bone plays in the global material properties.

8.2 Likelihood of voids on surface

The computational analysis created two models for both the longitudinal and transverse orientations: those with surface perforations and those with a continuous surface. Both models represent an extreme condition and opposite size effects were observed for each case. In comparing the experimentally observed size effect from bovine cortical bone with that of an idealised material it is necessary to identify the likelihood and the average depth by which the surface of a real specimen of cortical bone is intersected by the Haversian canal system (Figure 76).

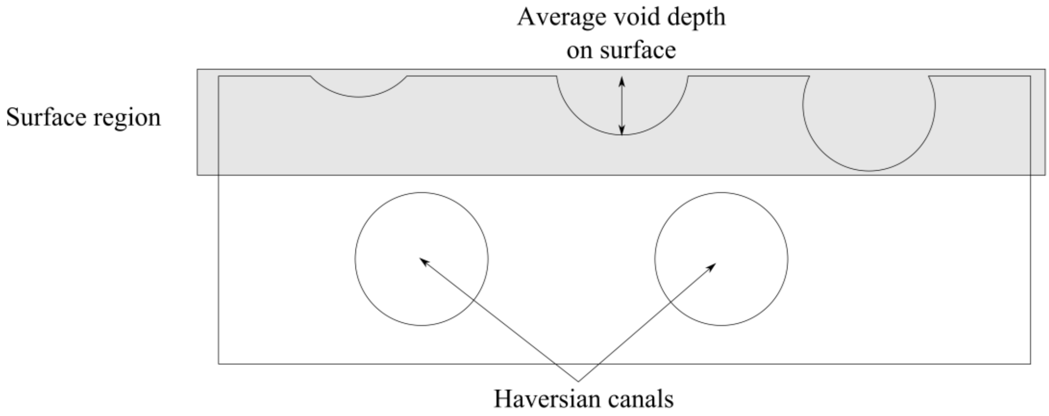

Figure 76 – Vascular channels intersect the surface of a cortical bone cross section

The experimental results showed a negative anti-micropolar size effect congruent with the computational models in which the surface is corrugated by the internal microstructure. Therefore it is surmised that the surface of the experimental specimens has been intersected by the internal microstructure causing a size softening size effect. Thi9s is backed up by imaging of the surface (Figure 22) which indicates the majority of vascular channels are orientated along the length of a long bone consistent with the numerical models. By determining the degree to which the surface has been corrugated by the internal microstructure will allow a direct comparison with the extreme cases of the numerical results. Whilst it may be fairly obvious that the mean depth of the surface voids will be approximately equal to the void radius (Figure 76) the distribution of the void radius is not immediately obvious and should be investigated also.

8.2.1 **Methodology**

A two dimensional array of voids was created, using Matlab (Mathworks Inc, USA), to represent the cross sectional arrangement of voids in cortical bone. The voids were arranged in a random perturbation of the uniform equilateral triangular array used in the FE analysis models where $S_Y = 0.866S_X$ (Figure 77). The horizontal separation of the voids was prescribed as 300μm while the void fraction was set to 0.1, these values were chosen to represent typical values representative of cortical bone where the void fraction is typically between 8-10% and the diameter of an osteon is typically 250-400μm (Wang & Ni 2003; Bensamoun et al. 2004). The void position was then randomly perturbed to a maximum of ±50μm using a normal distribution around the void radius value determined from the specified void fraction value. Five millimetre lines were then repeatedly imposed at random orientations on the void array to represent the possible cut surface of an experimental specimen (Figure 77) and in total ten thousand 5mm lines were imposed on the void array. Both the mean number of surface voids along the breadth and the mean depth of surface void on the surface were calculated in order to determine the likelihood of voids intersecting the surface and to what depth the surface had been broken.

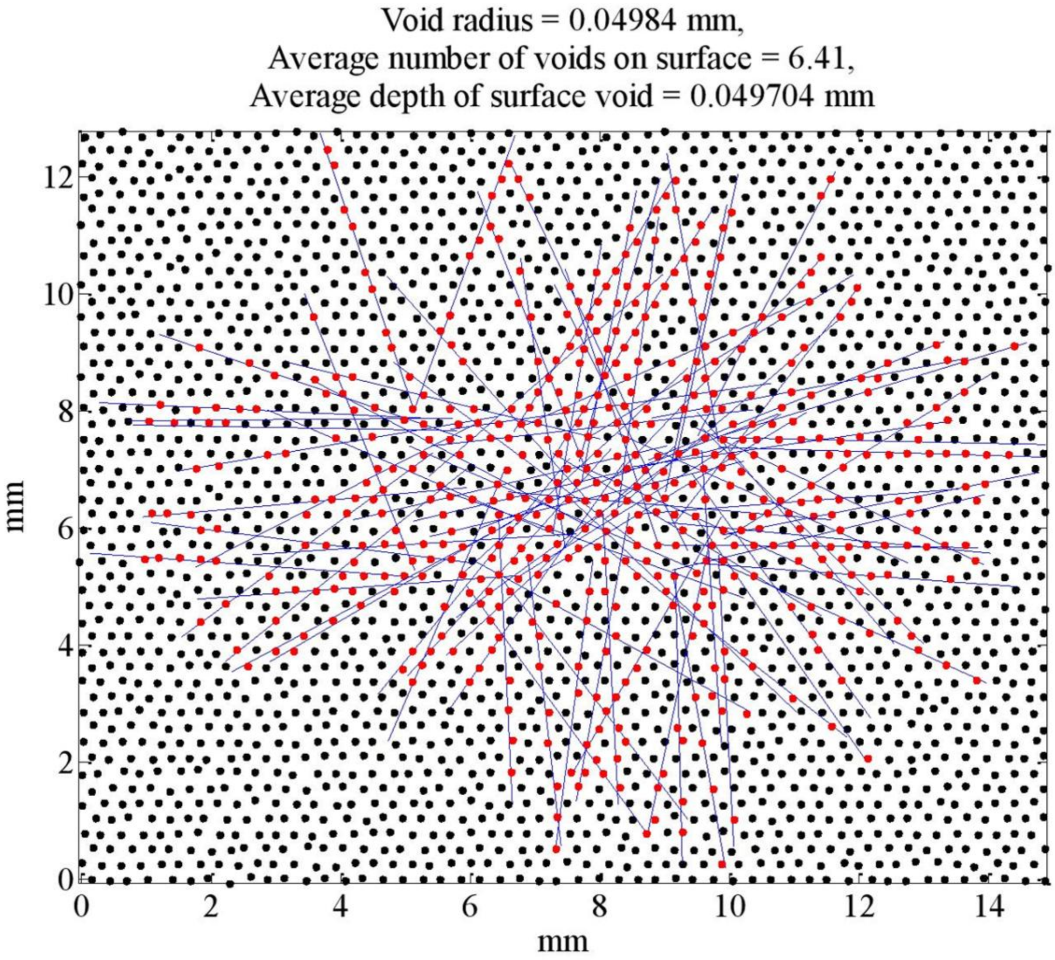

Figure 77 – A two dimensional array of voids representative of the Haversian canal system in a cross section of cortical bone. The blue lines represent randomly distributed cuts through the material.

8.2.2 Results and discussion

The results showed that on average the surface of each 5mm line was intersected by 6.41 Haversian canals. This is representative of 6.41 Haversian canals across the breadth perforating the surface along the length of a 5mm wide specimen. The mean depth of each surface void was found to be 0.0497mm with a standard deviation of 0.007mm which as expected compares to the void radius of 0.0498mm (Figure 78). This indicates that the mean depth of the surface perforations in a five millimetre wide specimen is equivalent to the radius of a Haversian canal.

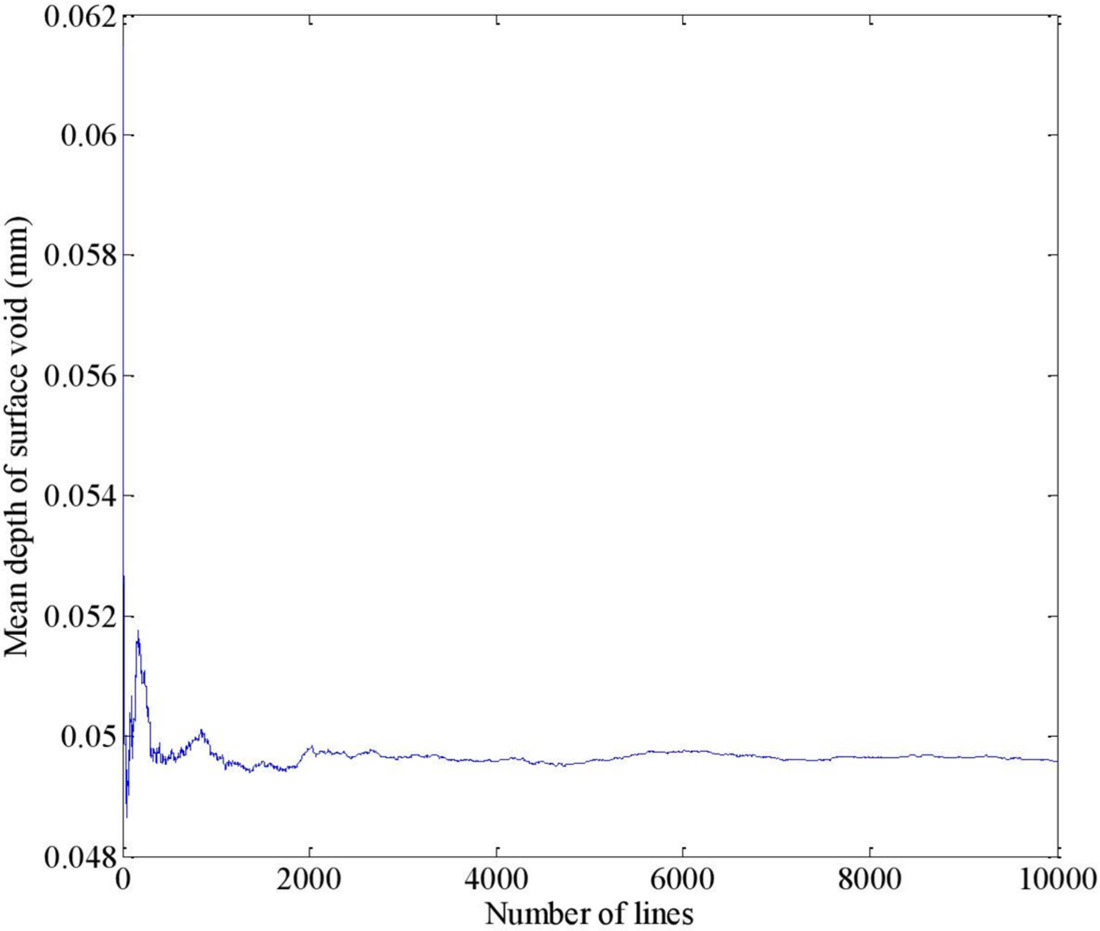

Figure 78 – The mean depth of surface voids plotted against the number of lines plotted.

The significance of these findings is that the mean depth of voids along the surface of a randomly orientated beam is equivalent to the radius of the internal voids in the material. In the case of cortical bone the surface voids are of the same radius as the Haversian canals. This suggests that the experimental specimens of bovine cortical bone were produced with voids intersecting the surface, in accordance with Figure 22, thereby producing a negative anti-micropolar size softening size effect. The computational models of beams with voids perforating the surface were created with half voids along the surface equivalent to voids of half diameter along the surface region. This suggests the size effect produced experimentally is directly comparable to the computational models where the surface is intersected by microstructural voids because both the experimental and computational beams represent materials where the surface is perforated by the internal microstructure to a depth of the void radius.

8.3 Comparison of experimental and FEA results

The results from the Numerical analysis of idealised heterogeneous materials chapter (p40) show the size effects observed in idealised computational models where $S_Y = 0.866S_X$. In cortical bone the separation of vascular channels in the x and y axes are equivalent to the diameter of an osteon typically 250 - 400μm. For this reason the computational results need to be scaled to account for the difference between void size and distribution in the idealised case and the real material. The most appropriate fit of the computational results to the experimental results when considering the distribution of voids in the material is to set the smallest computational specimen size equivalent to the smallest experimental specimen size. To do this S_Y was set to 0.433mm, which compares favourably with the upper threshold of osteon diameter and allows the smallest computational model to approximately coincide with the smallest experimental specimen size. Figure 79 and Figure 80 show the comparison between computational and experimental results for the longitudinal and transverse orientated specimens respectively. It may be noticed that the smallest numerical model is of the same order of magnitude as the smallest experimental model, thereby allowing a more accurate comparison between computational and experimental results.

The root mean square error between the finite element results and experimental results for each void fraction in both the longitudinal and transverse orientations is shown in Table 15. This clearly shows that for both the longitudinally and radially-circumferential orientations a void fraction of 0.145 has the strongest correlation with the experimental results. The void fraction of bovine cortical bone is in the region of 10% which is comparable to the 14.5% void fraction of the most representative numerical model. Figure 81 shows the plot of the experimental results for longitudinal and transverse orientations plotted with the void fraction of 0.145. It can be seen that the longitudinal specimens exhibited a greater size effect than that predicted by the numerical modelling for a void fraction of 0.145, whilst the transverse specimens exhibit a weaker size effect trend at the 0.145 void fraction. This suggests that specimens orientated longitudinally have a more complicated micropolar behaviour and may also indicate that there are multiple influences which might be responsible for the size effect, beyond solely the influence of longitudinally orientated voids. This could be explained by a greater influence of structural features such as cement lines being more influential longitudinally rather than transversely and as a result creating a more pronounced size effect in a longitudinal orientation.

Table 15 – The root mean square error for longitudinally and transversely orientated specimens with the equivalent computational size effect trends for each void radius and void fraction. Where S_X = 0.5mm S_Y = 0.433mm.

Void Fraction	**Normalised Void Radius, V_R/S_Y**	**Longitudinal RMSE with experimental results (N/mm^2)**	**Transverse RMSE with experimental results (N/mm^2)**
0.009	0.06	16.8	19.6
0.036	0.12	13.6	17.0
0.082	0.17	9.2	9.1
0.145	**0.23**	**5.4**	**1.2**
0.227	0.28	8.2	6.9
0.326	0.35	15.6	13.6

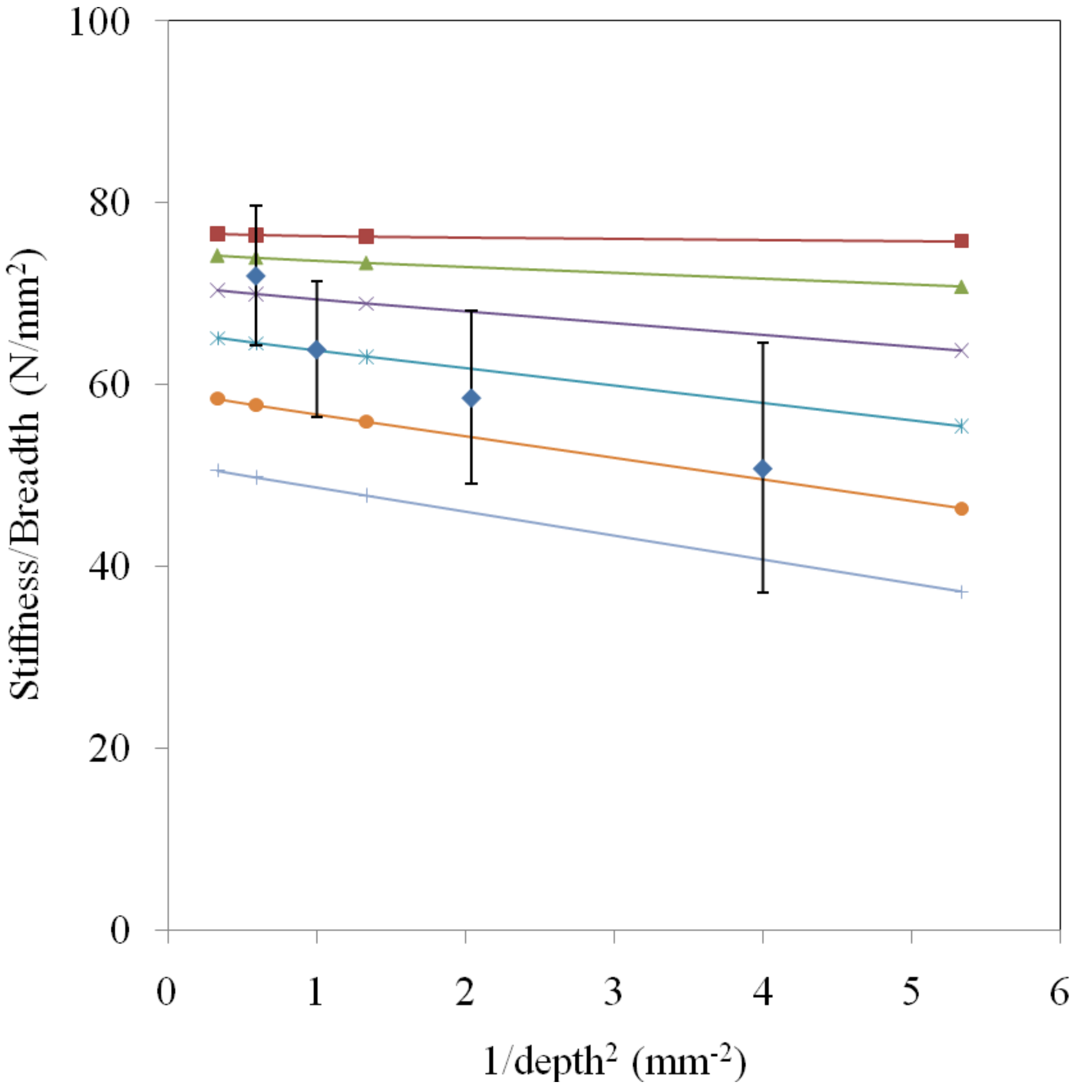

Figure 79 - Comparative plot of the experimental longitudinally results with standard deviation (blue diamonds) and the FE results for different void fractions. S_X = 0.5mm S_Y =0.433mm. Red squares, V_R/S_Y=0.06; green triangles, V_R/S_Y=0.12; purple crosses, V_R/S_Y=0.27; blue stars, V_R/S_Y=0.23; orange circles, V_R/S_Y=0.29; blue crosses, V_R/S_Y=0.35.

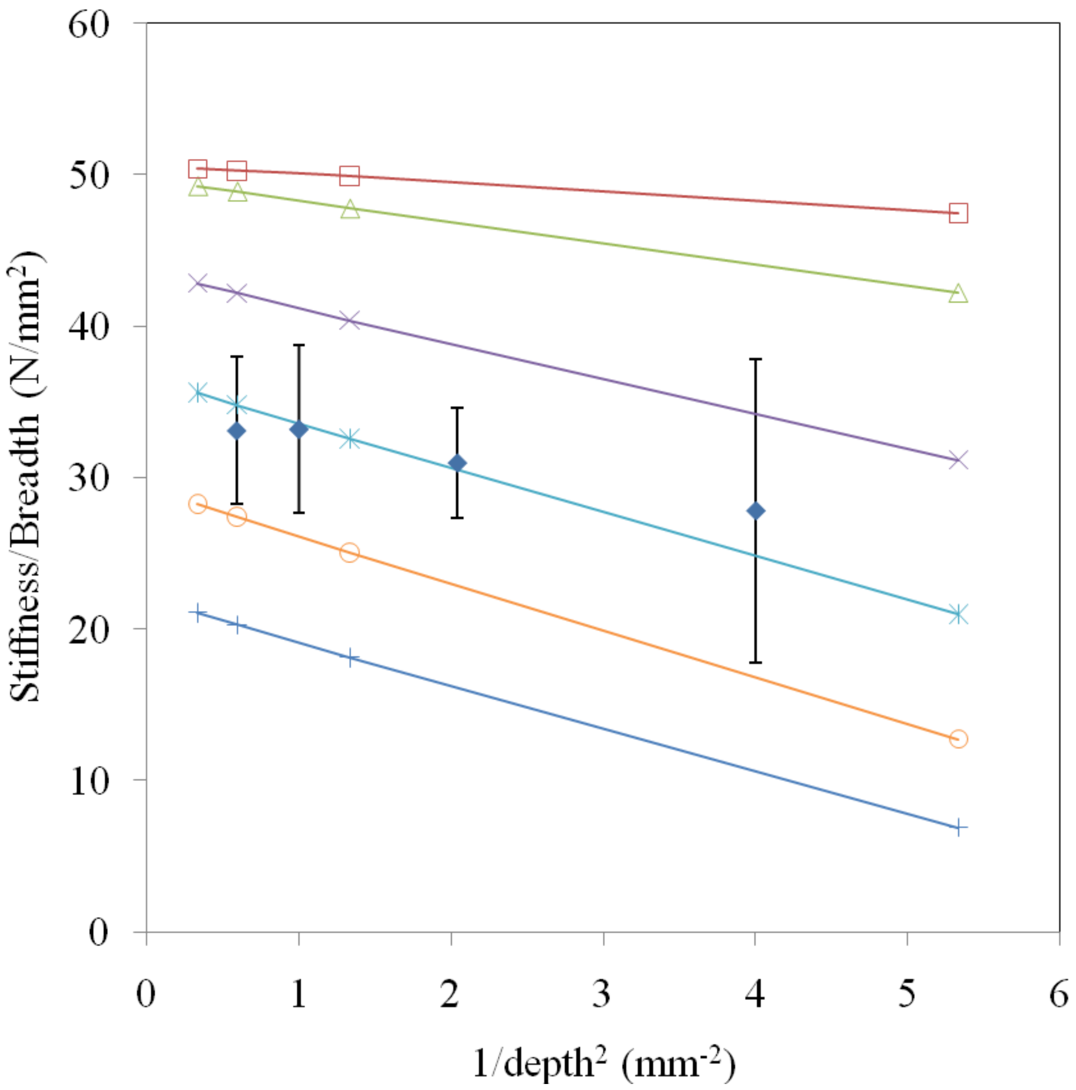

Figure 80 - Comparative plot of the experimental radial-circumferential results (blue diamonds) with the FE results for different void fractions. S_X = 0.5mm S_Y =0.433mm. Red squares, V_R/S_Y=0.06; green triangles, V_R/S_Y=0.12; purple crosses, V_R/S_Y=0.27; blue stars, V_R/S_Y=0.23; orange circles, V_R/S_Y=0.29; blue crosses, V_R/S_Y=0.35.

The micropolar material properties calculated from the computational results give a micropolar characteristic length in bending of 50μm and micropolar Young's modulus of 16.4GPa for the longitudinal models. For the transversely orientated models the micropolar characteristic length in bending from 0.145 void fraction models was found to be 82μm and the micropolar Young's modulus was found to be 8.4GPa. A comparison between these values and the values obtained directly from the trend line of the experimental results can be seen in Table 16.

Table 16 – A comparison between the values for micropolar Young's modulus and characteristic length in bending for the longitudinal and transverse specimens for both the experimental trend fit and FE results for a void fraction of 0.145, S_X of 0.5mm and matrix Young's modulus of 20GPa..

	E_m longitudinal	**l_b longitudinal**	**E_m transverse**	**l_b transverse**
Experimental best fit	17.9GPa	80 µm	8.6GPa	63 µm
FE best fit	16.4GPa	50 µm	8.4GPa	82 µm

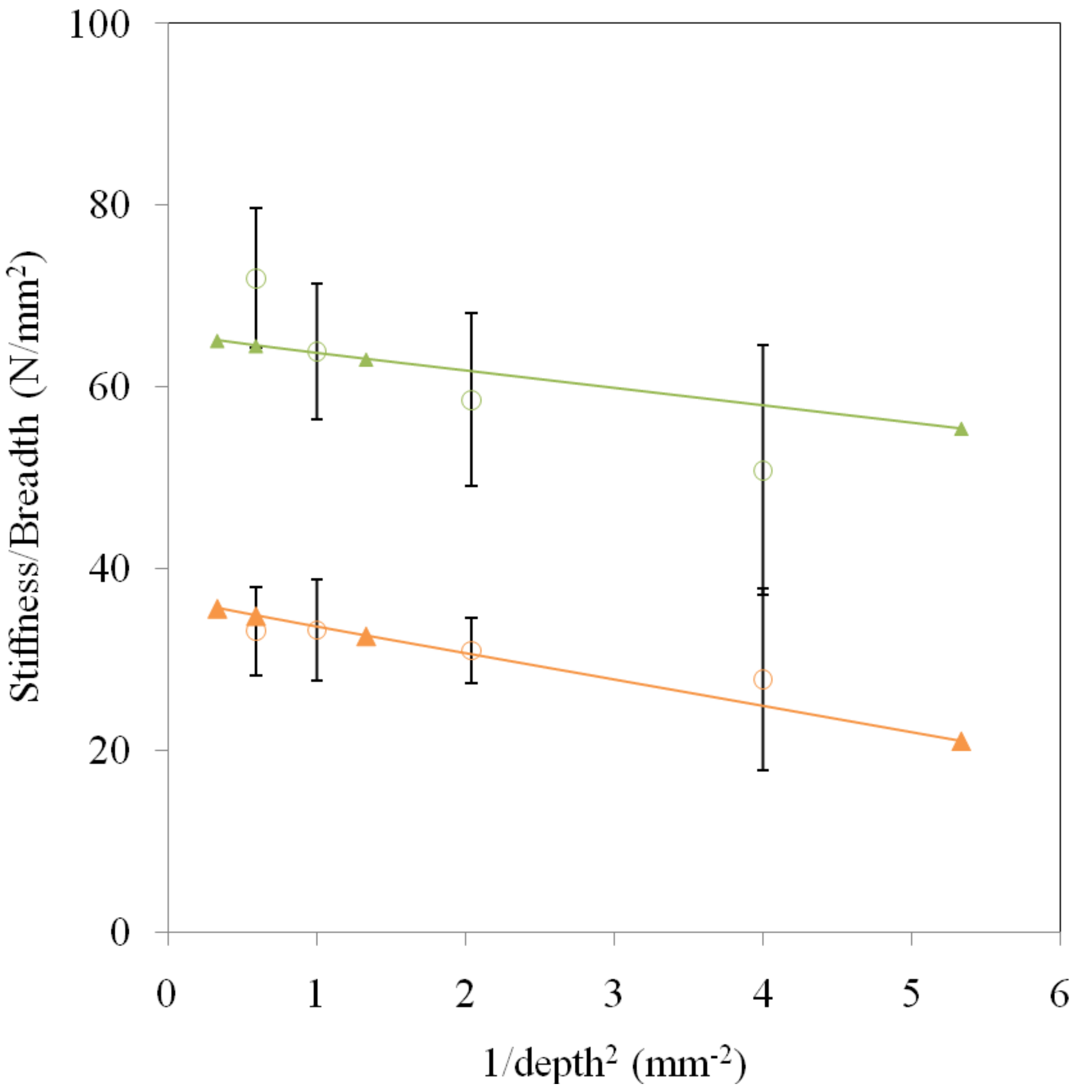

Figure 81 – Experimental results plotted with the numerical results for a void fraction of 0.145 with S_X=0.5mm and S_Y=0.433mm. Green lines are for longitudinal specimens orange are for transverse specimens. Triangles represent the numerical results and circles are for the experimental results.

8.4 Variation in S_X, V_F and matrix Young's modulus (E_{mat})

Although a good agreement between the experimental results and the computational models has been established it is worth discussing the significance of other variables in the computational models and how they may influence the correlation between an idealised model and real materials.

The idealised heterogeneous material may be defined by three parameters: Void spacing (S_X), void fraction (V_F) and matrix Young's modulus (E_{mat}); by altering each of these variables it is possible to create a different size effect. In understanding the significance of a numerically created size effect it is worthwhile determining the material characteristics of the model in order to compare geometrical features as well as material properties. The interdependence of the geometry of the computational model with the observed size effect is an important aspect in understanding similar size effects observed in real materials.

8.4.1 **Separation of voids, S_X**

As mentioned previously the numerical results needed to be scaled to the size of the microstructure in cortical bone. In cortical bone the diameter of an osteon is typically 250-400 μm (Black et al. 1974; J Y Rho et al. 2002; J Y Rho et al. 1997b). For this reason a more representative void spacing was used to compare the numerical and experimental results. To gain a fuller representation of the size effect predicted by the numerical models S_X may be varied through a range of values.

8.4.2 **Void fraction**

The void fraction of cortical bone is typically reported being between 8-10%. The closest correlation between the computational and experimental results was observed where the void fraction was 0.145. Although this is not an exact match, it is a close correlation and suggests that the void fraction responsible for the size effect in the material does not solely consist of the physical voids within the material, but may also be accounting for the differences in the material properties of the different phases of the material (J Y Rho et al. 2002; Hoffler et al. 2000). For example the collagen phase of cortical bone may not contribute significantly to the stiffness and could be considered to contribute towards the void fraction of the material which would undoubtedly increase the void fraction of the overall material as would the contribution of other microstructures such as cement lines.

8.4.3 **Matrix Young’s modulus**

The Young’s modulus of the matrix material is perhaps the most difficult variable to define because of the anisotropy in material properties within cortical bone. Cortical bone is an inherently heterogeneous material at multiple length scales and as a consequence regions of the material may display stiffer material behaviours than other regions because the material is more densely packed and has fewer voids. The Young’s modulus value for the matrix material in cortical bone should take into account the porosity of the material and therefore should be regarded as a stiffer material than the global properties of cortical bone itself. Nano-indentation experiments on regions of the microstructure of cortical bone have suggested that there is a significant difference between osteonal bone and interstitial bone, where the interstitial bone is noticeably stiffer. It is suggested that interstitial bone has a Young's modulus of 22GPa whereas osteonal bone has a modulus of 18-20GPa (Zhang et al. 2008; Ghanbari & Naghdabadi 2009; Rho et al. 2002). Because the idealised model used in this study does not differentiate between osteonal and interstitial cortical bone a generic Young's modulus representative of the matrix material properties was used. For these reason a Young's modulus in the region of 20-22GPa for the matrix material was thought to be representative of cortical bone.

8.4.4 **Methodology**

To determine the closest agreement between the experimental results and the numerical analysis the variables of void fraction V_F and matrix Young's modulus (E_{mat}) were varied for a fixed void spacing, S_X. For each variation the RMSE was calculated to both the longitudinal and transverse experimental results. Voids were maintained in an equilateral array and the separation in the x-axis was fixed to equal 0.5mm (S_Y = 0.433mm), the void fraction was varied between six unique values representative of six void radii (0.01, 0.04, 0.08, 0.15, 0.23, and 0.33) and the matrix Young's modulus was varied between six values (18, 20, 22, 24, 26 and 28GPa).

8.4.5 **Results and discussion**

There was a variation in the RMSE which was dependent upon the three defining variables of the FE model. Table 17 shows the RMSE values for the longitudinally orientated specimens where S_X is equal to 0.5mm. It can be seen that the lowest RMSE which indicates the strongest correlation between experimental and numerical results is for a matrix Young's modulus of 26GPa and a void fraction of 0.33. The equivalent set of RMSE values for transversely orientated specimens is shown in Table 18 where S_X was again set to equal 0.5mm. This indicates that the strongest correlation between experimental and numerical results for the transverse specimens occurs where the matrix Young's modulus is set to 20 GPa and the void fraction is 0.15, which again highlights the difference between the longitudinal and transverse results and their corresponding fit to numerical predictions of micropolar behaviour. Figure 82 shows the values in Table 17 plotted in a three dimensional graph. It can be seen that there is not one clear global minimum in the graph but rather, a valley of minima.

Table 17 – Variation in RMSE where void fraction and matrix Young's modulus have been varied for an S_X value of 0.5mm for longitudinal specimens.

Matrix Young's Modulus (GPa)	Void Fraction					
	0.01	**0.04**	**0.08**	**0.15**	**0.23**	**0.33**
	RMSE of experimental results to FEA results (N/mm)					
18	10.5	8.2	6.2	7.8	13.2	20.2
20	16.7	13.6	9.2	**5.4**	8.2	15.6
22	23.8	20.3	15.0	8.6	**4.7**	11.2
24	31.1	27.2	21.3	14.0	**6.0**	6.9
26	38.6	34.4	28.0	19.9	10.5	**3.8**
28	46.1	41.5	34.7	25.9	15.6	**4.9**

Table 18 - Variation in RMSE where void fraction and matrix Young's modulus have been varied for an S_X value of 0.5mm for transverse specimens.

Matrix Young's Modulus (GPa)	Void Fraction					
	0.01	**0.04**	**0.08**	**0.15**	**0.23**	**0.33**
	RMSE of experimental results to FEA results (N/mm)					
18	14.8	12.4	**5.3**	**2.5**	9.2	15.3
20	19.6	17.0	9.1	**1.2**	6.9	13.6
22	24.5	21.7	12.9	**4.0**	**4.6**	11.9
24	29.4	26.3	16.8	7.1	**2.5**	10.3
26	34.3	31.0	20.7	10.2	**1.6**	8.7
28	39.3	35.7	24.6	13.3	**3.2**	7.1

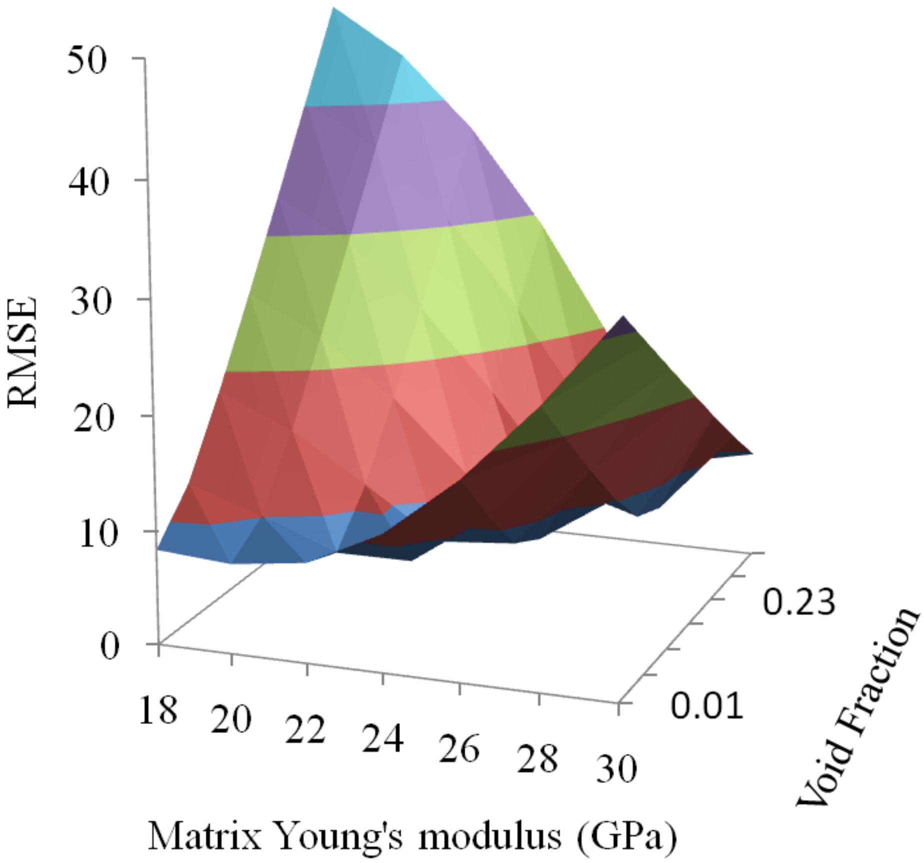

Figure 82 – A three-dimensional plot of the RMSE of the experimental results with computational results plotted against the matrix Young's modulus and void fraction for S_X=0.5mm for longitudinal specimens.

What these findings indicate is that the parameterisation of the FE model may be considered to be a process of curve fitting to the experimental results. By softening the matrix material and reducing the void fraction for a given void separation a more representative fit, which fits with literature values, of the experimental trend can be obtained. Moreover, these findings suggest that the FE model in itself is not a definitive representation of cortical bone, but may be more accurately described as a representation of the material properties exhibited by cortical bone. Nevertheless, what may be inferred from the FE results is that a micropolar behavioural trend is apparent in idealised heterogeneous materials.

Although a broad range of values were used as the parameter inputs for V_F and E_{MAT} the representation of cortical bone as an idealised heterogeneous material is effectively done by selecting input values which closely match those of cortical bone. Selecting input values which are unrealistic in terms of observed material properties may produce a better statistical match but it does not describe the material in real terms. Furthermore, only by obtaining material characteristics from experimental techniques such as image analysis or nano-indentation is it possible for an impression of the input parameters of cortical bone be obtained. This allows a more realistic comparison between the computational and the experimental models because it is comparing similar materials in terms of geometry and mechanical character. In short it is not the output (the desired size effect) which is the important measure of cortical bone's behaviour, but rather, the correlation between the input parameters, the real material properties and the experimental and computational size effects. Although it is possible to obtain a more accurate fit between experimental and computational results by varying the matrix Young's modulus and void fraction, essentially this becomes an exercise in curve fitting. The fact that a matrix Young's modulus of 28GPa and void fraction of 0.33 (and potentially other values) may produce a more accurate fit to the experimental results may only be highlighting the representative nature of the computational models, rather than bear any significance to physical material properties or characteristics. The computational models are a representation of an idealised microstructure, which in itself is representative of the vascular channels in cortical bone.

Bone exhibits more intense micropolar behaviour than the numerical results from idealised heterogeneous materials would suggest. When fitting these idealised heterogeneous models to experimental data the added tissue complexity manifests itself as an increase in void fraction, i.e. the structure causing the micropolar behaviour. The numerical model generated in this study is a simplification of the complex hierarchy present in cortical bone and should not be considered as a realistic microstructural depiction of cortical bone. Rather, the numerical model should be considered a generalisation of the microstructural complexities present in cortical bone. For example the influence of cement lines are not directly included in the numerical representation of vascular channels, however they are a microstructural ferature which is commonly thought to be an important influence on the plastic and viscoelastic material behaviour of cortical bone. This may indicate that the increased micropolar size effect observed in the longitudinally orientated specimens is suggestive of a higher degree of micropolar behaviour which could be attributed to cement lines around osteons acting in conjunction with the natural porosity of the vascular channels. Thus, collagen fibre orientation, cement lines and other structural organisations may all play their parts in the micropolar description of bone. The complexity may be represented by the unphysiological nature of the idealised heterogeneous model.

8.5 Conclusions

The comparison between the experimental results obtained through three-point bending experiments on bovine cortical bone and the numerical analyses of idealised three-dimensional heterogeneous materials show striking similarities. The two orientations of cortical bone specimens experimentally tested revealed identifiable micropolar material properties in the transverse and longitudinal directions. This is consistent with the computational results obtained from the 2-dimensional and 3-dimensional analogue models. Both experimental and numerical models exhibit negative anti-micropolar size effects. A study was undertaken to determine the likelihood of voids intersecting a surface when randomly prepared from a section of cortical bone. It was found that on average the surface will be intersected by voids to a depth of half a void diameter, validating the choice of idealised heterogeneous models. By comparing both the experimental and numerical negative size effects with those obtained numerically for the complimentary positive size effect in beams without surface perforations it has been possible to calculate the micropolar material properties from the experimentally observed size effects.

When the experimental size effects were overlayed onto the FE results it was observed that for a void fraction of 0.145 there was the greatest agreement between both sets of results. This indicated that an idealised 3-dimensional model with a void fraction in the region of 15%, a matrix Young’s modulus of 20GPa and a void separation of 0.5mm produced a realistic description of the microstructure of cortical bone. This was further evidenced by the agreement between micropolar material properties obtained experimentally and numerically.

The input variables for the idealised FE models may be varied in order to adjust the size effects produced. Although these input values may be changed to generate a more accurate correlation between the experimental and numerical results it was decided that the chosen values offered a more realistic description of the nature of cortical bone.

9 Discussion, Conclusions and Further Work

Cortical bone exhibits size effect trends in three-point bending which are consistent with those predicted by micropolar elasticity. The micropolar material properties of micropolar Young’s modulus and micropolar characteristic length in bending were calculated from the negative size effects observed from the three-point bending experiments on two orientations of cortical bone. The longitudinal micropolar Young’s modulus of cortical bone was calculated to be 17.9GPa and longitudinal micropolar characteristic length was calculated to be 80μm. The transverse micropolar Young’s modulus of cortical bone was calculated to be 8.6GPa and transverse micropolar characteristic length in bending was calculated to be 63μm. These compare favourably with published values for the diameter of Haversian canals in secondary osteons, the vascular channels in plexiform bone and the longitudinal and transverse Young’s modulus values of cortical bone (Black et al. 1974; Wang & Ni 2003; Rho et al. 1993).

It has been shown that computational models of idealised heterogeneous materials display size effect trends which are in agreement with the predictions of micropolar elasticity. This is the case for both two-dimensional planar idealised heterogeneous materials and three-dimensional idealised heterogeneous materials. However, there is a fundamental difference in size effect predicted by the numerical models for beams in bending where the surface is broken by the underlying microstructure. In this case a negative size effect approximately opposite to the scenario where the surface is smooth occurs. By showing that the opposing size effects represent extremes of the material behaviour the micropolar material properties may be inferred from the negative size effect. This was further corroborated by a study into the likelihood of voids intersecting a surface in a randomly sectioned beam, which revealed that on average the surface will contain surface voids of half the depth of the internal microstructural void. This allowed the experiments on bovine cortical bone to be compared directly with the computational findings and the micropolar material properties to be calculated.

For the first time ever complementary numerical and experimental size effects in cortical bone have been observed. Both the longitudinal and transverse specimens exhibited distinct micropolar size effect behaviours. When the micropolar material properties were compared they revealed strong agreement between both the numeric and experimental results and further suggest that the diameter of the vascular channels found in cortical bone are a key dimension in understanding the mechanical importance of the microstructure. Experiments on longitudinal specimens exhibited a stronger size effect, as indicated by the gradient of stiffness against $1/d^2$, than that predicated by numerical calculations. However, the strength of the size effect of transversely oriented specimens was well predicted by the numerical models. This suggests a longitudinally aligned microstructural feature of bone which adds to its micropolar behaviour, over and above that due to vascular channels. One possible hypothesis is that the interface between osteons and interstitial bone, i.e. the cement lines, act to increase micropolar behaviour. Thus further work could examine whether a “double micropolar” description may be appropriate for longitudinal specimens where there are two characteristic lengths: one approximately the diameter of the canals, and one approximately the diameter of the primary and/or secondary osteons.

At present cortical bone is generally modelled using classical elasticity. This research has shown that in reality this is a generalisation which is not fully descriptive of the complexities of the material. The presence of a size effect in three-point bending suggests that classical elasticity is an inadequate material model to properly describe the mechanical behaviour of cortical bone in all circumstances. This research may herald the introduction of micropolar elasticity into the mainstream modelling of cortical bone. Although classical elasticity may be an adequate continuum model to describe the mechanical behaviour of cortical bone in general terms, it is not wholly robust for situations where the influence of the microstructure becomes significant. The results presented here strongly suggest that micropolar elasticity is a more appropriate continuum model for describing the material behaviour of cortical bone and that micropolar elasticity may be a more appropriate continuum model for fully incorporating the microstructure into bone’s mechanical description. This is especially true where the scale of the microstructure becomes significant in relation to the macroscale deformations and stresses. In situations where there is an interaction between cortical bone and a prosthetic device for example, the slight deformations and stress concentrations surrounding the microstructure may aid the loosening of an implant over time. There are many common instances where implant loosen over time, and the reasons for this are not well understood at present (Bauer & Schils 1999; J.-H. Lee et al. 2005; Baggi et al. 2008). A possible cause of implant failure may be because the modelling of the implant in cortical bone is performed using classical elasticity and subsequently does not properly describe the translation of stresses between the bone and the implant. This is particularly important when considering stress concentrations around a rigid inclusion. Micropolar elasticity predicts that in such situations the stress concentration will be lower than that predicted by classical elasticity (Beveridge & Wheel 2010; Beveridge et al. 2013; Eringen 1966; Fatemi et al. 2002). It is apparent that a screw, for example, which is holding a hip implant in place, could be considered to be a rigid inclusion in cortical bone and because cortical bone has been shown to behave in accordance with micropolar elasticity, it therefore follows that the stress concentrations which are predicted by modelling a hip implant using classical elasticity may not properly describe the true material behaviour. The result of this may be that stress concentrations are relocated and areas of stress shielding occur, resulting in demineralisation and weakening of regions of the bone which would otherwise be more densely mineralised, or more directly the weakening of regions of bone which should be strong to enable the proper function of the implant. It may be more effective to design an implant and the interaction between an implant and the surrounding region of cortical bone using a micropolar finite element calculation rather than a classical elastic element then. This would enable the effects of the microstructure surrounding an implant screw for example to be generalised by micropolar elasticity rather than using more computationally intensive methods such as micro CT scanning the microstructure and applying a classically elastic material model. The input parameters to the micropolar FE model would be determined from the nature of the microstructure, where the characteristic length is related to the size of the Haversian system and the matrix Young's modulus is related to the Young's modulus of the surrounding osteons and interstitial bone. An example of how a FE material model has been created for a micropolar element is given by Beveridge (Beveridge et al 2013; Waseem & Beveridge 2013; Beveridge et al 2011). The creation of a micropolar FE code which is able to accurately represent cortical bone may ultimately be seen as the continuation of this research and could build upon the findings presented here.

The finite element analyses in this research project have demonstrated the strong link between the magnitude of observed size effects and the void fraction of the microstructure. In relation to cortical bone this finding has a strong significance to the void fractions associated with the Haversian canal system and it has been demonstrated that the characteristic length in bending is scalable to the relative size of the microstructural features. Osteoporosis is a condition where there is a reduction in the mineral content of cortical bone and consequently increases in the void fraction. This suggests that the micropolar characteristic length in bending would be altered depending upon the degree of demineralisation. In understanding the importance of increased void size it follows that the micropolar characteristic length will change depending upon the degree of increased void fraction. This resultantly will produce altered stress concentration patterns in bone with increased osteoporosis. This would enable a more accurate representation and description of the behaviour of osteoporotic bone if micropolar elasticity were used to generalise the increase in void fraction. A micropolar finite element model would be able to account for an increase in void fraction by increasing the input parameter of micropolar characteristic length. Moreover a reduction in mineral content would also imply that the matrix Young’s modulus may have decreased and subsequently this input parameter would be adjusted accordingly. If it is possible to define the character of the material being modelled in terms of the microstructural features and properties then it will be possible to accurately predict the material behaviour of cortical bone.

Micropolar material properties were calculated for the longitudinal and transverse orientations of specimens. In particular size effects were shown to exist in cortical bone where the vascular channels run along the length and through the breadth of specimens in bending. A third case exists where the Haversian canals run through the depth of the specimens. A new set of three-point bending experiments could allow these material properties to be calculated and matched with a complementary FE analysis, thereby providing a more complete material description. This could also be augmented by the creation of more sophisticated FE models which would include more of the microstructural detail and perhaps allow distinctions between microstructural levels of complexity within the material. For example a future FE model may attempt to include more microstructural detail at the intra-osteon level and be complemented by experimental tests on single osteons. However, it should also be noted that the general purpose of defining cortical bone as a micropolar material and the calculation of micropolar material properties is to simplify the simulation processes involved in modelling cortical bone. Once the material has been established as being micropolar, a general micropolar FE model can then be applied to future simulations which will greatly reduce the complexity of the computational model and simulations

Further experiments on cortical bone would enable the micropolar coupling number, which defines the boundary between couples stress elasticity and micropolar elasticity to be identified. This can be done by experimentally comparing the size effect trends produced at varying length to depth aspect ratios (Beveridge et al. 2013). It was not possible to obtain the coupling number from the experiments in this study because only one aspect ratio was tested in three-point bending. Therefore future work may be able to reproduce similar experiments to this study at varying aspect ratios and subsequently calculate the coupling number. The complications involved with this will be in maintaining a consistent experimental protocol between aspect ratios. Ideally a range of length to depth aspect ratios similar to the numerical range simulated in this study would need to be tested, however this requires specimens of both greater and less than a 10:1 aspect ratio being tested, which then introduces practical complications into the experiments.

The experiments on cortical bone in this study used only one discrete value for strain and strain rate for each specimen. It would be interesting to investigate if there was a significant variation in the observed size effect if the strain rate was increased or decreased. Cortical bone is a viscoelastic material and a higher strain rate would undoubtedly increase the observed elastic modulus of each specimen (Zioupos et al. 2008). Moreover, it is known that there is a relationship between observed elastic modulus and micropolar Young's modulus, but would the micropolar characteristic length in bending (related to the gradient of the size effect) be altered by an increase or decrease in strain rate? A study of this kind may also begin to highlight if there are significantly more dominant microstructural features which act at different length scales within cortical bone. For example, it may be possible for lower or higher strain rates to reveal more engagement of cement lines and interaction between cement lines and the surrounding osteons. This may reveal multifaceted degrees of micropolar behaviour which are not characterised by experiments at one strain rate alone. There is also a strong link between the strain rate and the propagation of microcracks in cortical bone (Gupta & Zioupos 2008; Zioupos & Currey 1994; Zioupos et al. 2008) and this could have an important influence on the observed micropolar size effects and in how the micropolar material properties relate to the underlying microstructure. In this study the strain rate was maintained at a relatively low value. At a higher value of strain rate the propagation of microcracks would be reduced and the material may behave in a more rigid classically elastic manner. By conducting further experiments at increased strain rates it may be possible to remove many of the viscoelastic elements of cortical bone's behaviour. Moreover, it may also be possible to remove other layers of heterogeneity in the material. For example at lower strain rates the propagation of microcracks is increased as a method by which cortical bone dissipates energy through the material. At higher strain rates the material is forced to behave in a more rigid manner and stiffens, this may allow a better comparison between the idealised models of the numerical analyses in this study to be compared with cortical bone. This would be because the influence of other possible contributing heterogeneous factors, such as the interaction between organic and mineral phases and the various scales of microstructural detail, which may have contributed to a size effect at lower strain rates would be minimised. Therefore a purer comparison between the idealised void lattice networks in the idealised computational material could be compared with the Haversian and vascular systems in cortical bone. A possible method to enhance the understanding of stress concentrations in micropolar material would be to use Digital Image Correlation

(DIC) to observe the strain behaviour of cortical bone around a rigid inclusion. Such an analysis could investigate the actual bone deformation response around screws which are currently used in implanted devices.

The computational models used in this study are relatively simple. They are linear elastic models which include detailed geometry designed to mimic the character of cortical bone. Once the idealised material has been shown to behave in accordance with micropolar size effect trends it is no longer necessary to include all the geometrical detail of the microstructure. Rather, it is more appropriate to create a micropolar finite element model with input parameters which will produce the same effect as modelling the entire microstructural geometry. The significance of this should not be underestimated, as the reduction in geometrical computational complexity may allow more specialised bone models to be created and subsequently provide advancements in prosthesis design. Many bone models at present use fairly complex geometries which include many of the details of the underlying microstructure. However, the suitability of such a complex geometry may be undermined by the assumptions made in using classical elasticity as the continuum model. If a micropolar element is created all the detail of the microstructure may be discarded and in its place input parameters which characterise the microstructural features may be used instead. For example the micropolar material properties obtained in this study could be used as input parameters to re-create the same size effects in a computational model which was independent of the physical microstructure. Moreover, for a material where the micropolar material properties were unknown, it may be possible to investigate the geometrical structure of the material microstructure and input the physically observed dimensions directly into a micropolar material model. Perhaps by having knowledge of the void size, spacing and matrix material properties, as discussed in the numerical and experimental comparison chapter, it will be possible to fully describe material behaviour using micropolar elasticity. It is hoped that this will create an avenue of advancement not just in prosthesis modelling but in material constitutive modelling in general.

References

Abdel-Wahab, A., Maligno, A.R. & Silberschmidt, V. V., 2011. Micro-scale modelling of bovine cortical bone fracture: Analysis of crack propagation and microstructure using X-FEM. *Computational Materials Science*, pp.1–8.

Akiva, U., Wagner, H. & Weiner, S., 1998. Modelling the three-dimensional elastic constants of parallel-fibred and lamellar bone. *Journal of materials science*, 33(6), pp.1497–1509.

Anderson, W. & Lakes, R., 1994. Size effects due to Cosserat elasticity and surface damage in closed-cell polymethacrylimide foam. *Journal of Materials Science*, 29(24), pp.6413–6419.

Baggi, L. et al., 2008. The influence of implant diameter and length on stress distribution of osseointegrated implants related to crestal bone geometry: a three-dimensional finite element analysis. *The Journal of prosthetic dentistry*, 100(6), pp.422–31.

Bala, Y. et al., 2011. Respective roles of organic and mineral components of human cortical bone matrix in micromechanical behavior: an instrumented indentation study. *Journal of the mechanical behavior of biomedical materials*, 4(7), pp.1473–82.

Bauer, T.W. & Schils, J., 1999. The pathology of total joint arthroplasty.II. Mechanisms of implant failure. *Skeletal radiology*, 28(9), pp.483–97.

Bayraktar, H.H. et al., 2004. Comparison of the elastic and yield properties of human femoral trabecular and cortical bone tissue. *Journal of biomechanics*, 37, pp.27–35.

Belanche, A. et al., 2011. The tensile behaviour of demineralized bovine cortical bone. *Journal of animal science*, 29(11), pp.1497–1501.

Bensamoun, S. et al., 2004. Spatial distribution of acoustic and elastic properties of human femoral cortical bone. *Journal of biomechanics*, 37(4), pp.503–10.

Beveridge, A., 2011. Novel computational methods to predict the deformation of macroscopic heterogeneous materials. *PhD Thesis, University of Strathclyde*.

Beveridge, A. & Wheel, M., 2010. Computational Modelling and Experimental Characterisation of Heterogeneous Materials. *Materials with Complex Behaviour*, 3(2), pp.257–268.

Beveridge, A., Wheel, M. & Nash, D., 2013. The micropolar elastic behaviour of model macroscopically heterogeneous materials. *International Journal of Solids and Structures*, 50(1), pp.246–255.

Beveridge, A., Wheel, M., 2010. Computational Modelling and Experimental Characterisation of Heterogeneous Materials. *Materials with Complex Behaviour,* 3(2), pp.257–268.

Bigoni, D. & Drugan, W.J., 2007. Analytical Derivation of Cosserat Moduli via Homogenization of Heterogeneous Elastic Materials. *Journal of Applied Mechanics,* 74(4), p.741.

Black, J., Mattson, R. & Korostoff, E., 1974. Haversian osteons: size, distribution, internal structure, and orientation. *Journal of biomedical materials research*, 8(5), pp.299–319.

Braidotti, P. et al., 1995. An elastic compound tube model for a single osteon. *Journal of biomechanics,* 28(4), pp.439–444.

Brezny, R. & Green, D.J., 1990. Characterization of edge effects in cellular materials. *Journal of Materials Science,* 25(11), pp.4571–4578.

Buechner, P.M. & Lakes, R.S., 2003. Size effects in the elasticity and viscoelasticity of bone. *Biomechanics and modeling in mechanobiology*, 1(4), pp.295–301.

Burstein, A.H. et al., 1975. Contribution of collagen and mineral to the elastic-plastic properties of bone. *Journal of Bone and Joint Surgery*.

Buskirk, R. & Rice, J.C., 1982. A continuous wave technique for the measurement of the elastic properties of cortical bone. *Journal of biomechanics*, 17(5), pp.349–361.

Choi, K. et al., 1990. The elastic moduli of human subchondral, trabecular, and cortical bone tissue and the size-dependency of cortical bone modulus. *Journal of biomechanics*, 23(11), pp.1103–13.

Cowin, S., 1989. *Bone mechanics*, CTC Press (Boca Raton, Florida).

Cristofolini, L. et al., 2009. Stress shielding and stress concentration of contemporary epiphyseal hip prostheses. *Proceedings of the Institution of Mechanical Engineers, Part H: Journal of Engineering in Medicine*, 223(1), pp.27–44.

Currey, J. D., 1969. The mechanical consequences of variation in the mineral content of bone. *Journal of Biomechanics*, 2(I), pp.1–11.

Currey, J. D. 1975. The effects of strain rate, reconstruction and mineral content on some mechanical properties of bovine bone. *Journal of Biomechanics*, 8, pp.81–86.

Currey, J.D., 1988. The effect of porosity and mineral content on the Young’s modulus of elasticity of compact bone. *Journal of Biomechanics*, 21(2), pp.131–139.

Dong, X.N. & Guo, X.E., 2004. The dependence of transversely isotropic elasticity of human femoral cortical bone on porosity. *Journal of biomechanics*, 37(8), pp.1281–7.

Ebacher, V. et al., 2012. Sub-lamellar microcracking and roles of canaliculi in human cortical bone. *Acta biomaterialia*, 8(3), pp.1093–100.

Ellison, B. et al., 2009. Minimal stress shielding with a Mallory-Head titanium femoral stem with proximal porous coating in total hip arthroplasty. *Journal of orthopaedic surgery and research*, 4, p.42.

Eringen, A., 1966. Linear theory of micropolar elasticity.

Eringen, A., 1967. Linear theory of micropolar viscoelasticity. *International Journal of Engineering Science*, 5(2), pp.191–204.

Evans, G.P. et al., 1990. Microhardness and Young’s modulus in cortical bone exhibiting a wide range of mineral volume fractions, and in a bone analogue. *Journal of Materials Science: Materials in Medicine*, 1(1), pp.38–43.

Fatemi, J., Van Keulen, F. & Onck, PR, 2002. Generalized Continuum Theories: Application to Stress Analysis in Bone. *Meccanica*, 37(4), pp.385–396.

Forest, S., Barbe, F. & Cailletaud, G., 2000. Cosserat modelling of size effects in the mechanical behaviour of polycrystals and multi-phase materials. *Science*, 37, pp.7105–7126.

Gauthier, R.D. & Jahsman, W.E., 1975. A quest for micropolar elastic constants. *Journal of Applied Mechanics*, 42, pp.369–374.

Ghanbari, J. & Naghdabadi, R., 2009. Nonlinear hierarchical multiscale modeling of cortical bone considering its nanoscale microstructure. *Journal of biomechanics*, 42(10), pp.1560–5.

Ghoniem, N. et al., 2003. Multiscale modelling of nanomechanics and micromechanics: an overview. *Philosophical Magazine*, 83(31), pp.3475–3528.

Gitman, I.M. et al., 2010. Stress concentrations in fractured compact bone simulated with a special class of anisotropic gradient elasticity. *International Journal of Solids and Structures*, 47(9), pp.1099–1107.

Goda, I. et al., 2012. A micropolar constitutive model of cancellous bone from discrete homogenization. *Journal of the Mechanical Behavior of Biomedical Materials*.

Gupta, H.S. & Zioupos, P, 2008. Fracture of bone tissue: The “hows” and the “whys”. *Medical engineering & physics*, 30(10), pp.1209–26.

Hasegawa, K. et al., 1995. Elastic properties of osteoporotic bone measured by scanning acoustic microscopy. *Bone*, 16(1), pp.85–90.

Hasegawa, K., Turner, C H & Burr, D.B., 1994. Contribution of collagen and mineral to the elastic anisotropy of bone. *Calcified tissue international*, 55(5), pp.381–6.

Hernandez, C.J. et al., 2001. The influence of bone volume fraction and ash fraction on bone strength and modulus. *Bone*, 29(1), pp.74–8.

Hoc, T. et al., 2006. Effect of microstructure on the mechanical properties of Haversian cortical bone. *Bone*, 38(4), pp.466–74.

Hoffler, C.E. et al., 2000. Heterogeneity of bone lamellar-level elastic moduli. *Bone*, 26(6), pp.603–9.

Hogan, H.A., 1992. Micromechanics modeling of Haversian cortical bone properties. *Journal of Biomechanics*, 5, pp.549–556.

Huiskes, R., 1990. The various stress patterns of press-fit, ingrown, and cemented femoral stems. *Clinical orthopaedics and related research*, (261), pp.27–38.

Iyo, T. et al., 2004. Anisotropic viscoelastic properties of cortical bone. *Journal of Biomechanics*, 37, pp.1433–1437.

Johnson, T.P.M., Socrate, S. & Boyce, M.C., 2010. A viscoelastic , viscoplastic model of cortical bone valid at low and high strain rates. *Acta Biomaterialia*, 6(10), pp.4073–4080.

Katz, J.L. & Yoon, H.S., 1984. The structure and anisotropic mechanical properties of bone. *IEEE transactions on bio-medical engineering*, 31(12), pp.878–84.

Kouznetsova, V., Geers, M.G.D. & Brekelmans, W. a. M., 2002. Multi-scale constitutive modelling of heterogeneous materials with a gradient-enhanced computational homogenization scheme. *International Journal for Numerical Methods in Engineering*, 54(8), pp.1235–1260.

Ladevèze, P., 2004. Multiscale modelling and computational strategies for composites. *International Journal for Numerical Methods in Engineering*, 60(1), pp.233–253.

Lakes, R., 1995. Experimental methods for study of cosserat elastic solids and other generalized elastic continua. *Continuum models for materials with microstructure*, Ch. 1, p. 1-22.

Lakes, R., 1983. Size effects and micromechanics of a porous solid. *Journal of Materials Science*, 18(9), pp.2572–2580.

Lakes, R., 1979. Viscoelastic properties of wet cortical bone. *Journal of Biomechanics*, 12, pp.679–687.

Lee, J.H. et al., 2005. Effect of implant size and shape on implant success rates: a literature review. *The Journal of prosthetic dentistry*, 94(4), pp.377–81.

Lees, S., Heeley, J.D. & Cleary, P.F., 1979. A Study of Some Properties of a Sample of Bovine Cortical Bone Using Ultrasound. *Bone*, 117, pp.107–117.

Macione, J. et al., 2010. Correlation between longitudinal, circumferential, and radial moduli in cortical bone: effect of mineral content. *Journal of the mechanical behavior of biomedical materials*, 3(5), pp.405–13.

Martin, R.B. et al., 1996. Collagen fiber organization is related to mechanical properties and remodeling in equine bone. A comparison of two methods. *Journal of biomechanics*, 29(12), pp.1515–21.

Martin, R.B. & Boardman, D.L., 1993. The effects of collagen fiber orientation, porosity, density, and mineralization on bovine cortical bone bending properties. *Journal of biomechanics*, 26(9), pp.1047–54.

Mayya, A., Banerjee, A. & Rajesh, R., 2013. Mammalian cortical bone in tension is non-Haversian. *Scientific reports*, 3, p.2533.

Najafi, a R. et al., 2007. Micromechanics fracture in osteonal cortical bone: a study of the interactions between microcrack propagation, microstructure and the material properties. *Journal of biomechanics*, 40(12), pp.2788–95.

Najafi, R. et al., 2009. A fiber-ceramic matrix composite material model for osteonal cortical bone fracture micromechanics: solution of arbitrary microcracks interaction. *Journal of the mechanical behavior of biomedical materials*, 2(3), pp.217–23.

Norman, T.L. & Wang, Z., 1997. Microdamage of human cortical bone: incidence and morphology in long bones. *Bone*, 20(4), pp.375–9.

Park, H. & Lakes, R., 1986. Cosserat micromechanics of human bone: strain redistribution by a hydration sensitive constituent. *Journal of biomechanics*, 19(5), pp.385–97.

Pazzaglia, U.E. et al., 2009. Anatomy of the intracortical canal system: scanning electron microscopy study in rabbit femur. *Clinical orthopaedics and related research*, 467(9), pp.2446–56.

Pidaparti, R.M. V & Chandran, A., 1996. Predictions of a composite model for osteonal. *Science*, 29(7), pp.909–916.

Pope, M.H., 1974. Mechanical properties of bone as a function of position and orientation. *Journal of Biomechanics*, 7, pp.61–66.

Ramézani, H. et al., 2012. Size effect method application for modeling of human cancellous bone using geometrically exact Cosserat elasticity. *Computer Methods in Applied Mechanics and Engineering*, 237-240, pp.227–243.

Reilly, G. C. & Currey, J. D., 1999. The development of microcracking and failure in bone depends on the loading mode to which it is adapted. *The Journal of experimental biology*, 202(Pt 5), pp.543–52.

Reilly, G. C. & Currey, J. D, 2000. The effects of damage and microcracking on the impact strength of bone. *Journal of Biomechanics*, 33, pp.337–343.

Remond, A. & Naili, S., 2005. Transverse isotropic poroelastic osteon model under cyclic loading. *Mechanics Research Communications*, 32(6), pp.645–651.

Rho, J. Y. et al., 2002. Microstructural elasticity and regional heterogeneity in human femoral bone of various ages examined by nano-indentation. *Journal of biomechanics*, 35(2), pp.189–98.

Rho, J. Y., Kuhn-Spearing, L. & Zioupos, P, 1998. Mechanical properties and the hierarchical structure of bone. *Medical engineering & physics*, 20(2), pp.92–102.

Rho, J. Y., Roy, M. & Pharr, G.M., 2000. Comments on “Elastic modulus and hardness of cortical and trabecular bone lamellae measured by nanoindentation in the human femur”. *Journal of biomechanics*, 33(10), pp.1335–7.

Rho, J. Y., Tsui, T.Y. & Pharr, G.M., 1997a. Elastic properties of human cortical and trabecular lamellar bone measured by nanoindentation. *Biomaterials*, 18(20), pp.1325–30.

Rho, J. Y., Ashman, R.B. & Turner, Charles H., 1993. Young’s modulus of trabecular and cortical bone material: Ultrasonic and microtensile measurements. *Journal of Biomechanics*, 26(2), pp.111–119.

Sasaki, N. & Enyo, A., 1995. Viscoelastic properties of bone as a function of water content. *Journal of biomechanics*, 28(7), pp.809–15.

Sasaki, N. et al., 2008. Effect of mineral dissolution from bone specimens on the viscoelastic properties of cortical bone. *Journal of biomechanics*, 41(16), pp.3511–4.

Sathappan, S.S. et al., 2009. Does stress shielding occur with the use of long-stem prosthesis in total knee arthroplasty? *Knee surgery, sports traumatology, arthroscopy : official journal of the ESSKA*, 17(2), pp.179–83.

Sevostianov, I. & Kachanov, M., 2000. Impact of the porous microstructure on the overall elastic properties of the osteonal cortical bone. *Journal of biomechanics,* 33(7), pp.881–8.

Smit, T.H., Huyghe, J.M. & Cowin, S.C., 2002. Estimation of the poroelastic parameters of cortical bone. *Journal of biomechanics,* 35(6), pp.829–35.

Swanson, S.R., 2001. Anticlastic effects and the transition from narrow to wide behavior in orthotropic beams. *Composite Structures,* 53, pp.449–455.

Tai, K. et al., 2007. Nanoscale heterogeneity promotes energy dissipation in bone. *Nature materials,* 6(6), pp.454–62.

Taylor, D. & Lee, T.C., 1998. Measuring the shape and size of microcracks in bone. *Journal of biomechanics*, 31(12), pp.1177–80.

Tekoglu, C. & Onck, P, 2008. Size effects in two-dimensional Voronoi foams: A comparison between generalized continua and discrete models. *Journal of the Mechanics and Physics of Solids,* 56(12), pp.3541–3564.

Turner, C H, Chandran, a & Pidaparti, R.M., 1995. The anisotropy of osteonal bone and its ultrastructural implications. *Bone*, 17(1), pp.85–9.

Vashishth, D., Behiri, J C & Bonfield, W., 1997. Crack growth resistance in cortical bone: concept of microcrack toughening. *Journal of biomechanics*, 30(8), pp.763–9.

Vashishth, D., Tanner, K.E. & Bonfield, W., 2000. Contribution, development and morphology of microcracking in cortical bone during crack propagation. *Journal of biomechanics,* 33(9), pp.1169–74.

Wang, X. & Ni, Q., 2003. Determination of cortical bone porosity and pore size distribution using a low field pulsed NMR approach. *Journal of orthopaedic research*, 21(2), pp.312–9.

Waseem, A. et al., 2013. The Influence of Void Size on the Micropolar Constitutive Properties of Model Heterogeneous Materials. *European Journal of Mechanics - A/Solids*, 40, pp. 148–157.

Wirtz, D.C. et al., 2000. Critical evaluation of known bone material properties to realize anisotropic FE-simulation of the proximal femur. *Journal of biomechanics*, 33(10), pp.1325–30.

Yamato, Y. et al., 2006. Distribution of longitudinal wave properties in bovine cortical bone in vitro. *Ultrasonics*, 44 Suppl 1, pp.e233–7.

Yang, J. & Lakes, R., 1982. Experimental study of micropolar and couple stress elasticity in compact bone in bending. *Journal of biomechanics*, 25, pp.91–98.

Zhang, J., Niebur, G.L. & Ovaert, T.C., 2008. Mechanical property determination of bone through nano- and micro-indentation testing and finite element simulation. *Journal of biomechanics*, 41(2), pp.267–75.

Zioupos, P., and Currey, J., 1994. The extent of microcracking and the morphology of microcracks in damaged. *Journal of Materials Science*, 29, pp. 978-986.

Zioupos, P., 1998. Recent developments in the study of failure of solid biomaterials and bone: “fracture” and “pre-fracture” toughness. *Materials Science and Engineering: C*, 6(1), pp.33–40.

Zioupos, P, Hansen, U. & Currey, John D, 2008. Microcracking damage and the fracture process in relation to strain rate in human cortical bone tensile failure. *Journal of biomechanics*, 41(14), pp.2932–9.

Zysset, Philippe K., Guo, X., Hoffler, C., Goldstein S., 1999. Elastic modulus and hardness of cortical and trabecular bone lamellae measured by nanoindentation in the human femur. *Journal of Biomechanics*, 32, pp.1005–1012.

Appendix

Example mesh convergence study

A convergence study was carried out on the 2-D finite element mesh for each void radius, V_R from 0.05 to 0.3 at 0.05 intervals with S_X and S_Y fixed at 1 and 0.866 respectively. The numbers of nodes in the mesh were altered by using a user defined refine variable which was added to the input file. The percentage variation in calculated deflection was calculated and the mesh was deemed to have converged when the values were within 0.5% from the previous mesh. It can be seen that even with a relatively coarse mesh of less than 5000 nodes the models converged fairly well.

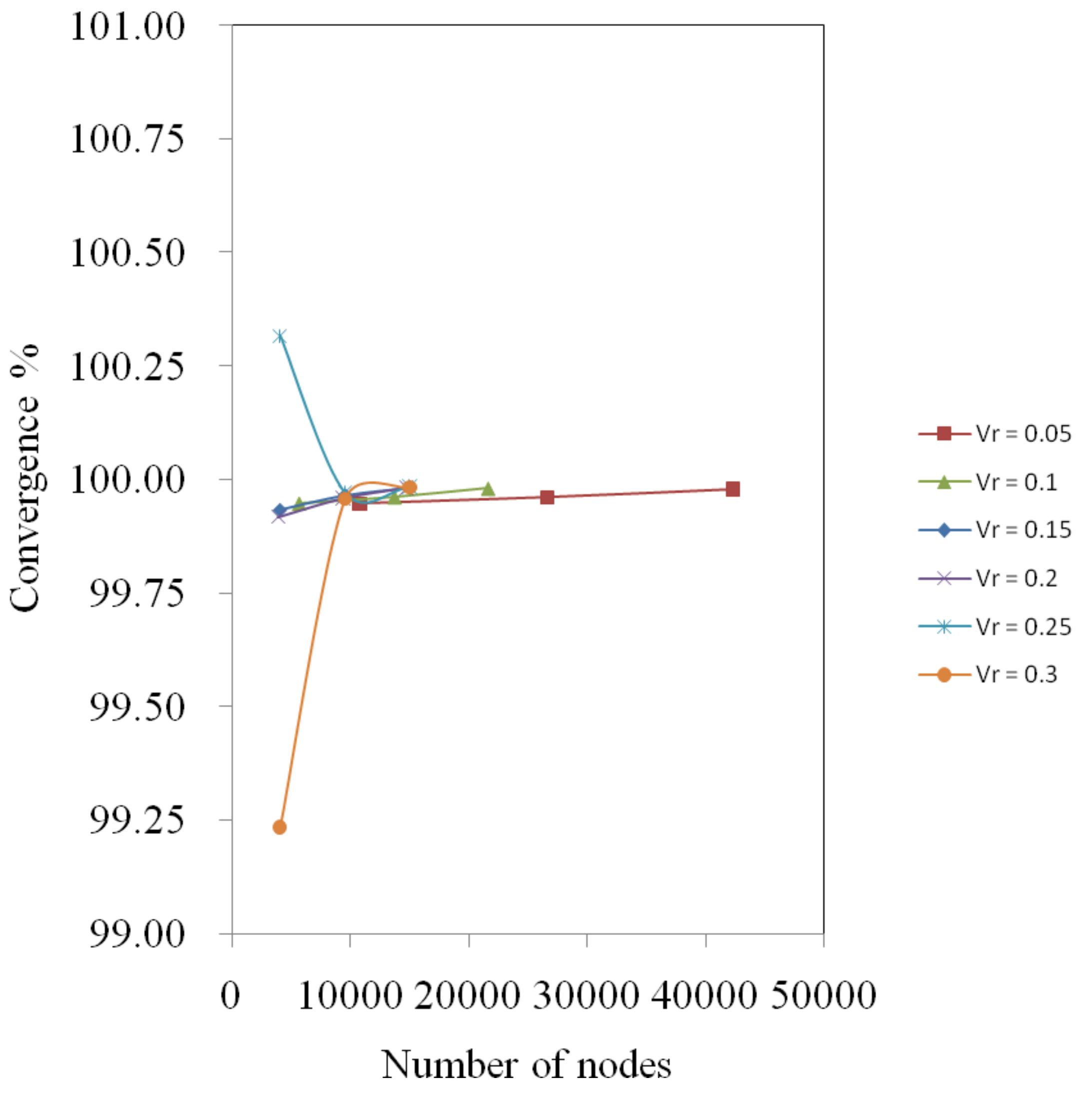

Publications

Simortho, Rostock, Germany August 2011, Oral presentation: The micropolar properties of bone.

Bose usergroup, University of Strathclyde, Glasgow, UK, April 2012, Oral presentation: Size effects in cortical bone.

Euromech Colloquium, Saint-Etienne, France, May 2012, Oral presentation: Haversian canal structures can be associated with size effects in cortical bone.

ESB, Lisbon, Portugal, July 2012, Oral presentation: Computational modelling of micropolar behaviour in cortical bone.

Glasgow Orthopaedic Research Group (GLORI), October 2012, Oral presentation: Modelling Micropolar Size Effects in Cortical Bone.

THE 10th HSTAM International Congress on Mechanics, Crete, Greece, August 2013, Oral presentation: On surface effects in model heterogeneous materials and the consequences for a real material:- cortical bone

ISB, Natal, Brazil, August 2013, Poster presentation: The micropolar behaviour of cortical bone: size and surface effects in 3-point bending.